



HAL
open science

Tailor-made conception of zeolites for catalysis: from the active site to the reactor

Marilyne Boltz

► **To cite this version:**

Marilyne Boltz. Tailor-made conception of zeolites for catalysis: from the active site to the reactor. Catalysis. Université de Strasbourg, 2014. English. NNT : 2014STRAF039 . tel-01127066

HAL Id: tel-01127066

<https://theses.hal.science/tel-01127066v1>

Submitted on 6 Mar 2015

HAL is a multi-disciplinary open access archive for the deposit and dissemination of scientific research documents, whether they are published or not. The documents may come from teaching and research institutions in France or abroad, or from public or private research centers.

L'archive ouverte pluridisciplinaire **HAL**, est destinée au dépôt et à la diffusion de documents scientifiques de niveau recherche, publiés ou non, émanant des établissements d'enseignement et de recherche français ou étrangers, des laboratoires publics ou privés.

ÉCOLE DOCTORALE DES SCIENCES CHIMIQUES

Institut de Chimie, UMR 7177

THÈSE

présentée par

Marilyne BOLTZ

soutenue le : 17 octobre 2014

pour obtenir le grade de :

Docteur de l'université de Strasbourg

Discipline/ Spécialité : Catalyse hétérogène

Tailor-made Conception of Zeolites for Catalysis : From the Active Site to the Reactor

THÈSE dirigée par :
Dr. LOUIS Benoît

Chargé de Recherches, Université de Strasbourg

RAPPORTEURS :
Pr. VEDRINE Jacques
Dr. VALTCHEV Valentin

Professeur Emérite, Université Pierre et Marie Curie
Directeur de Recherches, Ecole Nationale Supérieure
d'Ingénieurs de Caen

AUTRES MEMBRES DU JURY :
Pr. ROGER Anne-Cécile
Pr. PEREIRA Marcelo Maciel

Professeur, Université de Strasbourg
Professeur, Université Fédérale de Rio de Janeiro

“Une personne qui n’a jamais commis d’erreurs n’a jamais tenté d’innover.”

Albert Einstein

A tous ceux qui sont chers à mon Coeur...

REMERCIEMENTS

Je tiens en premier lieu à remercier le docteur Benoît Louis pour m'avoir soutenu tout au long de ma thèse. Il a été de très grands conseils, tant au niveau scientifique qu'au niveau personnel et m'a toujours aidé à faire avancer au mieux mon travail. Je lui évoque toute ma gratitude pour sa patience, sa générosité et ses qualités humaines.

Je remercie également tous les membres du jury pour avoir accepté de juger mon travail de thèse : Pr. Jacques Védrine, Dr. Valentin Valtchev, Pr. Anne-Cécile Roger et Pr. Marcelo Maciel Pereira.

Je tiens à remercier le professeur Patrick Pale pour m'avoir accueilli au sein de son équipe ainsi que tous les membres permanents du laboratoire, Dr. Valérie Bénéteau, Dr. Aurélien Blanc, Pr. Jean-Marc Weibel et Dr. Victor Mamane pour toutes les discussions que nous avons pu avoir lors de nos séminaires internes.

Mes remerciements vont aussi au Professeur Jean Sommer pour l'hospitalité et la gentillesse qu'il a pu m'accorder avant son départ en retraite.

Un grand merci à toutes les personnes qui ont pris soin de faire régner une bonne ambiance au LASYROC. J'aimerais citer les personnes qui sont devenues des amis pour moi. Je pense tout particulièrement à mon acolyte Pit Losch avec qui le contact est tout de suite passé. Pour nos discussions scientifiques mais surtout pour tous nos moments de délires dans le laboratoire... Je n'oublie pas Anne-Sophie pour tous les potins partagés. Et Catarina, notre portugaise toujours de bonne humeur.

J'aimerais saluer toutes les personnes qui ont contribué scientifiquement à la réalisation de ce travail :

- * Pr. Pierre Mothe Esteves pour ses grandes connaissances et les calculs de DFT.
- * Dr. Thomas Onfroy pour son expertise en spectroscopie infrarouge, sa disponibilité et sa gentillesse.

- * Thierry Roméro pour sa bonne humeur et pour les images MEB de qualité qu'il a pu tirer de mes échantillons lors des séances MEB à Cronenbourg.
- * le service RMN de la faculté de Chimie de Strasbourg et tout particulièrement Jean-Daniel Sauer pour les analyses H/D.
- * le laboratoire ICPEES pour l'accès au DRX et un merci au Dr. Ksenia Parkhomenko pour les analyses BET.
- * Suzanne Libs pour ses précieuses connaissances en chromatographie gazeuse.

Mes prochains remerciements vont à toutes les personnes des autres laboratoires côtoyées tout au long de ma thèse, Laetitia Angelo, Myriam Frey, Charlotte Lang, Kilian Kobl, Georges Khalil et bien d'autres encore.

Je remercie également le Professeur Marcelo Maciel Pereira pour m'avoir accueilli au sein de son laboratoire à Rio de Janeiro ainsi que toutes les personnes du LACES pour leur accueil chaleureux.

Ces prochaines lignes seront dédiées à toutes les personnes proches qui ont également contribué à la réussite de ce doctorat. Je pense notamment à Anne-Laure et Florian pour toutes les soirées passées ensemble (Rétro et autres) et celles à venir !! Toutes mes coéquipières de hand et tout le HC Marckolsheim pour la bonne ambiance dans les bons comme les mauvais moments « sportifs ».

Merci à ma belle-famille, Dominique et Dominique, Mallaury et Maxime pour les moments conviviaux passés ensemble. Je ne saurai comment remercier mes parents, Pascale et Philippe et ma petite sœur Elsa, pour leur soutien sans faille. Sans vous, je n'en serai pas là !! Finalement, je remercie mes grands-parents ainsi que toute ma famille proche.

Last but not least, Clément qui a partagé mes joies et mes déceptions tout au long de cette étape. Merci infiniment pour ton écoute, ton soutien constant, ton humour qui a rendu plus facile la vie de tous les jours.

TABLE OF CONTENTS

REMERCIEMENTS	I
TABLE OF CONTENTS	V
<hr/>	
RÉSUMÉ (EN FRANÇAIS)	I
<hr/>	
1. Introduction	III
2. Synthèse sur mesure et caractérisation de zéolithes	VI
3. Conversion du méthanol en oléfines légères sur des zéolithes de type ZSM-5	XI
4. Chloration semi-continue d'aromatiques avec l'acide trichloroisocyanurique sur des acides solides	XIV
5. Synthèse et applicabilité en MTH de zéolithes supportées sur des supports siliciques	XX
6. Conclusion	XXIII
<hr/>	
GENERAL INTRODUCTION	1
<hr/>	
1. Goal and scope of the Thesis	3
2. Outline of the Thesis	5
3. Selected references	6
<hr/>	
CHAPTER 1. LITERATURE BACKGROUND	9
<hr/>	
1. Zeolites	12
1.1 What are zeolites?.....	12
1.2 Zeolite properties and applications.....	16
1.3 Zeolite synthesis	26
1.4 Y and ZSM-5 zeolites	35
1.5 Hierarchical zeolites	39
1.6 Zeolites coatings.....	50
1.7 Conclusions.....	54
2. Zeolites = solid acid catalysts	54
2.1 Introduction.....	54

2.2 Chlorination of aromatics.....	55
2.3 Methanol-To-Olefins reaction	60

CHAPTER 2. EXPERIMENTAL 81

1. Experimental set-up.....	84
1.1 Aromatics chlorination reactions	84
1.2 Methanol to olefins reaction.....	86
2. Characterization methods.....	88
2.1 X-ray diffraction (XRD).....	88
2.2 Scanning electron microscopy (SEM)	89
2.3 High-Resolution transmission electron microscopy (HRTEM).....	90
2.4 Specific surface area and porosimetry measurements	91
2.5 H/D isotope exchange method.....	93
3. Conclusion.....	94

CHAPTER 3. TAILOR-MADE SYNTHESIS AND CHARACTERIZATION OF ZEOLITES..... 95

1. Introduction	98
2. Hydrothermal synthesis of zeolites	100
2.1 Alkaline route	100
2.2 Fluoride route.....	109
3. Preparation of hierarchical zeolites.....	115
3.1 Constructive synthesis strategy.....	115
3.2 Destructive synthesis strategy.....	118
4. Conclusion.....	140

CHAPTER 4. CONVERSION OF METHANOL INTO LIGHT OLEFINS OVER ZSM-5 ZEOLITES141

1. Introduction	144
2. Preliminary results.....	147
2.1 Characterization of the zeolites.....	147
2.2 Evaluation of catalytic properties in the methanol to hydrocarbons (MTH) reaction	151
2.3 Discussion	154
2.4 Summary	159
3. Toward the design of a second generation of MTP-catalysts.....	160

3.1 Influence of the Si/Al ratio	160
3.2 Influence of the crystal size	162
3.3 Replacement of HF by HCl	163
3.4 Total conversion capacity	165
4. Conclusion	168

CHAPTER 5. AROMATIC CHLORINATION WITH TRICHLOROISOCYANURIC ACID OVER ZEOLITES.....169

1. Introduction	172
2. Preliminary results.....	174
2.1 Liquid-phase chlorination	174
2.2 DFT calculations.....	179
2.3 Chlorination reaction mechanism	182
2.4 Summary	183
3. Semi-continuous chlorination	184
3.1 Screening of solid acid catalysts	184
3.2 Optimization of the reaction conditions	191
3.3 Kinetics study	195
3.4 Catalyst recycling	200
3.5 Chlorine consumption and catalyst stability versus time.....	202
3.6 Silylation of zeolite surface.....	203
3.7 Hierarchical zeolites in chlorination reactions	205
4. Conclusions	220

CHAPTER 6. SYNTHESIS AND APPLICABILITY OF ZEOLITE COATINGS ON SILICON-CONTAINING SUPPORT223

1. Introduction	226
2. Structured catalyst synthesis	228
2.1 Zeolite coated on glass monolith	228
2.2 Zeolite coatings on silicon carbide	232
3. Catalytic activity of zeolite coatings on SiC supports in MTH reaction	246
3.1 Catalytic activity of ANA/ α -SiC composite	246
3.2 Catalytic activity of ZSM-5/ β -SiC beads.....	247
4. Conclusions	249

GENERAL CONCLUSIONS AND FUTURE PROSPECTS.....	251
PUBLICATIONS.....	257
COMMUNICATIONS.....	259

RÉSUMÉ (EN FRANÇAIS)

1. Introduction

Le marché mondial fait pression sur l'industrie chimique et sur l'industrie des matériaux de pointe afin de réduire le temps écoulé entre la recherche et le développement. En particulier, les approches courantes de développement et d'insertion de matériaux sophistiqués dans les systèmes ayant trait à l'utilisation dans les secteurs vitaux (microélectronique, photonique, automobile, aérospatiale) consomment trop de temps et donc d'argent. Il y a par conséquent un gain potentiellement élevé dans le développement de méthodologies qui accéléreraient l'insertion de matériaux et économiseraient donc des millions d'euros en investissement. Ainsi une approche rationnelle, permettant de combiner un examen approfondi des bases de données scientifiques, comme la composition chimique, la structure et les propriétés de matériaux inorganiques apparaît bénéfique, tout en gardant à l'esprit la nécessité de faire ce choix en fonction de l'application visée. Cette stratégie apparaît être un moyen élégant de palier à ces problèmes et de s'imposer au sein de la chimie organique mais aussi de la chimie industrielle.

Dans cet esprit, les zéolithes apparaissent comme des candidats intéressants grâce à leur propriétés très modulables. En effet, les zéolithes sont des catalyseurs hétérogènes qui peuvent être conçus de manière tridimensionnelle en fonction de l'application voulue, c'est-à-dire à trois différentes échelles : au niveau de leur composition moléculaire, au niveau microscopique et leur structuration à l'échelle du réacteur.

D'un point de vue industriel, les zéolithes sont d'importants catalyseurs dans de nombreux procédés, allant de l'adsorption et l'échange ionique à la catalyse hétérogène. En terme de valeur, la catalyse représente de loin le plus grand marché pour les zéolithes, environ 55% du total et promet une large croissance dans les années à venir. Les zéolithes sont les catalyseurs hétérogènes possédant la plus grande production annuelle. Elles sont largement utilisées dans de nombreuses réactions de catalyse acide, notamment en

pétrochimie [1] mais également de plus en plus en chimie organique [2]. Les connaissances sur les zéolithes obtenues grâce à leur emploi en industrie pétrochimique notamment, ont permis d'accéder à de nombreuses possibilités disponibles pour leur conception sur mesure en fonction de l'application ciblée.

Ces travaux de Thèse s'inscrivent parfaitement dans cette problématique. Ainsi, il sera décrit dans le manuscrit la synthèse sur mesure, la caractérisation, ainsi que l'application de matériaux zéolithiques. En effet, les zéolithes sont des aluminosilicates cristallins de structure microporeuse, possédant une surface spécifique élevée ainsi qu'une forte acidité (de Lewis et de Brønsted) les rendant très utiles pour la catalyse acide. Ainsi, les travaux décrits dans cette Thèse visent au développement de diverses zéolithes et ceux à trois échelles : (i) site actif en jouant sur leur force acide et accessibilité, (ii) au niveau microscopique en adaptant la taille des cristaux et (iii) au niveau de leur structuration à l'échelle du réacteur en déposant les cristaux de zéolithes sur différents supports (Figure 1.1).

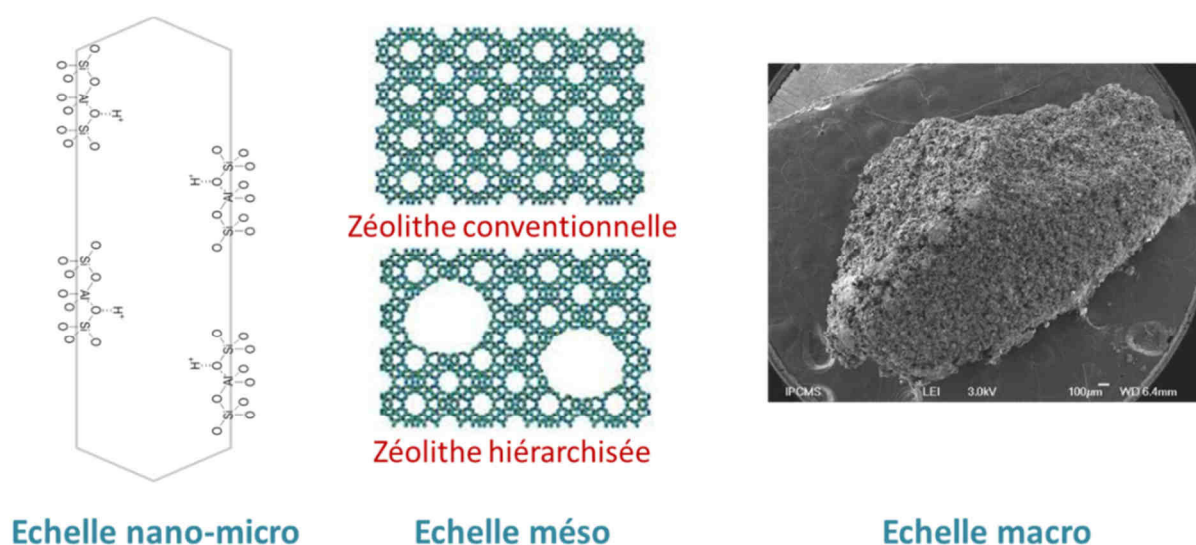


Figure 1.1 Du site actif...au réacteur

[1] A. Corma, *Chem. Rev.* **1995**, *95*, 559–614.

[2] S. Borghèse, P. Drouhin, V. Bénéteau, B. Louis, P. Pale, *Green Chem.* **2013**, *15*, 1496.

De plus, le second aspect qui sera développé est l'utilisation de ces zéolithes dans deux réactions distinctes de catalyse acide : une plus classique du domaine de la catalyse hétérogène et une réaction de chimie organique ; la conversion du méthanol en oléfines légères (MTO) et la chloration d'aromatiques désactivés, respectivement.

Premièrement, afin d'atteindre ce but, des zéolithes hiérarchisées, c'est-à-dire mésoporeuses, ont été préparées *via* plusieurs méthodes et minutieusement caractérisées à l'aide de nombreuses techniques. Des techniques destructives, comme la désilication et la déalumination, ou des techniques constructives comme la méthode de « double templating », ont été essayées sur des zéolithes de topologies FAU et MFI. En plus d'une optimisation de ces traitements individuels, une exploration sur l'enchaînement de ces traitements a été étudiée. Le dépôt de zéolithes sur divers supports siliciques a été étudié. Ainsi, deux techniques de préparation ont été envisagées : (i) une préparation avec ajout supplémentaire de source de silicium et (ii) une préparation sans ajout supplémentaire de source de silicium.

Différentes topologies de zéolithes ont été modifiées par des traitements pré- ou post-synthèses selon la réaction visée. Concernant la réaction de MTO, seule la structure MFI tridimensionnelle et bien définie de la zéolithe ZSM-5 a été testée. En effet, une attention particulière sur les conditions de synthèse *via* la procédure par voie fluorure a été donnée. D'autre part, les activités catalytiques des zéolithes hiérarchisées ont été évaluées dans la réaction de chloration des aromatiques. Enfin, l'évaluation de zéolithes supportées a été effectuée dans des applications en MTO.

Finalement, les performances catalytiques de ces différentes zéolithes seront directement liées à leur propriétés intrinsèques. En d'autres termes, le lien entre l'activité catalytique et la structure de la zéolithe (après modification) des différents catalyseurs a été évalué.

2. Synthèse sur mesure et caractérisation de zéolithes

Premièrement, des matériaux zéolithiques conventionnels ont été synthétisés par méthode hydrothermale en milieu alcalin afin d'obtenir des zéolithes classiques (ZSM-5, EMT et FAU) qui ont pu servir de référence dans les tests catalytiques.

Ainsi, nous avons pu synthétiser, par voie hydrothermale alcaline, des zéolithes de topologie MFI présentant des tailles de cristaux variées. Une zéolithe ZSM-5 ayant des cristaux classiques en forme de « pastille Vichy » d'une dizaine de micron et une autre présentant des cristaux sous forme d'empilement de nanofeuillets ont pu être obtenues (Figure 1.2).

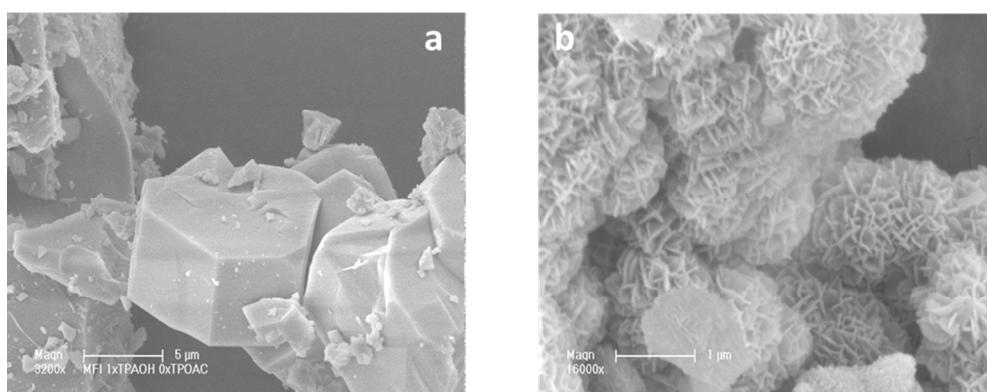


Figure 1.2 Images MEB des zéolithes a) ZSM-5R et b) ZSM-5NS

Des zéolithes de topologies similaires (FAU et EMT) ont également été préparées (Figure 1.3).

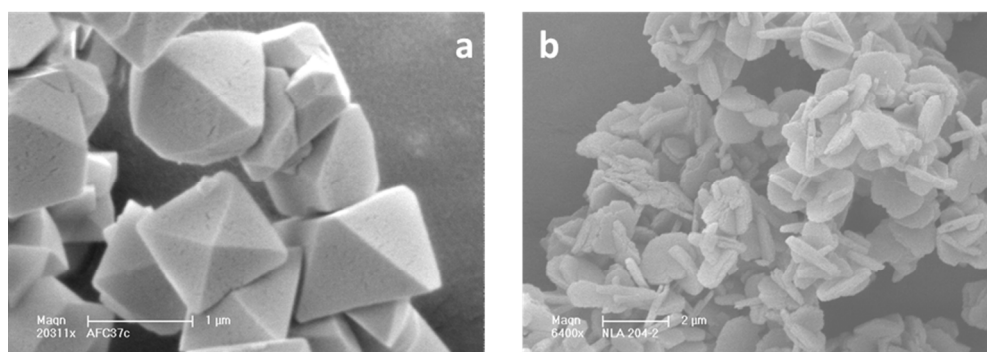


Figure 1.3 Images MEB des zéolithes a) EMC-1 et b) EMC-2

D'autre part, une partie des travaux de thèse a été focalisée sur la synthèse de zéolithes ZSM-5 en présence d'anions fluorures. La voie fluorure s'effectue en présence d'une source de fluorures servant d'agent minéralisant (NH_4F , HF) dans des conditions de pH neutre (pH \sim 6-7). Une synthèse conventionnelle de zéolithe réalisée par voie basique, utilisant de la soude, à des pH \sim 9-10 a été effectuée à titre comparatif. Des zéolithes présentant des tailles de cristaux « géants », de l'ordre de plusieurs dizaines de microns ont été obtenues (Figure 1.4).

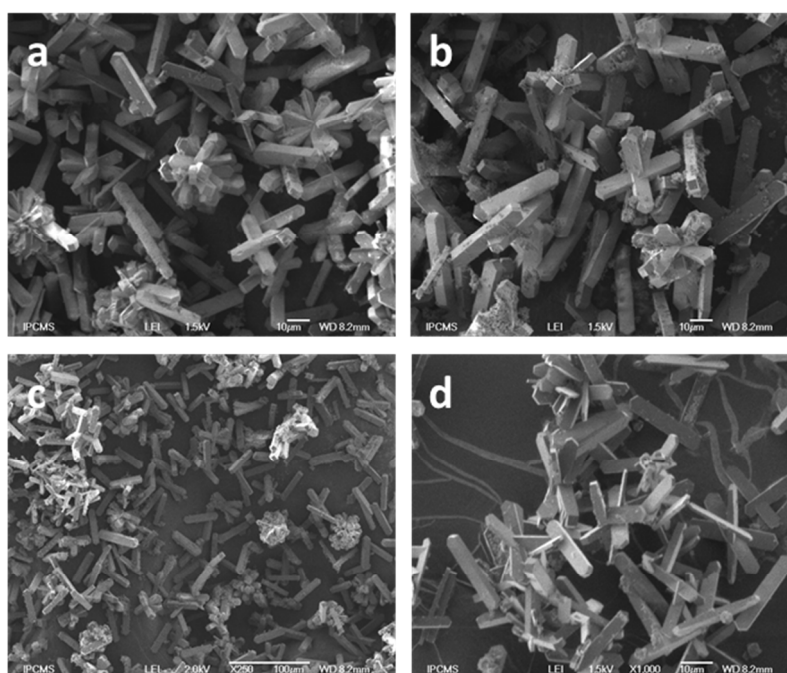


Figure 1.4 Images MEB de zéolithes préparées par voie fluorure

De plus, les tailles de cristaux, la cristallinité du matériau ainsi que de faibles acidités (Lewis et Brønsted) ont été modulées par simple variation des paramètres de synthèse (durée, source de silicium, quantité d'aluminium, concentration, etc). De plus, le remplacement de l'acide fluorhydrique par de l'acide chlorhydrique a été également étudié afin de rendre la synthèse plus verte. Des zéolithes présentant une morphologie similaire à celles obtenues lors de l'emploi d'HF ont été synthétisées. Les comportements catalytiques de ces zéolithes « géantes » ont été principalement étudiés dans la réaction MTO.

Finalement, un axe d'étude centré sur la hiérarchisation de la porosité au sein des catalyseurs a été étudié. En effet, l'insertion de mésoporosité au sein d'un solide

microporeux permet d'améliorer l'accessibilité aux sites actifs ainsi que les capacités de diffusion des réactifs et des produits à l'intérieur du réseau (Figure 1.5). En conséquence, une zéolithe hiérarchisée est obtenue, intégrant dans un seul matériau à la fois les propriétés uniques des micropores natifs et un accès et une diffusion facilités induits par le réseau mésoporeux complémentaire. Ces processus de hiérarchisation de la porosité ont été développés afin d'ouvrir les capacités des zéolithes à des réactions impliquant des molécules de plus grande taille.

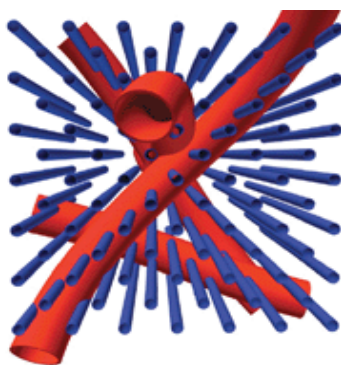


Figure 1.5 Schématisation des mésopores au sein d'un réseau microporeux

Ainsi, il existe deux approches pour la création de mésoporosité dans les zéolithes : la voie constructive et la voie destructive, respectivement.

Dans le cas de la voie constructive, l'insertion de mésoporosité s'effectue dès la formation du réseau microporeux de la zéolithe, c'est-à-dire directement lors de sa synthèse. Lors de ce travail, la méthode de « *double templating* » a été utilisée. Cette méthode consiste à mettre, en plus de l'agent structurant de la zéolithe qui permet de former le réseau microporeux, un agent structurant supplémentaire qui va permettre de créer un réseau complémentaire ayant des pores de plus grand diamètre (mésopores > 2nm). Ces mésopores ont la particularité d'être bien ordonnés au sein du cristal de la zéolithe. Dans notre cas, nous avons utilisé la spermine, une polyamine, qui grâce à des phénomènes d'interaction ou de répulsion avec le réseau de la zéolithe va induire la formation de mésoporosité intra-cristalline. Malheureusement, la caractérisation de cette zéolithe a pu mettre en évidence le fait qu'aucune mésoporosité significative n'a été insérée.

Parallèlement, la voie destructive a également été étudiée. Cette méthode a pour principe d'effectuer des post-traitements sur des zéolithes déjà synthétisées. Il est à noter

que ces traitements permettent d'obtenir une mésoporosité aléatoire dans le cristal et ont pour conséquence la destruction (en partie) du réseau cristallin de la zéolithe. Le premier type de post-traitement employé était la désilication. Ce traitement induit l'extraction sélective d'une partie du silicium intra-réseau en présence d'un milieu alcalin (une solution de NaOH ou de tétrapropylammonium plus ou moins concentrée), ce qui engendre la formation de mésoporosité intra-cristalline (Figure 1.6).

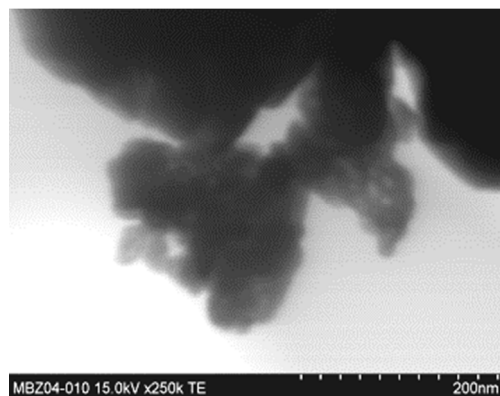


Figure 1.6 Image MET d'une zéolithe traitée à la soude

Grâce à différentes techniques de caractérisation (MEB, DRX, BET, dosage des sites acides, FTIR avec adsorption de CO à basse température), les effets des divers traitements ont pu être analysés.

Finalement, l'insertion de mésoporosité par déalumination a également pu être vérifiée. Lors de ces travaux, diverses méthodes de déalumination ont été employées afin d'évaluer leurs effets sur l'activité catalytique des zéolithes modifiées. Le traitement à la vapeur d'eau (dans des conditions de température plus ou moins drastiques), ainsi que des traitements acide ou chimique à l'acide oxalique, à l'acide éthylène diamine tétraacétique (EDTA) ont été étudiés lors de ces travaux de thèse. Le traitement à la vapeur d'eau permet de générer, par extraction d'une partie de l'aluminium intra-réseau formant ainsi des mésopores, des espèces d'aluminium extra-réseaux, nommés EFAl. La création d'EFAl par traitement à la vapeur d'eau est dépendante des conditions de température. En effet, il a été montré, grâce à des études de RMN du solide ^{27}Al , que la quantité d'espèces d'EFAl générées lors du traitement est proportionnelle à la température de celui-ci. Les mesures d'adsorption par la méthode BET ont permis de mettre en évidence la formation de

mésoporosité intra-cristalline. De plus, la présence de ces espèces d'EFAl, en particulier des espèces de type acide de Lewis, au sein des pores de la zéolithe peut induire une acidité exaltée grâce à une synergie entre l'acidité de Brønsted et l'acidité de Lewis. Au contraire, les méthodes chimiques utilisant l'acide oxalique et l'EDTA induisent la création d'espèces d'EFAl qui sont immédiatement lessivées hors des pores de la zéolithe. Ces post-traitements permettent de ce fait de former de la mésoporosité et de libérer les pores du matériau des espèces d'EFAl, améliorant ainsi l'accessibilité aux sites actifs. Cette mésoporosité a pu être caractérisée par mesures d'adsorption et désorption d'azote. La distribution de la taille de ces mésopores est d'environ 7 nm de diamètre (Figure 1.7).

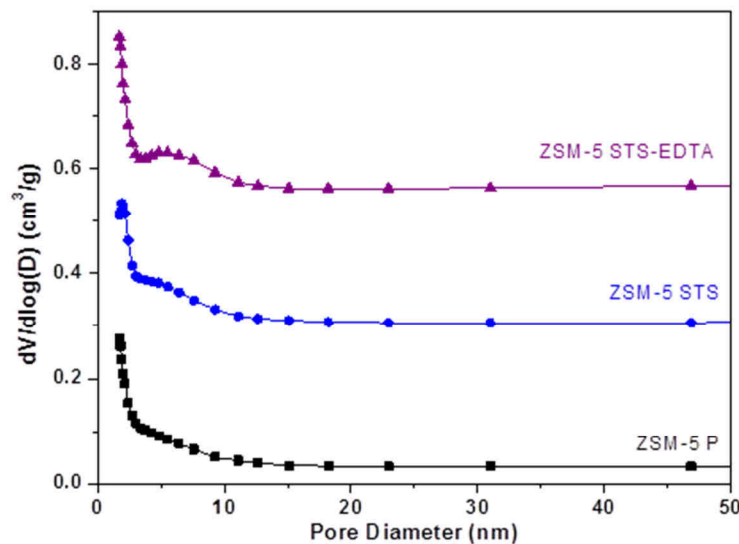


Figure 1.7 Distribution de la taille des pores de zéolithes déaluminées

D'autre part, l'acidité de ces matériaux a pu être analysée par analyse FTIR classique et d'adsorption de CO. Les zéolithes traitées à la vapeur d'eau ont montré moins de sites acides de Brønsted du fait du blocage des pores par les débris d'EFAl mais une force acide légèrement supérieure à celle de la zéolithe parente. Les échantillons traités à la fois à la vapeur d'eau et à l'EDTA ont montré une acidité similaire à la zéolithe parente (Figure 1.8). Les réactivités de l'ensemble de ces zéolithes hiérarchisées ont été étudiées dans la réaction de chloration d'aromatiques désactivés.

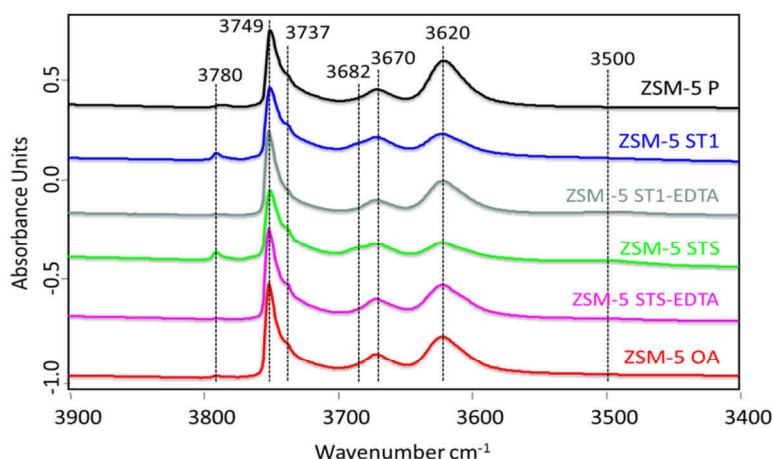


Figure 1.8 Spectres IR des zéolithes déaluminées dans la région des OH

3. Conversion du méthanol en oléfines légères sur des zéolithes de type ZSM-5

De nos jours, les procédés de conversion du méthanol en oléfines légères (Figure 1.9) et plus particulièrement du méthanol en propylène (MTP) sont considérés comme des voies attractives et viables pour la valorisation des ressources en gaz naturel [3].

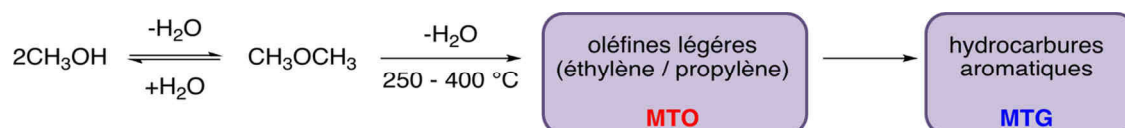


Figure 1.9 Description des procédés de conversion du méthanol en hydrocarbures (MTH)

Afin de palier, dans les prochaines décennies, à l'augmentation de la demande en propylène, brique élémentaire indispensable pour l'industrie des polymères, les chercheurs poursuivent le développement de ces procédés que ce soit en termes de conception du catalyseur acide ou en termes d'amélioration du procédé global, pour obtenir un procédé encore plus sélectif et rentable. Notre stratégie était de développer un catalyseur

[3] G.A. Olah, A. Goepfert, G.K.S. Prakash, *Beyond oil and Gas: The Methanol Economy*, Wiley VCH, Weinheim, Germany (2006) pp. 246.

zéolithique « optimisé » pour la conversion du méthanol en propylène (MTP), de type ZSM-5, à la fois via des procédures classiques et plus originales décrites précédemment. Les tests catalytiques ont montré une amélioration notable pour une famille de zéolithes préparées en milieu fluorure, permettant d'atteindre une sélectivité en propylène de 40% (Figure 1.10). Ainsi un rapport propylène / éthylène > 5 a été atteint, représentant une valeur bien supérieure à une zéolithe ZSM-5 commerciale (propylène / éthylène ~ 2). La meilleure activité du catalyseur préparé par voie fluorure peut être liée à plusieurs facteurs : (i) une faible acidité, (ii) faible quantité de défauts structuraux (silanols) et (iii) taille de cristaux « géants » empêchant les réactions consécutives et donc la formation de coke.

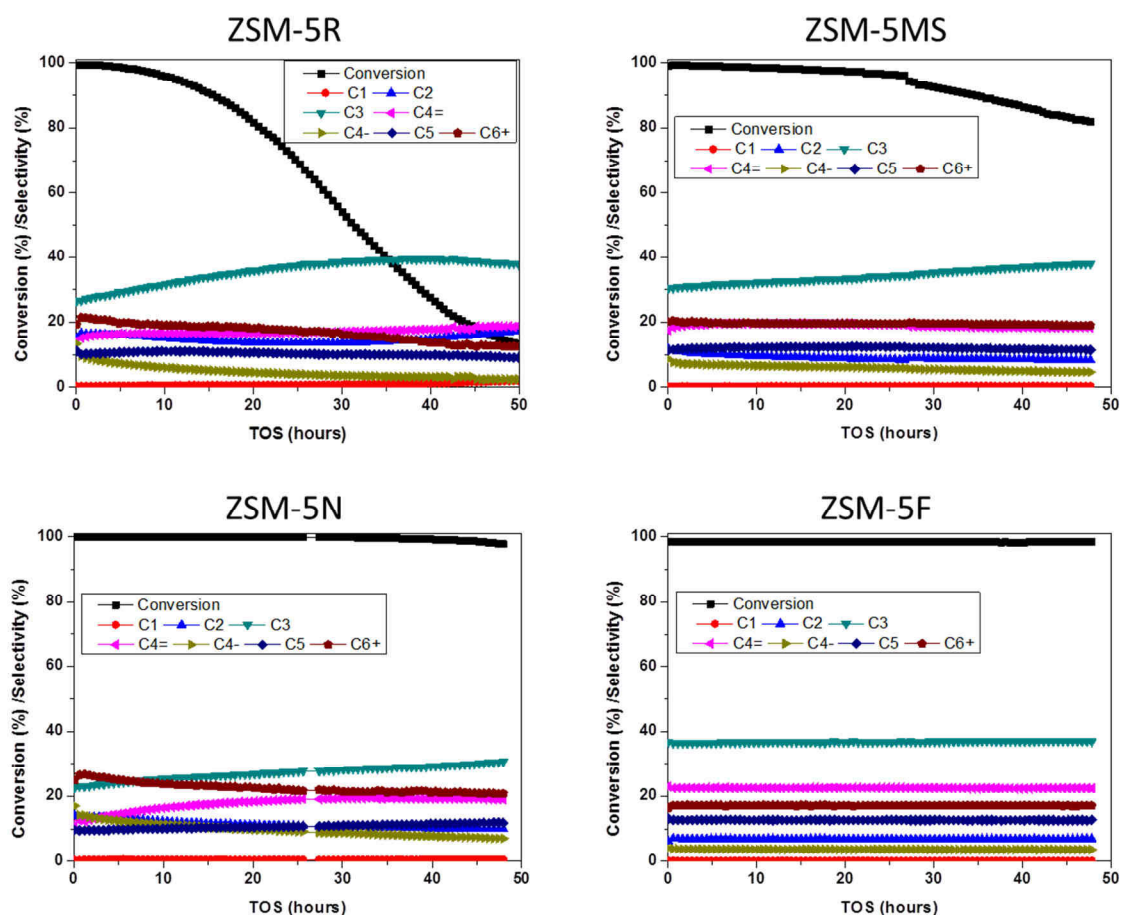


Figure 1.10 Résultats catalytiques de quatre zéolithes ZSM-5 en MTH

Une seconde génération de catalyseur a pu être développée grâce à l'emploi de la procédure par voie fluorure. Durant cette étude, l'influence du rapport Si/Al a été analysée. De manière surprenante, il en est ressorti que les catalyseurs présentant les plus faibles

acidités permettaient d'obtenir les meilleurs résultats catalytiques en terme de conversion du méthanol et de sélectivité en propylène. De plus, l'influence de la taille des cristaux a été étudiée. Nous avons pu mettre en évidence la présence d'un volume optimale d'environ $540 \mu\text{m}^3$. Grâce à ces études, un catalyseur optimal, en terme d'acidité ($\text{Si}/\text{Al} = 136$) et de taille de cristaux ($30 \mu\text{m}$ en longueur), a permis d'obtenir une conversion de 94% en méthanol avec des sélectivités très intéressantes ($S_{\text{oléfines légères}} = 85\%$, $S_{\text{propylène}} = 58\%$) et un ratio C_3/C_2 de 5,3 (Figure 1.11).

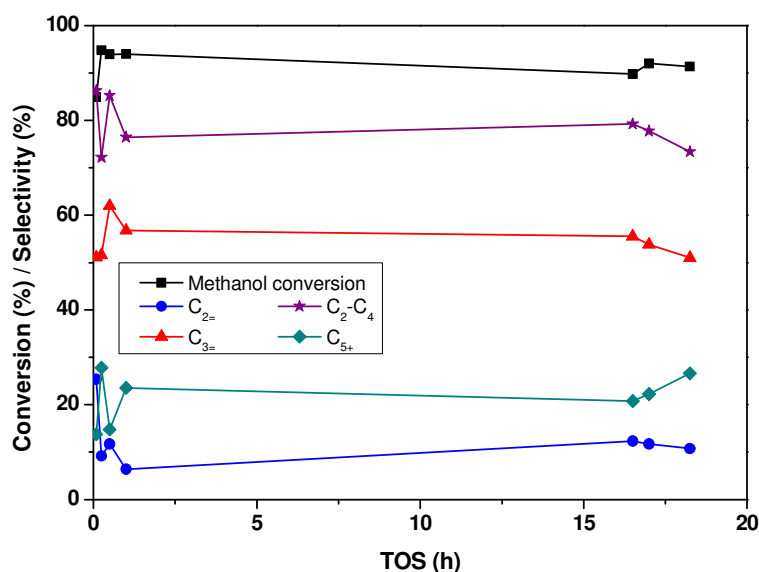


Figure 1.11 Profil catalytique du catalyseur optimale en MTP

Finalement, les zéolithes synthétisées par voie fluorure avec utilisation d'acide chlorhydrique (ZSM-5FCl) ont également été testées en réaction MTO. Le meilleur candidat de cette série de catalyseur a permis de convertir 69% de méthanol avec des sélectivités en oléfines légères et propylène de 76% et 35%, respectivement (Figure 1.12).

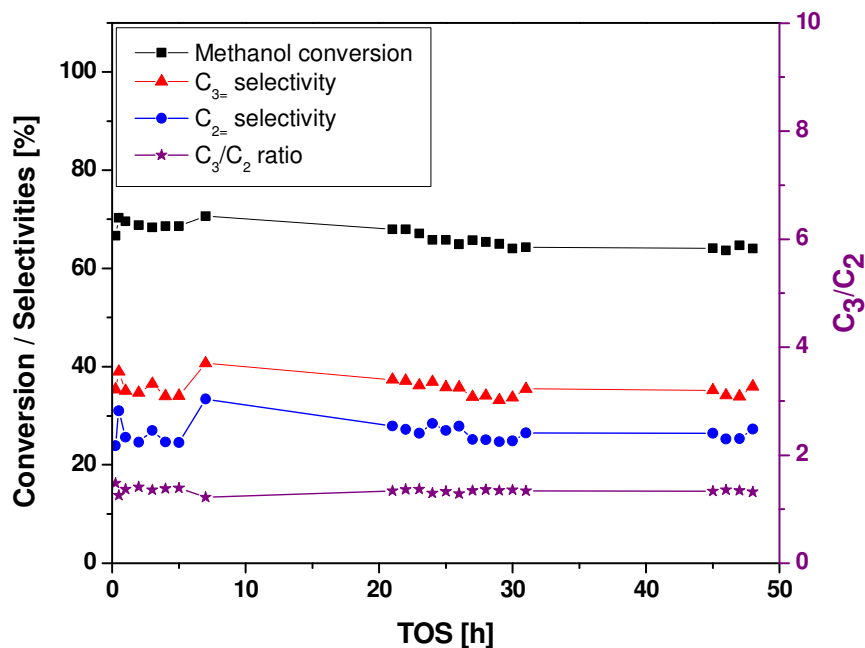


Figure 1.12 Profil catalytique du meilleur candidat ZSM-5/FCI

Ainsi, cette étude a permis de montrer que l'acide fluorhydrique peut être efficacement remplacé par un autre acide moins nocif. Malgré les taux de conversion et sélectivités envers le propylène plus modérés, ces catalyseurs présentaient une stabilité similaire à celle des catalyseurs préparés par voie fluorure classique.

4. Chloration semi-continue d'aromatiques avec l'acide trichloroisocyanurique sur des acides solides

Finalement, le dernier objectif, mais non le moindre, était de développer une nouvelle méthode de chloration d'aromatiques plus éco-compatible que les procédés industriels existants. Les dérivés aromatiques chlorés sont d'importantes molécules de base dans la chimie fine, en l'occurrence pour la synthèse de colorants et de composés bio-actifs comme les pesticides ou les composés pharmaceutiques [4]. Malheureusement, les méthodes

[4] J.I. Kroschwitz, M. Howe-Grant, C.A. Treacy, L.J. Humphreys, Encyclopedia of Chemical Technology, vol. 6, Wiley, New York (1993) pp. 109.

industrielles, utilisées pour la chloration d'aromatiques, produisent des mélanges de régioisomères difficiles à séparer et engendrent des coûts supplémentaires. Ainsi, durant les dernières décennies, la communauté scientifique s'est intéressée à développer des procédés de chloration d'aromatiques plus efficaces et sélectifs [5-6]. Esteves *et al.* ont notamment développé une méthode de chloration d'aromatiques désactivés utilisant un nouvel agent de chloration, l'acide trichloroisocyanurique (TCCA, $C_3N_3O_3Cl_3$) en présence d'un milieu superélectrophile. Notre stratégie était de remplacer les acides liquides utilisés jusqu'à présent par des acides solides : les zéolithes. De plus, nous avons développé un procédé semi-continu (procédé gaz-solide) applicable à divers aromatiques désactivés. Nos études se sont focalisées sur la chloration du nitrobenzène et celle du chlorobenzène (Schéma 1.1). Il était important d'étudier la réactivité du TCCA avec les composés aromatiques en milieu acide (ou superacide).

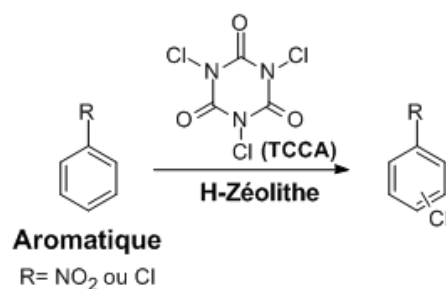


Schéma 1.1 Chloration d'aromatiques désactivés sur zéolithes

Ainsi, durant notre étude, nous avons pu tester de nombreuses structures zéolithiques afin d'analyser leur aptitude à activer le TCCA. Nous avons également pu mettre en évidence le besoin d'une synergie entre la force acide et la taille des pores de l'acide solide, pouvant favoriser la réaction. En effet, la zéolithe de type FAU s'est avérée être le meilleur candidat pour la chloration du nitrobenzène alors que dans le cas du chlorobenzène le catalyseur de type ZSM-5 s'est révélé le plus efficace (Figure 1.13).

[5] K. Smith, G. A. El-Hiti, *Green Chem.* **2011**, *13*, 1579–1608.

[6] G. F. Mendonça, M. R. M. R. Senra, P. M. Esteves, M. C. S. de Mattos, *Appl. Catal. A* **2011**, *401*, 176–181.

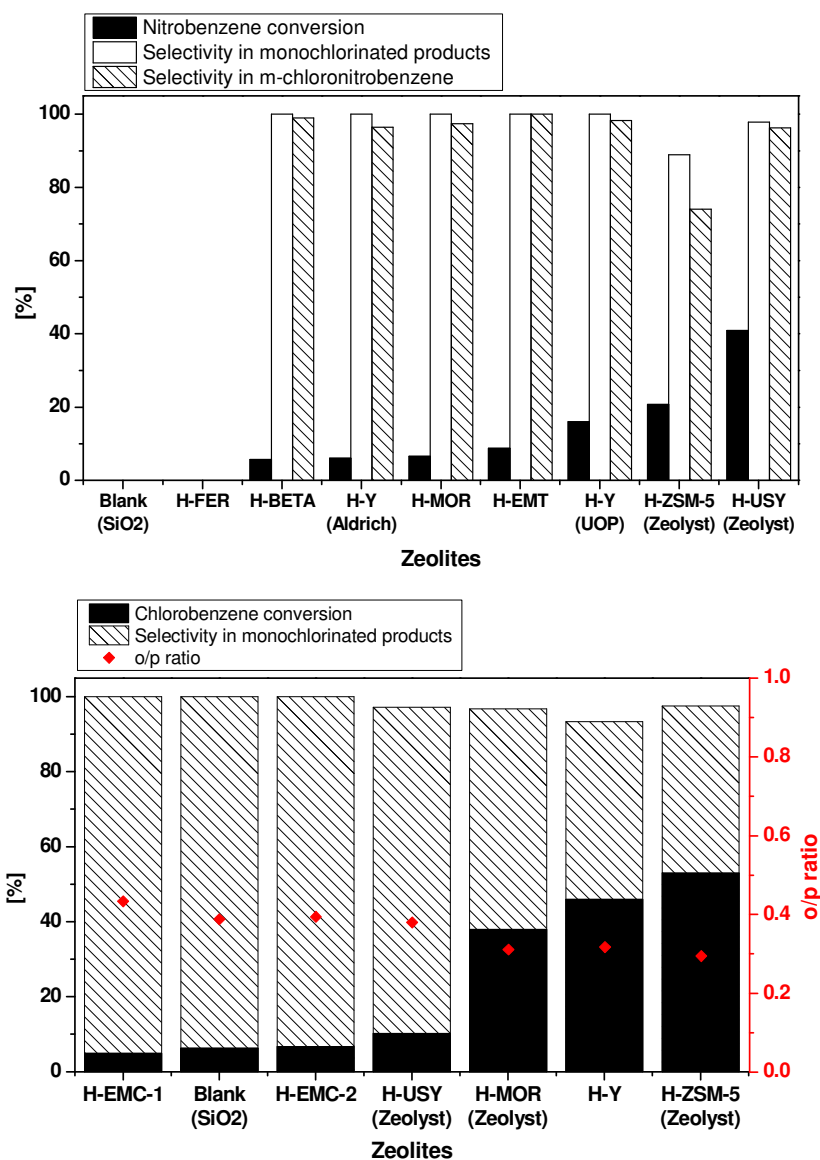


Figure 1.13 Activité catalytique de différentes zéolithes en chloration du nitrobenzène (haut) et chlorobenzène (bas)

Grâce à une collaboration avec le Prof. Esteves, nous avons pu réaliser des calculs DFT afin de mieux comprendre le mécanisme réactionnel (Figure 1.14) et une étude cinétique de cette réaction a été entreprise.

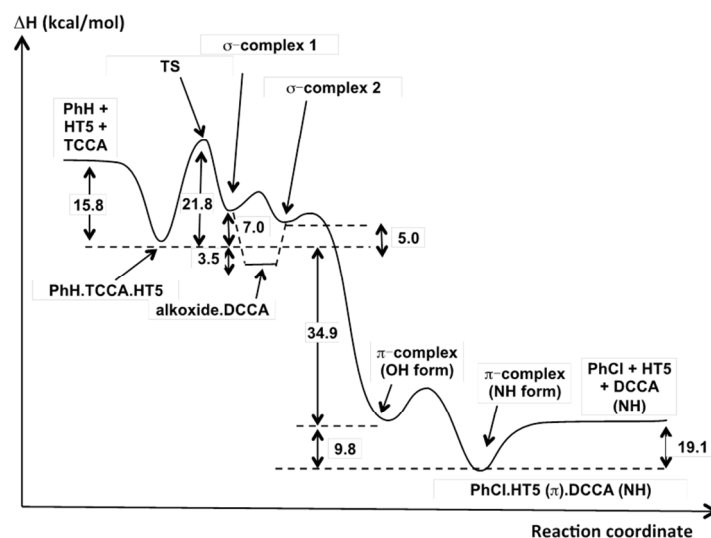


Figure 1.14 Représentation schématique des coordonnées réactionnelles pour la réaction entre le site actif (HT5), l'aromatique et le TCCA

Une étude plus poussée sur l'influence de la porosité hiérarchisée des catalyseurs a été menée. Ainsi, dans la chloration du nitrobenzène, nous avons pu mettre en évidence l'influence positive de la présence de mésoporosité dans la zéolithe de type FAU. En effet, un traitement à l'EDTA de la zéolithe USY a permis d'obtenir une zéolithe exempte de débris d'EFAl et présentant deux type de mésopores (4 et 20 nm). Ainsi la zéolithe traitée à l'EDTA mène à une activité catalytique améliorée par rapport à la zéolithe parente. Une conversion de 82% de nitrobenzène avec une sélectivité en produits de monochloration quasi similaire à la zéolithe parente ont été atteints (Figure 1.15).

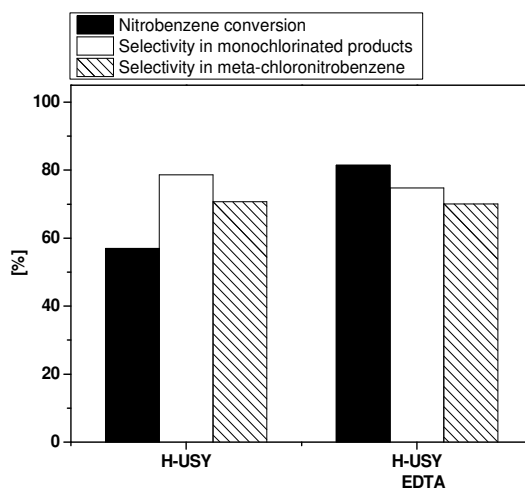


Figure 1.15 Comparaison des activités catalytiques en chloration du nitrobenzène entre la zéolithe H-USY et H-USY traitée à l'EDTA

Différentes zéolithes de type ZSM-5 déaluminées ont été testées dans la chloration du chlorobenzène (Figure 1.16). Les zéolithes traitées à la vapeur d'eau (ZSM-5 ST), exceptée la zéolithe traitée de manière intermédiaire (ZSM-5 ST2), présentent des conversions de chlorobenzène supérieures à celle de la zéolithe parente. Ce phénomène peut être attribué à la présence d'EFAL au sein des micropores de ces zéolithes. En effet, ces espèces peuvent interagir avec les sites acides de Brønsted et exalter leur force, grâce à une synergie qui s'opère entre ces deux acidités. Il est important de noter que ces catalyseurs conservent une importante sélectivité en produits de monochloration > 90%. D'autre part, la zéolithe traitée à la fois avec la vapeur d'eau et avec l'EDTA présente quant à elle une importante amélioration en terme de conversion de chlorobenzène (88% vs. 53% pour la zéolithe parente). Cette augmentation peut être reliée à la présence significative de mésoporosité dans ce catalyseur. En effet, cette mésoporosité peut améliorer les propriétés de diffusion du catalyseur à la fois du chlorobenzène mais aussi des produits de chloration. Malheureusement cette amélioration de réactivité s'effectue au dépens de la sélectivité en produits de monochloration. Cette mésoporosité facilitant la formation des produits de polychloration plus encombrants. L'utilisation d'acide oxalique comme méthode de déaluminisation permet également d'améliorer la réactivité du catalyseur.

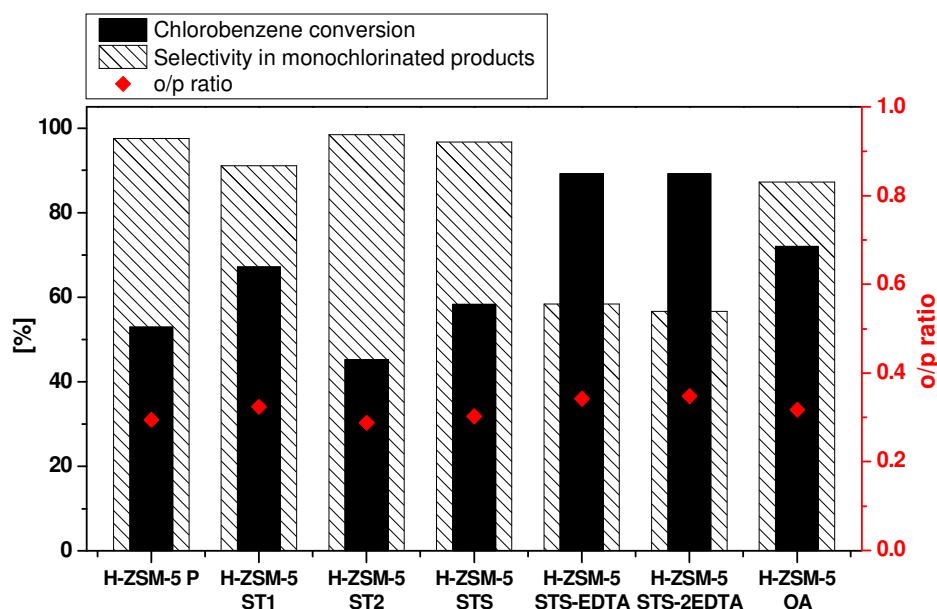


Figure 1.16 Comparaison des activités catalytiques en chloration du chlorobenzène entre la zéolithe parente et les zéolithes déaluminées

Finalement, des zéolithes ZSM-5 traitées à la soude selon différentes conditions (H-ZSM-5 IDS) ont également pu être évaluées dans la réaction de chloration du chlorobenzène (Figure 1.17). Exceptée la zéolithe H-ZSM-5 IDS3, tous les catalyseurs traités par solution alcaline montrent de meilleures performances catalytiques comparé à la zéolithe ZSM-5 parente. La réactivité plus faible de la zéolithe ZSM-5 IDS3 peut être attribuée à l'amorphisation du catalyseur durant le traitement, rendant cette zéolithe moins efficace. Trois catalyseurs présentent une amélioration significative en conversion du chlorobenzène supérieure à 48% (ZSM-5 IDS2, IDS4 et IDS5). Les propriétés mésoporeuses de ces zéolithes pourraient permettre de diminuer les limitations diffusionnelles dans le réseau microporeux et ainsi faciliter leur réactivité comme dans le cas de la zéolithe déaluminée ZSM-5 STS-EDTA. Le catalyseur ZSM-5 IDS5 possède néanmoins une sélectivité en produits de monochloration plus faible comparé à la zéolithe parente. De la même manière que pour la zéolithe ZSM-5 STS-EDTA, la mésoporosité présente dans ce catalyseur favorise la formation de produits de polychloration.

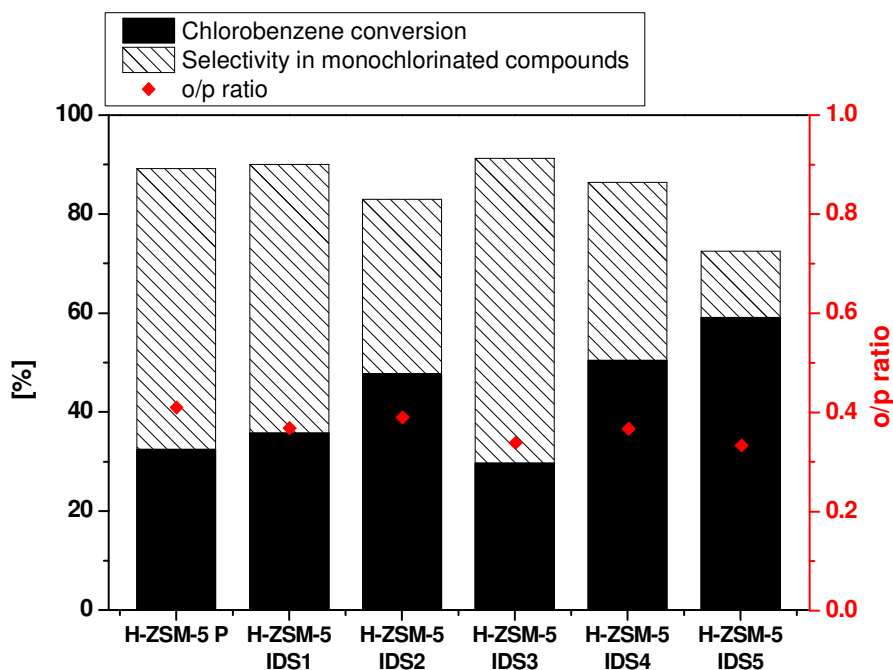


Figure 1.17 Comparaison des activités catalytiques en chloration du chlorobenzène entre la zéolithe parente et les zéolithes traitées à la soude

5. Synthèse et applicabilité en MTH de zéolithes supportées sur des supports siliciques

Enfin, après avoir étudié et tenté de rationaliser les propriétés intrinsèques indispensables des catalyseurs en fonction de leur application en MTO ou en chloration, nous avons voulu préparer des lits catalytiques structurés à l'échelle du réacteur. Deux types de support ont été utilisés pour favoriser la croissance de cristaux de zéolithes sans l'ajout d'un *binder*; des monolithes en verre et du carbure de silicium (SiC), respectivement (Figure 1.18).

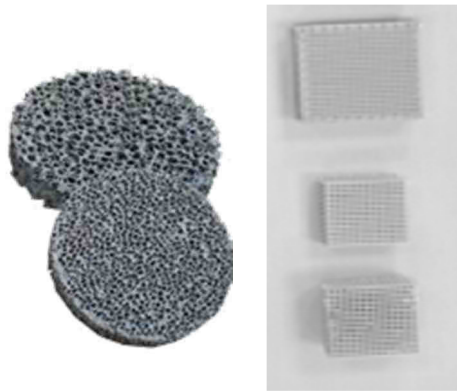


Figure 1.18 Mousses de SiC (gauche) et monolithes en verres (droite)

Les céramiques présentent de nombreux avantages par rapport à d'autres supports comme les métaux. En effet, une plus grande affinité chimique opère entre un support de silice amorphe et la future couche de silice cristalline déposée. De plus, ce genre de support silicique a l'avantage d'être chimiquement inerte. Les supports en SiC possèdent des propriétés supplémentaires très importantes, à savoir une conductivité thermique élevée, une résistance mécanique élevée, une résistance à l'oxydation et une mise en forme aisée [7]. Ainsi, une technique de dépôt de zéolithes sans ajout de source de silicium a été envisagée pour les deux types de support, via une synthèse hydrothermale faisant croître de manière *in-situ* les cristaux de zéolithes à la surface du support. Le lien entre le support et les

[7] a) I.-H. Song, I.-M. Kwon, H.-D. Kim, Y.-W. Kim, J. Eur. Ceram. Soc. 30 (2010) 2671. b) M. Lacroix, P. Nguyen, D. Schweich, C. Pham Huu, S. Savin-Poncet, D. Edouard, Chem. Eng. Sci. 62 (2007) 3259.

cristaux de zéolithes devrait grâce à cette méthode être d'autant plus fort. Des cristaux de zéolithes de type ZSM-5 ont été obtenus par recristallisation de la surface de monolithes en verre (Figure 1.19).

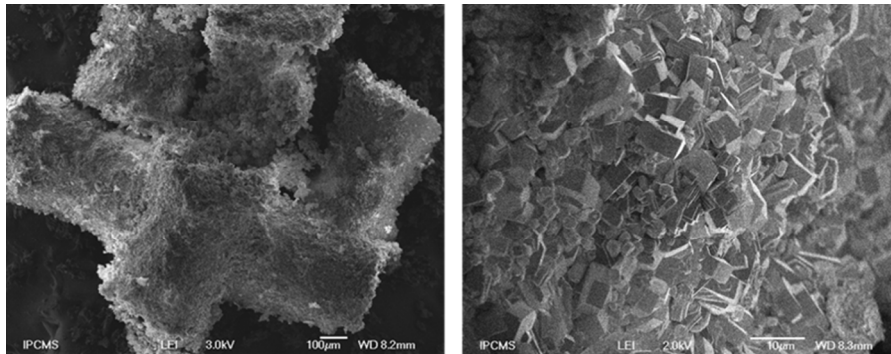


Figure 1.19 Images MEB du monolithe en verre recouvert de zéolithes ZSM-5

D'autre part, il a été nécessaire d'améliorer la réceptivité du support en SiC grâce à une calcination sous air à 550°C pendant 15h. Ce traitement permet de créer à la surface du support SiC une couche de SiO₂ plus facile à recristalliser en structure zéolithique. Deux types de SiC ont été employés lors de ces travaux, le polymorphe α et le polymorphe β . Le polymorphe α utilisé possède une structure alvéolaire alors que le polymorphe β est non alvéolaire et sous forme sphérique. Les cristaux de zéolithes obtenus à la surface de chacun diffèrent en fonction de la composition du gel de zéolithe mis en contact avec le support. Ainsi, nous avons pu recristalliser une partie de la surface de ces supports en différentes zéolithes : Analcime (ANA), zéolithe A (LTA) et ZSM-5.

Une étude sur l'influence du temps de synthèse a permis de démontrer que différents niveaux de recouvrements en cristaux de zéolithes de type ANA peuvent être atteints grâce à cette méthode de recristallisation. En effet, plus le temps de synthèse augmente, plus le taux de recouvrement de la surface du SiC en cristaux de zéolithes augmente (Figure 1.20).

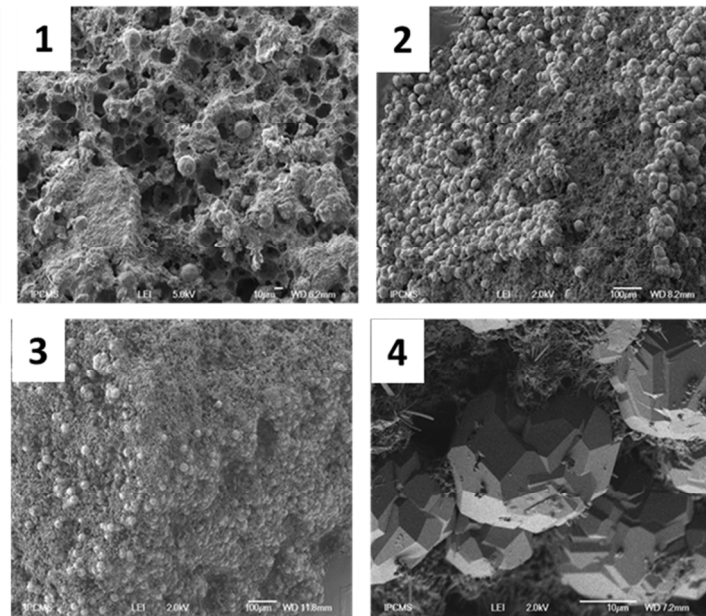


Figure 1.20 Influence du temps de synthèse sur la recristallisation d' α -SiC en cristaux d'analcime : 1) 48h, 2) 60h, 3) 333h et 4) 768h

De plus, en fonction de la composition du gel de zéolithe et notamment en jouant sur l'alcalinité de celui-ci, nous avons pu obtenir la croissance de diverses topologies de zéolithes. En effet, les zéolithes étant des structures métastables, la prévision de formation de telles ou telles zéolithes est difficilement prévisible par l'emploi de cette méthode de recristallisation de la surface. Ainsi, en diminuant l'alcalinité du gel, des cristaux cubiques de type LTA ont pu croître à la surface du SiC. A l'inverse, en augmentant l'alcalinité du gel, des fibres (non définies) sont apparues à la surface de notre support. Finalement, en variant à la fois l'alcalinité et le temps de synthèse, des cristaux typique de la topologie MFI ont pu croître à la surface du α -SiC.

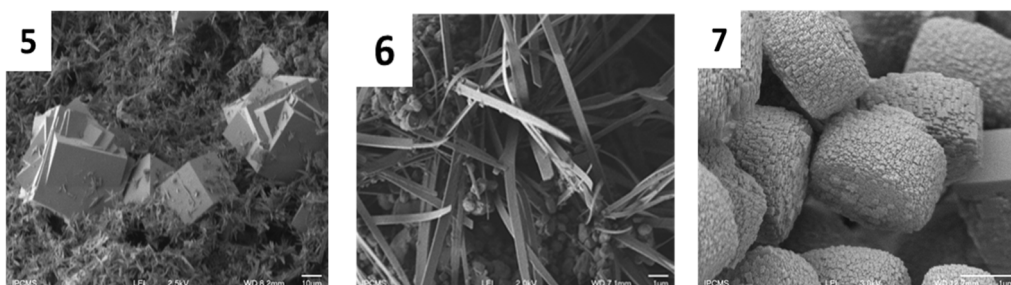


Figure 1.21 Différents types de zéolithes à la surface du α -SiC : 5) LTA, 6) inconnu et 7) MFI

Les composites les plus intéressants ont par la suite été engagés dans la conversion du méthanol en hydrocarbures afin d'évaluer leur comportements catalytiques et de les comparer à leur zéolithe parente non supportée. Ainsi, les composites ZSM-5/ β -SiC, obtenus grâce à la méthode de préparation avec ajout supplémentaire de source de silicium, ont été testés et comparés avec leurs équivalents non supportés. Il en est ressorti que le composite ayant un double dépôt de zéolithe présentait une activité catalytique similaire à la zéolithe non supportée en terme de conversion de méthanol et sélectivités en oléfines légères et propylène. De plus, un test de stabilité du composite a montré qu'il se désactivait immédiatement à raison de 10% en relatif toutes les 10h.

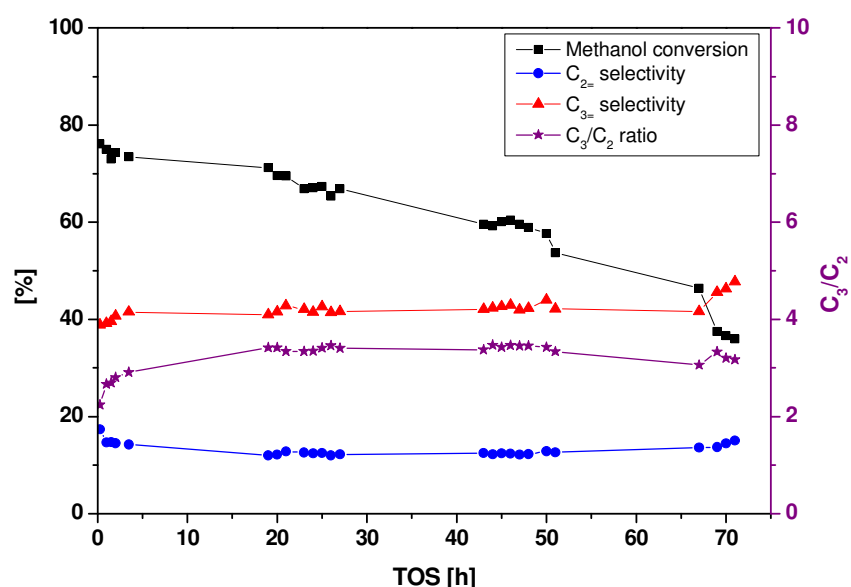


Figure 1.22 Profil catalytique du composite ZSM-5/ β -SiC double dépôt en MTH

6. Conclusion

Grâce à un design sur mesure à trois échelles: au niveau du site actif, de l'insertion de porosité auxiliaire et de leur structuration à l'échelle du réacteur, nous avons pu développer différents catalyseurs ayant les propriétés appropriées en fonction de la réaction ciblée.

De mon point de vue, la conception rationnelle d'un catalyseur « idéal » devrait combiner ces différents aspects, afin d'acquérir une composition chimique adéquate (force et densité acides), une porosité hiérarchisée, une taille de cristaux adaptée mais également une forme macroscopique adaptée au réacteur. En effet, l'ensemble de ces propriétés semble être nécessaire pour élargir l'applicabilité des zéolithes en pétrochimie mais aussi en chimie fine. Chaque niveau joue un rôle défini : nature et densité des sites acides dans le réseau microporeux ; les mésopores facilitent la diffusion intra-cristalline ; et la structuration macroscopique permet d'accéder plus aisément à une utilisation en industrie.

GENERAL INTRODUCTION

1. Goal and scope of the Thesis

The global market lays stress on chemical and material industries to reduce the time between research and development. Particularly, the development of high valuable and advanced materials used in strategic sectors including micro-electronics, photonics, automotive and space industries, consumes too much time and therefore money. Consequently, there is a potential high gain in the development of methodologies which would increase the insertion of materials and therefore save millions of investment. Thus, a rational approach allowing the combination of thorough examination of the literature, the chemical composition, the structure and properties of inorganic materials, appears to be beneficial depending on the aimed application. Such strategies represent an elegant way to solve time loss and money. Moreover, they could be used both in fine chemistry and chemical industry.

Bearing this in mind, zeolites appear to be valuable candidates, thanks to their tunable properties. Indeed, zeolites are heterogeneous catalysts which can be three-dimensionally customized at a triple scale in terms of their molecular composition, microscopic level and macroscopic design, according to any targeted application.

From an industrial point of view, zeolites are important in many processes, ranging from adsorption and ion-exchange to catalysis. In value terms, catalysis represents by far the largest market for zeolites, approximately 55% of the total and promising high rates of market growth. Zeolites are the heterogeneous catalysts with the highest annual production. They are used in a large variety of acid-catalyzed reactions. The knowledge on zeolites obtained through the petrochemical applications allowed assessing the rich possibilities available for the design of zeolites as catalysts molecularly tailored to suit any desired application.

The work described in this Thesis aims in the design of zeolites at three levels: (i) acid site by playing on the acid strength and on the accessibility, (ii) microscopic scale by adapting the crystal size and (iii) reactor level by coating zeolite crystals on different supports (Figure 1).

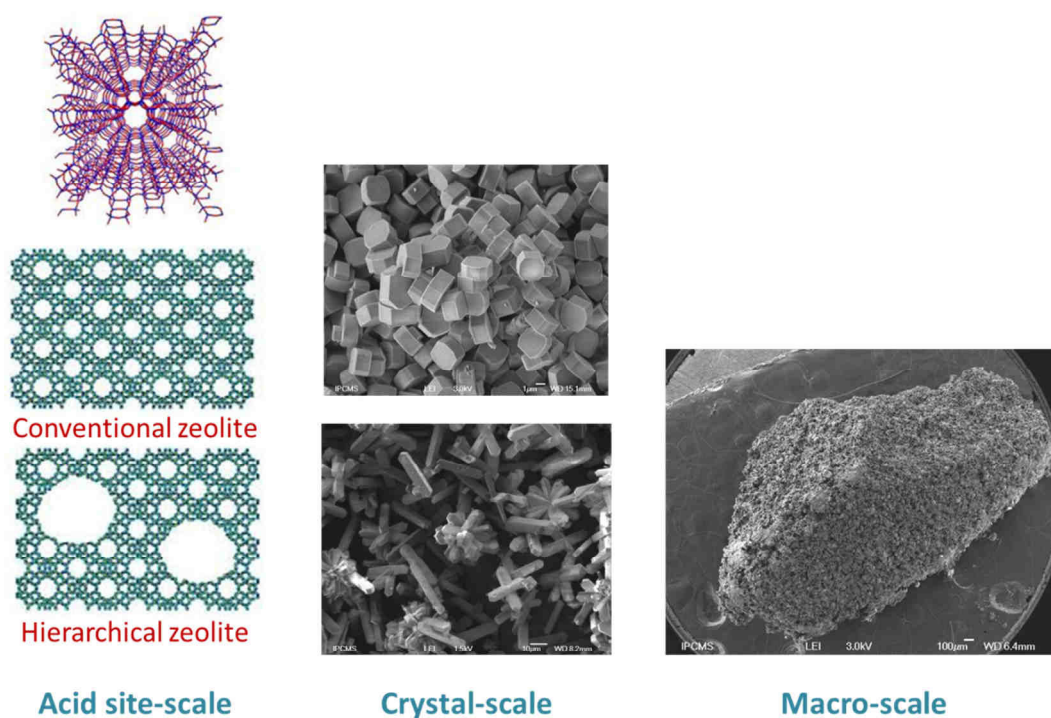


Figure 1 From the active site to... the reactor

Therefore, the second aspect addressed is the use of customized zeolites in acid-catalysis by selection of reactions, *i.e.*, the chlorination of aromatics and the conversion of methanol into light olefins (MTO).

Firstly, to achieve this goal, hierarchical zeolites have been prepared *via* several methods and thoroughly characterized. Top-down techniques, such as desilication and dealumination, as well as bottom-up methods like double templating, have been attempted. Besides optimization of individual treatments, an important focal point comprises the exploration of strategic sequences of treatments.

Several zeolite topologies were modified by pre- or post-synthesis methods according to the aimed reaction. For the MTO reaction, only the well-defined three-dimensional MFI structure of ZSM-5 is tested. Indeed, a special focus on the synthesis conditions *via* the fluoride-mediated route is given. On the other hand, the catalytic activities of hierarchical zeolites, *i.e.*, ZSM-5 and FAU type zeolites, were evaluated in the chlorination of aromatics. In addition, the evaluation of zeolite coatings as structured catalytic bed have been performed in the field of the MTO application.

Finally, it is hoped that their catalytic performances could be directly related to their intrinsic properties. In other words, the link between the catalytic activity and the zeolite structure (after modification) of the different catalysts was evaluated.

2. Outline of the Thesis

The Thesis consists of 6 chapters, starting with a literature background on zeolites and on chosen applications, ending with general conclusions and outlook.

Chapter 2 describes the experimental setups used for gas-phase reactions. Furthermore, this section also presents the different physico-chemical techniques employed to characterize the catalysts.

Chapter 3 describes the tailor-made syntheses of all zeolites, either for the chlorination of aromatics or for the MTO reactions. This part is divided in two sub-sections: (i) the preparation and characterization of hydrothermally synthesized zeolites, either in alkaline or fluoride medium and (ii) the design and characterization of hierarchical zeolites, either *via* the constructive or destructive methods.

Chapter 4 addresses the catalytic activities of ZSM-5 zeolites in the conversion of methanol into light olefins. The first section reports preliminary results obtained over four different ZSM-5 zeolites: a reference, mesoporous, nanocrystals and fluoride-mediated “giant” ZSM-5 crystals. The results show the highest catalytic performances of the crystals synthesized in the presence of fluoride anions. Hence, the second section focused on the preparation of ZSM-5 catalysts in fluoride media. The influence of several synthesis parameters, *i.e.*, silicon source nature, amount of alumina source, utilization of hydrofluoric or hydrochloric acid, was investigated in terms of zeolite crystal formation and activity in the MTO.

In chapter 5, the chlorination of deactivated aromatics in the presence of trichloroisocyanuric acid over zeolites is presented. Preliminary results were obtained under liquid phase conditions. This work has shown the efficiency of zeolites to activate TCCA to perform electrophilic aromatic substitution. Furthermore, a semi-continuous process has

been settled to render the chlorinations more environmental-friendly. H-USY and H-ZSM-5 zeolites were found to be the best candidates in terms of performances in nitro- and chlorobenzene chlorination, respectively. Finally, hierarchical zeolites have been tested in both halogenation reactions to determine the required catalyst properties for such reactions.

Chapter 6 reports the development of zeolite coatings on silicon-containing supports (glass monolith and silicon carbide). The design of zeolite coatings on SiC without the use of any additional silica source during the synthesis will be highlighted. In addition, the catalytic activity of ZSM-5 crystals coated on SiC was evaluated in the MTO reaction.

A general conclusion summarizes the most promising results and proposes interesting opportunities for the development of triple-scale designed zeolites.

3. Selected references

Chapter 4

- * Conversion of methanol into light olefins over ZSM-5 zeolite: Strategy to enhance propene selectivity, *Applied Catalysis A* 447–448, 178–185 (2012).
- * A general overview on the methanol to olefins reaction: recent catalyst developments, *Advanced Chemistry Letters* 1, 247–256 (2013).

Chapter 5

- * Green route for the chlorination of nitrobenzene, *Applied Catalysis A* 449, 1–8 (2012).
- * Electrophilic chlorination of Arenes with trichloroisocyanuric acid over acid zeolites, *Applied Catalysis A* 461, 46–51 (2013).

- * Gas-phase chlorination of aromatics over FAU- and EMT-type zeolites, *Catalysis Communications* 39, 10–13 (**2013**).
- * MFI-type zeolite nanosheets for gas-phase aromatics chlorination: a strategy to overcome mass transfer limitations, *RSC Advances* 4, 27242–27249 (**2014**).

Chapter 6

- * Binderless zeolite coatings on macroporous α -SiC foams, *Microporous Mesoporous Materials* 188, 99–107 (**2014**).

Chapter 1. LITERATURE BACKGROUND

ABSTRACT

The literature background of this Thesis is divided into two main sections:

- (i) the first presenting a smattering of zeolite chemistry, namely: generalities, structure, intrinsic properties, synthesis and growth mechanisms. Then, a brief focus is given for two topologies, *i.e.*, ZSM-5 and Y type zeolites. Finally, the design and applications of hierarchical porosity and structured catalytic beds are presented;
- (i) the second section is divided in two parts devoted to the discussion of zeolite applications. General points on halogenation processes, as well as the chlorinating agents used and a focus on the application of solid catalysts in chlorination reactions are presented. Afterwards, an overview on methanol conversion into hydrocarbons is given. The state of the art in terms of conditions, catalysts, mechanisms, various catalyst modifications and reactors is discussed.

Porous materials could be of different nature; those from mineral origin are highly used and of big interest in industry. Porous materials share the common feature of regular and uniform porous structures. To describe a porous structure, several parameters may be used and these include pore size and shape, channel dimensionality and direction, composition and features of channel walls, etc. Among these parameters, pore size and pore shape are the most important [1]. One may distinguish and classify according to their pore aperture and the IUPAC nomenclature as follows:

- * Microporous solids having aperture diameter less than 2 nm
- * Mesoporous solids having aperture diameter of 2-50 nm
- * Macroporous solids having aperture diameter larger than 50 nm

Within the frame of this Thesis, among the porous materials described above, we have decided to focus our attention on zeolites.

1. Zeolites

1.1 What are zeolites?

1.1.1. From natural to synthetic zeolites

In 1756 the Swedish mineralogist, Alex Fredrik Crønsted, discovered the first natural zeolite, named Stilbite (Figure 1.1), in basaltic rocks [2]. He observed that in contact with heat, this mineral rapidly released an important amount of water from its core giving the impression of boiling. Hence, he baptized this material as zeolite, from Greek “zein” (to boil) and “lithos” (stone), literally boiling stone. Natural zeolites are formed, after several million years, from volcanic ashes deposited in salted lake. A rapid crystallization occurred after hydrothermal transformation of volcanic glasses in the presence of high-pH saline groundwater. Natural zeolites are rarely pure and are contaminated in varying degrees by

[1] M. E. Davis, *Nature* **2002**, 417, 813–821.

[2] A. F. Cronsted, *Akad. Handl. Stockholm* **1756**, 18, 120–130.

other minerals, metals, quartz, or other zeolites. For this reason, naturally occurring zeolites are excluded from many important commercial applications where uniformity and purity are required. Thus, their principal use relies in geological museums, jewelry or construction materials.



Figure 1.1 Natural Stilbite zeolite

A significant breakthrough in the field of zeolites occurred in 1948 with the discovery of the first synthetic zeolite by R. M. Barrer, in similar crystal form than their natural counterparts [3]. In the late 1940s, R. M. Milton and co-workers successfully synthesized A, X and P zeolites by hydrothermal crystallization [4]. They tried to mimic the natural synthesis conditions; *i.e.*, high temperatures and salt concentrations under autogenous pressures. Since this first discovery, the family of zeolites grew up and counts more than 200 unique different zeolite structures identified, among 40 being natural zeolites. Today, The International Zeolite Association (IZA) database shows that the number of structural types of unique microporous frameworks has been growing rapidly, from 27 in 1970, to 64 in 1988 and to 133 in 2001, whereas in 2007, this number has reached 174. In fact, during the past half century, many microporous compounds containing diverse elements and primary building units have been synthesized thanks to the development of synthetic techniques [5].

[3] a) R. M. Barrer, *J. Chem. Soc.* **1948**, 127–132. b) R. M. Barrer, L. Hinds, E. A. White, *J. Chem. Soc.* **1953**, 1466–1475.

[4] R. M. Milton, *Molecular Sieve Adsorbents*, **1959**, US Patent, 2882243.

[5] C. Baerlocher, L. B. Mccusker, D. H. Olson, *Atlas of Zeolite Framework Types*, 6th Revised Edition, Elsevier B.V., **2007**.

1.1.2. Nomenclature and morphologies of zeolites

Zeolites are highly crystalline aluminosilicates belonging to the family of tectosilicates. One can define and characterize them by their three-dimensional porous structure arising from a framework of SiO_4^{4-} and AlO_4^{5-} tetrahedra (TO_4 where T represent Si or Al atom) linked together by all their corners (O atoms) as depicted in Figure 1.2.

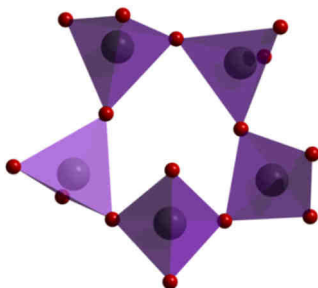
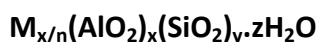


Figure 1.2 TO_4 tetrahedra connected together to create the 3D structure

The unit cell formula of zeolites is usually written as:



where M is the cation (alkali; *i.e.*, Na^+ , K^+ ... or alkaline earth metal; *i.e.*, Ca^{2+} , Ba^{2+} ...) which balances the negative charge associated with framework aluminum ions, n is the charge of the cation, x is the number of Al per formula unit, y is the number of Si, and z is the number water molecules in the channel system. The y/x ratio represents the Si/Al ratio, which is always larger than or equal to one, and can vary infinitely to obtain a purely siliceous material (silicalite). Silicon atoms being tetravalent, the mineral skeleton is electrically neutral. Whereas, insertion of trivalent Al atoms bonded to four shared oxygen anions introduces negative charges, which are compensated by cations (mono or divalent) inserted into channels or cavities to maintain electrical neutrality throughout the microporous structure. A direct linkage between two AlO_4 entities is strictly forbidden by the Loewenstein rule [6]. In addition, water molecules are present in the void volume of the cavities/channels.

Zeolites are characterized by their framework architecture which is described in terms of the pores' size and the dimensionality of the channel system. The 3D arrangement is sophisticated since tetrahedra assemble into repeating structural subunits, called Secondary

[6] W. Loewenstein, *Am. Mineral.* **1954**, 39, 92–96.

Building Units (SBU's). These SBU's include simple polyhedra which self-arrange together to form either an array of interconnecting channels or a system of cage-like voids. Figure 1.3 presents numerous structural features (cages, channels, chains and sheets) that are common to different zeolite framework types. There are 23 known SBU's which have been listed [5]. These SBU's only reflect the aluminosilicate skeleton (*i.e.*, the relative positions of Si, Al and O atoms in space) but exclude consideration of the compensation cation and water moieties present within the void cavities and channels.

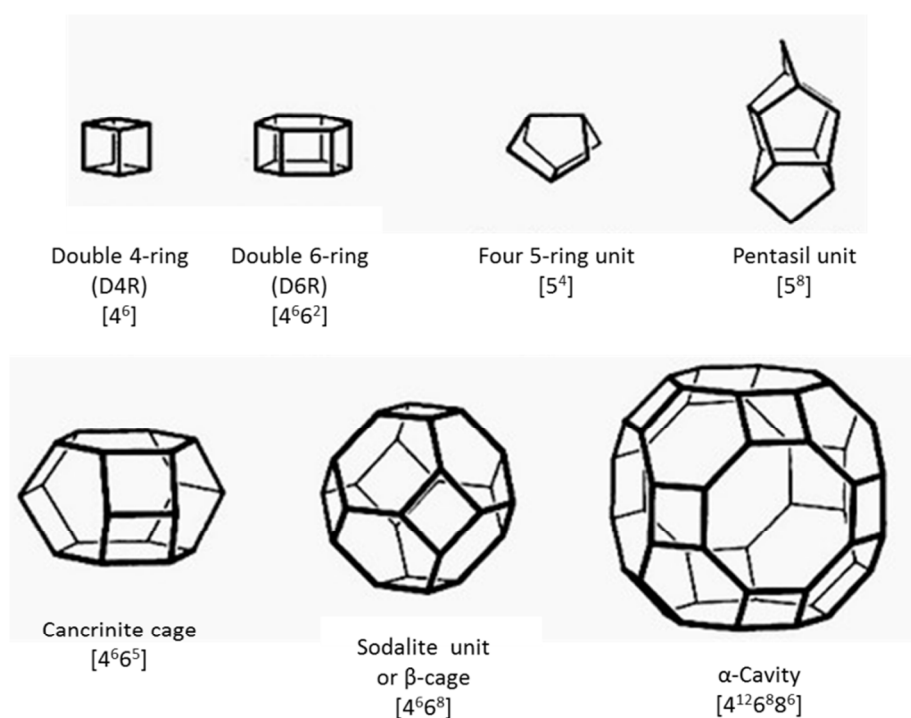


Figure 1.3 SBU's and cages often encountered in zeolite framework types

A global classification of zeolites has been adopted by the IZA including all known zeolite frameworks described by a combination of one or more SBU types. In addition, zeolites are named by a three letters code derived from their original names according to the rules set up by IUPAC Commission in 1979 [5,7].

The zeolite channels are characterized by the ring size forming the pore. The opening size is defined by the number of T-atoms in the ring, called n -membered ring (n -MR). Thus, zeolites can be classified according to their pore size:

[7] IUPAC Physical Chemistry Division, *Pure Appl. Chem.* **1979**, 51, 1091–1100.

- * Small pore zeolites: 8-MR with a diameter of about 4 Å such as LTA, SOD and GIS
- * Medium pore zeolites: 10-MR having a pore diameter of approximately 5.5 Å like MFI
- * Large pore zeolites: 12-MR with diameter of about 7.5 Å such as FAU, MOR and BEA
- * Extra-large pores zeolites: > 12-MR having pore diameter larger than 8 Å

At present, only three silicate/germanosilicate zeolites with pores larger than 18-MR have been synthesized: ITQ-37 (30-MR, ~26 Å) [8], ITQ-43 (28-MR, ~22 Å) [9] and PKU-12 (20-MR, ~13 Å) [10].

All these specific structural peculiarities, namely the structure in channels and cages (in 1, 2 or 3 dimensions), but also the Si/Al ratio of the skeleton and the presence of mobile cations in the void volume, are responsible for the interesting physico-chemical properties exhibited by zeolite materials.

1.2 Zeolite properties and applications

Among inorganic oxides, zeolites are rather special, and exhibit a number of specific properties. Indeed, the high surface area (> 300 m²/g) and high thermal stability of zeolites make them promising materials for a wide range of applications. However, their main features can be classified into three groups: ion-exchange properties, adsorption and heterogeneous catalysis [11].

[8] J. Sun, C. Bonneau, A. Cantín, A. Corma, M. J. Díaz-Cabañas, M. Moliner, D. Zhang, M. Li, X. Zou, *Nature* **2009**, *458*, 1154–1157.

[9] J. Jiang, J. L. Jorda, J. Yu, L. a Baumes, E. Mugnaioli, M. J. Diaz-Cabanias, U. Kolb, A. Corma, *Science* **2011**, *333*, 1131–1134.

[10] J. Su, Y. Wang, J. Lin, J. Liang, J. Sun, X. Zou, *Dalton Trans.* **2013**, *42*, 1360–1363.

[11] a) A. Dyer, *An Introduction to Zeolite Molecular Sieves*, John Wiley & Sons, New York, **1988**. b) A. Corma, H. Garcia, *Catal. Today* **1997**, *38*, 257–308. c) A. Corma, *Chem. Rev.* **1995**, *95*, 559–614. d) H. Ghobarkar, O. Schäf, U. Guth, *Prog. Solid State Chem.* **1999**, *27*, 29–73. e) L. B. Mccusker, C. Baerlocher, in *Introduction to Zeolite Molecular Sieves, 3rd Revised Ed.* (Eds.: J. Cejka, H. van Bekkum, A. Corma, F. Schüth), Elsevier B.V., Amsterdam, The Netherlands, **2007**, pp. 13–37. f) J. Weitkamp, *Solid State Ionics* **2000**, *131*, 175–188.

1.2.1. Ion-exchange properties and separation

The compensation cations present in zeolite void channels and cages are loosely bonded to the zeolite framework. Hence, they can be easily exchanged with other cations in aqueous solution. This exchange ability is defined by the amount of cations present in the void volume. This amount is directly linked to the Si/Al ratio. Indeed, the more zeolite is rich in aluminum, the higher its exchange capacity is. Hence, these ion-exchange properties can be tailored to specific tasks. Zeolites are often used as water softener (mainly Na-LTA), where alkali metals such as sodium or potassium prefer to exchange out of the zeolite, being replaced by the "hard" calcium and magnesium ions from the water. Thus, one can find substantial amounts of zeolites in many commercial washing powders and soaps (up to 30 wt.%) [11d]. In this field, zeolites have effectively replaced phosphates, such as sodium tripolyphosphate, in detergent builders, which are responsible for the eutrophication of surface water bodies. It is even possible to remove radioactive isotopes from contaminated water and soils, as demonstrated after nuclear accidents at Chernobyl and Fukushima by $^{137}\text{Cs}^+$ -trapping. In addition, this cationic exchange ability has been recently used to design heterogeneous catalyst for fine chemistry. Many papers deal with metal-doped zeolites for organic catalysis [12].

1.2.2. Adsorption and separation

The shape-selective properties of zeolites, thanks to their porous structure, are also the basis for their use in molecular adsorption. The ability to adsorb preferentially certain molecules, while excluding others, has opened up a wide range of molecular sieving applications. The first use of zeolite as adsorbents began in the 1955-1959 period in dry and purification of refrigerated and natural gases [13]. Later, zeolites have been used in a variety of adsorption and separation processes such as the drying, the removal of CO_2 from air and natural gas, the desulfurization of natural gas, and the separation of xylene isomers, alkenes,

[12] a) D. E. De Vos, M. Dams, B. F. Sels, P. A. Jacobs, *Chem. Rev.* **2002**, *102*, 3615–3640. b) P. Kuhn, P. Pale, J. Sommer, B. Louis, *J. Phys. Chem. C* **2009**, *113*, 2903–2910. c) A. Olmos, S. Rigolet, B. Louis, P. Pale, *J. Phys. Chem. C* **2012**, *116*, 13661–13670.

[13] J. J. McKetta, Ed., *Petroleum Processing Handbook*, Marcel Dekker, Inc., New York, **1992**.

and O₂/N₂ from air. The adsorption properties are directly linked to dipolar interactions between the zeolite framework and molecules having adequate size to diffuse within the zeolite pores. These applications strongly depend on the shape and size aperture of pores, the compensation cation nature and on the hydrophobic/hydrophilic character of the zeolite framework. One can easily modify this character by varying the Si/Al ratio, *i.e.* zeolites with high Si/Al ratio are more hydrophobic and allow higher selectivity toward organic molecules. In contrast, hydrophilic zeolites exhibiting low Si/Al ratio, facilitate the adsorption of water molecules. Thus, zeolites can separate molecules based on differences in size, shape and polarity.

1.2.3. Heterogeneous catalysis

The most interesting application and also the one with higher added value of zeolites is undoubtedly heterogeneous catalysis. The exceptional performance of zeolites in catalyzed reactions stems from their strong acidity and uniformly-sized micropores [14]. These assets enable to catalyze a wide variety of chemical transformations, while yielding narrow product distributions.

1.2.3.1. Shape selectivity

Analogously to enzymes, zeolites with their regular well-defined pore dimensions are able to discriminate reactants and products by size and shape when they present significant differences in diffusivity through a given pore channel system [15]. Indeed, the zeolite pores have dimensions in the same range of molecules which interact with the zeolite surface. This phenomenon, called shape selectivity, leads to unique effects in catalysis. Indeed, the product distribution of a wide range of chemical reactions can deviate from the thermodynamical distribution if the formation of the molecules is inhibited by the

[14] E. M. Flanigen, R. W. Broach, S. T. Wilson, in *Zeolites in Industrial Separation and Catalysis* (Ed.: S. Kulprathipanja), Wiley-VCH Verlag GmbH & Co. KGaA, Weinheim, Germany, **2010**, pp. 1–26.

[15] J. Weitkamp, *Solid State Ionics* **2000**, *131*, 175–188.

constraints imposed by the pores. One can distinguish three types of shape selectivity, as shown in Figure 1.4.

- * **Reactant shape selectivity:** molecules too large to enter the zeolite pore cannot reach internal active acid sites to perform the reaction and are therefore not converted into products. Thus, the less bulky molecules will react preferentially with respect to larger reactants which are hindered to diffuse inside the zeolite channels. Clearly, this type of selectivity depends on the geometry at the entrance of the pore and on the intra-pore diffusional characteristics of the reacting molecules. Relevant examples are the selective cracking of n-olefins and n-paraffins with respect to their branched-isomers in small pore zeolites [16].
- * **Product shape selectivity:** products formed in parallel or consecutively in the zeolite intersections (cages) have different molecular dimensions and only the product with dimension in the range of the zeolite pore openings can diffuse outside the molecular sieve. For example, the selective toluene disproportionation over ZSM-5 zeolite produces high selectivities in *para*-xylene [17].
- * **Transition state shape selectivity:** when the catalytic reaction occurs inside the zeolite pores, the effective diameter of the channels or the intersections can impose steric constraints to the transition state and thus strongly inhibit the formation of bulky transition states or reaction intermediates. In favorable cases, these states are completely suppressed and the zeolite architecture selects the preferred reaction pathway by favoring only certain configurations. The inhibition of coke formation and the cracking of paraffins within the MFI-type zeolite are well-known examples for this kind of shape selectivity [18].

[16] A. Corma, *J. Catal.* **2003**, *216*, 298–312.

[17] a) M. A. Abdal Kareem, S. Chand, I. M. Mishra, *J. Sci. Ind. Res.* **2001**, *60*, 319–327. b) I. Fecheté, Y. Wang, J. C. Védrine, *Catal. Today* **2012**, *189*, 2–27.

[18] J. S. Buchanan, *Catal. Today* **2000**, *55*, 207–212.

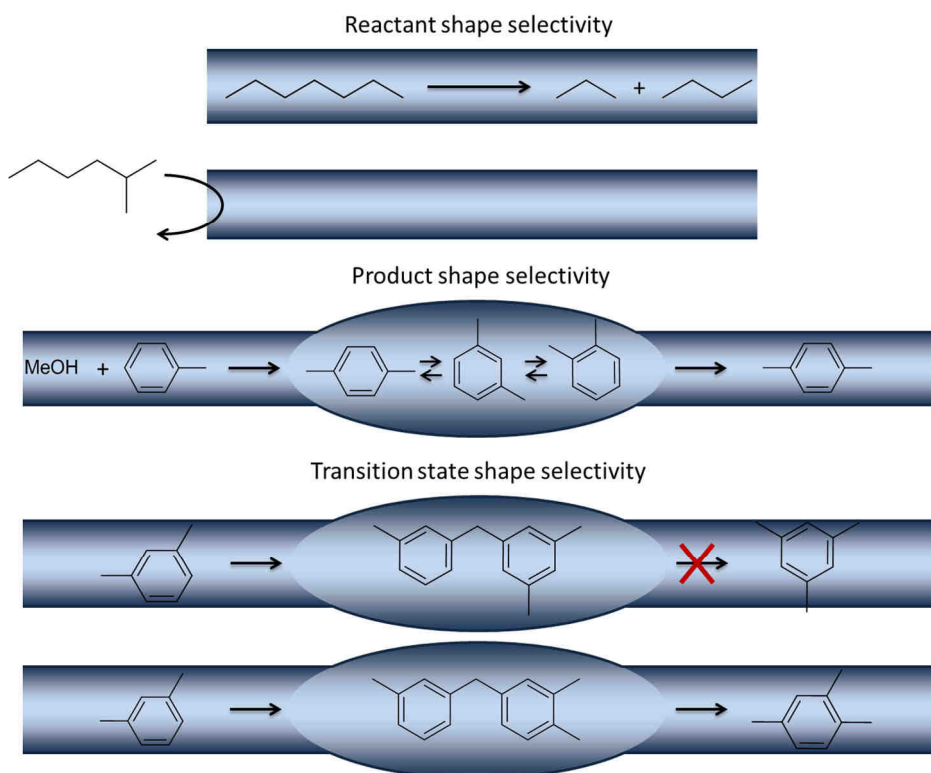


Figure 1.4 Different types of shape selectivity

Consideration of these three different effects underlying shape selectivity can give precious hints regarding molecules likely to form. But for more reliable (ideally quantitative) predictions, we also need to take into account thermodynamic effects [19]. Moreover, other theories based on shape selectivity are still debated such as inverse shape selectivity, molecular traffic control, pore mouth and key-lock shape selectivity, the “Window Effect,” and the “Nest Effect” [20].

1.2.3.2. Acidity

An important class of reactions is catalyzed by protonic zeolites, whose framework protons give rise to high acidity. However, the determination of zeolite absolute acidity and strength remains complicated and requires a huge variety of characterization tools. For more

[19] B. Smit, T. L. M. Maesen, *Nature* **2008**, 451, 671–678.

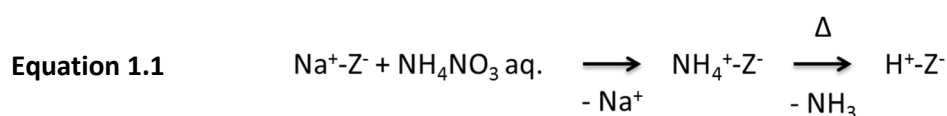
[20] T. F. Degnan, *J. Catal.* **2003**, 216, 32–46.

clarity, it is recommended to distinguish the chemical nature of the acid sites (Brønsted vs. Lewis), the density of these sites, their strength and their location in the solid acid.

Nature and location of the acid sites

The zeolite acid properties are directly related to the aluminum content of the zeolite skeleton. Two types of acid sites are identified in zeolite: Brønsted acid sites and Lewis acid sites.

Brønsted acid sites are generated by the ionic exchange of the metallic cation (present in the zeolite channels and cages to compensate the negative charge on the Al tetrahedra) with ammonium molecules (NH_4^+). The typical procedure to generate Brønsted acid sites (Equation 1.1) relies in aqueous cationic exchange, typically using NH_4NO_3 solution, followed by a calcination step at 550 °C.



Bridging hydroxyls groups (Si-OH-Al) formed by a proton and a framework oxygen in a AlO_4 tetrahedron are depicted in Figure 1.5. They exhibit the highest strength among existing hydroxyl groups. At the outer surface of zeolite crystals or in framework defects, one can find another type of hydroxyl groups, the silanol groups (SiOH) also called terminal OH groups. Their acid strength, comparable to the acidity of silica, is low. The formation of rather framework defects and silanol groups appears during dealumination processes such as calcination, hydrothermal treatment or treatment with strong acids. Depending on dealumination conditions, partial curing of the lattice may occur by silicon migration and reinsertion, formation of silanol groups or hydroxyls formation associated with extra-framework aluminum (EFAI) species.

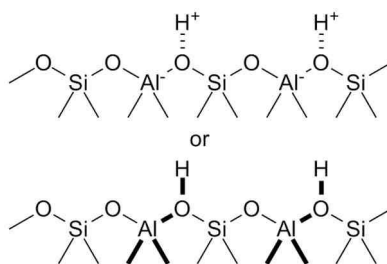


Figure 1.5 Brønsted acid site

Upon severe thermal treatment ($> 500\text{ }^{\circ}\text{C}$), these hydroxyl groups are more or less affected and can be degraded by dehydroxylation. Some of these groups with water are removed from the framework and subsequently Lewis acid sites are generated (Figure 1.6). The exact structure/nature of these acid species is still unclear but they were looked upon as tricoordinated aluminum and silicon species in the framework [15]. These sites are quite unstable, especially in the contact of vapour, therefore, an annealing reaction appends which stabilizes the framework. Thus, the removal/ejection of aluminum species allows to encounter this effect and create new Lewis acid sites, the EFAl species. The formation and the nature of EFAl species is tentatively given in a later Section .

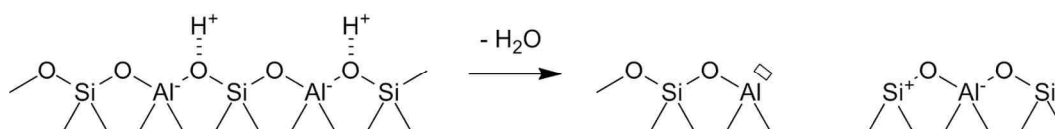


Figure 1.6 Formation of Lewis acid sites

Density and strength of the acid sites

Obviously, the density of acid sites is directly related to the framework aluminum content. The Si/Al ratio gives us important information regarding the relative acidity of the zeolite.

The Si-O-Al bond angle, which depends on the zeolite type, affects the partial charge and the acid strength of the hydroxyl protons [21]. For example, in ZSM-5 zeolite, the Si-O-Al bond angles vary between 137° and 177° with respect to Y zeolite which exhibits bond angles ranging from 138° to 147° .

In addition to the above-mentioned local effects, the global composition of the zeolite skeleton influences the acid strength of the zeolite. Indeed, the distribution of aluminum atoms in the zeolite framework has a great impact on acid strength. This effect is related to the global electronegativity of the framework (silicon atoms possess a higher electronegativity with respect to aluminum atoms), defined by Sanderson [21]. Generally, an increase in the electronegativity, thus a decrease in the Al content, leads to a stronger acid strength in the zeolite. In addition, the next nearest neighbors (NNN) theory relies on this

[21] M. Hunger, in *Zeolites and Catalysis Synthesis, Reactions and Applications* (Eds.: J. Čejka, A. Corma, S. Zones), Wiley-VCH Verlag GmbH & Co. KGaA, Weinheim, Germany, **2010**, pp. 493–546.

basis. The NNN concept takes into account the T-atoms in the coordination sphere of Al atom. For instance, in FAU-type zeolites each framework aluminum atom is linked to four silicon atoms *via* oxygen bridges. These four silicon atoms are further connected to nine T-atoms in the next coordination sphere, which are called NNN [5]. Hence, the acid strength of the zeolite can be determined according to the number of Al atoms present on NNN positions. The lower these aluminum atoms are, the higher the acid strength is. FAU zeolites are characterized by a 9-NNN configuration (Si/Al ratio ≈ 1) leading to the lowest acid strength. A 0-NNN configuration, being a completely isolated AlO_4 tetrahedron (Si/Al ratio $\gg 11$), allows the higher acid strength [22].

Various techniques and methods are usually employed to measure the intrinsic acidity of zeolites. Calorimetric methods measuring the heat of adsorption of nitrogen-containing bases are probably the most reliable to measure the strength of a solid acid, but it requires very experienced specialists [23]. In contrast, semi-quantitative data could be obtained by IR spectroscopy with probe molecules (for example, CO, NH_3 , pyridine), temperature-programmed desorption (TPD) of bases, NMR spectroscopy and titration methods. Combination of these techniques may offer a more complete and sound result.

1.2.3.3. Confinement effect

The description of zeolites as solid solvent was first introduced in 1979 by D. Barthomeuf [24]. Her studies pointed out the influence of electric field gradient due to the aluminum and cation distribution. In the late 80s, Derouane elaborated a new concept in zeolite abilities, the so-called confinement [25]. He originally proposed this effect as the “Nest effect” [25a]. Besides the molecular shape selectivities, confinement effects stem from longer range and attractive interactions, *i.e.*, van der Waals forces, which are of

[22] L. A. Pine, P. J. Maher, W. A. Wachter, *J. Catal.* **1984**, *85*, 466–476.

[23] a) A. Auroux, V. Bolis, P. Wierzchowski, P. Gravelle, J. C. Védrine, *J. Chem. Soc. Faraday Trans.* **1978**, *75*, 2544–2555. b) J. C. Védrine, A. Auroux, V. Bolis, P. Dejaifve, C. Naccache, P. Wierzchowski, E. G. Derouane, J. B. Nagy, J. Gilson, J. H. C. van Hooff, et al., *J. Catal.* **1979**, *59*, 248–262.

[24] D. Barthomeuf, *J. Phys. Chem.* **1979**, *83*, 249–256.

[25] a) E. G. Derouane, *J. Catal.* **1986**, *100*, 541–544. b) E. G. Derouane, J. Andre, A. A. Lucas, *Chem. Phys. Lett.* **1987**, *137*, 336–340.

supramolecular nature. Indeed, this effect is based on non-covalent interactions between the framework and molecules located in the zeolite void volume. One can distinguish two different forces responsible for this phenomenon; *i.e.*, the repulsive Pauli interaction in the short range and the attractive van der Waals force in the long range. These remarkable properties arise from the surface curvature of the internal surface of zeolites (internal pores and cages, and external “pockets”) [26]. These effects are responsible for the shape selectivity, selective adsorption and enhanced diffusivity. Hence, Derouane assimilated zeolites to solid solvents [26c].

Molecules occupying the intracrystalline volume of molecular sieves are known to be in strong interaction with their environment. Derouane suggested first in his “nest effect” that special activity and selectivity of different zeolites in cracking of n-pentane are associated with the zeolite pores. According to van der Waals forces, molecules present inside zeolite pores, tend to adopt the best conformation in terms of shape, size and electronic structure. By this way, molecules will reach minimum energy points on the sorbate-zeolite van der Waals potential surface, which in turn will affect the final activity and selectivity [25a]. Smallest molecules accommodate first to the smallest pores. Moreover, reactants can be differently polarized depending on the cage type. These induced dipoles and multipoles within some C-C bonds will weaken or strengthen these bonds and induce different cracking mechanisms [27]. Recently, Lercher *et al.* highlighted the importance of the zeolite structure in n-pentane cracking [28].

Furthermore, Derouane exposed another concept related to confinement, called “Floating molecule” [26b]. This concept describes the interactions between the relative size of adsorbed molecules and van der Waals forces. The extreme cases correspond to (floating molecules) a flat surface and molecules with almost the same size than the pore opening. In the latter case, Derouane and co-workers found that the molecules achieve a state of supermobility, which is induced by the absence of van der Waals interactions (causes adsorption) by an equal opposite repulsive force. In other words, when the size of sorbate

[26] a) E. G. Derouane, *Chem. Phys. Lett.* **1987**, *142*, 200–204. b) E. G. Derouane, J.-M. Andre, A. A. Lucas, *J. Catal.* **1988**, *110*, 58–73. c) E. G. Derouane, *J. Mol. Catal. A* **1998**, *134*, 29–45.

[27] G. Sastre, A. Corma, *J. Mol. Catal. A* **2009**, *305*, 3–7.

[28] S. Schallmoser, T. Ikuno, M. F. Wagenhofer, R. Kolvenbach, G. L. Haller, M. Sanchez-Sanchez, J. A. Lercher, *J. Catal.* **2014**, *316*, 93–102.

matches the pore aperture, the channel will behave as a guide for the direction of the global diffusion and the probability of perpendicular motions becomes negligible.

Finally, one can cite another remarkable positive result of confinement on the diffusion properties inside zeolite pores. Indeed, Derouane suggested that preferentially large molecules may keep a certain distance between themselves and pore walls, by finding the optimal positions of their atoms, to reach the minimum attractive van der Waals energy. Thus, only when a significant number of atoms simultaneously present a minimal energy toward the pore area, they will have a collective short jump and molecules will translate through the channel following the so-called “Creep motion”.

All these above-mentioned concepts can act separately or in addition to acid strength. Hence, the interpretation of zeolite catalytic performances, in given reactions, could be complicated.

1.2.4. Zeolites in industrial applications

Thanks to all these features, naturally and synthetic occurring zeolites form an important group of minerals for industrial purposes [29]. Among the 200 existing zeolite structures, nearly 17 are currently used in industry and all produced synthetically, *i.e.*, AEL, AFI, BEA, CHA, EDI, FAU, FER, GIS, LTA, LTL, MER, MFI, MOR, MTT, MWW, TON and RHO [11e].

Besides first applications in separation and purification, the development of synthetic zeolites led an annual market for these materials to grow immensely. Nowadays, worldwide consumption of zeolites (natural and synthetic) is estimated to be nearly 5 million metric tons per years [30]. The consumption of synthetic zeolites represents only 36% of the total zeolite consumption. Conventional applications can be separated in three major groups: detergents, adsorbents and catalysis. The biggest market for synthetic zeolites relies in laundry detergents with 73% of total consumption (Figure 1.7). However, the use of zeolites in catalyzed reactions represents the highest value.

[29] F. R. Ribeiro, A. E. Rodrigues, L. D. Rollmann, C. Naccache, Eds., *Zeolites: Science and Technology*, Martinus Nijhoff Publishers, The Hague, **1984**.

[30] B. Yilmaz, N. Trukhan, U. Müller, *Chinese J. Catal.* **2012**, *33*, 3–10.

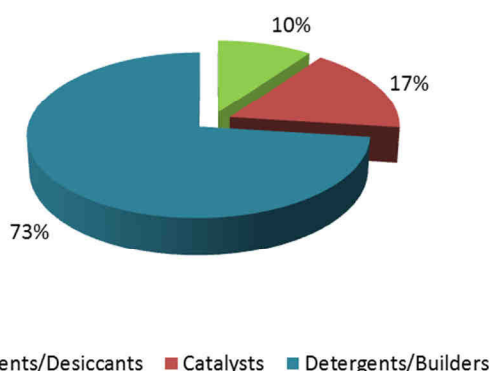


Figure 1.7 Global consumption of synthetic zeolites

The low-priced natural zeolites are typically applied in bulk industry as construction, agriculture and water/waste treatment. Whereas, synthetic zeolites, being more valuable due to their production cost, find applications as detergents builders, catalysts and adsorbents/desiccants [14,31]. Nowadays, zeolites are used in more than 70 industrial processes in oil refining, petrochemistry, and fine chemical industries [32]. Among those applications, FCC reaction accounts for about 95% of synthetic zeolite consumption [33].

According to Marcilly's proposal, there will be several new application fields in petroleum refining and petrochemical industries in next 20 years [34].

1.3 Zeolite synthesis

In this Thesis studies, different synthesis routes for preparing zeolites have been followed, in particular in alkaline and fluoride medium.

Since the earliest reports of Barrer, hundreds of patents and many papers have been published in this field and scientific researches will continue to develop new zeolite potentialities [35]. Zeolites are prepared *via* sol-gel hydrothermal synthesis under auto-

[31] F. A. Mumpton, *Proc. Natl. Acad. Sci. USA* **1999**, 96, 3463–3470.

[32] K. Tanabe, W. F. Hölderich, *Appl. Catal. A* **1999**, 181, 399–434.

[33] W. Vermeiren, J.-P. Gilson, *Top. Catal.* **2009**, 52, 1131–1161.

[34] C. Marcilly, *Stud. Surf. Sci. Catal.* **2001**, 135, 37–60.

[35] C. S. Cundy, P. A. Cox, *Microporous Mesoporous Mater.* **2005**, 82, 1–78.

genous pressure in a temperature range between room temperature up to 300 °C. The zeolite gel generally requires:

- * Reactants/sources of T atoms (Si and Al) forming the zeolitic skeleton
- * An organic (TPA^+ , TEA^+) or alkaline (Na^+ , K^+) template/structure-directing agent (SDA)
- * A mineralizer (OH^- or F^- anions)
- * Solvent (mainly water)

The starting point in zeolite synthesis is crystallization from inhomogeneous gel, called hydrogel, formed by silica and alumina sources combined to water under high pH (generated by the mineralizer) *via* a supersaturated solution (Figure 1.8) [36]. Roles of temperature, pressure, time, ageing, are not fully understood yet.

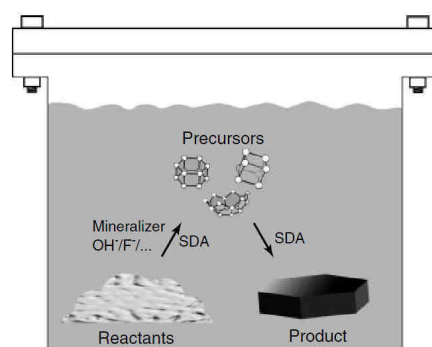


Figure 1.8 Schematic representation of zeolite formation process [36]

1.3.1. Components for zeolite synthesis

Si and Al sources

The nature of the silica source is a key parameter, as its dissolution may favor the crystallization of a particular zeolite type. Silica sources are mostly used in the form of colloidal suspension of acid silica, fumed silica, pyrogenic silica or silicon alkoxides; *i.e.*,

[36] C. E. A. Kirschhock, E. J. P. Feijen, P. A. Jacobs, J. A. Martens, in *Handbook of Heterogenous Catalysis, Volume 1* (Eds.: G. Ertl, H. Knözinger, F. Schüth, J. Weitkamp), **2008**, pp. 160–178.

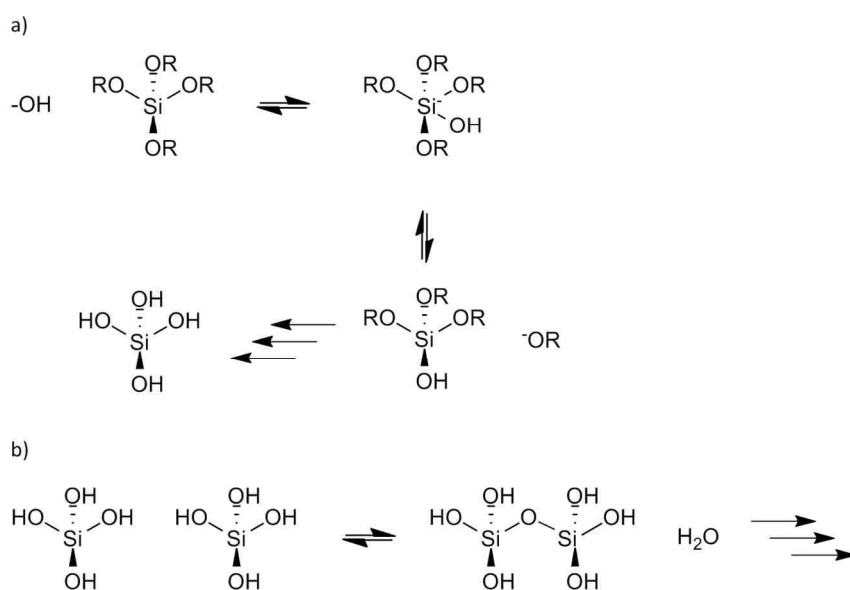
tetraethyl- or methyl-orthosilicate (TEOS and TMOS, respectively). The sole difference between these sources relies in the degree of polymerization of the silicate [37].

The aluminum source is not so crucial, and most of the laboratories are using aluminate salts, aluminum alkoxides or aluminum metal powder. Zeolite formation is enhanced by the presence of $[\text{Al}(\text{OH})_4]^-$ moieties at $\text{pH} > 10$.

Mineralizing agent

Zeolite syntheses are performed under alkaline conditions, mainly at pH between 9 and 13. The role of the mineralizers; *i.e.*, OH^- or F^- anions, are crucial in the catalytic crystallization of inorganic sources. Thus, the role of the mineralizer is to solubilize and/or depolymerize the alumino-silicate species at an appropriate rate.

The solubilization reaction, catalyzed by OH^- anions, proceeds *via* two steps: (i) the hydrolysis of the silica source and (ii) the silanol condensation, as shown in Scheme 1.1.



Scheme 1.1 Scheme of the mechanisms involving the mineralizer OH^-

The first step consists in a nucleophilic $\text{S}_{\text{N}}2$ mechanism (Scheme 1.1a), *via* the OH^- attack. This reaction is followed by a condensation step providing the reversible T-O-T structure (Scheme 1.1b), which occurs *via* an attack of a nucleophilic deprotonated (in

[37] J. Yu, in *Introduction to Zeolite Molecular Sieves, 3rd Revised Ed.* (Eds.: J. Cejka, H. van Bekkum, A. Corma, F. Schüth), Elsevier B.V., **2007**, pp. 39–104.

alkaline media) silanol group on a neutral species [36]. These steps form the basis of the microporous framework. In contrast, once solubilized, aluminum tetrahedron ($[\text{Al}(\text{OH})_4]^-$) stays in its monomeric form, the Al-OH function being hardly ionized. Furthermore, the alkalinity of the zeolite gel has an impact on final Si/Al ratio. The average Si/Al ratio in the zeolite shows a tendency to decrease with increasing pH of the hydrogel.

During the polymerization process, a network made of aluminosilicate species is formed. Under the influence of OH^- anions and SDAs (alkaline or organic) and mainly when the OH^- concentration increases, the condensation abilities of silicate species vanish; *i.e.*, SiO^-/SiOH ratio increase. In contrast, the condensation of aluminate species remains constant. Consequently, aluminum-rich zeolites are forming at high pH values with respect to silicon-rich zeolites (low pH). In addition, at high concentration of OH^- anions, framework defects as SiOH are preferentially formed.

Hydrothermal synthesis of microporous solids in the presence of fluoride anions allows their crystallization under nearly neutral or acidic conditions. The addition of F^- anions in the zeolite gel was first introduced by E. M. Flanigen and R. L. Patton in the late 70s to prepare an all-silica MFI zeolite [38]. Subsequently, J. L. Guth and H. Kessler systematically studied this field and developed this fluoride-mediated approach [39]. During their investigations, they observed for each new fluoride-mediated zeolite the formation of unusually large crystals with few lattice defects.

Compared with the hydrogel formed in the presence of OH^- anions, the presence of fluoride anions leads to a mixture in the form of a slurry with a viscosity depending on the nature of the SDA and the amount of water [40]. Furthermore, materials prepared in fluoride medium exhibit a low density of silanols groups. This can be attributed to a combination of several factors such as low pH conditions and charge balance between F^- and SDA^+ moieties. Corma *et al.* have found that in the presence of F^- anions, defect formation was pH-dependent and there was a threshold pH for the generation of constant defect amount.

[38] E. M. Flanigen, R. L. Patton, **1978**, US Patent 4073865.

[39] J. L. Guth, H. Kessler, J. M. Higel, J. M. Lamblin, J. Patarin, A. Seive, J. M. Chezeau, R. Wey, *ACS Symp. Ser.* **1989**, 398, 176–195.

[40] a) M. A. Cambor, L. A. Villaescusa, *Top. Catal.* **1999**, 9, 59–76. b) P. A. Barrett, M. A. Cambor, A. Corma, R. H. Jones, L. A. Villaescusa, *J. Phys. Chem. B* **1998**, 102, 4147–4155.

Structure-directing agent (SDA)

Templates are crucial molecules, which contribute to the formation of the crystalline solid. They have an impact on different crystallization steps, *i.e.*, gelation, precursor formation, nucleation and crystal growth processes. The incorporation of templates in the zeolite micropores allows the stabilization of the structure by different interactions; *i.e.*, hydrogen bonding, van der Waals and electrostatic interactions. SDAs play a fundamental role in the organization of oxide tetrahedra in specific topology around themselves through geometrical factors (size and form) [37]. Figure 1.9 shows a mechanism of auto-assembly that occurs through the aforementioned interactions between the hydrophobic silicate species and the template [36,41].

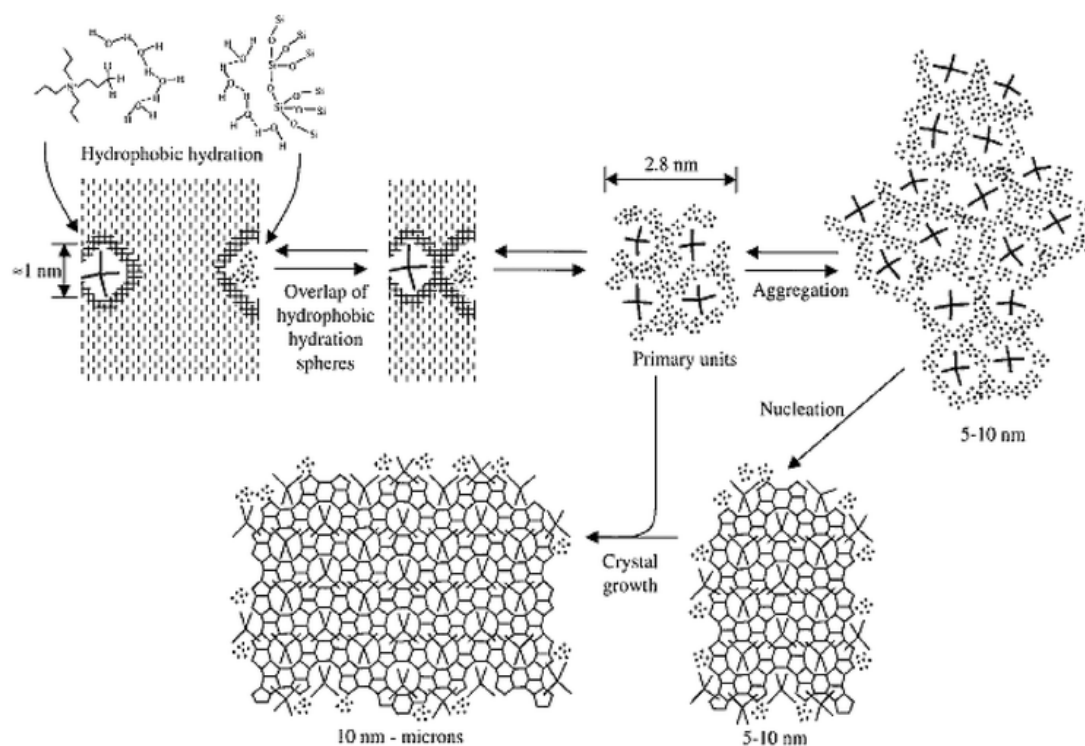


Figure 1.9 Schematic representation of the crystallization mechanisms involved in MFI synthesis (SDA = TPA⁺) [42]

The driving force of the process is the replacement of water molecules by Si and Al moieties around the organic/alkaline cation. The nature and the type of the template have

[41] X. S. Zhao, F. Su, Q. Yan, W. Guo, X. Y. Bao, L. Lv, Z. Zhou, *J. Mater. Chem.* **2006**, *16*, 637–648.

[42] P.-P. E. A. De Moor, T. P. M. Beelen, B. U. Komanschek, L. W. Beck, P. Wagner, M. E. Davis, R. A. Van Santen, *Chem. Eur. J.* **1999**, *5*, 2083–2088.

to be properly chosen depending on desired zeolite topology. After the synthesis, templates are trapped inside the microporous structure. Their removal has to be performed without alteration of the zeolite framework. Simple calcination step for organic cations or cationic exchange for inorganic cations is generally required. The extraction of template can be performed with solvents to avoid structure destruction or even recycle expensive templates.

1.3.2. Key parameters governing zeolite growth

The formation of zeolites depends on the combination of different variables such as molar composition, temperature, duration, template nature and amount, ageing and pressure. First of all, the composition is one of the most important factors determining the outcome of the crystallization. Reaction mixtures are a combination of appropriate sources to achieve required Si/Al zeolite composition. Likewise, the choice of the template is crucial to obtain the targeted zeolite structure. The chemical composition of a zeolite is usually expressed as molar ratios of oxides: $a \text{ SiO}_2 : b \text{ Al}_2\text{O}_3 : c \text{ M}_x\text{O} : d \text{ T} : e \text{ H}_2\text{O}$, where M represent alkali metal anions and T the organic template, while $a-e$ are molar ratios. Each zeolite possesses its specific compositional range, which can be either broad or extremely narrow [36]. The ratios of $\text{H}_2\text{O}/\text{SiO}_2$, OH^-/SiO_2 , $\text{SiO}_2/\text{Al}_2\text{O}_3$ and SiO_2/T are key values to give information on the concentration, solubility and the zeolite type and thus characterize the zeolite growth process. These crystallization parameters are usually represented in the form of ternary diagrams [43].

Moreover, the synthesis temperature has an influence on the zeolite crystallization. Usual crystallization temperature is ranging from room temperature to 200 °C and the syntheses are performed in sealed vessels where the pressure is autogenously generated by the vapor phase at high temperatures. Temperature could have an impact on the final nature of the crystallized zeolite phase. Thus, a raise in temperature provides denser phases, since under hydrothermal synthesis the fraction of water in the liquid phase decreases.

In general, the crystallinity increases with time. The time is a key parameter which can act in two ways: (i) an induction period during which the mixture is held at ambient temperature (ageing); (ii) since zeolites are thermodynamically metastable phases, zeolite

[43] A. Erdem, L. B. Sand, *J. Catal.* **1979**, *60*, 241–256.

crystallization is governed by the occurrence of successive phase transformations depending on time. The latter is known as the Ostwald's law. The thermodynamically least favorable phase crystallizes first, and is successively replaced by more stable and often denser phases [36,44].

The proper combination of all these parameters is not trivial [45]. Figure 1.10 shows typical phase transition diagram for a given gel composition at different temperatures.

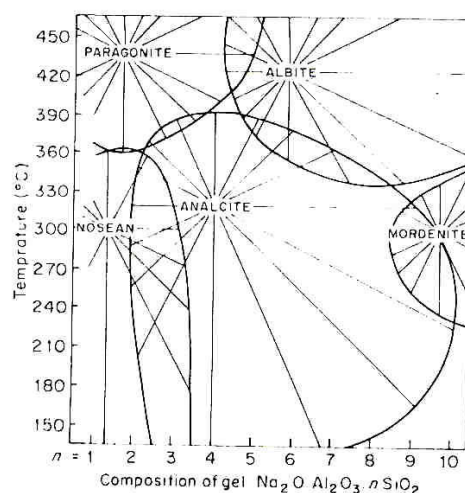


Figure 1.10 Typical zeolite crystallization field showing the phases formed at different reaction temperature from a sole gel composition [11a]

Furthermore, one can use the “seeding” method in order to guide crystallization toward an expected material, by simply adding small amounts of desired zeolite to the synthesis mixture during ageing period.

1.3.3. Nucleation/crystallization

The main event occurring in the synthesis is the zeolite formation from amorphous material. The mechanisms involving nucleation and crystal growth of zeolites have been thoroughly investigated since the mid-70s but still remain unclear [46]. The crystallization

[44] J.-L. Guth, H. Kessler, in *Catalysis and Zeolites: Fundamentals and Applications*. (Eds.: J. Weitkamp, L. Puppe), Springer-Verlag, Berlin, Germany, **1999**, pp. 1–52.

[45] M. Maldonado, M. D. Oleksiak, S. Chinta, J. D. Rimer, *J. Am. Chem. Soc.* **2013**, *135*, 2641–2652.

[46] C. S. Cundy, P. A. Cox, *Microporous Mesoporous Mater.* **2005**, *82*, 1–78.

process of zeolite can be subdivided into three phases: (i) supersaturation, (ii) nucleation and (iii) crystal growth [36,47].

Supersaturation

A solution with specific concentration and temperature can be in three different states: stable, metastable and labile states, as depicted in Figure 1.11. The metastable and stable states are separated by the solubility curve, which determines the equilibrium saturation concentration of a component. In labile area, nucleation as well as crystal growth are possible, whereas in the stable region, neither nucleation nor crystal growth can occur. The metastable region is only characterized by crystal growth phenomenon.

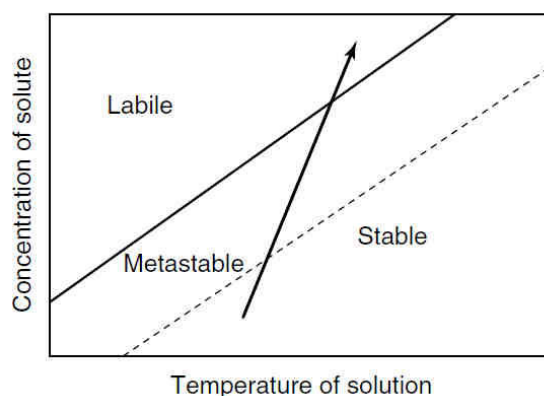


Figure 1.11 Solubility-supersolubility diagram [36]

When a synthesis mixture has reached its zeolite formation temperature, crystallization can only be expected after an induction period during which nucleation occurs. Indeed, during ageing, and especially while temperature rising, the concentration of aluminosilicate precursor species increases with time due to the dissolution of amorphous solid phase. During this ageing, the mixture shifts from a stable state to a metastable one up to the labile one. This transformation is indicated by an arrow in Figure 1.11. Chemically, the gel and the species present in the solution rearrange from a continuously changing phase of monomers to clusters of silicates and aluminosilicates. These oligomers form and disappear by condensation and hydrolysis under the influence of high temperature. In this

[47] E. J. P. Feijen, J. A. Martens, P. A. Jacobs, in *Preparation of Solid Catalysts* (Eds.: G. Ertl, H. Knözinger, J. Weitkamp), Wiley-VCH Verlag GmbH, Weinheim, Germany, **1999**.

reorganization process some particles become stable and small nuclei (in the nanometer range) are formed before crystallization starts.

Nucleation

All these features suggest that crystal growth is preceded by a slow nucleation step initiated by local concentration fluctuations inside the mixture and followed by a spontaneous growth of nuclei exceeding a critical size [48]. Furthermore, several theoretical models and experimental techniques have been applied in order to analyze the elementary reactions involved in the crystallization process of zeolites [46,49]. A combination of different methods of investigation is necessary to provide all the informations needed to understand the zeolite nucleation process.

Primary nucleation from a supersaturated solution has been strongly studied and is not understood so far. There is still a disagreement in the scientific community regarding the mechanism involved during nucleation. Hence, two different pathways are opposed for the nucleation in solution, namely heterogeneous or homogeneous mechanisms [36,46]. The latter supposes the nucleation directly from the liquid phase. This mechanism consists of a partial dissolution of amorphous particles (aluminosilicate species) present in the mixture by the action of the mineralizing agent (OH^- or F^-) in monomers or dimers. Subsequently, these entities condense into more complex structures, the SBUs, which arrange around the template ions to form stable nuclei. Once these nuclei reach a critical size, they grow into crystals by the successive introduction of soluble species. In this case, the amorphous solid phase acts as a reservoir of nutrients that are consumed as the growth progresses. Many works have been devoted to this mechanism pathway but no evidence for the location of nucleation has been given. Fan and co-workers while combining *in-situ* small angle and wide angle X-ray scattering (SAXS/WAXS) techniques investigated the nucleation of nanosized zeolite A and came to the conclusion that the mechanism was homogeneous [50]. They observed the formation of small precursors (5-15 nm in size) consumed during the growth of

[48] F. Schüth, *Curr. Opin. Solid State Mater. Sci.* **2001**, *5*, 389–395.

[49] a) F. Schüth, P. Bussian, P. Ågren, S. Schunk, M. Lindén, *Solid State Sci.* **2001**, *3*, 801–808. b) J. D. Epping, B. F. Chmelka, *Curr. Opin. Colloid Interface Sci.* **2006**, *11*, 81–117. c) S. A. Pelster, R. Kalamajka, W. Schrader, F. Schüth, *Angew. Chem. Int. Ed.* **2007**, *46*, 2299–302. d) A. Palčić, B. Subotić, V. Valtchev, J. Bronić, *CrystEngComm* **2013**, *15*, 5784–5791.

[50] W. Fan, M. O'Brien, M. Ogura, M. Sanchez-Sanchez, C. Martin, F. Meneau, K.-I. Kurumada, G. Sankar, T. Okubo, *Phys. Chem. Chem. Phys.* **2006**, *8*, 1335–1339.

LTA crystals, prior to the onset of crystallization. In contrast, the heterogeneous mechanism proceeds *via* the formation of the nuclei from impurities present in the solution. This mechanism has been proposed in numerous studies in order to explain the formation of A and Y zeolites [51].

Another wide studied mechanism of nucleation proceeds *via* the reorganization of an amorphous solid phase, named hydrogel. Nucleation takes place within this hydrogel and the crystals are formed through solid-solid transformations [52]. Clear solutions are special case of synthesis gel in which the amorphous particles remain of colloidal or sub-colloidal dimensions (≤ 50 nm) [53]. The presence of such particles inside the gel was highlighted by electronic microscopy studies. It is worthy to mention the outstanding work from Mintova, who provided images of the formation of crystalline structure; *i.e.*, A zeolite, within amorphous gel particles of nanometer dimensions [53b].

In summary, the understanding of the nucleation process in zeolite crystallization remains elusive and a combination of different pathways, such as the nucleation in solution and the formation of nuclei in the gel, should be envisaged.

Zeolite crystal growth occurs at the crystal-solution interface by condensation of dissolved preassembled building units onto the crystal surface.

1.4 Y and ZSM-5 zeolites

1.4.1. FAU zeolite type

Faujasite structures were discovered by R. M. Milton and D. W. Breck in the late 40's, namely types A, X and Y. FAU-type zeolites were first commercialized by Union Carbide Corporation in 1954 and are one of the industrially most important zeolite, which find

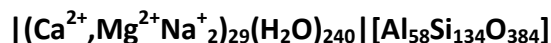
[51] a) T. Brar, P. France, P. G. Smirniotis, *J. Phys. Chem. B* **2001**, *105*, 5383–5390. b) J. Bronić, B. Subotić, *Microporous Mater.* **1995**, *4*, 239–242.

[52] D. P. Serrano, R. van Grieken, *J. Mater. Chem.* **2001**, *11*, 2391–2407.

[53] a) B. J. Schoeman, O. Regev, *Zeolites* **1996**, *17*, 447–456. b) S. Mintova, N. H. Olson, V. Valtchev, T. Bein, *Science* **1999**, *283*, 958–960. c) L. Itani, Y. Liu, W. Zhang, K. N. Bozhilov, L. Delmotte, V. Valtchev, *J. Am. Chem. Soc.* **2009**, *131*, 10127–39. d) A. Palčić, B. Subotić, V. Valtchev, J. Bronić, *CrystEngComm* **2013**, *15*, 5784–5791.

several utilizations such as ion-exchange (Na-X), adsorption and catalysis applications (FCC process) [54].

Zeolite Y belongs to the FAU-type framework. Its unit cell formula is given by:



This type of zeolite framework exhibits a three-dimensional pore structure with pores running perpendicular to each other in the x, y and z planes and is made of secondary building units 4, 6, and 6-6 (Figure 1.12). The window aperture is approximately 7.4 Å and is composed of 12-MR.

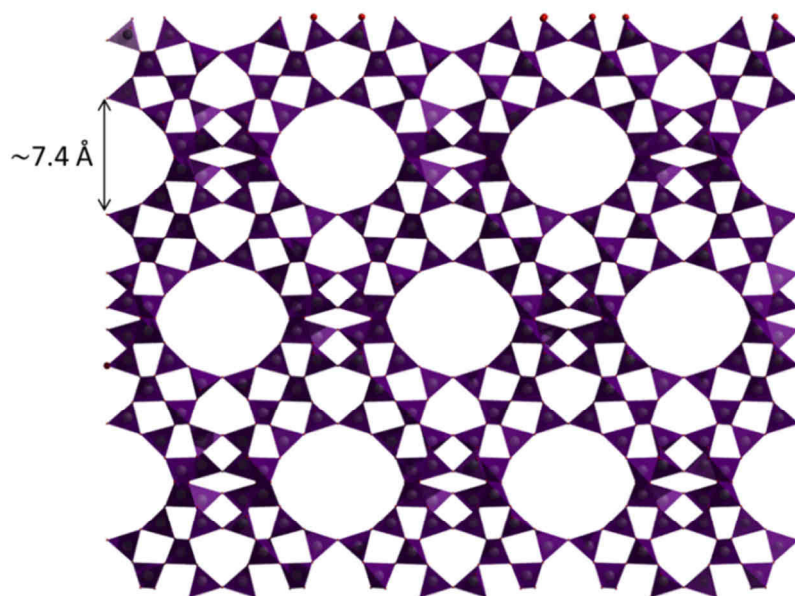


Figure 1.12 Framework of Y zeolite orthogonally viewed in the b axis

The pore walls are provided by the assembly of ten sodalite cages, through hexagonal prisms (D6R), leading to the formation of supercages, which are roughly spherical (dodecahedral) and having a diameter of approximately 12 Å (Figure 1.13) [5].

[54] E. M. Flanigen, in *Introduction to Zeolite Science and Practice* (Eds.: H. van Bekkum, E.M. Flanigen, P.A. Jacobs, J.C. Jansen), Elsevier Science B.V., Amsterdam, The Netherlands, **2001**, pp. 11–36.

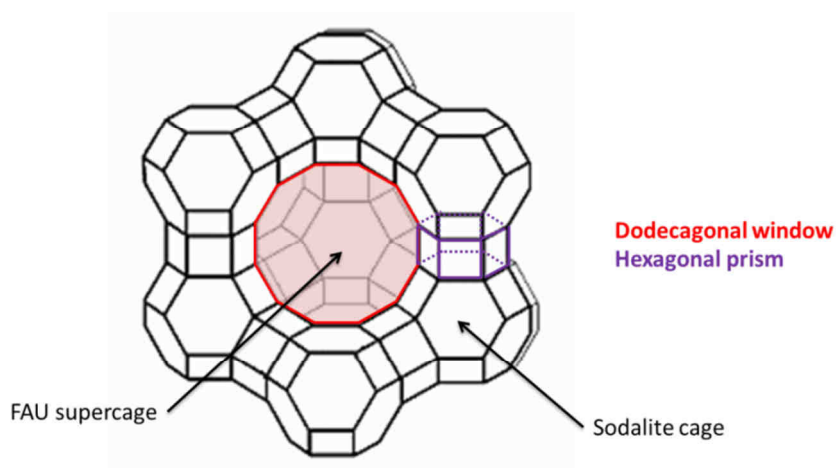


Figure 1.13 Schematic representation of FAU-supercage viewed along [111]

The most important use of zeolite Y is as a cracking catalyst in the refinery. It is used in acidic form in FCC units to enhance the yield of gasoline and diesel fuel from crude oil feedstocks. It is also used in hydrocracking units as a support for platinum/palladium to increase aromatic content in refinery products [13].

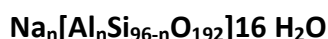
Zeolites with a FAU-type topology generally exhibit low Si/Al ratio. Thus, one can distinguish synthetic faujasite zeolites, depending on Si/Al ratio of the framework. The Si/Al ratio of X and Y zeolites is between 2 and 3. The synthesis of “low-silica” zeolites, as Y zeolite, is usually performed under hydrothermal conditions, with a silica and an alumina source as well as an exchangeable cation (typically Na^+) being dissolved in water and playing the role of template. Crystallization is induced by heating the gel for a while usually at 100 °C. A high pH value is obtained by adding a base (typically NaOH) in order to favor the dissolution of all chemicals. The Na^+ -form should be exchanged in NH_4^+ -form or in its acid form in order to keep the framework stability. The Y zeolite formation has also been investigated in numerous papers [55]. Furthermore, high-silica Y zeolites, named Ultra-Stable Y (USY), can be obtained through the removal of some framework aluminum atoms by hydrothermal treatment.

[55] a) M. W. Anderson, J. R. Agger, J. T. Thornton, N. Forsyth, *Angew. Chem. Int. Ed.* **1996**, *35*, 1210–1213. b) S. Mintova, N. Olson, T. Bein, *Angew. Chem. Int. Ed.* **1999**, *38*, 3201–3204.

1.4.2. MFI zeolite type

Zeolite ZSM-5 (Zeolite Socony Mobil-5) was discovered in the 70s at Mobil in the USA [56] and belongs to the MFI structure topology [5]. The Mobil scientists were immediately aware of the prime importance of this new material. ZSM-5 zeolite actually is not a single material but a family of zeolites, also known as pentasils. It is widely used in the petroleum industry as a catalyst for hydrocarbons cracking and isomerization reactions.

The unit cell formula of ZSM-5 zeolites is:



ZSM-5 zeolite belongs to the medium pore size family. It has a 3D channel structure with a pore system consisting of intersecting straight and sinusoidal channels having almost the same size: 5.1x5.5 and 5.3x5.6 Å (Figure 1.14). Moreover, ZSM-5 is composed by several pentasil units linked together through oxygen bridges to form pentasil chains. The ZSM-5 contains 10-MR and larger cavities of approximately 7 Å.

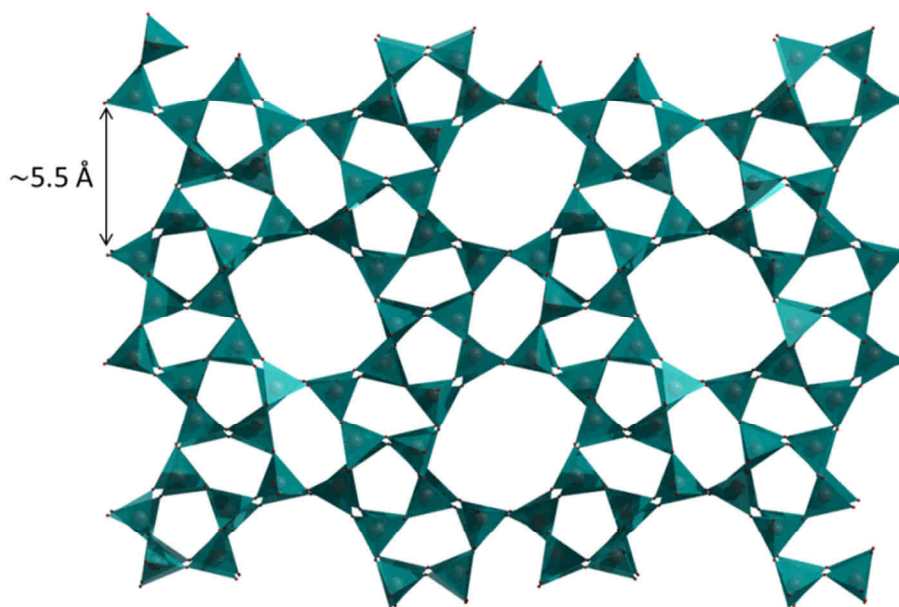


Figure 1.14 MFI-framework representation viewed along [010]

[56] R. J. Argauer, G. R. Landolt, *Crystalline Zeolite ZSM-5 and Method of Preparing the Same*, **1972**, US 3702886.

Pentasil-type zeolites have higher stability and Si/Al ratio than other structures (*i.e.*, Si/Al \geq 11). An organic SDA has to be added in order to obtain the desired topology. For ZSM-5 zeolites, a wide range of templates has been employed such as tetrapropylammonium hydroxide or halide, ethylenediamine, propylamine, tripropylamine and 1.6-hexanediamine [57]. Templates act in the zeolite crystallization in two ways: first by promoting the formation of desired building blocks in the gel, and secondly by acting as a hydrophobic pore filler preventing the dissolution and recrystallization of crystals already formed. Alkylamine templates must be removed after the synthesis by calcination, *via* Hofmann elimination, at high temperature (\geq 500 °C). However, template-free syntheses have also been described [58].

Neutral medium is particularly appropriate for the synthesis of “high-silica” materials as ZSM-5 zeolites. The crystallinity of these catalysts produced in the presence of F⁻ anions is generally higher than for materials obtained in alkaline media [39]. Moreover, fluoride-mediated ZSM-5 zeolites exhibit a regular crystal size ranging from 10 to 100 μ m. This peculiarity of fluoride-mediated zeolites is due to the fact that the synthesis mixture is less supersaturated than in alkaline synthesis, leading to fewer metastable phases. The synthesis in fluoride medium allows to form zeolites in their NH₄⁺-form, which is advantageous compared to alkaline media since further ion-exchange steps are not necessary. In this procedure, only one calcination step is needed to burn the template and generate acidic H-ZSM-5.

1.5 Hierarchical zeolites

Zeolites are the heterogeneous catalysts that have the highest annual production and are used in numerous acid-catalyzed reactions. With the necessity for the refining industry to deal with heavier feedstocks, there is a clear demand for improved zeolites displaying

[57] a) F. J. van der Gaag, J. C. Jansen, H. van Bekkum, *Appl. Catal.* **1985**, *17*, 261–271. b) S. Mintova, V. Valtchev, E. Vulcheva, S. Veleva, *Mater. Res. Bull.* **1992**, *27*, 515–522.

[58] a) F. J. Machado, C. M. Lopez, M. A. Centeno, C. Urbina, *Appl. Catal. A* **1999**, *181*, 29–38. b) F. Pan, X. Lu, Y. Wang, S. Chen, T. Wang, Y. Yan, *Mater. Lett.* **2014**, *115*, 5–8.

better accessible surface areas and higher pore sizes/volumes in order to capitalize on their effectiveness. Indeed, zeolites can show several limitations and constraints on the reactants, intermediates and products, especially regarding diffusion limitations.

Ordered mesoporous materials have shown to be an attractive solution to overcome these diffusion limitations. For example, MCM-41 solid possesses larger pores and well manageable pore size distribution with respect to zeolites. This mesostructured material exhibits an hexagonal arrangement of cylindrical mesopores of approximately 2-6 nm depending on the choice of the template (*i.e.*, ionic surfactants) [59]. Without post-synthetic modifications, MCM-41 framework is electrically neutral and does not exhibit any strong Brønsted acidity, therefore its catalytic activity is very limited. The incorporation of heteroatoms by grafting methods, in particular aluminum, allows to provide acidic properties [60]. Nevertheless, aluminum-doped mesoporous catalysts present weak acidity comparable to amorphous silica-alumina. Additionally, their thermal and hydrothermal properties turn out less stable than zeolites [61]. Due to these limitations, ordered mesoporous materials have not succeeded to replace zeolites in petrochemical and refining processes.

With this in mind, the development of “hierarchical” zeolite catalysts has opened new possibilities and perspectives in acid-catalyzed processes for over a decade now [62]. New methodologies and strategies have been tempted to minimize diffusion limitations and enhance catalysts effectiveness. Thus, an intense and persistent scientific effort focused on improving the accessibility to the acid sites by widening the zeolites openings [63], reducing

[59] a) J. S. Beck, J. C. Vartuli, W. J. Roth, M. E. Leonowicz, C. T. Kresge, K. D. Schmitt, C. T. W. Chu, D. H. Olson, E. W. Sheppard, *J. Am. Chem. Soc.* **1992**, *114*, 10834–10843. b) C. T. Kresge, M. E. Leonowicz, W. J. Roth, J. C. Vartuli, J. S. Beck, *Nature* **1992**, *359*, 710–712.

[60] a) A. Corma, M. S. Grande, V. Gonzalez-Alfaro, A. V Orchilles, *J. Catal.* **1996**, *159*, 375–382. b) A. Corma, *Chem. Rev.* **1997**, *97*, 2373–2420. c) T. Kugita, S. K. Jana, T. Owada, N. Hashimoto, M. Onaka, S. Namba, *Appl. Catal. A* **2003**, *245*, 353–362.

[61] S. Hitz, R. Prins, *J. Catal.* **1997**, *168*, 194–206.

[62] a) J. Pérez-Ramírez, C. H. Christensen, K. Egeblad, J. C. Groen, *Chem. Soc. Rev.* **2008**, *37*, 2530–2542. b) K. Na, M. Choi, R. Ryoo, *Microporous Mesoporous Mater.* **2013**, *166*, 3–19.

[63] a) C. C. Freyhardt, M. Tsapatsis, R. F. Lobo, K. J. Balkus Jr, M. E. Davis, *Nature* **1996**, *381*, 295–298. b) A. Corma, M. J. Díaz-Cabañas, J. Martínez-Triguero, F. Rey, J. Rius, *Nature* **2002**, *418*, 514–517. c) J. Sun, C. Bonneau, A. Cantín, A. Corma, M. J. Díaz-Cabañas, M. Moliner, D. Zhang, M. Li, X. Zou, *Nature* **2009**, *458*, 1154–1157. d) J. Jiang, J. L. Jorda, J. Yu, L. A. Baumes, E. Mugnaioli, M. J. Diaz-Cabanias, U. Kolb, A. Corma, *Science* **2011**, *333*, 1131–1134.

the zeolite crystal size to decrease the intracrystalline diffusion path length [64], or introducing a secondary pore system consisting of intracrystalline mesopores [65]. Larger pore zeolites allow to raise the diffusion of molecules inside the micropores, whereas hierarchical zeolites facilitate diffusion by coupling the intrinsic microporous system with an auxiliary mesopore network being inter- or intracrystalline (Figure 1.15) [66].

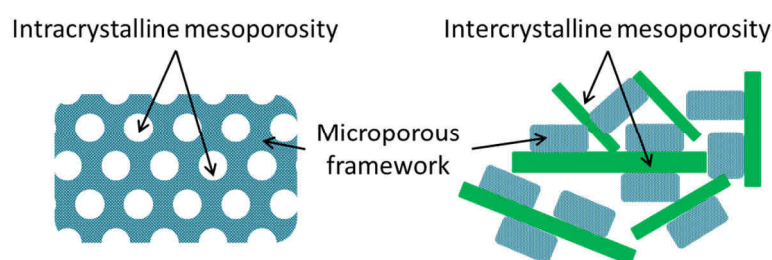


Figure 1.15 Schematic representation of hierarchical zeolites

In the latter case, each porosity level fulfills a distinct complementary task: the micropores hold catalytically active sites, whose access is facilitated by the newly introduced mesoporosity [62a]. Figure 1.16 summarizes the different strategies leading to materials combining micro- and mesoporosity [67].

There are two strategies leading to hierarchical materials combining micro- and mesoporosity: either through top-down routes or so-called “destructive” modifications, as well as by bottom-up routes, namely “constructive” pathways [67]. The first one lies in an “*a priori*” tailoring of the shape, size and connectivity within zeolite by using multiple templates or small zeolite-based building blocks during crystallization [65b]. Whereas the second method involves already synthesized zeolites followed by destructive post-treatments by

[64] a) A. Corma, V. Fornes, S. B. Pergher, T. L. M. Maesen, J. G. Buglass, *Nature* **1998**, 396, 353–356. b) M. Choi, K. Na, J. Kim, Y. Sakamoto, O. Terasaki, R. Ryoo, *Nature* **2009**, 461, 246–249. c) E.-P. Ng, D. Chateigner, T. Bein, V. Valtchev, S. Mintova, *Science* **2012**, 335, 70–73.

[65] a) M. Choi, H. S. Cho, R. Srivastava, C. Venkatesan, D.-H. Choi, R. Ryoo, *Nature Mater.* **2006**, 5, 718–723. b) K. Egeblad, C. H. Christensen, M. Kustova, C. H. Christensen, *Chem. Mater.* **2008**, 20, 946–960. c) J. Pérez-Ramírez, S. Abello, A. Bonilla, J. C. Groen, *Adv. Funct. Mater.* **2009**, 19, 164–172. d) F. C. Meunier, D. Verboekend, J.-P. Gilson, J. C. Groen, J. Pérez-Ramírez, *Microporous Mesoporous Mater.* **2012**, 148, 115–121. e) F. Ocampo, H. Yun, M. M. Pereira, J.-P. Tessonier, B. Louis, *Cryst. Growth Des.* **2009**, 9, 3721–3729.

[66] S. Lopez-Orozco, A. Inayat, A. Schwab, T. Selvam, W. Schwieger, *Adv. Mater.* **2011**, 23, 2602–2615.

[67] R. Chal, C. Gérardin, M. Bulut, S. van Donk, *ChemCatChem* **2011**, 3, 67–81.

demetallation [68]. Several examples have been published, comprising steaming [69], acid [70] or base [71] leaching, and more refined approaches like ion irradiation [72] and/ or strong oxidizing agents [73].

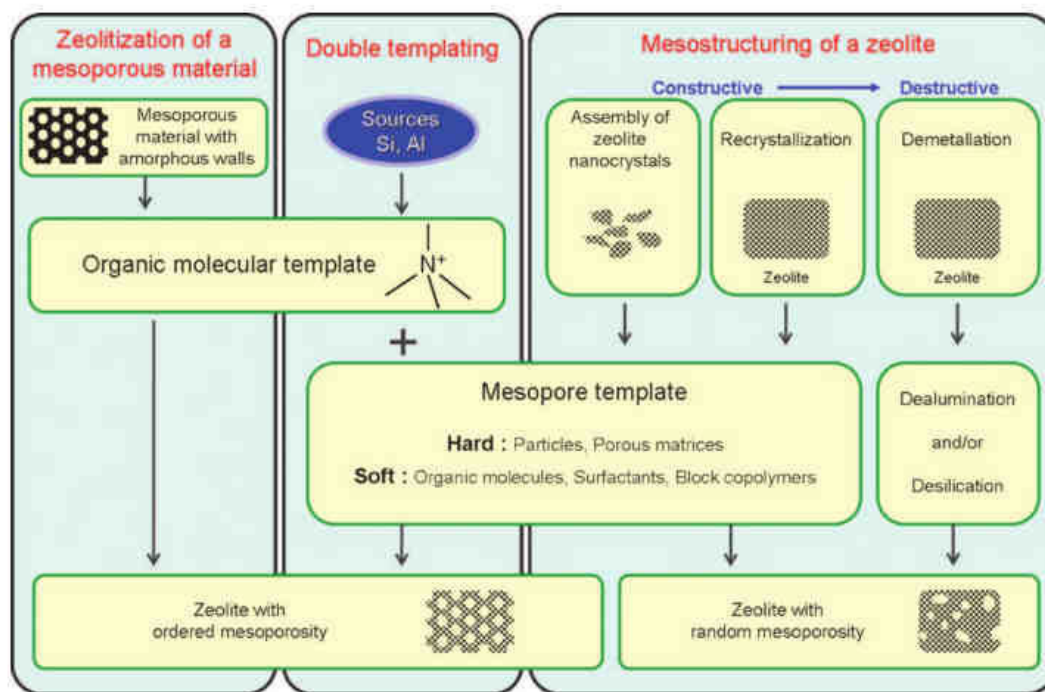


Figure 1.16 Summary of the methods for designing micro-mesostructured zeolites [67]

1.5.1. Destructive methods

Mesopores introduced in zeolite frameworks by destructive post-modifications are obtained by means of selective extraction of structure atoms from a pre-synthesized zeolite crystal. As zeolites are aluminosilicates, the most studied demetallation treatments are

[68] M.-C. Silaghi, C. Chizallet, P. Raybaud, *Microporous Mesoporous Mater.* **2014**, *191*, 82–96.

[69] a) K. P. de Jong, J. Zečević, H. Friedrich, P. E. de Jongh, M. Bulut, S. van Donk, R. Kenmogne, A. Finiels, V. Hulea, F. Fajula, *Angew. Chem. Int. Ed.* **2010**, *49*, 10074–10078. b) S. M. T. Almutairi, B. Mezari, E. A. Pidko, P. C. M. M. Magusin, E. J. M. Hensen, *J. Catal.* **2013**, *307*, 194–203.

[70] a) J. C. Groen, L. A. A. Peffer, J. A. Moulijn, J. Pérez-Ramírez, *Microporous Mesoporous Mater.* **2004**, *69*, 29–34. b) N. Viswanadham, M. Kumar, *Microporous Mesoporous Mater.* **2006**, *92*, 31–37.

[71] S. Abello, A. Bonilla, J. Pérez-Ramírez, *Appl. Catal. A* **2009**, *364*, 191–198. b) Abello, A. Bonilla, J. Pérez-Ramírez, *Appl. Catal. A* **2009**, *364*, 191–198.

[72] a) S. Abello, J. Pérez-Ramírez, *Phys. Chem. Chem. Phys.* **2009**, *11*, 2959–2963. b) V. Valtchev, E. Balanzat, V. Mavrodinova, I. Diaz, J. El Fallah, J.-M. Goupil, *J. Am. Chem. Soc.* **2011**, *133*, 18950–18956.

[73] C. Pavel, R. Palkovits, F. Schüth, W. Schmidt, *J. Catal.* **2008**, *254*, 84–90.

desilication and dealumination. Moreover, top-down methods lead to the formation of non-ordered mesopores inside the zeolite microporous framework (Figure 1.17).

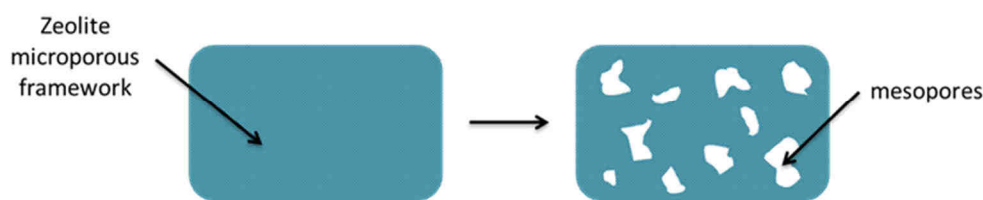


Figure 1.17 Representation of the mesoporosity introduced by destructive treatments

1.5.1.1. Desilication

The introduction of mesopores by the alkaline-mediated leaching of framework silicon atoms has become an attractive method due to the combination of both experimental simplicity and efficiency of the hierarchical zeolites obtained [62a]. The mesopores generated by this approach are interconnected and accessible from the external surface of the zeolite crystal, improving the catalytic performance of access-limited and diffusion-limited reactions [62a,74,75]. The first description of post-synthetic modifications by alkaline treatment was patented by Young and Yorba in the 60s [76]. They claimed that alkaline-treated mordenite exhibited preserved crystallinity and enhanced performances in benzene adsorption.

In the past decade, a great attention focused on the design of mesoporous zeolites by desilication and reported the corresponding benefits, in terms of activity, selectivity, and/or lifetime, in several catalyzed reactions such as isomerization, cracking, conversion of methanol to hydrocarbons, acylation, etc. [62a,77]. The treatment of zeolites by alkaline leaching is the most studied desilication method to design hierarchical materials. Different post-synthesis parameters have been investigated: nature of the base, base concentration,

[74] J. C. Groen, W. Zhu, S. Brouwer, S. J. Huynink, F. Kapteijn, J. A. Moulijn, J. Pérez-Ramírez, *J. Am. Chem. Soc.* **2007**, *129*, 355–360.

[75] Y. Tao, H. Kanoh, L. Abrams, K. Kaneko, *Chem. Rev.* **2006**, *106*, 896–910.

[76] D. A. Young, L. Yorba, *Hydrocarbon Conversion Process and Catalyst Comprising a Crystalline Alumino-Silicate Leached with Sodium Hydroxide*, **1967**, US3326797.

[77] a) B. Gil, Ł. Mokrzycki, B. Sulikowski, Z. Olejniczak, S. Walas, *Catal. Today* **2010**, *152*, 24–32. b) J. Kim, M. Choi, R. Ryoo, *J. Catal.* **2010**, *269*, 219–228. c) S. J. You, E. D. Park, *Microporous Mesoporous Mater.* **2014**, *186*, 121–129.

post-treatment duration and presence of organic additives to better control the desilication extend [78].

Groen *et al.* established optimal desilication conditions for alkaline treatment of ZSM-5 zeolite in the presence of NaOH, *i.e.*, 0.2M of base at 338 K for 30 min [79]. Moreover, they identified that the presence of framework Al plays an important role in the mechanism of mesopores formation in alkaline medium [80]. They report an optimal aluminum amount in ZSM-5 zeolites, *i.e.*, Si/Al ratio between 25 to 50, for this method to generate mesopores in the range of 5-20 nm. Above this ratio, aluminum atoms prevent Si extraction and hinder the formation of mesopores. In contrast, high Si/Al ratios (≥ 50) exhibit uncontrollable and unselective Si dissolution, leading to the formation of large meso- and also macropores weakening the zeolite framework. Figure 1.18 summarizes the mechanism of mesopores formation in alkaline medium. Another intrinsic characteristic of alkaline treatment is the decreased Si/Al ratio in the solid due to the selective silicon dissolution.

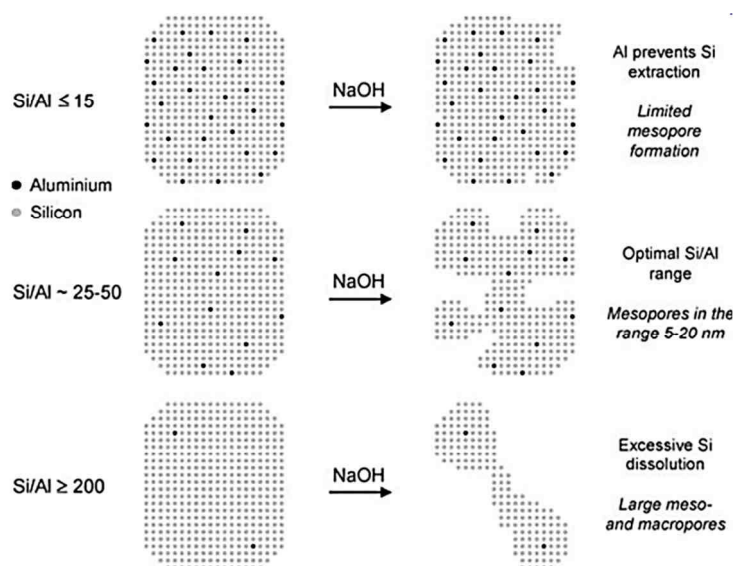


Figure 1.18 Schematic representation of the Si/Al ratio during the desilication of ZSM-5 zeolite upon NaOH treatment. Illustrated mechanism of mesoporosity formation [80]

Recently, hierarchical zeolites have been prepared by desilication using aqueous solution of organic bases such as tetrapropylammonium hydroxide (TPAOH) or

[78] D. Verboekend, G. Vilé, J. Pérez-Ramírez, *Adv. Funct. Mater.* **2012**, 22, 916–928.

[79] J. C. Groen, L. A. A. Peffer, J. A. Moulijn, J. Pérez-Ramírez, *Colloids Surf., A* **2004**, 241, 53–58.

[80] J. C. Groen, J. C. Jansen, J. A. Moulijn, J. Pérez-Ramírez, *J. Phys. Chem. B* **2004**, 108, 13062–13065.

tetrabutylammonium hydroxide (TBAOH) [81]. However, it was found that organic bases are less reactive and less selective toward silicon extraction with respect to inorganic bases. Hence, the desilication process is more controllable under these conditions. These treatments need to be performed at higher temperature and longer duration to achieve significant mesoporosity. In addition, higher aluminum leaching was observed, compared with NaOH treatment, and therefore higher Si/Al ratios were found in resulting zeolites.

1.5.1.2. Dealumination

This demetalation method is the most used strategy in industry [82]. Dealumination approach leads to the partial removal of aluminum atoms from the zeolite framework. Various methods have been investigated to achieve the hydrolysis of the Si-O-Al bonds, *i.e.*, calcination, steaming, acid leaching and chemical treatment. The pioneering work of R. M. Barrer and M. B. Makki described this post-synthetic process with the use of mineral acids [83]. Several reviews have been published regarding dealumination and its relative effect on intrinsic properties and catalytic activity of as-modified zeolites [67,68,84].

The most renowned way to create mesopores in zeolites is by hydrothermal treatment in the presence of steam, even though thermal treatment without the addition of steam can be used [85]. It is worthy to note that the presence of water molecules during the thermal treatment facilitates largely the mobility of silicon and aluminum atoms [85a,86]. Various zeolite types, *i.e.*, MOR, ZSM-5 or FER, have been modified by dealumination process but Y types were the most studied ones [87]. The steaming process is generally performed over the

[81] S. Abello, A. Bonilla, J. Pérez-Ramírez, *Appl. Catal. A* **2009**, *364*, 191–198.

[82] a) P. E. Eberly, S. M. Laurent, H. E. Robson, *High Silica Crystalline Zeolites and Process for Their Preparation*, **1970**, US3506400. b) G. T. Kerr, A. W. Chester, *Ultra High Silicon-Content Zeolites and Preparation Thereof*, **1978**, US4093560. c) P.-S. E. Dai, D. E. Sherwood Jr., B. R. Martin, *Zeolite Treating Process*, **1991**, US5069890.

[83] R. M. Barrer, M. B. Makki, *Can. J. Chem.* **1964**, *42*, 1481–1487.

[84] S. van Donk, A. H. Janssen, J. H. Bitter, K. P. de Jong, *Catal. Rev.* **2003**, *45*, 297–319.

[85] a) S. Moreno, G. Poncelet, *Microporous Mater.* **1997**, *12*, 197–222. b) M. Müller, G. Harvey, R. Prins, *Microporous Mesoporous Mater.* **2000**, *34*, 135–147.

[86] G. T. Kerr, *J. Phys. Chem.* **1967**, *71*, 4155–4156.

[87] a) R. Beaumont, D. Barthomeuf, *J. Catal.* **1972**, *26*, 218–225. b) J. Lynch, F. Raatz, P. Dufresne, *Zeolites* **1987**, *7*, 333–340. c) A. Janin, M. Maache, F. Raatz, J. C. Lavalley, J. F. Joly, N. Szydłowski, *Zeolites* **1991**, *11*, 391–396. d) H. Miessner, H. Kosslick, U. Lohse, B. Parltitz, V. A. Tuan, *J. Phys. Chem.* **1993**, *97*, 9741–9748. e) S. M. T. Almutairi, B. Mezari, E. A. Pidko, P. C. M. M. Magusin, E. J. M. Hensen, *J. Catal.* **2013**, *307*, 194–203. f) E. Senderov, I. Halasz, D. H. Olson, *Microporous Mesoporous Mater.* **2014**, *186*, 94–100.

ammonium or acidic form of the zeolite at high temperatures (≥ 500 °C). The hydrolysis of Si-O-Al bonds occurs while the contact with steam and causes the extraction of Al atoms from the zeolite framework, leading to the formation of defects (Al vacancies) and silanol rich domains (hydroxyl nests [87f]), and/or the partial amorphization of the structure [84]. This corresponds to the first step of the well-established mechanism proposed by Marcilly in the 80s [88]. In a second step, the new defects created in the framework can be partially healed by amorphous debris containing mobile silica and alumina species. Thus, part of these mobile fragments can refill some vacancies, while others vacancies grow up to form mesopores, as shown in Figure 1.19. The pores formed during steaming are either cavities inside the zeolite crystals or cylindrical pores connecting the external surface with the interior of the crystal [89]. Their size depends on the severity of the steaming treatment.

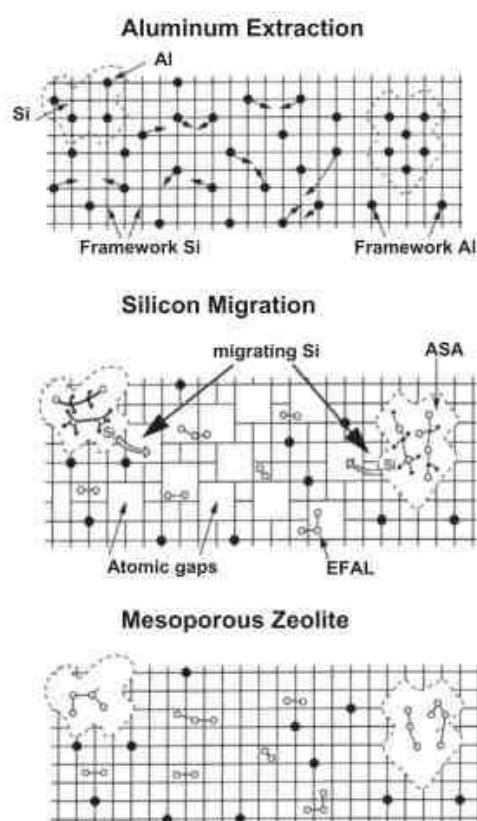


Figure 1.19 Mechanism proposed by Marcilly for the dealumination process [88]

[88] C. Marcilly, *Petrole et Techniques* **1986**, 328, 12–18.

[89] a) A. H. Janssen, A. J. Koster, K. P. de Jong, *J. Phys. Chem. B* **2002**, 106, 11905–11909. b) L. Teyssier, M. Thomas, C. Bouchy, J. A. Martens, E. Guillon, *Microporous Mesoporous Mater.* **2007**, 100, 6–11.

The main disadvantage of the steaming remains the partial amorphization of the zeolite framework, obviously leading to a lower crystallinity, which further diminishes with increasing the severity of the steaming treatment, along with the decrease of active sites. Furthermore, the formation of extra-framework aggregates into micro- and native mesopores may partially block the accessibility to the active sites [84]. The bulk Si/Al ratio after steaming treatment remains the same, whereas the Si/Al ratio of the framework increases.

As previously exposed, extracted Al atoms are not removed from the zeolite structure. They remain present as extra-framework aluminum (EFAl) species which are located within the micro- and mesopores. Though, the precise nature of EFAl species is not well established, different species have been proposed, either at tetrahedral or octahedral state: cations (Al^{3+} , AlO^+), neutral species, up to a certain degree polymerized and hydroxylaluminates ($\text{Al}(\text{OH})_3$, $\text{Al}(\text{OH})_2^+$, $[\text{Al}(\text{OH})_2]^+$ or $[\text{AlO}(\text{OH})]$) [90]. Hence, there is part of EFAl fragments which exhibits Lewis acidity. The spatial proximity between Brønsted (Si-OH-Al bridgings) and Lewis acid sites (EFAl species) was found and this proximity can lead to an enhanced Brønsted acid strength provided by a synergy effect [91]. However, the removal of Al from the framework results in a lower density of Brønsted acid sites [92]. The presence of EFAl species affects differently the catalytic activity with respect to the considered reaction. Indeed, the extent of influence of extra-framework species to activate the reactants, of mesopores to alleviate diffusion limitations, and of isolation of the Brønsted acid sites will depend on the kind of reaction that is targeted as well as on operating conditions [93].

[90] a) D. L. Bhering, A. Ramirez-Solis, C. J. A. Mota, *J. Phys. Chem. B* **2003**, *107*, 4342–4347. b) N. Rosenbach Jr., C. J. A. Mota, *Appl. Catal. A* **2008**, *336*, 54–60.

[91] a) N. Malicki, G. Mali, A.-A. Quoineaud, P. Bourges, L. J. Simon, F. Thibault-Starzyk, C. Fernandez, *Microporous Mesoporous Mater.* **2010**, *129*, 100–105. b) Yu, S. Li, Q. Wang, A. Zheng, X. Jun, L. Chen, F. Deng, *J. Phys. Chem. C* **2011**, *115*, 22320–22327. c) S. M. T. Almutairi, B. Mezari, G. A. Filonenko, P. C. M. M. Magusin, M. S. Rigutto, E. A. Pidko, E. J. M. Hensen, *ChemCatChem* **2013**, *5*, 452–466. d) C. Mirodatos, D. Barthomeuf, *Chem. Comm.* **1981**, 39–40.

[92] A. Maijanen, E. G. Derouane, J. B. Nagy, *Appl. Surf. Sci.* **1994**, *75*, 204–212.

[93] J. A. van Bokhoven, N. Danilina, in *Zeolites and Catalysis Synthesis, Reactions and Applications* (Eds.: J. Čejka, A. Corma, S. Zones), Wiley-VCH Verlag GmbH & Co. KGaA, Weinheim, Germany, **2010**, pp. 283–300.

Dealumination can also occur *via* either acid leaching or chemical treatment [67,94]. These techniques are usually used after calcination or steaming treatment in order to remove EFAl species and amorphous materials present in the void volume of the micropores [95]. Although, framework Al atoms can also be extracted by concentrated acid solution which break Si-O-Al bonds [96]. Both inorganic acids such as nitric, hydrochloric and sulfuric acid, or organic acids (acetic and oxalic acid) are able to dealuminate zeolites [95b,97]. The preparation of hierarchical zeolites can be performed *via* chemical post-modifications. Generally, chemicals that are involved in dealumination are strong chelating agents such as ethylenediaminetetraacetic acid (EDTA) [87a,98], or compounds able to substitute extracted aluminums with silicon atoms such as ammonium hexafluorosilicate (AHFS) [94b,99] or silicon tetrachloride [94a].

Finally, a combination between desilication and dealumination has been employed to design an optimal catalyst in terms of acidity and mesoporosity for various applications [100].

1.5.2. Constructive methods

A large variety of bottom-up techniques permits to synthesize hierarchical zeolites. One can cite the zeolitization of mesoporous materials [101], the double templating [102], the

[94] a) M. Müller, G. Harvey, R. Prins, *Microporous Mesoporous Mater.* **2000**, *34*, 135–147. b) C. S. Triantafyllidis, A. G. Vlessidis, L. Nalbandian, N. P. Evmiridis, *Microporous Mesoporous Mater.* **2001**, *47*, 369–388.

[95] a) P. J. Kooyman, P. van der Waal, H. van Bekkum, *Zeolites* **1997**, *18*, 50–53. b) R. Giudici, H. W. Kouwenhoven, R. Prins, *Appl. Catal. A* **2000**, *203*, 101–110. c) S. M. C. Menezes, V. L. Camorim, Y. L. Lam, R. A. S. San Gil, A. Bailly, J. P. Amoureux, *Appl. Catal. A* **2001**, *207*, 367–377.

[96] H. Najar, M. S. Zina, A. Ghorbel, *React. Kinet. Mech. Catal.* **2010**, 385–398.

[97] a) M. R. Apelian, A. S. Fung, G. J. Kennedy, T. F. Degnan, *J. Phys. Chem.* **1996**, *100*, 16577–16583. b)

[98] B. Xu, S. Bordiga, R. Prins, J. A. van Bokhoven, *Appl. Catal. A* **2007**, *333*, 245–253.

[99] A. Corma, V. Fornes, F. Rey, *Appl. Catal.* **1990**, *59*, 267–274.

[100] a) M. Milina, S. Mitchell, N.-L. Michels, J. Kevin, J. Pérez-Ramírez, *J. Catal.* **2013**, *308*, 398–407. b) J. H. Ahn, R. Kolvenbach, S. S. Al-Khattaf, A. Jentys, J. A. Lercher, *Chem. Comm.* **2013**, *49*, 10584–6. c) S. J. You, E. D. Park, *Microporous Mesoporous Mater.* **2014**, *186*, 121–129.

[101] a) M. J. Verhoef, P. J. Kooyman, J. C. van der Waal, M. S. Rigutto, J. A. Peters, H. van Bekkum, *Chem. Mater.* **2001**, *13*, 683–687. b) B. Louis, F. Ocampo, H. Yun, J.-P. Tessonnier, M. M. Pereira, *Chem. Eng. J.* **2010**, *161*, 397–402.

[102] W. Kim, J.-C. Kim, J. Kim, Y. Seo, R. Ryoo, *ACS Catal.* **2013**, *3*, 192–195.

hard templating [103], the recrystallization of zeolites [104], *etc.* Among previous cited methods, the double (or dual) templating method consists of the utilization of both micro- and mesopore-directing agents in the synthesis gel.

Kloetstra and co-workers first introduced the synthesis of a material with a bimodal pore size distribution combining meso- (MCM-41 type) and micropores (FAU zeolite) [105]. The preparation of this material was performed *via* a one-pot synthesis containing both MCM-41 and Y templates. Hence, the final composite was composed by MCM-41 phase covering the microporous structure of FAU zeolite.

Recently, Ryoo *et al.* reported an advanced method for the preparation of several microporous zeolites, *i.e.*, LTA, aluminophosphate and MFI, having an additional mesoporous skeleton [106]. Their approach consisted of adding an additional compound in the synthesis gel, *i.e.*, amphiphilic organosilane molecules, playing the role of meso-structuring agent. The covalent binding between the silica precursor moieties and the self-assembling organic chains, avoids expelling the surfactant-based mesostructures out of the forming zeolite phase during the synthesis. Likewise, they reported the synthesis of different mesophase in MFI like and BEA zeolites while using such surfactants [107]. The mesopore apertures can be tailored according to surfactant tail length or addition of swelling agents.

The use of an excess of classic organic template has been reported by Wang *et al.* [108]. Hierarchical zeolite composites, named TUD-C, with ZSM-5 crystals embedded in a well-connected mesoporous matrix, have been obtained by applying the sole ZSM-5 template (TPAOH) through a two-step procedure. Thus, assemblies of TPAOH serve as a scaffold for the meso-structure.

[103] C. J. H. Jacobsen, C. Madsen, J. Houzvicka, I. Schmidt, A. Carlsson, *J. Am. Chem. Soc.* **2000**, *122*, 7116–7117.

[104] S. Wang, T. Dou, Y. Li, Y. Zhang, X. Li, Z. Yan, *Catal. Commun.* **2005**, *6*, 87–91.

[105] K. R. Kloetstra, H. W. Zandbergen, J. C. Jansen, H. van Bekkum, *Microporous Mater.* **1996**, *6*, 287–293.

[106] a) M. Choi, H. S. Cho, R. Srivastava, C. Venkatesan, D.-H. Choi, R. Ryoo, *Nature Mater.* **2006**, *5*, 718–723.

b) M. Choi, R. Srivastava, R. Ryoo, *Chem. Comm.* **2006**, 4380–4382. c) K. Cho, H. S. Cho, L.-C. de Ménorval, R. Ryoo, *Chem. Mater.* **2009**, *21*, 5664–5673.

[107] K. Na, C. Jo, J. Kim, K. Cho, J. Jung, Y. Seo, R. J. Messinger, B. F. Chmelka, R. Ryoo, *Science* **2011**, *333*, 328–332.

[108] a) J. Wang, J. C. Groen, W. Yue, W. Zhou, M.-O. Coppens, *Chem. Comm.* **2007**, 4653–4655. b) J. Wang, W. Yue, W. Zhou, M.-O. Coppens, *Microporous Mesoporous Mater.* **2009**, *120*, 19–28.

1.6 Zeolites coatings

1.6.1. Generalities

Through their great importance in industry, fixed-bed reactors present some drawbacks such as pressure drop, sensibility to fouling by dust, limited heat and mass transfers, and flow maldistribution. On that basis and in particular for process intensification, scientists focused their studies on the development of structured catalysts at the reactor level, also called structured catalytic beds [109]. Three different kinds of structured catalysts can be distinguished, *i.e.*, monolithic catalysts, membrane catalysts and arranged catalysts. These structures are spatially arranged within a reactor.

In the last decades, monolithic honeycomb structures, have been evaluated in many applications, *i.e.*, chemical process and refining industries, catalytic combustion, environmental applications, *etc.* [110]. Monolith catalysts are known to allow low pressure-drop and moderate surface area for reactions requiring low residence time and high space velocities. Monoliths possess a porous shape in the range of meso- and/or macrosized. In addition, the monolith can be post-modified, by surface functionalization, with an additional porous material to generate a large porosity (micro-, meso- and/or macrosized), provided by the coated active phase and/or the monolith support itself. In this regard the use of appropriate catalysts, such as zeolites, allows the development of a hierarchical organization of the porosity in two (micro-/macroporosity) or three (micro-/meso/macroporosity) levels. Thanks to the properties given by both zeolite thin layer and support itself, these coatings on monoliths offer various advantages with respect to micropellets or extrudates, such as an improved accessibility to the active sites, an effective heat removal from the reaction zone *via* a metal substrate, mechanical stability, pressure drop reduction and increased mass transport [111].

[109] A. Cybulski, J. A. Moulijn, in *Structured Catalysts and Reactors* (Eds.: A. Cybulski, J.A. Moulijn), CRC, Taylor & Francis Group, United States, **2005**, pp. 1–17.

[110] a) V. Tomašič, Z. Gomzi, *Chem. Biochem. Eng. Q.* **2001**, *15*, 109–115. b) J. L. Williams, *Catal. Today* **2001**, *69*, 3–9. c) M. T. Kreutzer, F. Kapteijn, J. A. Moulijn, *Catal. Today* **2006**, *111*, 111–118.

[111] a) A. Zampieri, P. Colombo, G. T. P. Mabande, T. Selvam, W. Schwieger, F. Scheffler, *Adv. Mater.* **2004**, *16*, 819–823. b) S. Ivanova, B. Louis, B. Madani, J.-P. Tessonnier, M.-J. Ledoux, C. Pham-Huu, *J. Phys. Chem. C* **2007**, *111*, 4368–4374. c) A. Renken, L. Kiwi-Minsker, *Adv. Catal.* **2010**, *53*, 47–122.

Different methods for preparing zeolite coatings can be distinguished; either by hydrothermal synthesis in the form of a layer on a support surface (called *in-situ* coating) or by depositing a layer of pre-synthesized zeolite crystals on the support (called *ex-situ* coating or dip-coating). The latter consists of the immersion of the structured support in a suspension of zeolite in a solvent containing often a binder. Afterwards, the solvent is evaporated by drying and calcination [112]. In contrast, *in-situ* coating is one of the most promising methods for obtaining zeolite coating. It is based on the special formulation of zeolite in the presence of the support and yields a thin, crystalline and densely packed layer of crystals which are directly bonded to the support surface (through covalent bonds) [113].

Various supports have been reported for the preparation of zeolite coatings. One can cite for instance, both meso- and macroporous glass monoliths [114], alumina [115], metals [113a,116], ceramic foam [117], sacrificial biological supports [118], which have been used as supports for the development of structured catalytic beds.

-
- [112] a) A. E. W. Beers, T. A. Nijhuis, N. Aalders, F. Kapteijn, J. A. Moulijn, *Appl. Catal. A* **2003**, *243*, 237–250. b) M. Navlani-Garcia, F. J. Varela-Gandia, A. Bueno-Lopez, D. Cazorla-Amoros, B. Puertolas, J. M. Lopez, T. Garcia, D. Lozano-Castello, *ChemSusChem* **2013**, *6*, 1467–1477.
- [113] a) Z. Wang, Y. Yan, *Chem. Mater.* **2001**, *13*, 1101–1107. b) S. Ivanova, E. Vanhaecke, L. Dreibine, B. Louis, C. Pham-Huu, *Appl. Catal. A* **2009**, *359*, 151–157.
- [114] a) M. Rauscher, T. Selvam, W. Schwieger, D. Freude, *Microporous Mesoporous Mater.* **2004**, *75*, 195–202. b) F. Ocampo, H. Yun, M. M. Pereira, J.-P. Tessonier, B. Louis, *Cryst. Growth Des.* **2009**, *9*, 3721–3729. c) B. Louis, F. Ocampo, H. Yun, J.-P. Tessonier, M. M. Pereira, *Chem. Eng. J.* **2010**, *161*, 397–402.
- [115] N. van der Puil, F. M. Dautzenberg, H. van Bekkum, J. C. Jansen, *Microporous Mesoporous Mater.* **1999**, *27*, 95–106.
- [116] a) V. Valtchev, S. Mintova, *Zeolites* **1995**, *15*, 171–175. b) S. Mintova, J. Hedlund, B. Schoeman, V. Valtchev, J. Sterte, *Chem. Comm.* **1997**, 15–16. c) B. Louis, P. Reuse, L. Kiwi-Minsker, A. Renken, *Appl. Catal. A* **2001**, *210*, 103–109.
- [117] a) G. B. F. Seijger, O. L. Oudshoorn, W. E. J. van Kooten, J. C. Jansen, H. van Bekkum, C. M. van den Bleek, H. P. A. Calis, *Microporous Mesoporous Mater.* **2000**, *39*, 195–204. b) A. Zampieri, P. Colombo, G. T. P. Mabande, T. Selvam, W. Schwieger, F. Scheffler, *Adv. Mater.* **2004**, *16*, 819–823. c) S. Ivanova, B. Louis, M.-J. Ledoux, C. Pham-Huu, *J. Am. Chem. Soc.* **2007**, *129*, 3383–3391. d) S. Ivanova, E. Vanhaecke, B. Louis, S. Libs, M.-J. Ledoux, S. Rigolet, C. Marichal, C. Pham, F. Luck, C. Pham-Huu, *ChemSusChem* **2008**, *1*, 851–857. e) S. Ivanova, E. Vanhaecke, L. Dreibine, B. Louis, C. Pham-Huu, *Appl. Catal. A* **2009**, *359*, 151–157. f) Y. Jiao, C. Jiang, Z. Yang, J. Zhang, *Microporous Mesoporous Mater.* **2012**, *162*, 152–158.
- [118] a) A. Zampieri, H. Sieber, T. Selvam, G. T. P. Mabande, W. Schwieger, F. Scheffler, M. Scheffler, P. Greil, *Adv. Mater.* **2005**, *17*, 344–349. b) A. Zampieri, G. T. P. Mabande, T. Selvam, W. Schwieger, A. Rudolph, R. Hermann, H. Sieber, P. Greil, *Mater. Sci. Eng. C* **2006**, *26*, 130–135. c) M. W. Anderson, S. M. Holmes, N. Hanif, C. S. Cundy, *Angew. Chem. Int. Ed.* **2000**, *39*, 2707–2710.

1.6.2. Silicon-containing supports

The *in-situ* hydrothermal process is advantageous because the supports are used as a basis for nucleation and a chemical/covalent bonding between the zeolite crystals and the outer layer of supports is formed. A natural transition from the support to the zeolite layer and consequently a high thermal, chemical and mechanical stability of the composite can be achieved. Despite the numerous reports on zeolite coatings over ceramics, zeolite coatings on siliceous materials did not receive much attention, due to the possible support dissolution in alkaline media. However, the presence of silicon in the composition represents a great advantage for the coating process. Indeed, with such siliceous-containing supports, any pre-treatment of the support is required to obtain a chemical link between the zeolite crystals and the support surface. Glass monoliths and silicon carbide (SiC) supports could therefore be promising materials. Figure 1.20 shows several shapes of glass and SiC supports.

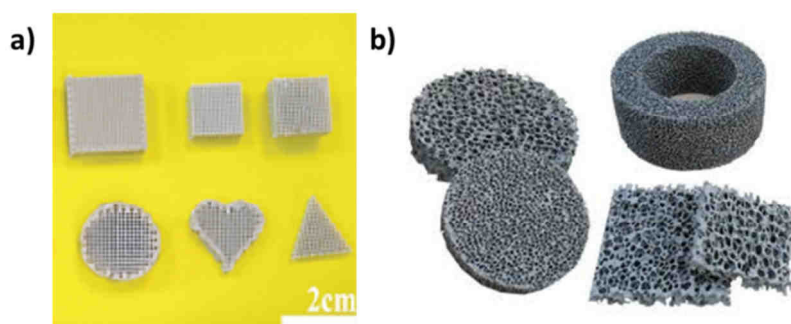


Figure 1.20 Macroscopic shapes of a) glass monoliths and b) SiC foams

Glass exhibits a high mechanical strength as well as relative thermal and chemical stability. Since these supports contain Si units, a higher affinity between crystalline Si material and amorphous Si support can be expected. Thus, crystallization of zeolites on porous glass in alkaline media has already been reported [119]. The glass matrix is partially transformed into zeolite, forming a biphasic composite with a bimodal pore system. The

[119] a) B. Louis, C. Tezel, L. Kiwi-Minsker, A. Renken, *Catal. Today* **2001**, *69*, 365–370. b) W. Schwieger, M. Rauscher, R. Monnig, F. Scheffler, D. Freude, *Stud. Surf. Sci. Catal.* **2000**, *129*, 121–130. c) B. Louis, F. Ocampo, H. Yun, J.-P. Tessonnier, M. M. Pereira, *Chem. Eng. J.* **2010**, *161*, 397–402.

synthesis procedure takes place in basic media at high pH [117a,120]. The gel is formed from the silica source present in the synthesis mixture (*i.e.*, TEOS) and condenses onto the support. This layer creates a nutrient-rich environment for zeolite nucleation, which is mediated by the template cations [121]. However, the strong basicity of the zeolite growth medium renders less effective the use of silica or alumina supports due to their partial dissolution, leading both to the deterioration of the support and a modification of the gel composition [119a].

Among the various types of monoliths, silicon carbide exhibits the necessary intrinsic properties required to become a valuable candidate as zeolite support: high thermal conductivity and mechanical resistance, chemical inertness, and ease of shaping [122]. Macroporous SiC structures can be coated with microporous or micro-mesoporous zeolites to obtain a hierarchical system at two (macro-/micro-) or even three levels (macro-/meso-/micro-) of porosity, respectively. The synthesis of zeolite/SiC composites implies to have a strong affinity between the zeolite crystals and the SiC surface.

Finally, the *in-situ* hydrothermal process on silicon-containing supports exhibits the possibility to grow zeolite crystals without the use of an additional silica source. Indeed, the silicon atoms present at the outer surface of the support can be used as nutrients for the zeolite nucleation. Indeed, zeolite layer formation was thought to be initiated by dissolution of the siliceous support. Louis *et al.* reported the preparation of zeolite coatings on glass and SiC supports without the use of silica source [111b,117c,119a,123]. Unfortunately in many cases, the final zeolite topology can barely be predicted.

[120] a) K. Okada, Y. Kameshima, C. D. Madhusoodana, R. N. Das, *Sci. Technol. Adv. Mater.* **2004**, *5*, 479–484. b) F.-C. Buciuman, B. Kraushaar-Czarnetzki, *Catal. Today* **2001**, *69*, 337–342. c) J. E. Antia, R. Govind, *Appl. Catal. A* **1995**, *131*, 107–120.

[121] J. H. Koegler, A. Arafat, H. van Bekkum, J. C. Jansen, *Stud. Surf. Sci. Catal.* **1997**, *105*, 2163–2170.

[122] a) M.-J. Ledoux, J.-L. Guille, S. Hantzer, D. Dubots, *Process for the Production of Silicon Carbide with a Large Specific Surface Area and Use for High-Temperature Catalytic Reactions*, **1990**, US4914070. b) M. J. Ledoux, C. Pham-Huu, *Cattech* **2001**, *5*, 226–246. c) M. Lacroix, P. Nguyen, D. Schweich, C. Pham Huu, S. Savin-Poncet, D. Edouard, *Chem. Eng. Sci.* **2007**, *62*, 3259–3267.

[123].a) P. Losch, M. Boltz, K. Soukup, I.-H. Song, H. S. Yun, B. Louis, *Microporous Mesoporous Mater.* **2014**, *188*, 99–107.

1.7 Conclusions

In this first section, an overview of the general properties of zeolites (structure, synthesis, acidity) was reminded. Major attention was paid to ZSM-5 and FAU zeolites which exhibit non exhaustive properties.

The preparation and properties of hierarchical zeolites were also presented. Two main routes can lead to the formation of mesoporosity within zeolite crystals, *i.e.* the constructive and the destructive routes.

Finally, another way to obtain structured zeolites by coating methods was shown. Zeolite coatings can be prepared in many ways, but the most versatile and promising method appears to be the *in-situ* synthesis on silicon-containing supports.

2. Zeolites = solid acid catalysts

2.1 Introduction

Zeolites are crystalline materials exhibiting ordered interconnected microporous channels with openings ranging from 0.2 to 2.0 nm. By virtue of their structure; *i.e.*, microporosity, surface area, acidity, *etc.*, they find useful applications in all fields of human life where chemical, biochemical and physicochemical processes are involved.

Nowadays, hydrocarbon transformations such as cracking, alkylation, and isomerization are preferably conducted over these environmental-friendly catalysts [124]. On the other hand, organic chemistry is increasingly moving toward “green chemistry”, where both homogeneous and heterogeneous catalysis are at the core of this concept [125]. The search for alternative cleaner, safer, and environmentally friendly technologies is one of the priorities in chemistry. Bearing this in mind, the reduction of waste along with the use of

[124] a) T. F. Degnan, *Top. Catal.* **2000**, *13*, 349–356. b) J. Weitkamp, *Solid State Ionics* **2000**, *131*, 175–188.

[125] P. T. Anastas, T. C. Williamson, in *Green Chemistry* (Eds.: P.T. Anastas, T.C. Williamson), American Chemical Society, Washington, DC, **1996**, pp. 1–17.

renewable feedstocks, green reagents and catalysts are important parameters to achieve more sustainable processes [126]. Heterogeneous catalysts are promising candidates to attain such improvements. In particular, thanks to their internal porosity, zeolites provide a highly organized channel structure as well as high thermal stability and strong acidity. The combination of these properties led them to exhibit high conversions and selectivities to produce bulk and fine chemicals [127].

The research work described in this Thesis focuses on the design in acid catalysis of new zeolite materials with improved properties. Hence, the catalytic activity of our home-made zeolites was evaluated in two different applications: (i) the chlorination of aromatics; and (ii) the conversion of methanol into hydrocarbons. The state of the art of both applications is reminded below.

2.2 Chlorination of aromatics

2.2.1. Generalities

Halogenation relies in the incorporation of halogen atoms in organic compounds. There are several processes for the halogenation of organic compounds, including free radical halogenation, ketone halogenation, electrophilic halogenation, and halogen addition reaction. The halogenation of aromatics can be classified in the family of electrophilic substitution reactions [128]. Both the regioselectivity and rate of these reactions depend upon the nature of existing substituent which can be *ortho*-, *meta*- or *para*-selective. In terms of regioselectivity, some substituent/group can promote the substitution at the *ortho*- and *para*-positions or at the *meta*-position. Substituents can generally be divided into two classes regarding electrophilic substitution, *i.e.*, activating and deactivating towards the aromatic ring. Thus, groups with unshared pairs of electrons, such as methoxy- or amino-

[126] a) I. T. Horváth, P. T. Anastas, *Chem. Rev.* **2007**, *107*, 2167–2168. b) I. T. Horváth, P. T. Anastas, *Chem. Rev.* **2007**, *107*, 2169–2173.

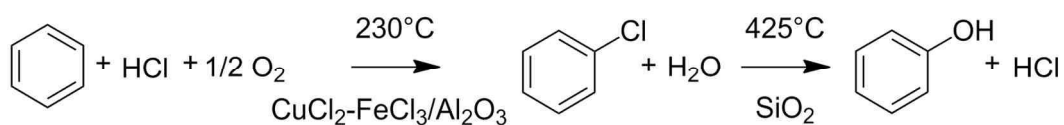
[127] a) N. Y. Chen, W. E. Garwood, F. G. Dwyer, Eds., *Shape Selective Catalysis in Industrial Applications, Second Edition*, Marcel Dekker, Inc., New York, United States of America, **1996**. b) B. Louis, G. Laugel, P. Pale, M. M. Pereira, *ChemCatChem* **2011**, *3*, 1263–1272. c) M. J. Climent, A. Corma, S. Iborra, *Chem. Rev.* **2011**, *111*, 1072–1133.

[128] J. Clayden, N. Greeves, S. Warren, P. Wothers, *Organic Chemistry*, Oxford University Press Inc., New York, **2001**, pp. 547.

group, are strongly activating thanks to their electron-donating effect and *ortho*-/*para*-directing substituents. However, halogens having unshared pairs of electrons are also *ortho*-/*para*-directors but their electron-withdrawing effect destabilizes the aromatic ring. For this reason, they are considered as deactivating groups. On the other hand, groups being more electronegative than carbon atom and having strong electron-withdrawing effect, such as nitro- or carboxylic acid groups, are strongly deactivating and *meta*-directing groups. Deactivating substituents destabilize the intermediate cation during the reaction and thus decrease the reaction rate.

Organic halides present a great synthetic interest. They can be efficiently converted into other functionality by well-known methodologies, such as halogen-metal exchange, palladium-catalyzed reaction for new C-C bond formation, nucleophilic substitution, *etc.* [129]. Chloroarenes are valuable starting molecules in fine chemistry, for the synthesis of dyes, bio-active compounds such as pesticides or pharmaceuticals [130]. Unfortunately, the conventional industrial methods used for the chlorination of aromatics usually produce mixtures of regioisomers, difficult to separate, thus raising the costs [131].

One can cite the industrial Raschig-Hooker process, developed in the 30s, which was a chemical process for the production of phenol [132]. This process, no longer used in industry, consisted of the chlorination of benzene at 230 °C by a vapor phase composed of HCl and air in the presence of Al₂O₃-supported Cu-Fe catalyst (Scheme 1.2). In a second step, the chlorobenzene was hydrolyzed over silica at 425 °C to obtain phenol.



Scheme 1.2 Raschig process

[129] P. L. Spargo, *Contemp. Org. Synth.* **1994**, *1*, 113–124.

[130] a) H.-G. Franck, J. W. Stadelhofer, Eds., *Industrial Aromatic Chemistry: Raw Materials*, Springer-Verlag, Berlin Heidelberg, **2011**, pp. 224–226.

[131] H.-G. Franck, J. W. Stadelhofer, Eds., *Industrial Aromatic Chemistry: Raw Materials*, Springer-Verlag, Berlin Heidelberg, **2011** pp 218–220.

[132] A. Chauvel, G. Lebfèvre, L. Castex, *Procédés de pétrochimie Tome 2*, Edition Technip, **1985**.

2.2.2. Chlorination agent

Several reagents are known for the chlorination of activated and deactivated arenes [133]. Indeed, one can cite electrophilic chlorination procedures of fairly broad scope (with respect to the substrate), which generally provide high yield and include the use of N-chlorosuccinimide with catalytic perchloric acid or N-chloro-saccharin with pyridinium poly(hydrogen fluoride) [129]. Recently, Prakash developed a more efficient chlorination procedure [134]. Indeed, they efficiently halogenated aromatics including deactivated ones using the N-halosuccinimide/BF₃-H₂O system at room temperature. Rodriguez *et al.* reported the invention of new guanidine-based reagent, named “Palau’chlor”, for the direct electrophilic chlorination of heteroaromatic compounds [135].

Although several reagents introducing halogen atoms in organic substrates were demonstrated to be efficient, the typical route to prepare vicinal dihalo compounds remains the electrophilic molecular halogen (X₂) addition to alkenes. For chlorination of organic molecules, molecular chlorine (Cl₂), as chlorine source produces a large quantity of non-recyclable wastes. Such halogens are corrosive, difficult to handle and strong oxidants [136]. Another disadvantage is the use of toxic acid catalysts such as Lewis acids (aluminum chloride or boron trifluoride), which are consumed and need to be neutralized after the reaction. In parallel, strong Brønsted acid catalysts such as H₂SO₄ remain very corrosive and generate a lot of salts.

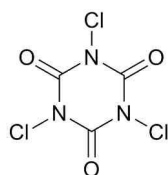
Among all these chlorination agents, trichloroisocyanuric acid (TCCA, C₃N₃O₃Cl₃) represents a stable and inexpensive solid, easily available in pool supplies, being thus frequently used as swimming-pool disinfectant and bleaching agent (Scheme 1.3).

[133] F. A. Carey, R. J. Sundberg, Eds., in *Advanced Organic Chemistry: Part B: Reaction and Synthesis*, 5th Ed., Springer, New York, **2007**, pp. 1008–1014.

[134] G. K. S. Prakash, T. Mathew, D. Hoole, P. M. Esteves, Q. Wang, G. Rasul, G. A. Olah, *J. Am. Chem. Soc.* **2004**, *126*, 15770–15776.

[135] R. A Rodriguez, C.-M. Pan, Y. Yabe, Y. Kawamata, M. D. Eastgate, P. S. Baran, *J. Am. Chem. Soc.* **2014**, *136*, 6908–6911.

[136] R. Stringer, P. Johnston, Eds., *Chlorine and the Environment: An Overview of the Chlorine Industry*, Kluwer Academic Publishers, Dordrecht, **2001**, pp. 14-17.



Scheme 1.3 Trichloroisocyanuric acid

It is an efficient chlorine source due to its high chlorine content, being 45.5% in weight, allowing *a priori* a higher atomic efficiency than its N-chloro analogues [137]. TCCA was successfully used for chlorination of electron-rich arenes [137], alkenes [138], carbonyl compounds [139], preparation of N-chloro substrates [140] and in diverse oxidation reactions [141]. The reaction with deactivated arenes is only possible under strong acidic conditions [138a], the reactivity being highly influenced by the acidity of the reaction medium [142]. For instance, nitrobenzene was fully brominated to pentabromonitrobenzene by TCCA in 2 min at room temperature by using 65% oleum as solvent [143]. Other impressive results are the electrophilic chlorination [138a], bromination [143], and iodination [144] of m-dinitrobenzene respectively by TCCA, TBCA and TICA in 98% H₂SO₄, which afforded the corresponding halogenated products in good yields.

2.2.3. Chlorination over solid catalysts

The beneficial effects of solid surfaces on the rates of halogenation reactions were observed more than 75 years ago. The nature of heterogeneous catalysts used is broad but the most popular include silica, alumina, activated carbon and chromia [145]. The use of

[137] a) G. F. Mendonça, M. C. S. de Mattos, *Quim. Nov.* **2008**, *31*, 798–801. b) G. F. Mendonça, M. C. S. de Mattos, *Curr. Org. Synth.* **2013**, *10*, 820–836. c) A. Hubbard, T. Okazaki, K. K. Laali, *Aust. J. Chem.* **2007**, *60*, 923–927.

[138] a) S. D. F. Tozetti, L. S. de Almeida, P. M. Esteves, M. C. S. de Mattos, *J. Braz. Chem. Soc.* **2007**, *18*, 675–677. b) G. F. Mendonça, A. M. Sanseverino, M. C. S. De Mattos, *Synthesis* **2003**, 45–48.

[139] G. A. Hiegel, K. B. Peyton, *Synth. Commun.* **1985**, *15*, 385–392.

[140] a) L. De Luca, G. Giacomelli, *Synlett* **2004**, 2180–2184. b) A. Shiri, A. Khoramabadi-zad, *Synthesis* **2009**, 2797–2801.

[141] U. Tilstam, H. Weinmann, *Org. Process Res. Dev.* **2002**, *6*, 384–393.

[142] G. F. Mendonça, M. R. Senra, P. M. Esteves, M. C. S. de Mattos, *Appl. Catal. A* **2011**, *401*, 176–181.

[143] L. S. de Almeida, P. M. Esteves, M. C. S. de Mattos, *Tetrahedron Lett.* **2009**, *50*, 3001–3004.

[144] R. S. da Ribeiro, P. M. Esteves, M. C. S. de Mattos, *Synthesis* **2011**, 739–744.

[145] P. Ratnasamy, A. P. Singh, in *Handbook of Heterogenous Catalysis, Volume 1* (Eds.: G. Ertl, H. Knözinger, F. Schüth, J. Weitkamp), Wiley-VCH Verlag GmbH & Co. KGaA, Weinheim, Germany, **2008**, pp. 3564–3578.

zeolites in halogenation reactions began in the early 1970s. Hölderich reviewed the halogenation of arenes over aluminosilicates [146]. Most of the examples presented in this review showed high degree of selectivity with lower *o/p* ratios of isomers than conventional catalysts such as FeCl₃. Despite these interesting results, halogenation in the presence of hydrogen halides causes irreversible damage in the zeolite structure [147]. In 1999, Smith *et al.* reported a chlorination procedure using zeolites as catalyst [148]. Indeed, they performed the monochlorination of a wide range of aromatic substrates at mild conditions in the presence of various chlorination agents. Singh *et al.* performed several studies between 1996 and 2002 on the chlorination of various substituted-benzenes [149]. The *para*-selective chlorination of cumene over K-L zeolite was performed [149c]. They tested two different conditions, either in the presence of sulfuryl chloride (SO₂Cl₂) or with chloroacetic acid combined with gaseous chlorine, allowing a cumene conversion of nearly 30% and 70%, respectively. When SO₂Cl₂ was used as chlorinating agent, the electrophile, Cl⁺, is generated by the dissociation of SO₂Cl₂, which can act itself as chlorinating agent.

2.2.4. Conclusions

The chlorination reagent, TCCA, appears to be a valuable option for the chlorination of activated and deactivated aromatics. The different papers on the use of TCCA as chlorination agent have shown a great efficiency and a more eco-friendly behavior for the chlorination of various molecules compared with conventional catalysts used in industry.

In addition, halogenations over heterogeneous catalysts present many advantages, leading to a great potential of solid catalysts for nuclear halogenations (especially chlorination and bromination) of aromatics in the liquid phase with respect to Lewis acid catalysts (*i.e.*, AlCl₃ and FeCl₃). The use of zeolites in such cases might lead to enhanced yields in *para*-isomer, thus lowering not only the formation of byproducts but also the separation costs.

[146] W. Hölderich, M. Hesse, F. Näumann, *Angew. Chem. Int. Ed.* **1988**, *27*, 226–246.

[147] T. M. Wortel, D. Oudijn, C. J. Vleugel, D. P. Roelofsen, H. van Bekkum, *J. Catal.* **1979**, *60*, 110–120.

[148] a) K. Smith, M. Butters, W. E. Paget, D. Goubet, E. Fromentin, B. Nay, *Green Chem.* **1999**, *1*, 83–90.

[149] a) P. Ratnasamy, A. P. Singh, S. Sharma, *Appl. Catal. A* **1996**, *135*, 25–55. b) S. Sharma, S. G. Hegde, A. P. Singh, *Appl. Catal. A* **1997**, *162*, 201–211. c) A. P. Singh, S. Sharma, S. M. Kale, *J. Mol. Catal. A* **1997**, *127*, 101–111. d) S. M. Kale, A. P. Singh, *Appl. Catal. A* **2002**, *228*, 1–13.

2.3 Methanol-To-Olefins reaction

2.3.1. Generalities

Nowadays, the world global energy is largely based on fossil fuel resources. Oil, coal and natural gas represent nearly 80% of the global energy consumption, petroleum being the highest (35%). However, those fossil fuel reserves will (in a more or less close future) disappear: 40 years expected for oil, 70 years for natural gas and around 170 years for coal at the present rate of consumption [150]. In addition, oil also serves as an important feedstock for the production of numerous key petrochemical building blocks [150].

With the raise in energy demand, technologies producing liquid hydrocarbon fuels play an important role in the global energy chain and are therefore attractive. From this perspective, biomass, natural gas, carbon dioxide and coal appear to be alternate carbon sources. Hence, different transformations of these carbon feedstocks may serve as alternative to oil as for instance in the methanol production. Methanol is indeed an attractive product to diminish the dependence on fossil fuels and the lack of energy sources. This simple molecule, safe and easy to store, can be a promising candidate for efficient oil and natural gas resource utilizations. Methanol is mainly synthesized from synthesis gas (syngas mixture of carbon monoxide and hydrogen) which is obtained from steam reforming of natural gas or coal gasification. Besides, methanol can also be prepared from biomass. The so-called “wood alcohol” can be directly used as an oxygenated additive for gasoline or converted *via* a catalytic step into liquid hydrocarbons.

With the oil crisis in the 70s, the methanol-to-hydrocarbons (MTH) technology became a powerful tool to produce either gasoline (methanol-to-gasoline; MTG) or olefins (methanol-to-olefins; MTO). In 1973, a new interest in synfuels and other chemicals appeared both in academia and industry [151]. During the same period, the development of ZSM-5 zeolite and its unique catalytic properties at the Mobil Oil company allowed them to discover by accident the MTG reaction [152]. While tempting to alkylate isobutane with methanol into different oxygen-containing compounds (like MTBE) over an acidic ZSM-5

[150] G. A. Olah, A. Goepfert, G. K. S. Prakash, *Beyond Oil and Gas: The Methanol Economy*, Wiley-VCH Verlag GmbH & Co. KGaA, **2009**.

[151] C. D. Chang, *Catal. Rev. Sci. Eng.* **1983**, *25*, 1–118.

[152] M. Stöcker, *Microporous Mesoporous Mater.* **1999**, *29*, 3–48.

catalyst; Mobil researchers were surprised to obtain liquid hydrocarbons, similar to the gasoline fraction. The MTG process was ready to be commercialized in 1985 [153]. The first plant (600 kton/year) has been established in New Zealand. The MTG process consists of two separated reactors. The first reactor allows the catalytic dehydration of methanol into an equilibrium of dimethyl ether and water. The second reactor allows to transform the former mixture into gasoline (paraffins, aromatics, naphthenes and olefins). The MTG reaction runs at approximately 400 °C under a methanol partial pressure of $2 \cdot 10^6$ Pa over a fixed-bed reactor. As the conversion of methanol is exothermic, reactors are operated under adiabatic conditions, the temperature being controlled by the recycling of light hydrocarbons. ZSM-5 zeolite used in the MTG process leads to a high selectivity in gasoline but an important coking phenomenon appears after few hours on stream. This deactivation can be controlled and the initial catalyst activity can be restored by setting up an in-situ regeneration. During this later step, the coke is burned off at high temperature. One can notice that light olefins are produced in the methanol-to-hydrocarbons (MTH) process as important intermediates. The fluidized-bed version of the MTH process generates a higher thermal efficiency and induces substantial gain in octane number with respect to the fixed-bed technology [153c].

Another ZSM-5 based process is the Mobil Olefin to Gasoline and Distillate (MOGD) process, originally developed as a refinery process, which operates in parallel to the MTO process. In the MOGD plant, ZSM-5 zeolite catalyzes the oligomerization of light olefins, from either refinery streams or MTO, into higher molecular weight olefins that conduct to gasoline and middle-distillate products. High octane MTO gasoline is separated before the MOGD reactor and blended with MOGD gasoline. Generally, the process intensification involves four fixed-bed reactors: three on-operation plus one working in a regeneration mode. A large-scale MOGD refinery test run was conducted by Mobil in 1981 (Figure 1.21).

[153] a) S. Yurchak, *Stud. Surf. Sci. Catal.* **1988**, 36, 251–272. b) C. D. Chang, *Catal. Today* **1992**, 13, 103–111. c) H. A. Zaidi, K. K. Pant, *Catal. Today* **2004**, 96, 155–160.

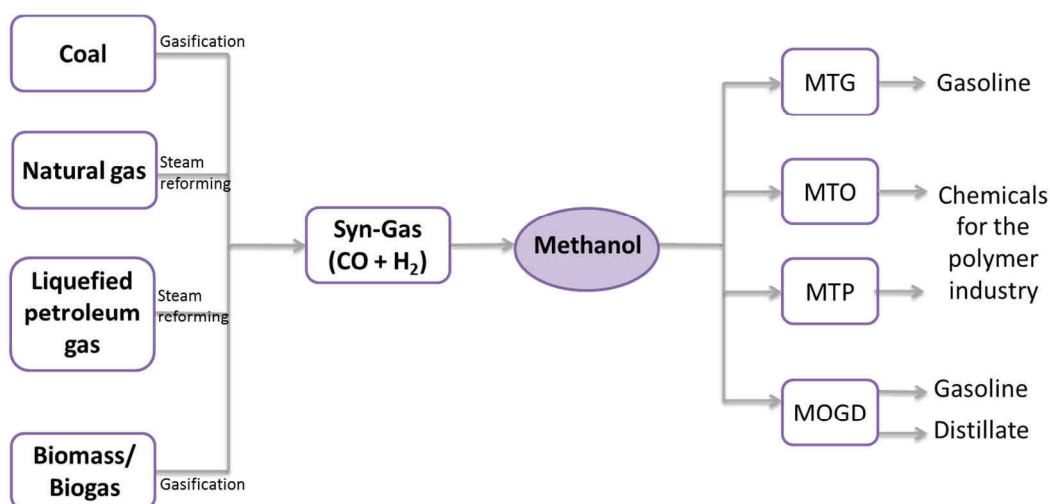


Figure 1.21 Production route of methanol up to its conversion into raw chemicals

A MTG alternative process, developed in the mid-80s by Haldor Topsøe, called Topsøe Integrated Gasoline Synthesis (TIGAS) is based on the conversion of syngas into gasoline *via* a single-loop process, thus eliminating the need for upstream methanol production and intermediate storage [154]. Figure 1.22 shows the principal differences between the Mobil MTG process and the TIGAS process.

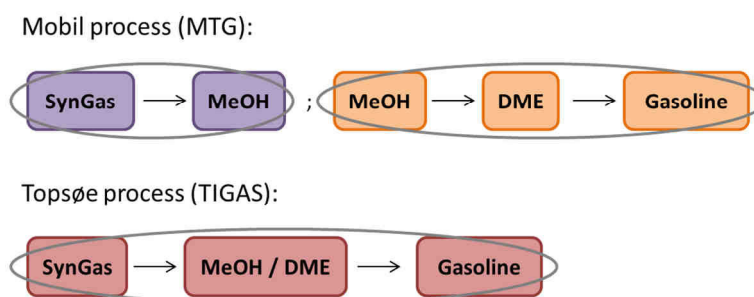


Figure 1.22 Schematic representation of the Mobil and the TIGAS processes

The discovery of small pore zeolite analogues, SAPO type molecular sieves, led to the development of a new process, derived from the MTG reaction: the methanol-to-olefins technology (MTO). Union Carbide scientists found out that H-SAPO-34 zeolite significantly improved the selectivity towards light olefins (ethylene and propylene). By properly adjusting the reaction conditions, as raising the temperature to 500 °C and changing the

[154] J. Topp-Joergensen, *Stud. Surf. Sci. Catal.* **1988**, 36, 293–305.

catalyst, the olefin yield could exceed 80% with high-octane gasoline as major by-product. Such results led to the development of the MTO technology. The conversion of methanol into light olefins proceeds through the dehydration of methanol to dimethyl ether (DME), which then reacts further over the catalyst to produce ethylene and propylene. In the nineties, UOP and Norsk Hydro (now INEOS) improved the MTO reaction by using the H-SAPO-34 catalyst in a low-pressure fluidized-bed reactor that allowed an efficient temperature control and a continuous regeneration [155]. The MTO process is now ready for commercialization, UOP has launched a SAPO-34 based MTO process of nearly 250 ktons per year plant in Nigeria. Thanks to its collaboration with UOP, Total Petrochemicals has achieved an increase in ethylene/propylene selectivity by combining the UOP/INEOS process with an olefin cracking process (OCP). A demonstration unit in Belgium (Feluy), has been built in 2009 processing 10 tons per day methanol feed and a construction of a plant (295 kt per year) was announced in China in 2011. Another plant developed by researchers at Dalian Institute of Chemical Physics, based on SAPO-34 zeolite and a recirculation of C₄₊ olefins to improve ethylene/propylene yield (DMTO process), was constructed in 2010 in China (Baotou). Finally, the development of a MTO process based on H-ZSM-5 catalyst by Lurgi was also settled [156]. This technology promotes propylene selectivity and will become a new process named methanol-to-propylene (MTP). Undesired products, such as ethylene and butenes are recycled thanks to parallel fixed-bed reactors. The first plant has been developed in China in 2010 with a production of 500 kt propylene per year.

2.3.2. Development of tailored MTO-catalysts

In this section, we will focus on the different strategies for MTO catalysts development. The design of a catalyst remains an important task to achieve a competitive process in terms of conversion and selectivity. To tailor the properties, one has to tune the following features:

[155] U. Olsbye, S. Svelle, M. Bjørgen, P. Beato, T. V. W. Janssens, F. Joensen, S. Bordiga, K. P. Lillerud, *Angew. Chem. Int. Ed.* **2012**, *51*, 5810–5831.

[156] http://www.lurgi.com/website/fileadmin/user_upload/pdfs/19_Methan-Propylen-E_rev060707.pdf

- * acidity nature, density and strength
- * pore topology (channel type, cages, pore openings)
- * morphology, crystal size
- * porosity (micro- and/or mesoporosities)
- * chemical composition (metal doping), coatings.

Only the most representative catalysts are listed and discussed in this section.

The MTH reactions have been studied over different kinds of zeolites or molecular sieves and metal oxides. H-ZSM-5 and H-SAPO-34 are the key zeolites used [157,158]. Both microporous solids exhibit well-defined three-dimensional crystalline structures. Figure 1.23 [159] presents these two catalysts, ZSM-5 (MFI topology) and SAPO-34 (CHA topology), which possess Brønsted acid sites located within ordered micropores of molecular dimensions. H-ZSM-5 zeolite is an aluminosilicate possessing a 3D pore structure consisting of 10 T-atoms. Its pore openings are classified as medium, having 5.5 Å in diameter, whilst H-SAPO-34 zeolite-type material is a small-pore silicoaluminophosphate consisting of 8-ring channels with a cage structure and a pore size of only 3.8 Å. These two zeolites allow shape selectivity, being thus able to promote the formation of small products like light olefins. The presence of small cavities and restricted space within the framework of zeolites can hinder the diffusion and also the formation of larger molecules. Hence this can induce a high selectivity into light and linear olefins as propylene and ethylene. Since aromatics and branched hydrocarbons are too large to easily diffuse throughout the pore network, light olefins are naturally predominant in the product streams [160]. For instance, ZSM-5 allows an easier formation and diffusion of para-xylene than SAPO-34. In contrast a CHA-type zeolite exhibits a faster deactivation by coke formation, than the MFI structure, *via* pore blocking.

[157] a) H.-G. Jang, H.-K. Min, J. K. Lee, S. B. Hong, G. Seo, *Appl. Catal. A* **2012**, 437–438, 120–130. b) M. Bjørgen, S. Svelle, F. Joensen, J. Nerlov, S. Kolboe, F. Bonino, L. Palumbo, S. Bordiga, U. Olsbye, *J. Catal.* **2007**, 249, 195–207.

[158] a) D. Chen, A. Grønvold, K. Moljord, A. Holmen, *Ind. Eng. Chem. Res.* **2007**, 46, 4116–4123. b) N. Fatourehchi, M. Sohrabi, S. J. Royaei, S. M. Mirarefin, *Chem. Eng. Res. Des.* **2011**, 89, 811–816. c) Z. Liu, J. Liang, *Curr. Opin. Solid State Mater. Sci.* **1999**, 4, 80–84.

[159] <http://www.iza-structure.org/databases/>

[160] a) D. Chen, K. Moljord, T. Fuglerud, A. Holmen, *Microporous Mesoporous Mater.* **1999**, 29, 191–203. b) J. W. Park, J. Y. Lee, K. S. Kim, S. B. Hong, G. Seo, *Appl. Catal. A* **2008**, 339, 36–44. c) B. P. C. Hereijgers, F. L. Bleken, M. H. Nilsen, S. Svelle, K.-P. Lillerud, M. Bjørgen, B. M. Weckhuysen, U. Olsbye, *J. Catal.* **2009**, 264, 77–87.

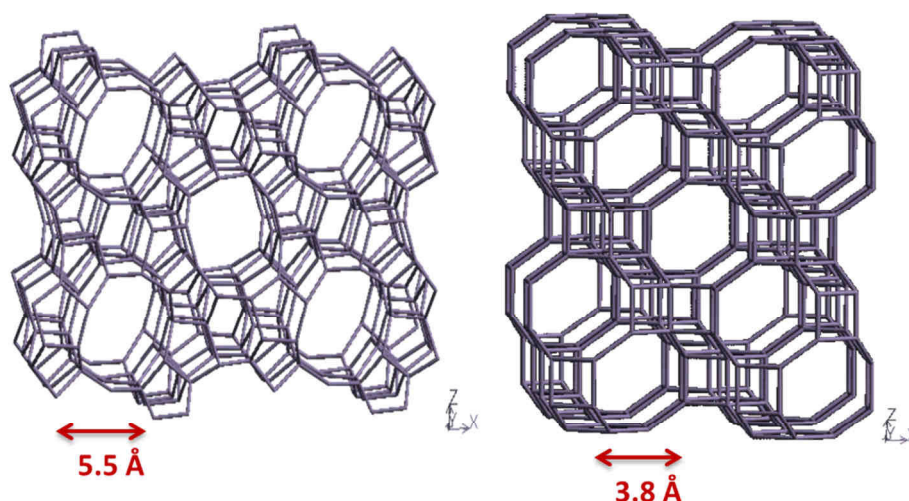


Figure 1.23 Schematic structures of ZSM-5 (left) and SAPO-34 (right) zeolites [159]

2.3.2.1. Acid strength and acid site density

It is important to note how framework atoms may change the acidity of a given material. The framework of SAPO-34 and SSZ-13 is the same. The nature of the T-atoms is the sole parameter that differs and hence influences the acidity. All materials of interest possess medium-to-high Brønsted acidity. MOR and BEA zeolites with 12-membered rings have been tested in spite of being rather non-effective catalysts for the MTO reaction, inducing low selectivity in light olefins and fast deactivation. However, MOR zeolite with a low Brønsted acid site density, modified by the removal of framework aluminum atoms, exhibited slower deactivation rate and higher selectivity in light olefins [161]. Likewise the careful dealumination of MOR zeolite to reduce its acid site density without destroying its pore structure could maintain its activity in the course of the MTO reaction. Park *et al.* [161c] showed that MOR zeolites, having low acid site densities, exhibited rather good selectivities and activities toward olefins. The low acid site density of these MOR zeolites improved the resistance toward deactivation by coking. Nevertheless, selectivities in ethylene and propylene remained always lower with respect to SAPO-34 material.

[161] a) Ø. Mikkelsen, S. Kolboe, *Microporous Mesoporous Mater.* **1999**, 29, 173–184. b) M. Bjørgen, S. Kolboe, *Appl. Catal. A* **2002**, 225, 285–290. c) J. W. Park, S. J. Kim, M. Seo, S. Y. Kim, Y. Sugi, G. Seo, *Appl. Catal. A* **2008**, 349, 76–85.

It is noteworthy that strong acid sites are mainly responsible for aromatization reactions, and thus for deactivation by coking [162]. Many authors have reported that catalyst deactivation occurs when both acid density and strength were high. For these reasons, the MTO process requires a catalyst with moderate acidity and the design of the catalyst has to take into account both the strength and the density of the acid sites. Bleken *et al.* [163] have recently reported the influence of acid strength on the stability and product selectivity of two microporous catalysts having CHA framework type, SSZ-13 and SAPO-34. These two CHA analogues presented similar acid site densities and crystal sizes, but with different acid strength. The H-SSZ-13 catalyst led to a higher activity than H-SAPO-34 but exhibited a fast deactivation due to its higher acid strength. One can note the promising behavior of H-SSZ-13 allowing to achieve a high degree of methanol conversion at lower temperature.

2.3.2.2. Influence of the pore topology

The effects of pore structure and acidity of zeolites on their product distribution and deactivation rates in the MTO reaction were extensively studied and reported by several authors [164]. It is difficult to perform direct comparisons between deactivation rates for zeolites with different pore topologies since the simultaneous influence of other parameters is known to affect catalyst deactivation: acid strength, acid site density (section 2.1) and crystal size. Park *et al.* [160b] compared four kinds of 8-membered ring (8-MR) small-pore molecular sieves with CHA (SAPO-34), ERI (UZM-12), LTA (UZM-9), and UFI (UZM-5) topologies. These molecular sieves possess different cavities but almost the same Si/Al ratio (~ 6). The selectivity to light olefins was high over the 8-MR catalysts, regardless their topologies. However, the ERI, LTA, and UFI catalysts deactivated rapidly, while the CHA catalyst demonstrated an enhanced stability under these experimental conditions. Zeolites

[162] a) S. Wilson, P. Barger, *Microporous Mesoporous Mater.* **1999**, *29*, 117–126. b) D. Chen, K. Moljord, A. Holmen, *Microporous Mesoporous Mater.* **2012**, *164*, 239–250. c) H. Schulz, *Catal. Today* **2010**, *154*, 183–194.

[163] F. L. Bleken, M. Bjørgen, L. Palumbo, S. Bordiga, S. Svelle, K.-P. Lillerud, U. Olsbye, *Top. Catal.* **2009**, *52*, 218–228.

[164] a) J. F. Haw, D. M. Marcus, *Top. Catal.* **2005**, *34*, 41–48. b) J. W. Park, G. Seo, *Appl. Catal. A* **2009**, *356*, 180–188. c) J. Li, Y. Wei, G. Liu, Y. Qi, P. Tian, B. Li, Y. He, Z. Liu, *Catal. Today* **2011**, *171*, 221–228. d) Y. Bhawe, M. Moliner-Marin, J. D. Lunn, Y. Liu, A. Malek, M. E. Davis, *ACS Catal.* **2012**, *2*, 2490–2495.

with large cages exhibit a faster deactivation than those with smaller intersections due to the possible formation of large polycyclic aromatics and a certain ease in pore blocking. The catalytic performance of the CHA catalyst can be explained by its pores, which possess the right shape and size to keep active the intermediates. Likewise, Bleken *et al.* [165] compared four 3D 10-MR zeolites divided in two topology groups; IM-5, TNU-9 and ZSM-11, ZSM-5. While the former group presents zeolites with larger cavities, in contrast the later consists zeolites possessing smaller intersections (with similar channel sizes). IM-5 and TNU-9 deactivated faster than ZSM-11 and ZSM-5 zeolites. Indeed, IM-5 and TNU-9 led to a high amount of methylated aromatics and polyaromatics and the formation of those species was related to this fast deactivation. These results clearly confirmed the correlation between pore topology and deactivation due to the formation of bulky molecules trapped inside zeolite cavities.

2.3.2.3. Developments of doped or coated zeolites

Several contributions dealing with the doping of zeolites by metals as nickel or magnesium in the framework have been found to yield high ethylene selectivity in the MTO reaction [166]. The incorporation of such metals allows to adjust the concentration of acid sites [166c]. Djieugoue *et al.* [167] developed a Ni containing SAPO-34 catalyst which led to raise both ethylene selectivity and catalyst lifetime. Recently, Hua *et al.* [168] reported the synthesis of B-doped ZSM-5 zeolites with mild acidity to diminish the coking rate and therefore to raise the catalyst lifetime.

[165] F. L. Bleken, W. Skistad, K. Barbera, M. Kustova, S. Bordiga, P. Beato, K. P. Lillerud, S. Svelle, U. Olsbye, *Phys. Chem. Chem. Phys.* **2011**, *13*, 2539–2549.

[166] a) D. R. Dubois, D. L. Obrzut, J. Liu, J. Thundimadathil, P. M. Adekkanattu, J. A. Guin, A. Punnoose, M. S. Seehra, *Fuel Process. Technol.* **2003**, *83*, 203–218. b) J. M. Thomas, Y. Xu, C. R. A. Catlow, J. W. Couves, *Chem. Mater.* **1991**, *3*, 667–672. c) M. Salmasi, S. Fatemi, A. Taheri Najafabadi, *J. Ind. Eng. Chem.* **2011**, *17*, 755–761. d) S. Ahmed, *J. Porous Mater.* **2012**, *19*, 111–117.

[167] M.-A. Djieugoue, A. M. Prakash, L. Kevan, *J. Phys. Chem. B* **2000**, *104*, 6452–6461.

[168] Y. Yang, C. Sun, J. Du, Y. Yue, W. Hua, C. Zhang, W. Shen, H. Xu, *Catal. Commun.* **2012**, *24*, 44–47.

In the last decade, another efficient way to improve the stability of MTO catalysts relied on the development of zeolite coatings on various macroporous supports [169,170]. Different procedures for zeolite coatings on silicon carbide have been reported elsewhere [170a-c]. ZSM-5 coatings were performed on SiC, in the form of extruded pellets or foam monoliths and their performances were evaluated in the MTO reaction. Ivanova *et al.* [170a] have shown that an appropriate tailoring of the MFI coating over β -SiC, led to drastic variations in product selectivities ranging from a 98% selectivity in C₁-C₄ saturated hydrocarbons [170a] to a nearly 70% into C₂-C₄ olefins [170c].

In general, an important enhancement in the catalyst lifetime was achieved over these structured catalysts [170d,e]. Finally, a further raise in propylene selectivity compared with its non-coated counterpart could often be achieved [170b,d].

2.3.2.4. Mesoporous zeolites

The introduction of additional mesopores in the zeolite microporous network allows the enhancement of molecular transport to and from the active sites. Hence, a catalyst improvement might therefore be expected. Up to date, only few reports dealing with the strategies for preparation of zeolites containing mesopores were applied to the MTH reaction [171]. In 2001, Ohayon *et al.* [172] reported an application of ZSM-5 catalysts treated with Na₂CO₃ to create mesopores inside the zeolite structure. This treatment had a beneficial influence on light olefins selectivities with a 30% raise (relative value) with respect

[169] a) S. Lopez-Orozco, A. Inayat, A. Schwab, T. Selvam, W. Schwieger, *Adv. Mater.* **2011**, *23*, 2602–2615. b) P. Wang, A. Lv, J. Hu, J. Xu, G. Lu, *Ind. Eng. Chem. Res.* **2011**, *50*, 9989–9997.

[170] a) S. Ivanova, B. Louis, M.-J. Ledoux, C. Pham-Huu, *J. Am. Chem. Soc.* **2007**, *129*, 3383–3391. b) S. Ivanova, C. Lebrun, E. Vanhaecke, C. Pham-Huu, B. Louis, *J. Catal.* **2009**, *265*, 1–7. c) S. Ivanova, B. Louis, B. Madani, J.-P. Tessonnier, M.-J. Ledoux, C. Pham-Huu, *J. Phys. Chem. C* **2007**, *111*, 4368–4374. d) Y. Jiao, C. Jiang, Z. Yang, J. Zhang, *Microporous Mesoporous Mater.* **2012**, *162*, 152–158. e) S. Ivanova, E. Vanhaecke, B. Louis, S. Libs, M.-J. Ledoux, S. Rigolet, C. Marichal, C. Pham, F. Luck, C. Pham-Huu, *ChemSusChem* **2008**, *1*, 851–857.

[171] a) J. Bandiera, C. Naccache, *Appl. Catal.* **1991**, *69*, 139–148. b) M. Choi, K. Na, J. Kim, Y. Sakamoto, O. Terasaki, R. Ryoo, *Nature* **2009**, *461*, 246–249. c) L. Sommer, D. Mores, S. Svelle, M. Stöcker, B. M. Weckhuysen, U. Olsbye, *Microporous Mesoporous Mater.* **2010**, *132*, 384–394. d) C. Sun, J. Du, J. Liu, Y. Yang, N. Ren, W. Shen, H. Xu, Y. Tang, *Chem. Commun.* **2010**, *46*, 2671–2673. e) C. Mei, P. Wen, Z. Liu, H. Liu, Y. Wang, W. Yang, Z. Xie, W. Hua, Z. Gao, *J. Catal.* **2008**, *258*, 243–249. f) L. Wu, V. Degirmenci, P. C. M. M. Magusin, B. M. Szyja, E. J. M. Hensen, *Chem. Commun.* **2012**, *48*, 9492–9494.

[172] D. Ohayon, R. Le van Mao, D. Ciaravino, H. Hazel, A. Cochenec, N. Rolland, *Appl. Catal. A* **2001**, *217*, 241–251.

to pristine zeolite. Bjørgen *et al.* [173] obtained an improved catalyst performance over mesoporous MFI materials synthesized by desilication with NaOH. Selectivity towards the gasoline fraction was increased by a factor of 1.7. In 2010, Ryoo *et al.* [174] investigated numerous MFI zeolites with different degrees of mesoporosity generated by using organosilane surfactants, along with desilication treatment and sacrificial carbon template use. The MTH catalytic activity did not change significantly but catalyst lifetime could be extended more than three times [174].

2.3.3. Mechanism of the MTO reaction

During the past three decades, many studies have been focused on MTH mechanisms understanding [152,155,175,176]. Herein, the major propositions described in the literature are summarized.

The initial step in the MTO reaction is the acid-catalyzed dehydration of methanol into dimethyl ether (DME), thus forming an equilibrium mixture composed of methanol, DME and water. This mixture reacts further to produce light olefins: ethylene, propylene and butenes. After, those light olefins can be further converted to produce higher olefins, alkanes and aromatics by several alkylation aromatization and/or polycondensation reactions (Figure 1.24).

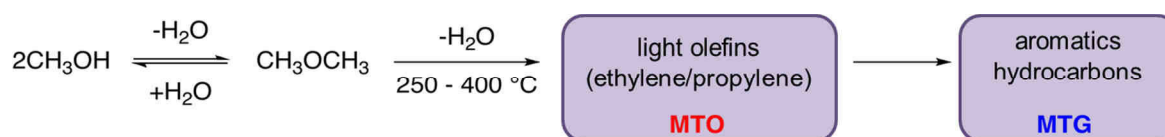


Figure 1.24 Principal steps occurring in the conversion of methanol to olefins

[173] M. Bjørgen, F. Joensen, M. Spangsborg Holm, U. Olsbye, K.-P. Lillerud, S. Svelle, *Appl. Catal. A* **2008**, *345*, 43–50.

[174] J. Kim, M. Choi, R. Ryoo, *J. Catal.* **2010**, *269*, 219–228.

[175] M. Stöcker, in *Zeolites and Catalysis* (Eds.: J. Čejka, A. Corma, S. Zones), Wiley-VCH Verlag GmbH & Co. KGaA, Weinheim, **2010**, pp. 687–711.

[176] J. F. Haw, W. Song, D. M. Marcus, J. B. Nicholas, *Acc. Chem. Res.* **2003**, *36*, 317–326.

The understanding of the first step occurring in the MTO reaction constitutes a general consensus where the intermediate in the dehydration of methanol to DME over solid acids is a protonated surface methoxy group, being subject to a nucleophilic attack by methanol [152]. Nevertheless, the second step yielding the first C-C bond formation from C₁ reactants has been widely debated. Numerous researchers have focused their studies on the mechanism and according to Stöcker [152] more than 20 possible mechanisms have been proposed to explain this first C-C bond formation. Among those mechanisms, one can mention oxonium ylide [177], carbene [178], carbocationic [179], and free radical mechanism [180].

The first proposal supposed an activation of methanol on the catalyst to form a carbenium ion: CH₃⁺, or a carbene: CH₂. Several free radical routes were also suggested as possible pathways for the direct conversion of methanol to species which containing the first C-C bond [181]. To illustrate one of these possible pathways, the oxonium ylide mechanism has been the matter of peculiar attention, involving the interaction between DME and a Brønsted acid site of the catalyst thus forming a dimethyloxonium ion intermediate, which reacts further with another DME molecule to generate a trimethyloxonium ion. The following step is a deprotonation of trimethyloxonium ion by a basic site to form a surface-associated dimethyloxonium methylide species [152]. The final step is either an intramolecular Stevens rearrangement, or more probably as suggested by Olah and co-workers [182], an intramolecular methylation, (the both) leading to ethane *via* a β-elimination step.

For a better understanding of mechanisms involved in the MTO, it is worthy to cite relevant works devoted to adsorption and diffusion of light molecules and cyclic molecules in

[177] G. J. Hutchings, G. W. Watson, D. J. Willock, *Microporous Mesoporous Mater.* **1999**, *29*, 67–77.

[178] E. A. Swabb, B. C. Gates, *Ind. Eng. Chem. Fund.* **1972**, *11*, 540–545.

[179] D. Kagi, *J. Catal.* **1981**, *69*, 242–243.

[180] J. K. A. Clarke, R. Darcy, B. F. Hegarty, E. O'Donoghue, V. Amir-Ebrahimi, J. J. Rooney, *J. Chem. Soc. Chem. Commun.* **1986**, 425–426.

[181] a) S. Xu, A. Zheng, Y. Wei, J. Chen, J. Li, Y. Chu, M. Zhang, Q. Wang, Y. Zhou, J. Wang, et al., *Angew. Chem. Int. Ed.* **2013**, 1–6.

[182] G. A. Olah, H. Doggweiler, J. D. Felberg, S. Frohlich, M. J. Grdina, R. Karpeles, T. Keumi, S. Inaba, W. M. Ip, K. Lammertsma, et al., *J. Am. Chem. Soc.* **1984**, *106*, 2143–2149.

different zeolites [183]. Denayer *et al.* [183a] pointed out the utmost importance of taking into account the diffusivity of various molecules, such alcohols, alkanes and alkenes, in CHA-type catalysts to better understand the catalytic cracking reactions. The adsorption of methanol in these zeolites is favored, versus alkanes or alkenes, thanks to its polar interaction with the zeolite network. Furthermore, they have also shown that CHA structure led to an opposite trend with respect to tubular pore zeolites in terms of adsorption. CHA catalysts were able to adsorb short chain molecules in contrast to tubular pore zeolites, which adsorbed long chain molecules. Likewise, Vlught and co-workers [183g,h] showed differences in the adsorption isotherms of normal and branched alkanes on silicalite.

It is now well-admitted that the MTH reaction proceeds auto-catalytically through olefins chain growth and cracking [184]. The product formation can indeed be promoted by the presence of small amounts of alkenes trapped inside the catalyst and thus leading to an enhanced degree of conversion during an induction period [185]. The presence of this induction period corresponds to a high methanol conversion without any detected products. None of the aforementioned direct mechanisms could satisfactorily explain this induction period. Dessau and LaPierre [186] performed investigations on MTH mechanism over ZSM-5 zeolite by studying the conversion of ^{13}C -labeled methanol in the presence of various olefins and aromatics. They concluded to an alkene-based model, where olefins were produced by successive methylation and cracking steps.

Dahl and Kolboe were the first to suggest a parallel-type mechanism, named hydrocarbon-pool mechanism (Figure 1.25) in the mid 90's, without specifying the chemical

-
- [183] a) I. Daems, R. Singh, G. Baron, J. F. M. Denayer, *Chem. Comm.* **2007**, 1316–1318. b) J. F. M. Denayer, L. I. Devriese, S. Couck, J. Martens, R. Singh, P. A. Webley, G. V Baron, *J. Phys. Chem. C* **2008**, *112*, 16593–16599. c) D. M. Ruthven, *Microporous Mesoporous Mater.* **2006**, *96*, 262–269. d) J. Kärger, S. Vasenkov, *Microporous Mesoporous Mater.* **2005**, *85*, 195–206. e) R. Rungsirisakun, T. Nanok, M. Probst, J. Limtrakul, *J. Mol. Graph. Model.* **2006**, *24*, 373–382. f) A. F. P. Ferreira, M. C. Mittelmeijer-Hazeleger, J. V. D. Bergh, S. Aguado, J. C. Jansen, G. Rothenberg, A. E. Rodrigues, F. Kapteijn, *Microporous Mesoporous Mater.* **2013**, *170*, 26–35. g) T. J. H. Vlught, W. Zhu, F. Kapteijn, J. A. Moulijn, B. Smit, R. Krishna, *J. Am. Chem. Soc.* **1998**, *120*, 5599–5600. h) T. J. H. Vlught, R. Krishna, B. Smit, *J. Phys. Chem. B* **1999**, *103*, 1102–1118.
- [184] a) J. F. Haw, J. B. Nicholas, W. Song, F. Deng, Z. Wang, T. Xu, C. S. Heneghan, *J. Am. Chem. Soc.* **2000**, *122*, 4763–4775. b) S. Kolboe, *Acta Chem. Scand. A* **1986**, *A40*, 711–713.
- [185] a) W. Wang, A. Buchholz, M. Seiler, M. Hunger, *J. Am. Chem. Soc.* **2003**, *125*, 15260–15267. b) Y. Ono, T. Mori, *J. Chem. Soc. Faraday Trans. 1* **1981**, *77*, 2209–2221.
- [186] R. M. Dessau, R. B. LaPierre, *J. Catal.* **1982**, *78*, 136–141.

composition of this pool [187]. The idea is that hydrocarbon species present on the catalyst are essential to guarantee methanol conversion into olefins, and thus act as co-catalysts during the reaction. Dahl and Kolboe showed by ^{13}C -labelled methanol over a SAPO-34 that ethene and propene possess poor reactivity with respect to methanol [187a]. These alkenes were observed to be relatively inert under operating conditions since most of the products were formed from starting methanol feed.

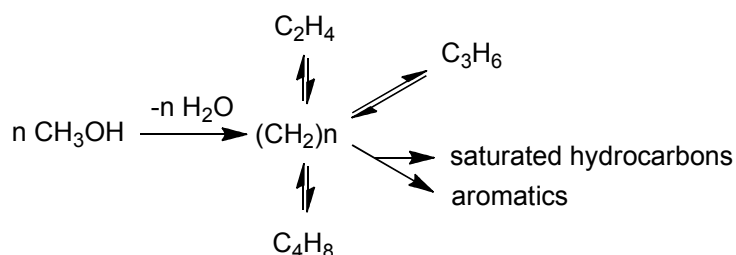


Figure 1.25 Schematic presentation of the hydrocarbon pool [187a]

The hydrocarbon pool mechanism is based on the presence of hydrocarbons on the catalyst, which continuously react with methanol and split off into light olefins. It has become clear that the main components of the hydrocarbon pool are polymethylated benzenes, which may possess many characteristics in common with ordinary coke. Haw *et al.* [184a,188] performed, *via* solid-state NMR spectroscopy, MTH mechanism investigations over H-ZSM-5 zeolite. They concluded that polymethylated cyclopentenyl ions played also a central role in light olefins formation. However different ring-structures and aromatics are particularly active in different zeolites, thus strengthening the importance of zeolite cages and channels in the stabilization of those intermediates. For instance, hexa- and penta-methylbenzenes were shown as main components of the hydrocarbon pool in SAPO-34 [189,190].

[187] a) I. M. Dahl, S. Kolboe, *J. Catal.* **1994**, *149*, 458–464. b) I. M. Dahl, S. Kolboe, *J. Catal.* **1996**, *161*, 304–309. c) I. M. Dahl, S. Kolboe, *Catal. Lett.* **1993**, *20*, 329–336.

[188] a) J. F. Haw, *Phys. Chem. Chem. Phys.* **2002**, *4*, 5431–5441. b) P. W. Goguen, T. Xu, D. H. Barich, T. W. Skloss, W. Song, Z. Wang, J. B. Nicholas, J. F. Haw, *J. Am. Chem. Soc.* **1998**, *120*, 2650–2651.

[189] B. Arstad, S. Kolboe, *Catal. Lett.* **2001**, *71*, 209–212.

[190] a) W. Song, J. F. Haw, J. B. Nicholas, C. S. Heneghan, *J. Am. Chem. Soc.* **2000**, *122*, 10726–10727. b) C.-M. Wang, Y.-D. Wang, H.-X. Liu, Z.-K. Xie, Z.-P. Liu, *J. Catal.* **2010**, *271*, 386–391.

These methylbenzenes play key roles in alkene formation *via* the hydrocarbon-pool mechanism. Marcus *et al.* [191] concluded that the only valid mechanism for the MTO reaction remains the hydrocarbon pool mechanism since it describes the prime formation of olefins on organic moieties centers, such as methylbenzenes, coupled with well-known secondary reactions involving olefins. Arstad and Kolboe [192] investigated different molecules confined into zeolite cavities after short times on stream. They showed that confined methylated aromatics were not spectator species, but do take part in the reaction. Several studies were extended to include BEA and ZSM-5 zeolites. Haw *et al.* [193] investigated the reactivity of different butylbenzene isomers on H-BEA and Svelle *et al.* [194] confirmed that hydrocarbon-pool mechanisms (methylation, polymethylbenzene formation and oligomerization) and cracking reactions are occurring at the same time over ZSM-5 zeolite.

To summarize, these studies support that certain organic reaction centers trapped within the zeolite pores such as methylbenzenes serve as scaffolds/co-catalysts where methanol is added and olefins are eliminated in a (closed) catalytic cycle. By finding a suitable compromise between the inorganic framework and the organic reaction centers, both the activity and selectivity in the MTO reaction can be optimized. The evolution of hydrocarbon pool species in the course of the reaction, has been suggested to follow two possible routes (Figure 1.26), namely the side-chain and the paring routes [195]. The side-chain route involves the stepwise growth of alkyl side chain on methylbenzenes, followed by the subsequent elimination of this side chain into light olefins, whilst in the paring route, olefins are obtained *via* the contraction of methylbenzene ring.

[191] D. M. Marcus, K. A. McLachlan, M. A. Wildman, J. O. Ehresmann, P. W. Kletnieks, J. F. Haw, *Angew. Chem. Int. Ed.* **2006**, *45*, 3133–3136.

[192] B. Arstad, S. Kolboe, *J. Am. Chem. Soc.* **2001**, *123*, 8137–8138.

[193] A. Sassi, M. A. Wildman, J. F. Haw, *J. Phys. Chem. B* **2002**, *106*, 8768–8773.

[194] S. Svelle, P. O. Rønning, S. Kolboe, *J. Catal.* **2004**, *224*, 115–123.

[195] D. Lesthaeghe, A. Horr , M. Waroquier, G. B. Marin, V. Van Speybroeck, *Chem. Eur. J.* **2009**, *15*, 10803–10808.

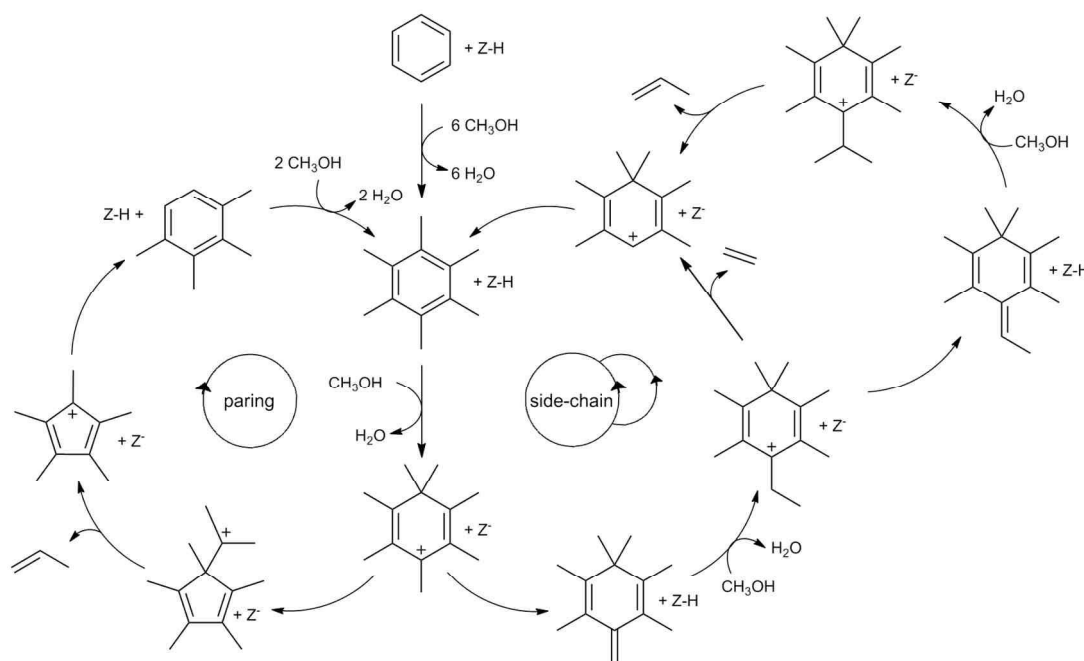


Figure 1.26 Representation of the two possible reaction pathways in MTH reaction [195]

It is worthy to mention that recently a novel concept in the MTH mechanism began to appear. Thanks to a better knowledge of the hydrocarbon-pool mechanism over ZSM-5 zeolites, it was observed that the predominant formation of ethylene occurs *via* aromatic-based feeds, whereas propylene and higher alkenes are mainly produced by methylation of alkenes which then crack further. It was suggested that these two cycles run in parallel during the MTH reaction over the catalyst. Figure 1.27 gives a schematic picture of this dual-cycle concept [157b,196].

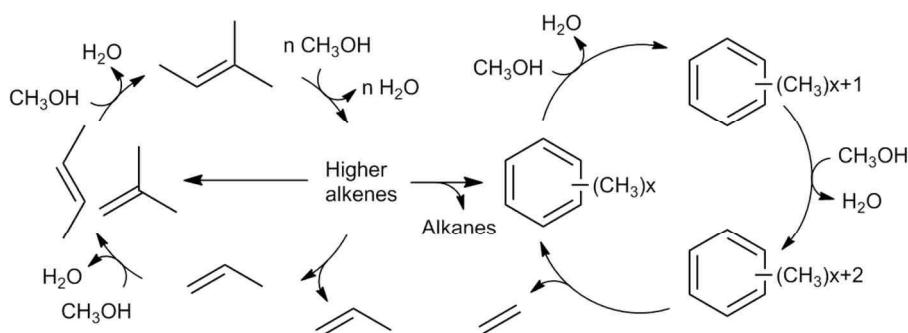


Figure 1.27 Suggested dual-cycle concept for the conversion of methanol over H-ZSM-5 [155]

[196] S. Svelle, F. Joensen, J. Nerlov, U. Olsbye, K.-P. Lillerud, S. Kolboe, M. Bjørgen, *J. Am. Chem. Soc.* **2006**, *128*, 14770–14771.

In 2009, Bjørngen *et al.* [197] consolidated this dual-cycle concept by following the conversion of ^{13}C -labelled methanol over two zeolites, H-ZSM-5 and H-BEA. It was found that under nearly identical conditions the yield in ethylene was up to 7 times higher versus propylene over H-ZSM-5 than H-BEA zeolite. They concluded that the amount of ethylene in H-BEA was mainly due to the aromatic hydrocarbon pool reaction intermediates (penta- and hexa-methylbenzenes) which promoted the formation of propylene and higher alkenes. In H-ZSM-5, ethylene is promoted by the presence of lower methylbenzene intermediates.

Recent investigations on MTH mechanisms showed new tools for the elucidation of MTH reaction over different solid acids [198]. Their study was performed over ZSM-22 zeolite, exhibiting one-dimensional 10-ring straight narrow and channels. In contrast to SAPO-34 and ZSM-5 zeolites, the hydrocarbon-pool mechanism is partially suppressed in this kind of topology because of the lack of space within the channels. Hence, the methylation/cracking mechanism of olefins is really favored (Figure 1.27 left side). Thanks to these studies, one may be able to control the selectivity in MTH reaction by designing new catalysts having the appropriate pore topology.

2.3.4. Methanol-to-Propylene technology

During the last decade, the MTO has been widely promoted and studied with respect to the MTG reaction. This can be explained by the strong demand in light olefins, principally ethylene and propylene. The world propylene consumption is forecasted to increase by close to 5% per year in coming years, compared to an ethylene expected growth rate of nearly 4% a year [150]. This driving force pushes scientists to the development of methanol-to-propylene (MTP) technology. Propylene is one of the key building blocks widely used as feedstock for a variety of polymers and chemical intermediates, like polypropylene, propylene oxide, acrolein, acrylonitrile, isopropyl alcohol and other miscellaneous intermediates. These compounds are mostly used in a wide range of industries such automotive, packaging and electronic industries. The current industrial production of

[197] M. Bjørngen, F. Joensen, K.-P. Lillerud, U. Olsbye, S. Svelle, *Catal. Today* **2009**, *142*, 90–97.

[198] a) S. Teketel, U. Olsbye, K.-P. Lillerud, P. Beato, S. Svelle, *Microporous Mesoporous Mater.* **2010**, *136*, 33–41. b) J. Li, Y. Wei, Y. Qi, P. Tian, B. Li, Y. He, F. Chang, X. Sun, Z. Liu, *Catal. Today* **2011**, *164*, 288–292.

propylene is performed either by steam cracking, fluidized catalytic cracking (FCC) and propane dehydrogenation. Besides the availability of low cost methanol, such expected growth in propylene demand renders the MTP process viable. At present, the Lurgi MTP process has been the sole commercialized yet, owned by the Lurgi Company, involving a ZSM-5 catalyst, developed by Süd-Chemie. This process allows a high selectivity in propylene (about 70%) at complete methanol conversion with gasoline range compounds as by-products and slow deactivation rate. This high selectivity in propylene is related to an efficient combination of a very selective and stable catalyst and a suitable reactor configuration. Such performances are achieved thanks to the engineering of two fixed-bed reactors, which operate in parallel at 425 °C and a pressure of 1.5 bar. Another important feature in this set-up is the recycling of olefins, which allows to maximize the propylene selectivity.

Several authors have reported different catalyst developments, specially designed to raise the selectivity to propylene [199-207]. In this section, we will discuss the strategies to modify catalyst properties: like crystal size, mesoporosity, zeolite coatings or dopings (with metals or not) to improve propylene selectivity.

Firstly, the crystal size is one of the critical parameters influencing the propylene selectivity [199,200]. Firoozi and co-workers [201] have studied the impact of ZSM-5 particle size on methanol conversion. Two samples comprising a micro and a nano-sized H-ZSM-5 were compared in the MTO reaction. Nano-sized zeolite demonstrated a higher performance in terms of conversion and selectivity in propylene, being 88% and 63% after 120 h time on stream, respectively. This can be attributed to higher external surface area and higher concentration of strong acid sites present in nano-sized H-ZSM-5 compared with micro-sized crystals. Bleken *et al.* [202] observed a higher catalytic activity and a slower deactivation rate over a “giant” crystal sized ZSM-5 catalyst. Surprisingly, they concluded that the huge crystal size along with a low density of Brønsted acid sites prevented consecutive reactions and hence maximized the formation of propylene. One may suppose that huge crystals would

[199] M. Asadi, A. M. Thalkhoncheh, *Propylene via Methanol over Aluminosilicate Catalyst*, **2010**, CA2642395.

[200] a) R. Wei, C. Li, C. Yang, H. Shan, *J. Nat. Gas Chem.* **2011**, *20*, 261–265. b) S. Hu, J. Shan, Q. Zhang, Y. Wang, Y. Liu, Y. Gong, Z. Wu, T. Dou, *Appl. Catal. A* **2012**, *445-446*, 215–220.

[201] M. Firoozi, M. Baghalha, M. Asadi, *Catal. Commun.* **2009**, *10*, 1582–1585.

[202] F. L. Bleken, S. Chavan, U. Olsbye, M. Boltz, F. Ocampo, B. Louis, *Appl. Catal. A* **2012**, *447-448*, 178–185.

increase the diffusion of reactants and products to yield longer chain alkenes, favoring the olefin methylation/cracking route.

Another key parameter for an improved propene formation could be the presence of mesoporosity inside the catalyst [171c-d,173,202]. In 2010, Sun *et al.* [203] performed the design of a mesoporous ZSM-5 zeolite, which exhibited prominent stability enhancement in MTP reaction. The presence of open mesopores in the crystal shortens the diffusion path of primary olefin products and renders easier the olefins (propylene and butenes) desorption from the active sites. This phenomenon hinders secondary reactions occurring on the acid site and thus the probabilities of aromatics and higher olefins formation. A higher catalyst stability can therefore be expected. Besides the hydrocarbon-pool mechanism, responsible for both ethylene and propylene formation, the olefin route involving methylation and cracking of olefins allows the preferential formation of propylene [157b]. The higher propylene selectivities observed over mesoporous ZSM-5 catalysts could be explained by an improved diffusion of olefins, favoring the olefin route [164d]. To summarize, the creation of open mesopores in ZSM-5 zeolite is important, in line with the proper adjustment of Brønsted acidity to properly design a competitive MTP catalyst.

Zeolite coatings could also favor the selectivity in propylene in the MTO reaction [170b]. Recently, Jiao *et al.* [170d] have suggested that ZSM-5 crystals coated on SiC foam with appropriate morphology led to an enhancement in the catalyst activity and stability. Thanks to their high thermal conductivity, high resistance toward oxidation, high mechanical strength, rapid heat evacuation, favored mass transfer and chemical inertness, silicon carbide foams are promising supports. These catalysts allow high dispersion of zeolite thin layer on support and render easier the access of reactants and the diffusion of products outside the zeolite pores. Thanks to improved diffusion, the olefin route may be favored and therefore the propylene selectivity can be raised over structured catalysts. In summary, these new composites showed substantial stability and yield improvement in comparison with zeolite pellets in the MTP reaction [170b,d].

[203] C. Sun, J. Du, J. Liu, Y. Yang, N. Ren, W. Shen, H. Xu, Y. Tang, *Chem. Comm.* **2010**, 46, 2671–2673.

Careful attention was paid to the development of ZSM-5 catalysts *via* the doping or the incorporation of different atoms within the zeolite structure [168,171c,204]. Besides the contribution from Hua *et al.* [171d], one can quote the study of Lee *et al.* [205] who tailored ZSM-5 acidity through the optimization of phosphorous loading in the binder to minimize side reactions to improve the propylene selectivity. Both an optimized P loading and operating conditions led to achieve a 50% propylene yield. The rate of deactivation by coking was also diminished with respect to non-promoted catalyst. The doping with boron in the zeolite structure [168] also allowed to tune the acidity by increasing the number of weak acid sites. Sun *et al.* [171c] proposed a novel route for raising MTP catalyst's resistance to deactivation *via* doping ZSM-5 zeolite with gold. Thanks to those gold nanoparticles, the catalytic stability was seriously enhanced by the inhibition of dehydrogenation reactions occurring during the coking process. Table 1.1 summarizes the nature of catalyst modifications performed and their influence on methanol conversion and propylene selectivity.

Table 1.1 Nature of MFI catalyst modifications and their influence on activity and selectivity

Refs	ZSM-5 modification	Reaction temperature [°C]	Methanol conversion [%]	Propylene selectivity [%]
156	Lurgi process	425	100	70 ^a
200b	Nanosheets of MFI zeolites	450	100	51
202	“Giant” ZSM-5crystal	350	98	38
203	Mesopores containing ZSM-5	460	99	49
204e	Ir-doped ZSM-5	480	98	48
205	P-ZSM-5	500	100	50
170b	ZSM-5 coated on SiC	400	60	40

^a selectivity achieved after proper reactor design and process intensification (cracking and recycling of alkenes)

[204] a) A. Mohammadrezaei, S. Papari, M. Asadi, A. Naderifar, R. Golhosseini, *Front. Chem. Sci. Eng.* **2012**, *6*, 253–258. b) D. Van Vu, Y. Hirota, N. Nishiyama, Y. Egashira, K. Ueyama, *J. Japan Pet. Inst.* **2010**, *53*, 232–238. c) K.-Y. Lee, H.-K. Lee, S.-K. Ihm, *Top. Catal.* **2010**, *53*, 247–253. d) J. Liu, C. Zhang, Z. Shen, W. Hua, Y. Tang, W. Shen, Y. Yue, H. Xu, *Catal. Commun.* **2009**, *10*, 1506–1509. e) S. Papari, A. Mohammadrezaei, M. Asadi, R. Golhosseini, A. Naderifar, *Catal. Commun.* **2011**, *16*, 150–154.
 [205] Y.-J. Lee, Y.-W. Kim, N. Viswanadham, K.-W. Jun, J. W. Bae, *Appl. Catal. A* **2010**, *374*, 18–25.

Finally, other ways to achieve a proper MTP catalyst design were tempted by proper particle shaping [206] or changing the catalyst topology [207].

2.3.5. Conclusions

MTO and MTP processes can now be considered as attractive options for the valorization of stranded natural gas reserves. They provide an economically viable alternative to naphtha cracking or shale gas associated ethane/propane dehydrogenation for the production of ethylene and propylene. In spite of high investment costs due to syngas production by reforming of methane and methanol synthesis, one commercial process for each technology, namely the UOP/Norsk Hydro (MTO process) production of C₂-C₄ olefins and the Lurgi's MTP process for the selective production of propylene have been settled (Section 2.3.1).

After investigation of the mechanisms involved in MTH reactions, the main parameters governing product selectivities are now identified. Hence, it is now well-admitted that the hydrocarbon-pool mechanism plays a central role in the formation of the final products *via* the involvement of hybrid organic-inorganic sites at the catalyst surface. The chemical composition of these hybrid sites and therefore the product selectivities are therefore strongly connected to the zeolite topology.

Further investigations devoted to catalyst design are warranted to maximize the selectivity toward propylene. An "ideal" catalyst needs therefore to demonstrate a high activity and stability versus time on stream, as well as being highly selective in propylene. In addition, costs of preparation and formulation have to be kept low for this large scale process. ZSM-5 zeolite is a viable candidate (Section 2.3.4), which could be further improved by adapting/tailoring its crystal size and acid strength. A viable MTP catalyst should therefore be the result of a compromise between **an appropriate crystal size** [171,208] in order to avoid mass transfer limitations, and **a tailored Brønsted acidity**: sites not too

[206] W. Guo, W. Xiao, M. Luo, *Chem. Eng. J.* **2012**, 207–208, 734–745.

[207] S. Hu, Y. Gong, Q. Xu, X. Liu, Q. Zhang, L. Zhang, T. Dou, *Catal. Commun.* **2012**, 28, 95–99.

[208] S. Mitchell, N.-L. Michels, K. Kunze, J. Pérez-Ramírez, *Nature Chem.* **2012**, 4, 825–831.

strongly acidic and highly-dispersed to hinder consecutive reactions leading to coke formation [199].

In parallel, mechanistic studies over acid zeolites have to be pursued through isotope labeling, kinetic studies and the use of computational tools [209] to come nearer the determination of each individual reaction steps. With those informations in hand, a certain level of predictability in products formation should be expected as a function of the zeolite topology.

Finally, a key approach to improve a MTP process is related to process engineering *via* proper reactor and/or plant design. Indeed, an appropriate reactor design (fixed versus fluidized bed) and process intensification (heat transfer, recirculation, catalyst regeneration, *etc.*), product selectivities and catalyst lifetime can be further maximized [210].

Based on all aforementioned points, one may overcome (in the future) the higher cost for methanol production with respect to shale-based feedstocks. Hence, MTP process may become even more viable.

[209] J. K. Norskov, T. Bligaard, J. Rossmeisl, C. H. Christensen, *Nature Chem.* **2009**, *1*, 37–46.

[210] F. J. Keil, *Microporous Mesoporous Mater.* **1999**, *29*, 49–66.

Chapter 2. EXPERIMENTAL

ABSTRACT

The experimental techniques and set-ups used in the present work are presented in this part. The installations for aromatics chlorination and for the methanol to olefins reactions, as well as the operating conditions are described in Section 1. Apparatus and techniques employed for catalysts characterization are described in Section 2.

1. Experimental set-up

1.1 Aromatics chlorination reactions

1.1.1. Reagents and catalysts

Trichloroisocyanuric acid (Aldrich, 98%), toluene (Carlo Erba, 99%), chlorobenzene (SDS, 99%), nitrobenzene (Merck, 99%) and solvents were used as received. Different commercial zeolites were tested H-USY (Zeolyst, CBV500), H-BEA (Zeolyst), H-EMT (IS2M, UHA, Mulhouse), H-MOR (Zeolyst), H-ZSM-5 (Zeolyst CBV3024, 5020 and 8020) and H-SAPO-5 (Louvain University, Belgium). Prior to use, these zeolites were activated at 550°C in static air for 4 h. Besides, non-zeolitic catalysts were used as received: Nafion SAC-13 (Aldrich, 20% nafion in MCM-41), $\text{SO}_4^{2-}/\text{ZrO}_2$ and $\text{H}_3\text{PW}_{12}\text{O}_{40}$ (Aldrich) [1].

1.1.2. Liquid phase reaction

TCCA was added at room temperature in small portions to a well-stirred suspension of aromatic and the solid acid in the appropriate solvent (see Table 2.1). After completion of the reaction, the reaction mixture was filtered and the solid washed with CH_2Cl_2 or 1.2 DCE. The solution was treated with a 10% aqueous $\text{Na}_2\text{S}_2\text{O}_3$ (5 mL), washed with water (5 mL) and then dried over anhydrous MgSO_4 . After filtration and evaporation of the solvent, the sample withdrawn was analyzed by a GC chromatograph with FID using a 30 m (length), 0.25 mm (ID), and 25 μm (phase thickness) RTX-5 capillary column and H_2 (flow rate 50 cm/s) as carrier gas (split: 1:10).

[1] Y. Sun, S. Walspurger, B. Louis, J. Sommer, *Appl. Catal. A* **2005**, 292, 200–207.

Table 2.1 Experimental conditions for aromatics chlorination reaction in liquid phase

Aromatic	TCCA equivalent [mmol]	Aromatic equivalent [mmol]	Acid site equivalent [mmol H ⁺]	Solvent [type, mL]	Synthesis duration [h]
Toluene	0.34	1.0	0.30	CH ₂ Cl ₂ , 5	between 1-x h ^a
Chlorobenzene	0.60	1.8	0.54	CH ₃ CH ₂ Cl ₂ , 10	24

^a determined by GC

1.1.3. Semi-continuous gas-solid set-up

All the catalytic tests were performed in an all-glass flow system with a cylindrical reactor (Figure 2.1).

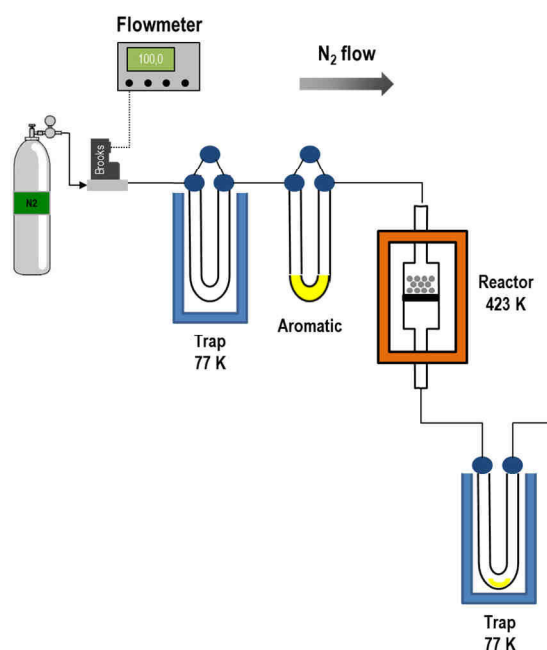


Figure 2.1 Experimental setup for the chlorination reactions in a semi-continuous gas-solid system

The gas flow (N₂) was regulated by means of Brooks 5850E mass flow controllers. The reactions were carried out by diluting the catalytic bed (TCCA and zeolite) in an amorphous matrix to maintain the same height for all catalytic beds. All catalytic beds exhibited similar granulometry (grains/particles smaller than 150 μm). To investigate the influence of the zeolite morphologies and crystal sizes on their catalytic performances, we have decided to

work at iso-site conditions. Table 2.2 summarizes the reaction conditions used for either chlorobenzene or nitrobenzene chlorination reactions. The solid acid catalyst, the TCCA and the inert matrix were blended closely by grinding. The intimate solid mixture was then transferred to a cylindrical reactor and fixed to the set-up. The catalytic bed was first dried under nitrogen flow at 423 K for 30 min. Then, the aromatic vapor pressure was flown through the catalytic bed for a defined reaction time.

The products were then trapped at 77 K and recovered downstream to the reactor with dichloromethane. The analysis was performed by gas chromatography (HP 6590) equipped with a capillary column (HP-5MS, 30 m). Retention times were compared with standards and used to characterize the different products. The degree of conversion and the selectivity toward the different products were calculated by taking into account the response factor of the aromatic substrate and those from the products (mono-, di- and trichlorinated aromatics) through the use of an external standard (styrene).

Table 2.2 Experimental conditions for aromatics chlorination reaction

Aromatic	TCCA equivalent (mol)	Aromatic equivalent (mol)	Acid site equivalent (mol)	Diluting agent	T _{reaction} (K)	T _{aromatic trap} (K)	Flow rate (mL/min)	Reaction duration (h)
Nitrobenzene	2.5×10^{-4}	2.5×10^{-4}	2.5×10^{-4}	Silica	423	r.t.	100	5
Chlorobenzene	5.0×10^{-4}	5.0×10^{-4}	1.0×10^{-4}	Glass rings	423	273	25	3

1.2 Methanol to olefins reaction

1.2.1. Materials

All the chemicals were used as received from the suppliers: methanol (Aldrich, 98.9%). All catalysts were calcined before each reaction and used in their H-form.

1.2.2. MTO set-up

Prior to use, catalysts were activated at 823 K in static air (with a gradient of 15 K/min). The zeolites were sieved and particles < 250 μm were used in the experiments. 60 mg of

zeolite were introduced in a tubular quartz reactor and packed between quartz wool plugs as shown in Figure 2.2.

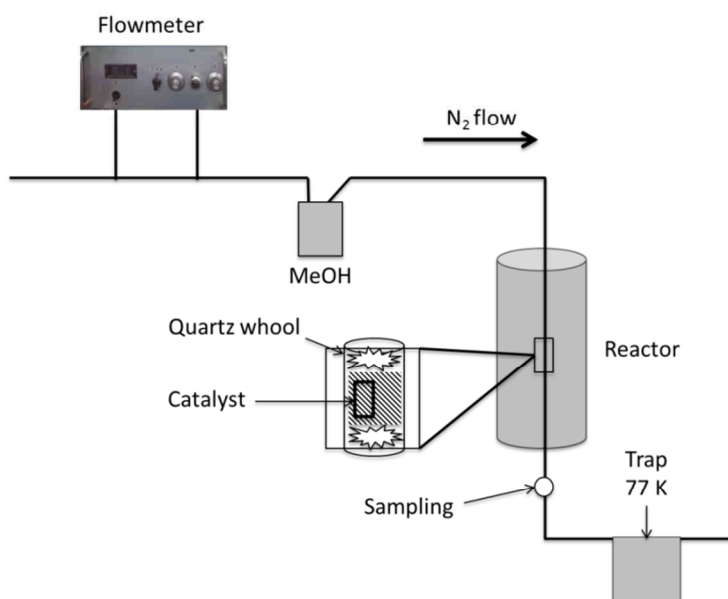


Figure 2.2 Experimental setup for the MTO reactions

A constant nitrogen flow, of 20 mL/min was flown through a methanol saturator, cooled at 273 K, to achieve a $WHSV = 1.12 \text{ g}_{\text{MeOH}}/\text{g}_{\text{cat}} \cdot \text{h}^{-1}$. The reactant was subsequently fed to the reactor containing the catalyst at 673 K. GC analysis was performed on a HP 5890 equipped with a 50 m capillary column (PONA) and a flame ionization detector (FID). The activity of the catalysts was expressed in terms of methanol- and dimethylether-conversion, calculated from the difference between inlet and outlet concentrations of methanol (DME is considered as a reactant). The selectivity was defined as the mole ratio of each product referred to the moles of converted methanol and dimethylether. Equations 2.1 - 2.3 were used to calculate the conversion, the respective selectivity and the C_3/C_2 ratio, respectively.

Equation 2.1

$$X = \frac{n \text{ MeOH In} - (n \text{ MeOH Out} + 2 * n \text{ DME})}{n \text{ MeOH In}} * 100 \%$$

Equation 2.2

$$S = \frac{(\sum) \alpha * n(\text{CH}_2)}{n \text{ MeOH In} - (n \text{ MeOH Out} + 2 * n \text{ DME})} * 100 \%$$

Where n represents the quantity of the desired fraction, α the number of C-atoms in the considered product, (Σ) applied for the calculation of the selectivity towards light olefins C₂-C₄ fraction. In addition, the denominator corresponds to consumed methanol and dimethylether.

Equation 2.3
$$C_3 / C_2 = \frac{n(C_3H_6)}{n(C_2H_4)}$$

2. Characterization methods

2.1 X-ray diffraction (XRD)

X-ray diffraction technique enables the identification of the different crystalline phases of a solid. Each crystalline phase gives characteristic diffraction reflections [2]. This technique is based on the Bragg's law shown in Equation 2.4. The basis for X-ray diffraction is the property of electromagnetic radiation, consisting in sending an X-ray beam through the sample and measuring the diffracted beam intensity. When incident X-ray beams have their path length difference equal to the integer number of their wavelength, a constructive interference will be observed. In other words, a reflection should be observed when the incident ray angle satisfies the Bragg's law.

Equation 2.4
$$2d \sin \theta = n \lambda$$

Where d : spacing between the planes in the atomic lattice
 θ : angle between the incident ray and the scattering planes, also called Bragg's angle
 n : integer number
 λ : wavelength of incident wave

[2] J. P. Eberhardt, *Analyse Structurale et Chimique Des Matériaux*, Paris, Dunod, **1989**.

X-ray diffraction is widely used for analysis of crystalline powders. Each crystalline material exhibits a diffraction pattern, which position (in 2θ degrees) reflects the distance between atomic planes in the crystals. The position and relative intensity of the lines in an X-ray diffraction pattern serve as a fingerprint for a given type of crystalline structure. By comparing an X-ray diffraction pattern to the patterns collected in JCPDS Tables, the structure of as-synthesized material can be determined.

Powder X-ray diffraction patterns were recorded systematically on a Bruker D8 Advance diffractometer, with a Ni detector side filtered Cu $K\alpha$ radiation (1.5406 \AA) over a 2θ range of $5\text{--}60^\circ$ and a position sensitive detector using a step size of 0.02° and a step time of 2 s.

2.2 Scanning electron microscopy (SEM)

Scanning electron microscopy is a powerful tool for studying zeolite materials. Parameters, such as surface morphology, crystal size and shape, degree of aggregation presence of other phases, distribution of elements in the material can be determined by EDX technique coupled with SEM chamber.

This technique consists of scanning the surface of the sample with a focused electron beam, accelerated by a 10 to 20 kV voltage, and in analyzing the interactions between the beam and atoms from the matter [2]. These interactions produce various signals that can be detected and that contain information about the sample surface topography and composition. Figure 2.3 presents a scheme of the SEM principle. Two types of interactions can occur and conduct to a SEM image:

- * Emission of secondary electrons (SE): when an incident electron excites the electronic level of a heart atom, this electron returns to its primary state by emitting a valence electron called secondary electron. The SE possesses a relative weak energy of nearly 50 eV. Thus, only the SE emitted by the superficial layer of the sample are expelled from the matter. The resulted SEM image (SEI mode) shows generally a good resolution of 3 to 5 nm.

- * Emission of backscattered electrons (BSE): part of the incident electrons undergo inelastic impacts which send them out of the sample with an energy close to their initial energy. These BSE could come from deeper layers of the matter compared with SE, leading to a SEM image with a lower resolution of 6 to 10 nm. However, the BSE gives access to additional information. Indeed, depending on the detector, BSE could provide a topographic image (contrast according to the surface roughness) or a composition image (contrast according to the atomic number Z).

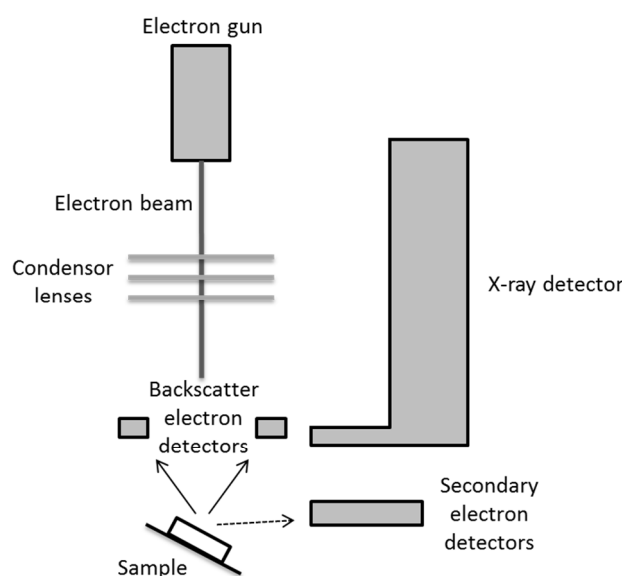


Figure 2.3 Schematic representation of a scanning electron microscope

SEM micrographs were recorded on a JEOL FEG 6700F microscope working at 9 kV accelerating voltage. The samples were maintained with an adhesive tape in carbon and are covered with a thin layer of carbon in order to increase their electric conductivity. The Si/Al ratio of the crystals was determined by energy-dispersive X-ray (EDAX) analysis in the SEM chamber.

2.3 High-Resolution transmission electron microscopy (HRTEM)

In transmission electron microscopy (TEM), the beam passes through the sample deposited on a thin metal grid typically coated with a thin layer of carbon and reaches the

detector. The image collected in bright field imaging mode gives information regarding the contrast of the sample. Thicker areas or areas with higher atomic number will be darker and vice versa. The choice of specimen support is important for high resolution TEM, since thicker support film decreases the resolution and may render difficult the detection of lattice fringes.

In this work, the microstructure of some mesoporous zeolites was investigated by TEM. The investigation was conducted in a Philips CM200 microscope with a LaB₆ emitter. The samples were dispersed in chloroform and deposited on a holey carbon film supported on a Cu grid. The measured lattice spacings were compared with reference X-ray powder diffraction patterns of the International Centre for Diffraction Data (ICCD 84039 file).

2.4 Specific surface area and porosimetry measurements

Adsorption of gases on the surface of porous materials provides crucial information related to the specific area, pore volume and pore size distribution. The basis for adsorption measurements is the physisorption of gas molecules on the surface. The most commonly used method was developed by Brunauer, Emmett and Teller (BET method) [3]. This method gives access to the BET surface area and to the pore size distribution of the solid.

The sample is submitted to a known gas pressure, at constant volume. The gas molecules adsorb onto the solid surface until equilibrium was reached. Brunauer, Emmet and Teller have shown the existence of a relationship between the adsorbed gas amount per gram of solid, the equilibrium pressure, the temperature, the gas nature and the nature of the studied solid (Equation 2.5).

This equation presents some limits. Indeed, it is only valid for an interval of relative pressures P/P_0 between 0.05 and 0.35. Except this interval, the surface heterogeneity at low relative pressure and the interaction between adsorbate molecules at higher relative pressure are not in agreement with the hypotheses of the BET method (based on Langmuir hypotheses).

[3] S. Brunauer, P. H. Emmett, E. Teller, *J. Am. Chem. Soc.* **1938**, *60*, 309–319.

Equation 2.5

$$\frac{P}{V(P_0 - P)} = \frac{1}{V_m C} + \frac{C-1}{V_m C} * \frac{P}{P_0}$$

Where P: equilibrium pressure
 P₀: vapor pressure of the adsorbate at the measured temperature
 V: vapor volume adsorbed per gram of solid at pressure P
 V_m: vapor volume needed to completely recover the surface with a mono-molecular layer of adsorbate
 C: constant of the studied gas-solid system

The basic textural properties involving the BET surface area S_{BET}, the mesopore surface area S_{meso} and the micropore volume V_μ were evaluated from nitrogen physical adsorption–desorption isotherms measured at 77 K by means of ASAP2020M and AP2050M instruments (Micromeritics, USA). The high precision of pressure measurements was insured by using low pressure transducer with the capacity of 0.1 Torr. The specific surface area, S_{BET}, was evaluated from the nitrogen adsorption isotherm branch in the range of relative pressures P/P⁰ = 0.05–0.25 (p is the adsorbate pressure and p₀ is the adsorbate vapor pressure at the measuring temperature). The mesopore surface area, S_{meso}, and the micropore volume, V_μ, were determined by the t-plot method [4] based on the Lecloux–Pirard standard isotherm [5,6] and thickness curve describing the statistical thickness of the film of adsorptive on a non-porous reference surface. The mesopore-size distribution was evaluated from the adsorption branch of the nitrogen adsorption–desorption isotherm using the Barrett–Joyner–Halenda (BJH) method [7,8], while taking into account the formation of liquid-like adsorbed layer of adsorbate on the pore walls prior to capillary condensation.

[4] J. B. DeBoer, B. C. Lippens, B. G. Linsen, J. C. P. Broekhoff, A. V. D. Heuvel, Th .J. Osinga, J. Colloid Interface Sci. **1966**, *21*, 405–414.

[5] A. Lecloux, J. P. Pirard, J. Colloid Interface Sci. **1979**, *70*, 265–281.

[6] P. Schneider, Appl. Catal. A **1995**, *129*, 157–165.

[7] E. P. Barret, L. G. Joyner, P. B. Halenda, J. Am. Chem. Soc. **1951**, *73*, 373–380.

[8] B. F. Roberts, J. Colloid Interface Sci. **1967**, *23*, 266–273.

2.5 H/D isotope exchange method

Home-made H/D exchange isotope technique was used to determine the total number of Brønsted acid sites present in solid acids [9,10]. Figure 2.4 presents the experimental set-up used to perform this titration method.

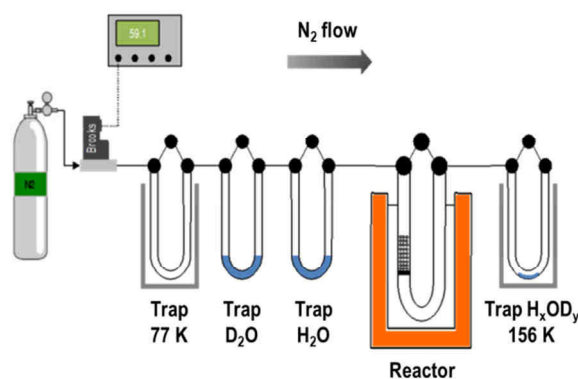


Figure 2.4 Experimental setup to perform the H/D isotope exchange technique

The catalyst (200 mg) was first activated under dry nitrogen flow (40 mL/min) at 723 K for 1 h. The deuteration of the catalyst was carried out at 473 K by flowing, through the catalyst, nitrogen (40 mL/min), previously bubbled at room temperature through a U-shaped tube containing D_2O (about 0.05 g), during 1 h. Dry nitrogen was then swept through the sample during 60 min to remove the excess of D_2O . After this purge, the titration of O-D sites was performed by back-exchanging the deuterium present on the solid surface with distilled water (3% of H_2O in N_2 stream) at 473 K for 1 h. During this step the partially exchanged water named H_xOD_y , composed by H_2O , D_2O and HDO, was collected in a cold U-tube trap at 156 K. Collected H_xOD_y was then weighted and allowed to react with trifluoroacetic anhydride, used in a two-fold excess. The acid solution obtained was then transferred to a NMR tube for analysis. Spectra were recorded on a Bruker AM600 spectrometer, after addition of a $CDCl_3$ (10 wt.%)/ $CHCl_3$ mixture used as reference. Finally, an accurate

[9] a) [1]B. Louis, S. Walspurger, J. Sommer, *Catal. Lett.* **2004**, *93*, 81–84. b) S. Walspurger, B. Louis, *Appl. Catal. A* **2008**, *336*, 109–115.

[10] B. Louis, A. Vicente, C. Fernandez, V. Valtchev, *J. Phys. Chem. C* **2011**, *115*, 18603–18610.

quantification of the H/D content in the different samples was achieved by the integration of $\text{CF}_3\text{COOH(D)}$ and CH(D)Cl_3 on both ^1H and ^2H spectra.

3. Conclusion

Section 1 described the different experimental setups used for the catalytic reactions (aromatic chlorination and MTO). Details of the procedures followed in these experiments, and of the calculations performed to determine the respective conversion and selectivities towards the respective products were also given.

Section 2 presented all physico-chemical techniques used to characterize the different catalysts. Many techniques were employed, each one being appropriate to get partial information regarding the success of the synthesis strategies (Chapter 3), as well as the molecular composition of the different as-synthesized materials.

**Chapter 3. TAILOR-MADE SYNTHESIS AND
CHARACTERIZATION OF ZEOLITES**

ABSTRACT

Various types of zeolites were prepared *via* different synthesis procedures. All as-prepared catalysts were thoroughly characterized by BET, XRD, SEM, ^{27}Al MAS NMR and FTIR techniques to investigate the effects of the different preparations.

Two main axes were followed during these studies being: (i) the hydrothermal synthesis of zeolites and (ii) the preparation of hierarchical zeolites. Section 2 deals with the preparation of different MFI and FAU zeolites *via* alkaline and fluoride-mediated routes. Section 3 focuses on preparation and characterization of mesoporous zeolites *via* constructive and destructive procedures.

1. Introduction

In heterogeneous catalysis, the catalyst choice and design are clue steps for reaching a competitive process. In this field, zeolites appear to be interesting materials for various applications. Indeed, their high surface area, as well as their tunable acidity are desirable properties, which lead them to be the prominent family of solid acid catalysts. However, it has been recognized that zeolites suffer from different drawbacks.

Firstly, zeolites exhibit a microporous structure with well-defined pore shape and size. Nevertheless, the microporous network of zeolite formed *via* the alkaline hydrothermal route, taking place at high pH, possesses connectivity defects [1]. These defects, generated by high concentration of positive charges during the synthesis, could have a negative impact on the catalytic reactivity. Hence, the fluoride-assisted synthesis, developed in the late 1970s, has been particularly used for the preparation of high-silica zeolites, such as ZSM-5 [2]. The fluoride route is usually carried out in the presence of F⁻ anions at nearly neutral pH. In contrast to zeolites synthesized *via* alkaline route, materials prepared in F⁻ aqueous media possess few connectivity defects [3]. The crystals formed in the fluoride medium exhibit therefore fewer network defects but these crystals are extremely large and may induce diffusion limitations.

Another zeolite drawback relies on their microporous structure and pore size dimensions close to the size of the molecules. Internal diffusion might be hindered which may seriously impact the catalyst activity, its selectivity and lifetime. Fundamental and practical interests of zeolites are a direct consequence of their intrinsic properties which can be manipulated through variations in their composition. Depending their applications, the zeolite properties can be customized and designed *via* different methods, thus leading to enhanced catalyst properties. Firstly, there is a great interest in the development of

[1] H. Koller, R. F. Lobo, S. L. Burkett, M. E. Davis, *J. Phys. Chem.* **1995**, *99*, 12588–12596.

[2] E. M. Flanigen, R. L. Patton, **1978**, US Patent 4073865.

[3] P. A. Barrett, M. A. Camblor, A. Corma, R. H. Jones, L. A. Villaescusa, *J. Phys. Chem. B* **1998**, *102*, 4147–4155.

nanosized zeolites. Several methods of synthesis and post-synthetic treatments have been developed to obtain nanocrystalline zeolites with thin frameworks [4]. These zeolites exhibit increased surface area, reduced diffusion paths and higher hydrophilicity [5]. Furthermore, the introduction of mesoporosity in addition to the microporous network of zeolites has been widely used to overcome their diffusion limitations [6]. Figure 3.1 shows a schematic representation of a mesoporous network (in red), complementary to the native microporous framework of the zeolite (in blue).

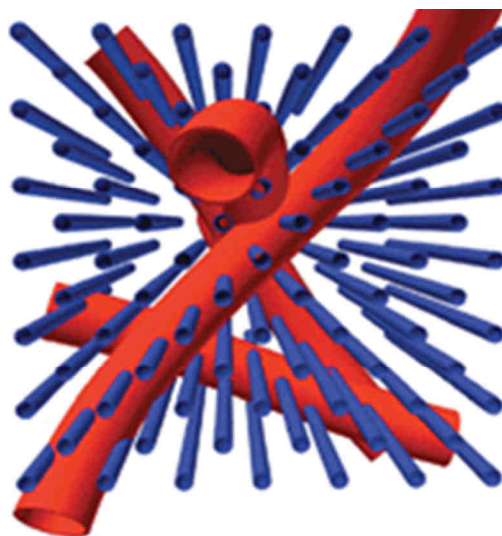


Figure 3.1 Schematic representation of mesoporosity inside the microporous zeolite network [6]

Hence, numerous methods (bottom-up or top-down, template-assisted or not) aimed to prepare hierarchical porous zeolites to overcome mass transfer limitations [7-8].

Bearing in mind all of these zeolite design improvements, the objectives of this Thesis were to prepare MFI and FAU-type zeolites, designed for their future application in either MTO or aromatics chlorination reaction. Hence, “giant” ZSM-5 zeolites were prepared by changing various parameters in the zeolite gel composition, such as the nature of silica source, the concentration in reactants and the synthesis duration. Finally, the replacement

[4] M. Choi, K. Na, J. Kim, Y. Sakamoto, O. Terasaki, R. Ryoo, *Nature* **2009**, *461*, 246–249.

[5] S. C. Larsen, *J. Phys. Chem. C* **2007**, *111*, 18464–18474.

[6] J. Pérez-Ramírez, C. H. Christensen, K. Egeblad, J. C. Groen, *Chem. Soc. Rev.* **2008**, *37*, 2530–2542.

[7] S. van Donk, A. H. Janssen, J. H. Bitter, K. P. de Jong, *Catal. Rev. Sci. Eng.* **2003**, *45*, 297–319.

[8] R. Chal, C. Gérardin, M. Bulut, S. van Donk, *ChemCatChem* **2011**, *3*, 67–81.

of hydrofluoric acid by safer acid (hydrochloric acid) was described. In addition, the development of hierarchical zeolites (FAU and ZSM-5 types) was followed for the design of a competitive chlorination catalyst. Two types of methods were tempted, namely the constructive method and the destructive one. Different characterizations of these materials were used to evaluate the effects of such treatments, thus to establish structure-activity relationships.

2. Hydrothermal synthesis of zeolites

2.1 Alkaline route

2.1.1. Procedures description

Various ZSM-5 and FAU type zeolites were synthesized according to the classical alkaline hydrothermal procedure.

2.1.1.1. Micron-sized ZSM-5 zeolite

The gel for ZSM-5 synthesis was prepared by adding sodium aluminate (52.5 wt.% NaAlO₂, Riedel-de Haën), tetrapropylammonium hydroxide (TPAOH, 1M in water, Alfa Aesar) and sodium chloride in demineralized water at room temperature. Afterwards, tetraethyl orthosilicate (TEOS, 98%, Aldrich) was introduced under vigorous stirring. The molar ratio was as follows: TPAOH: TEOS: NaAlO₂: NaCl: H₂O = 3: 8.07: 0.29: 3.91: 1000. Ageing and homogenization of the mixture run during 1 h. The gel was then poured in a PTFE-lined stainless steel autoclave and the synthesis took place during 168 h at 443 K. After being filtered over a nylon membrane, the solid was then dried at 383 K during 1h and calcined overnight at 823 K in static air. The MFI structure was obtained in its sodium form and was exchanged three times with ammonium nitrate (0.1M, NH₄NO₃, Aldrich) at 353 K, then calcined at 823 K overnight in air, resulting in acid H-ZSM-5 form, named ZSM-5R.

2.1.1.2. Nanosized ZSM-5 zeolite

This procedure was performed thanks to a collaboration with Jean Daou (IS2M, UHA, Mulhouse). The MFI-type nanosheets (called ZSM-5NS) were synthesized according to the following procedure: 0.24 g of sodium hydroxide (Riedel de Haën, 99%) was dissolved in 7.17 g of distilled water in a 45 mL Teflon-lined stainless steel autoclave. 0.73 g of $C_{22}H_{45}-N^+(CH_3)_2-C_6H_{12}-N^+(CH_3)_2-C_6H_{13}Br_2$ and 0.07 g of aluminum sulfate (Rectapur) were then added, under stirring. After homogenization, 2.13 g of TEOS were added, dropwise. Finally, 0.18 g of sulfuric acid (Aldrich) were added in order to set the molar composition of the gel to: 100 SiO_2 : 1 Al_2O_3 : 30 Na_2O : 18 H_2SO_4 : 10 $C_{22}H_{45}-N^+(CH_3)_2-C_6H_{12}-N^+(CH_3)_2-C_6H_{13}Br_2$: 4000 H_2O . The gel was stirred at 1000 rpm during 30 min, prior to be placed in a tumbling oven at a 423 K for 4 days. The autoclave was tumbled at 30 rpm. After synthesis, the product was filtered, washed with distilled water and dried overnight at 373 K. The surfactants were finally removed by calcination in a muffle furnace at 823 K during 8 h in air. The as-synthesized zeolite sample is denoted ZSM-5 nanosheets (ZSM-5NS).

For comparison, MFI-type zeolite nanocrystals were purchased from Zeolyst (CBV 5020) (denoted as ZSM-5NC) and a typical MFI zeolite with large crystals of coffin-shape morphology (denoted as big crystals) was synthesized in the same condition described above for MFI-type nanosheets by adding 2.03 g of a tetrapropylammonium hydroxyde (TPAOH) aqueous solution (20 wt.%, Fluka) instead of an appropriate amount of diquatery ammonium-type surfactant. The composition of the gel was therefore 100 SiO_2 : 1 Al_2O_3 : 30 Na_2O : 18 H_2SO_4 : 20 TPAOH : 4000 H_2O [9].

All samples were NH_4^+ -ion-exchanged with a 1 M NH_4NO_3 aqueous solution at 338 K. The ion exchange process was repeated twice. After filtration and drying, NH_4^+ -ion-exchanged samples were calcined in air at 823 K to obtain the zeolite H^+ -form.

[9] J. Dhainaut, T. J. Daou, Y. Bidal, N. Bats, B. Harbuzaru, G. Lapisardi, H. Chaumeil, A. Defoin, L. Rouleau, J. Patarin, *CrystEngComm* **2013**, *15*, 3009–3015.

2.1.1.3. Silylation procedure

The acid sites from the external surface of commercial nanosized zeolite (Zeolyst, CBV 5020, named ZSM-5NC) were passivated to obtain H-ZSM-5 nanocrystals-P (ZSM-5NCP). In a typical procedure, 1 g of H-ZSM-5 nanocrystals were suspended in a 4 wt.% of TEOS solution (in 25 mL n-hexane) [10]. The suspension was heated for 1h under reflux. Afterwards, the zeolite was filtered over a nylon membrane and passivated H-form was obtained through calcination in an oven at 823 K during 8 h in air. This procedure was repeated twice to obtain ZSM-5NCP2 and ZSM-5NCP3 zeolites.

2.1.1.4. FAU and EMT zeolite procedures

Y zeolite was prepared according to the verified procedure described in the Atlas of zeolites structures [11]. Firstly, the seed gel was prepared in a polypropylene bottle by mixing sodium hydroxide (0.050 mol, NaOH, Aldrich) and sodium aluminate (0.013 mol, 52.5 wt.% NaAlO₂, Riedel-de Haën) in water (10 mL) until complete dissolution. Then, sodium silicate solution (8.2 mL, 10.6 wt.% Na₂O, 26.5 wt.% (SiO₂)_x, Aldrich) was added and stirred for 10 min. the bottle was capped and the solution was aged at room temperature for 24h. Afterwards, sodium hydroxide (5.75.10⁻⁴ mol), sodium aluminate (0.027 mol) and water (22 mL) were stirred in a polypropylene bottle until complete dissolution. Then, sodium silicate solution (17.1 mL) was added to the previous mixture and stirred vigorously until the gel appeared smooth. Finally, 2.84 g of seed gel were slowly added and blended under vigorous stirring (1200 rpm). The polypropylene bottle was sealed and heated in an oven at 373 K for 6 h. The supernatant liquid must be cleared to achieve a complete crystallization. The mixture was cooled down to room temperature, filtered over a nylon membrane, washed with water until pH 9. The white solid was then dried in an oven overnight. The H-FAU form was obtained by exchanging three times the zeolite with a 1M ammonium nitrate aqueous solution at 353 K for 3 h, and then the catalyst was calcined at 853 K overnight in static air.

[10] S. Zheng, H. R. Heydenrych, H. P. Röger, A. Jentys, J. A. Lercher, *Top. Catal.* **2003**, 22, 101–106.

[11] H. Robson and K.P. Lillerud, in *Verified Syntheses of zeolitic materials*, Second edition (Ed.: H. Robson), Elsevier B.V., **2001**.

Finally, EMC-1 and EMC-2 zeolites, having FAU and EMT topology respectively, were synthesized in a PTFE-lined stainless steel autoclave using the following gel molar compositions 2.1 Na₂O: 10 SiO₂: 1 Al₂O₃: 0.5 15-crown-5: 100 H₂O (EMC-1); 2.1 Na₂O: 10 SiO₂: 1 Al₂O₃: 0.5 18-crown-6: 100 H₂O (EMC-2) at 383 K for 10 days. Sodium hydroxide (99.99 wt.%, Riedel de Haën), colloidal silica (Ludox AS-40, Aldrich), sodium aluminate (57 wt.% Al₂O₃, 40 wt.% Na₂O, Strem Chemicals), 15-crown-5 (98 wt.%, Alfa Aesar), 18-crown-6 (95 wt.%, Alfa Aesar) and distilled water were chemical reagents used in this step. After being filtered, washed with water and dried at 343 K overnight, the zeolite was calcined at 823 K during 6 h to remove the template.

2.1.2. Characterizations

Alkaline-synthesized zeolites were characterized thanks to different techniques in order to ascertain their morphologies and to analyze their intrinsic properties.

X-ray diffraction analyses (XRD)

The different catalysts were firstly characterized by X-ray diffraction. XRD patterns were recorded using a PANalytical MPD X'Pert Pro diffractometer operating with Cu K α radiation ($\lambda = 0.15418$ nm) equipped with an X'Celerator real-time multiple strip detector (active length = 2.122° 2 θ). This technique allows verifying topologies and crystallinities of each zeolites. The representative powder X-ray diffraction patterns are shown in Figure 3.2 for ZSM-5R, ZSM-5NC, ZSM-5NS zeolites [12].

According to these patterns, the sole crystalline MFI phase was obtained for all zeolites (Figure 3.2). As 'a priori' expected, XRD reflections of ZSM-5 nanocrystals and ZSM-5 nanosheets are broader than those of micron-sized ZSM-5 crystals synthesized in the presence of conventional structure directing agent (TPAOH). This can be explained by the smaller crystal size of the ZSM-5 nanosheets and nanocrystals with respect to ZSM-5 crystals synthesized in the presence of TPAOH. In addition, the major part of the reflections of ZSM-5NS sample belongs to the (h0l) crystallographic plane, providing the sign that a one-

[12] M. Boltz, P. Losch, B. Louis, G. Rioland, L. Tzanis, T. J. Daou, *RSC Adv.* **2014**, *4*, 27242–27249.

dimensional growth-inhibition is undertaken along the *b*-axis, thus confirming the formation of nanosheets [13]. Surprisingly, despite this expected *b*-axis growth inhibition, the [101] reflection could be observed for ZSM-5NS (Figure 3.2c). Taking into account that a reflection is usually discernible in the presence of 4/5 unit cells, one could hypothesize that the morphology of our ZSM-5NS crystals is rather of nanometric type than nanosheets' assembly.

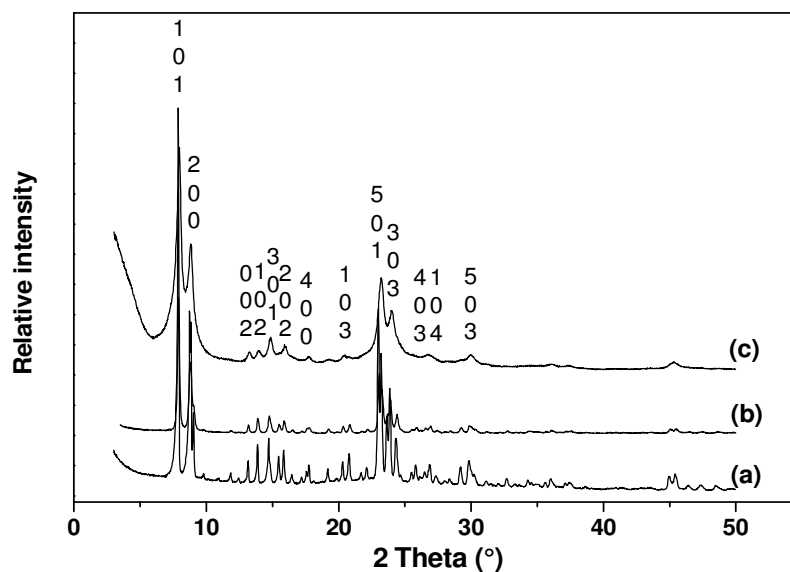


Figure 3.2. XRD patterns of ZSM-5 zeolites, big crystals ZSM-5R (a), nanocrystals ZSM-5NC (b), nanosheets ZSM-5NS (c)

The representative XRD patterns of EMC-1, EMC-2 and USY zeolites are presented in Figure 3.3. Furthermore, Figure 3.4 shows the XRD patterns of Y zeolite.

According to these patterns, pure crystalline FAU and EMT-type zeolites have been obtained for EMC-1, EMC-2 and FAU materials, a commercial USY zeolite has been used as a reference material.

[13] K. Na, M. Choi, W. Park, Y. Sakamoto, O. Terasaki, R. Ryoo, *J. Am. Chem. Soc.* **2010**, *132*, 4169–4177.

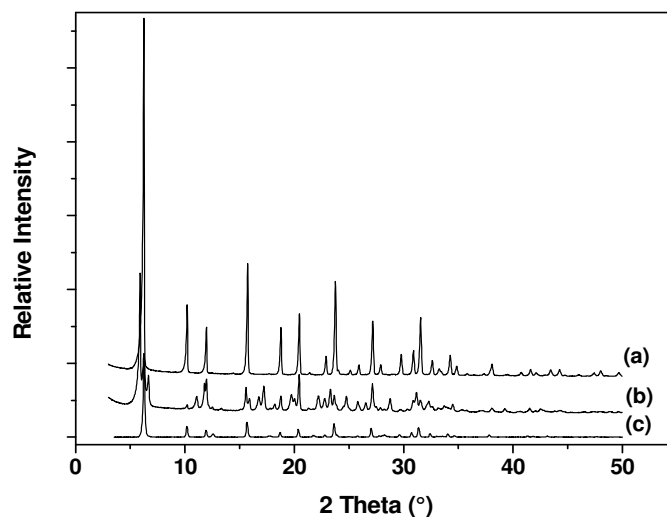


Figure 3.3 XRD patterns of as-synthesized EMC-1 (a), EMC-2 (b), and USY zeolites (c)

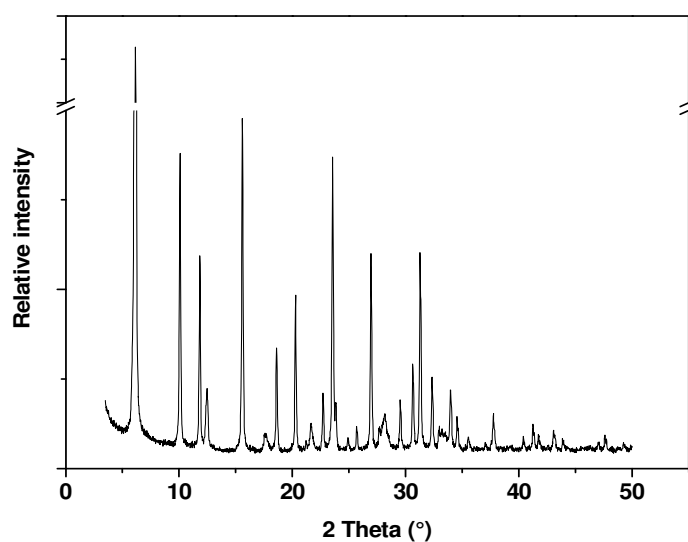


Figure 3.4. XRD pattern of Y zeolite

SEM analyses

All as-synthesized alkaline zeolites were analyzed by scanning electron microscopy to determine their crystal size and morphology with a Philips XL 30 FEG microscope or a JEOL FEG 6700F microscope working at 9 kV accelerating voltage.

The SEM micrographs given in Figure 3.5 reveal the shape of the zeolite crystals. The ZSM-5 big crystals synthesized in the presence of TPAOH exhibit the characteristic prismatic morphology shape and a 10-15 μm length. In contrast, MFI-type zeolite synthesized in the

presence of diquaternary ammonium surfactant exhibits a nanosheet morphology. A multi-lamellar stacking of MFI nanosheets has been three-dimensionally intergrown. The overall thickness of the lamellar stacking was normally 20–40 nm. The stacking was composed by alternating layers of 2-nm-thick MFI zeolite framework and 2.8-nm-thick surfactant micelles. The zeolite layer was composed of three pentasil sheets, which corresponds to a single unit cell dimension along the b-axis (1.974 nm) [4]. The commercial ZSM-5 nanocrystals exhibit a spherical shape with an average size between 200 and 400 nm (Figure not shown).

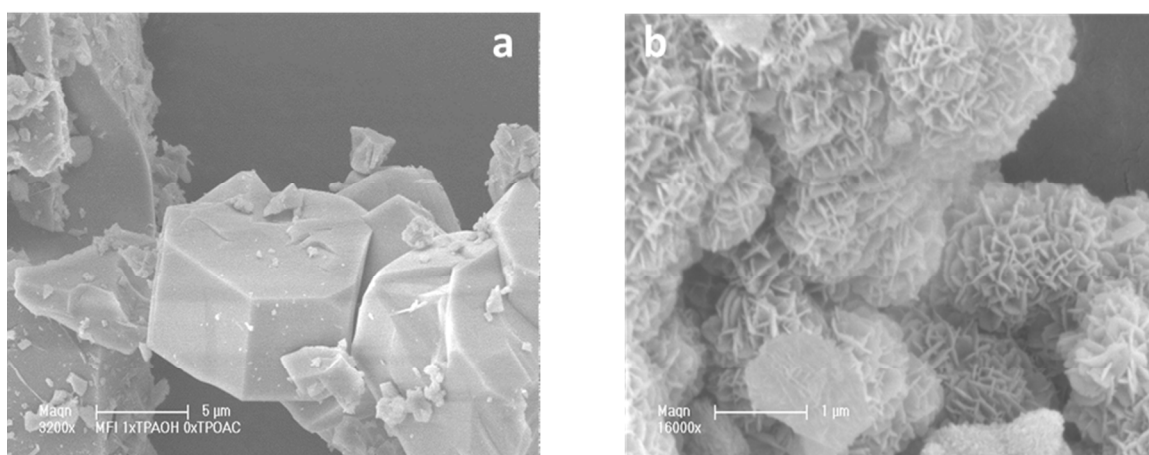


Figure 3.5 SEM micrographs of ZSM-5 zeolites, big crystals ZSM-5R (a) and nanosheets ZSM-5NS (b)

The SEM micrographs given in Figure 3.6 reveal the shape of zeolite particles. EMC-1 zeolite crystals exhibit characteristic pyramidal shape of about 1 μm. In contrast, EMC-2 zeolite (EMT-type) crystals exhibit a regular hexagonal platelet morphology of 2 μm.

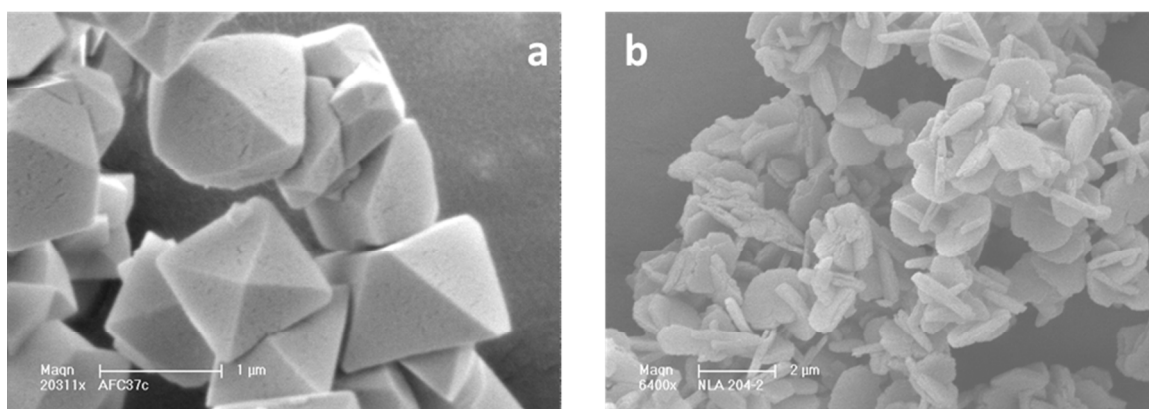


Figure 3.6 SEM images of EMC-1 (a) and EMC-2 zeolites (b)

Chemical composition and Brønsted acidity

The elementary analysis of alkaline catalysts was performed by X-Ray Fluorescence (Phillips, Magic X or XEPOS, AMETEK). Moreover, H/D exchange isotope technique was used to determine the number of Brønsted acid sites present in the different solid acids. Table 3.1 shows the silicon to aluminum ratio (Si/Al) and the Brønsted acidity of representative catalysts.

Table 3.1 Chemical composition and Brønsted acidity of representative alkaline zeolites

Zeolite	Si/Al ratio	Brønsted acid sites [mmol H ⁺ .g ⁻¹]
ZSM-5R	28	0.59
ZSM-5NC	25	0.86
ZSM-5NCP3	-	0.46
ZSM-5NS	48	1.17
EMC-1	4.0	4.63
EMC-2	4.0	4.36
Y	2.6	5.34

Surprisingly, ZSM-5NS sample exhibits a large quantity of titrated Brønsted acid sites compared to ZSM-5R and ZSM-5NC zeolites (1.17 vs. 0.59 and 0.86 mmol H⁺.g⁻¹, respectively). One could hypothesize that by this titration method, structural defects sites have been measured and render the measurement inaccurate for this sample.

N₂ adsorption-desorption measurements

Nitrogen adsorption / desorption isotherms were measured using a Micromeritics ASAP 2420 apparatus. The specific surface area (S_{BET}) and mesoporous volume (V_{meso}), and microporous volume (V_{micro}) were calculated using BET and t -plot methods, respectively.

As expected for microporous solids, typical type I isotherms were observed for ZSM-5 nanocrystals and big crystals (Figure 3.7), with a slight hysteresis for ZSM-5 nanocrystals due to nanocrystals agglomeration. In the presence of diquatery ammonium-type surfactant, the isotherms are of type I and IV. The presence of mesopores generated by the planar

stacking of ZSM-5 nanosheets (intercrystalline porosity) is responsible for the higher adsorbed volume (mesoporous volume).

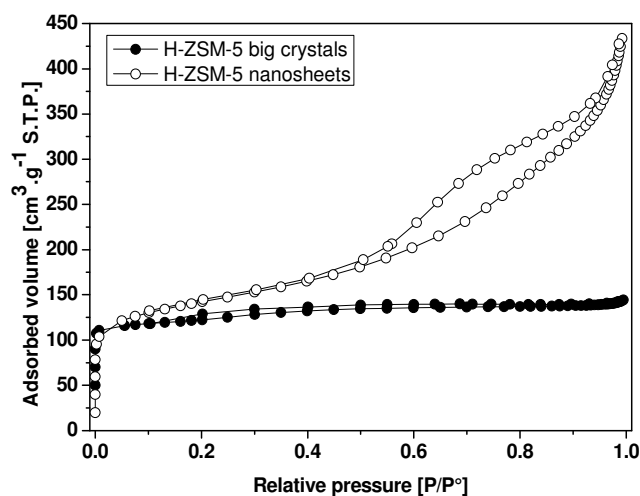


Figure 3.7 N_2 adsorption-desorption isotherms of ZSM-5R (solid circles), ZSM-5NS (empty circles) zeolites

Typical type I isotherms were observed in Figure 3.8 for FAU and EMT zeolites. As expected, classical microporous materials were obtained.

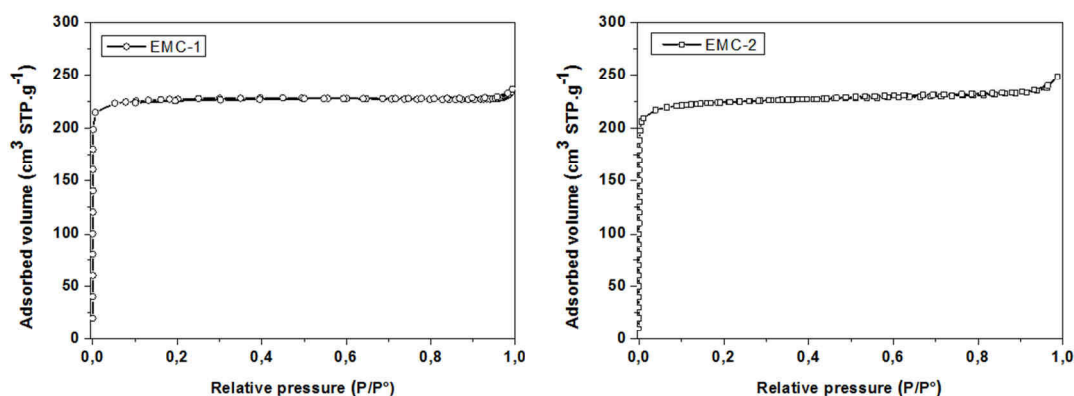


Figure 3.8 N_2 adsorption-desorption isotherms at 77 K of EMC-1 (left) and EMC-2 zeolites (right)

The associated Brunauer-Emmett-Teller (BET) surface area, microporous volume and external surface of alkaline type zeolites are reported in Table 3.2. It is worthy to note that ZSM-5 nanosheets exhibit a much higher BET surface area (S_{BET}) and a large mesopore volume ($503 \text{ m}^2/\text{g}$ and $0.48 \text{ cm}^3/\text{g}$, respectively) compared with big crystals ZSM-5R (351

m²/g and no mesopore volume). This can be attributed to the large number of intergrowths in nanosheet crystals and to the slight deviations of the crystal orientations in *a-c* planes [4].

Table 3.2 Textural properties of zeolites measured by N₂ sorption

Zeolite	S _{BET} ^a [m ² /g]	V _{micro} ^b [cm ³ /g]	V _{meso} ^c [cm ³ /g]	V _{tot} ^a [cm ³ /g]
H-ZSM-5R	351	0.18	-	-
H-ZSM-5NS	503	0.18	0.48	0.66
H-ZSM-5NC	402	0.14	0.11	0.25
H-ZSM-5NCP	349	-	-	0.21
H-ZSM-5NCP2	348	-	-	0.21
H-ZSM-5NCP3	321	-	-	0.20
H-EMC-1	935	0.34	-	-
H-EMC-2	895	0.33	-	-

^a BET method applied to the N₂ isotherm

^b t-plot method applied to the N₂ isotherm

^c V_{meso} = V_{tot} - V_{micro}. V_{tot} was determined from the amount of N₂ adsorbed at P/P₀ = 0.97

2.2 Fluoride route

2.2.1. Procedure

Several ZSM-5 zeolites were synthesized *via* fluoride-mediated route to investigate different parameters: density of Brønsted acid sites, crystal size, chemical composition (Table 3.3). MFI-F catalysts were prepared *via* the latter route according to previous studies [14]. In addition, this procedure was modified by substituting hydrofluoric acid by hydrochloric acid to maintain a neutral pH. These samples were named ZSM-5FCl.

All ZSM-5F zeolite syntheses were performed in a PTFE lined autoclave at 443 K for defined durations. All ZSM-5F samples obtained were calcined in static air during 6 h at 823 K.

[14] J. Arichi, B. Louis, *Cryst. Growth Des.* **2008**, *8*, 3999–4005.

Table 3.3 Summary of synthesis conditions of fluoride zeolites

Entry	Zeolite type	Si source	NaAlO ₂	NH ₄ F	TPABr	H ₂ O	Acid type	Duration (h)
F1	ZSM-5F	TEOS:100	3	112	7	7990	HF	168
F2	ZSM-5F	Aeroperl:100	1	112	7	7990	HF	46
F3	ZSM-5F	Aerodisp:100	1	112	7	7990	HF	46
F4	ZSM-5F	Aerodisp:100	1	112	7	7990	HF	144
F5	ZSM-5F	Aeroperl:100	1	112	7	7990	HF	144
F6	ZSM-5F	Aeroperl:100	3	112	7	7990	HF	144
F7	ZSM-5F	Aeroperl:100	10	112	7	7990	HF	144
F8	ZSM-5F	Aeroperl:100	3	56	7	7990	HF	144
F9	ZSM-5F	Aeroperl:100	1	112	7	7990	HF	24
F10	ZSM-5F	Aeroperl:100	1	100	7	7990	HF	166
F11	ZSM-5FCl	Aeroperl:100	1	112	7	7990	HCl	48
F12	ZSM-5FCl	Aeroperl:100	1	112	7	7990	HCl	166
F13	ZSM-5FCl	Aeroperl:100	1	168	7	7990	HCl	161
F14	ZSM-5FCl	Aeroperl:100	1	224	7	7990	HCl	161

2.2.2. Characterizations

The characterization data will be restricted to six ZSM-5F samples, to show the influence of various parameters.

XRD analyses

Figure 3.9 presents the XRD pattern of one fluoride-mediated zeolite (F2). All XRD patterns exhibit the sole MFI structure and present high crystallinities.

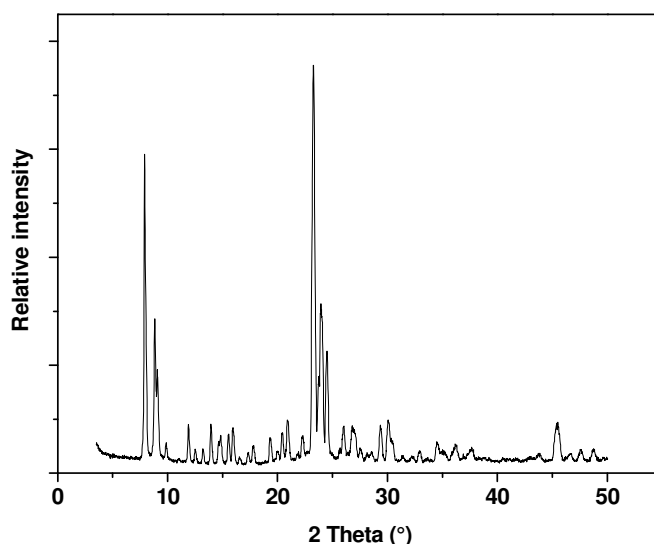


Figure 3.9 XRD pattern of fluoride-mediated zeolite (entry F2 in Table 3.3)

Chemical composition

The elementary analysis of alkaline catalysts was performed by X-Ray Fluorescence (XRF, XEPOS, AMETEK). Moreover, H/D exchange isotope technique was used to determine the number of Brønsted acid sites present in several solid acids and the values range from 0.15 to 0.30 mmol H⁺/g.

Table 3.4 shows the Si/Al ratio of representative catalysts.

Table 3.4 Chemical composition and Brønsted acidity of fluoride-mediated zeolites

Zeolite	Si/Al ratio
F2	136
F4	207
F5	165
F6	45
F7	41
F8	44
F9	142
F10	403
F12	196
F13	230

F14	237
-----	-----

SEM analyses

SEM characterizations were performed to evaluate the morphologies and determine the crystallization level of each catalyst. It is worthy to mention that each zeolite exhibits the classical coffin shape morphology, typical for MFI zeolites (Figure 3.10).

The crystal volume distribution in each samples is fairly narrow (Table 3.5). Indeed, one can note that smaller ZSM-5 crystals possess a volume of $270 \mu\text{m}^3$ (F6). In contrast, the bigger crystal exhibits a $6500 \mu\text{m}^3$ volume (F10). These dimension variations could be attributed to different factors. Indeed, the composition of the gel, in particular the Si/Al ratio, plays an important role. When the Si/Al ratio is diminished in the gel from 100/1 to 100/3, the crystal size is decreased from $1470 \mu\text{m}^3$ to $270 \mu\text{m}^3$ (F5 vs. F6). However, when the Si/Al gel ratio is further diminished to 100/10, there is no more effect in the crystal size (F6 vs. F7). The silicon source plays also an impact on the particle morphology. Aerodisp source allows forming less crystalline particles with a nearly tripled volume when compared with Aeroperl source (F2 vs. F3). Furthermore, the synthesis duration is another key parameter in crystal size design. For the same gel composition, a raise in the synthesis duration from 46 h to 144 h led to produce bigger crystals (F2 vs. F5). The level of intergrowth does not seem to follow the variation in synthesis parameters.

Finally, one can see that the replacement of HF by HCl was successful due to the formation of typical ZSM-5 crystals synthesized in a fluoride media. However, the crystallinity of these HCl-mediated zeolites appears lower than those obtained with HF (F5 vs. F12 in Figure 3.10). One can observe that the raise in the quantity of NH_4F is beneficial to achieve higher crystallinities (F12 vs. F14). The highest crystallinity was obtained for HCl-mediated zeolite prepared with a $\text{NH}_4\text{F}/\text{Al}$ molar ratio of 168 in the synthesis gel (F13 not shown).

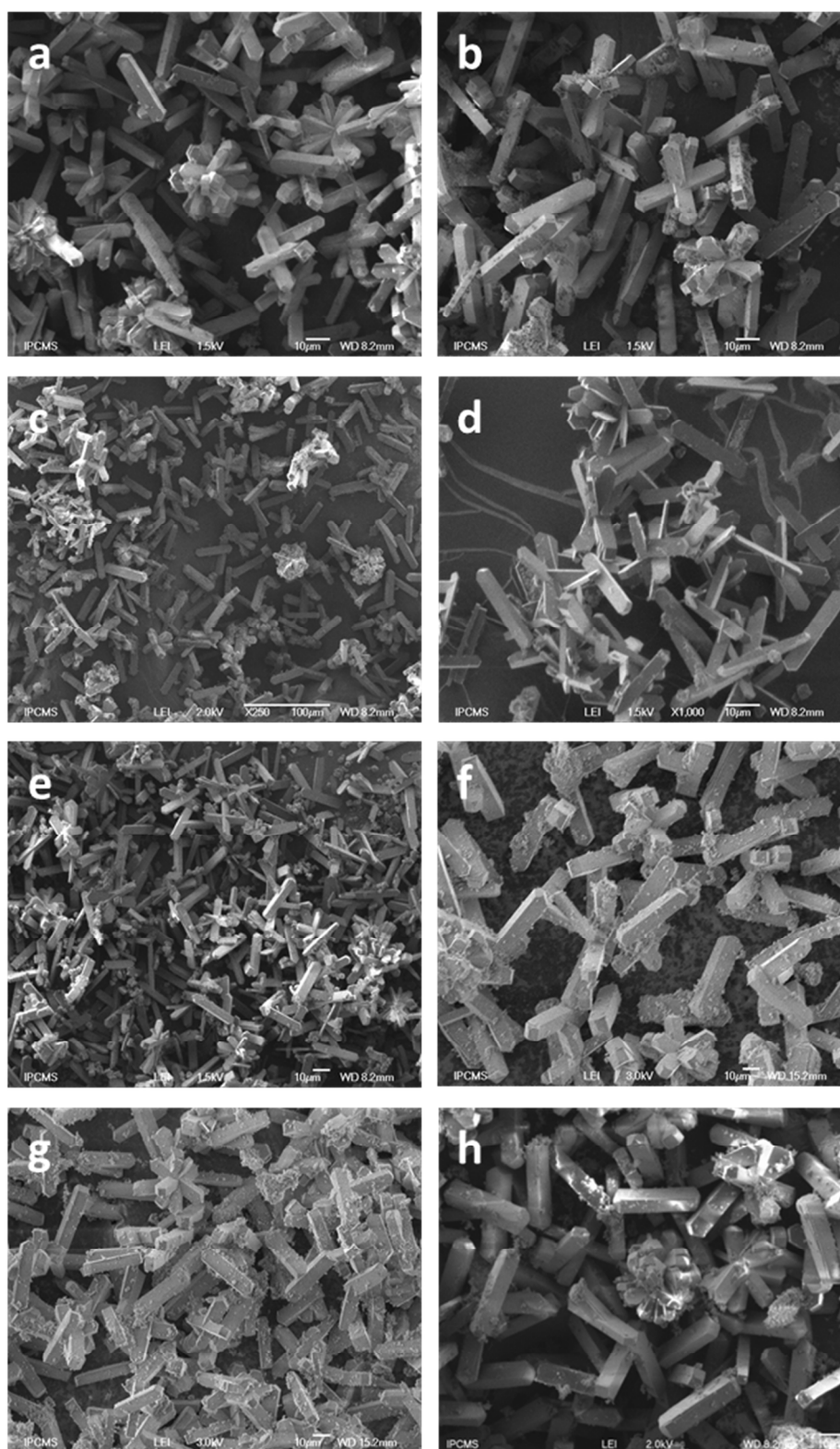


Figure 3.10 SEM images of fluoride-mediated zeolites, a) F2, b) F3, c) F5, d) F6, e) F7, f) F10, g) F12 and h) F14

Table 3.5 Morphologic characteristics of fluoride-mediated zeolites

Entry	Crystal length ^a [μm]	Crystal width ^a [μm]	Crystal thickness ^a [μm]	Crystal volume [μm^3]	Intergrowth amount
F2	30	6	3	540	many
F3	41	8	4	1475	few
F5	42	7	5	1470	few
F6	27	5	2	270	few
F7	26	5	3	390	few
F10	50	13	10	6500	few
F12	35	8	6	1680	very few
F13	31	7	3	651	many
F14	38	8	6	1824	many

^a average of 3 crystal size measures

N₂ adsorption-desorption measurements

The textural properties of two representative fluoride-mediated zeolites have been analyzed (F6 and F14 samples). Figure 3.11 presents the N₂ adsorption-desorption isotherms of the two samples. One can note that classical microporous materials were synthesized, since type I isotherms have been obtained for these two fluoride-mediated zeolites.

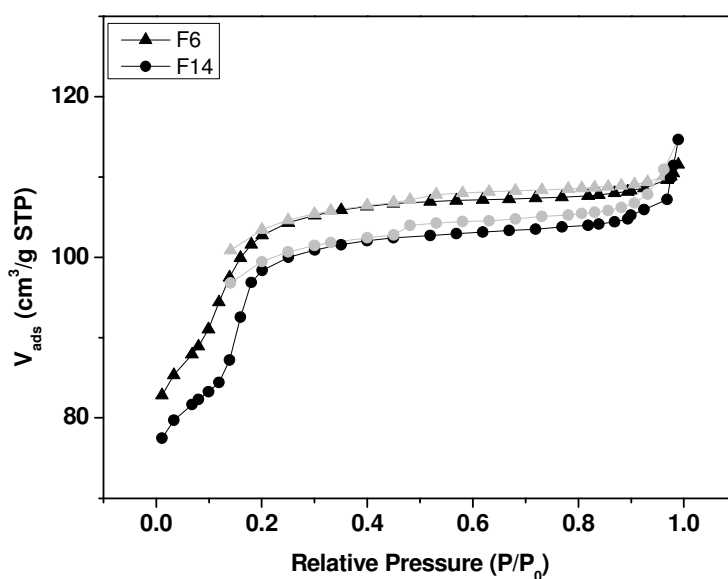


Figure 3.11 N₂ adsorption and desorption isotherms at 77 K of ($\blacktriangle, \triangle$) ZSM-5 synthesized in the presence of HF and (\bullet, \circ) ZSM-5 synthesized in the presence of HCl

Table 3.6 summarizes the textural properties of F6 and F14 zeolites. Similar BET surfaces have been calculated, 345 and 335 m²/g for the ZSM-5 synthesized in the presence of HF and HCl, respectively. Besides, these samples exhibit low microporous volume compared to classical ZSM-5 zeolite.

Table 3.6 Textural composition of two fluoride-mediated ZSM-5 zeolites

Entry	S _{BET} ^a [m ² /g]	V _{tot} ^a [cm ³ /g]
F6	345	0.17
F14	335	0.17

^a BET method applied to the N₂ isotherm

It appears therefore that no textural differences could be observed while replacing HF by HCl. Thus, the substitution of HF with HCl has been successfully performed. Typical fluoride zeolite crystals having similar intrinsic properties have been obtained by this strategy.

3. Preparation of hierarchical zeolites

3.1 Constructive synthesis strategy

3.1.1. Double templating approach

3.1.1.1. Procedure

The gel was prepared by adding sodium aluminate (52.5 wt.% NaAlO₂, Riedel-de Haën), sodium chloride (NaCl, Aldrich), and tetrapropylammonium hydroxide (TPAOH, 1M in water, Alfa Aesar) in demineralized water at room temperature. Then, spermine (C₁₀H₂₆N₄, ≥97%, Sigma) and finally TEOS were introduced under vigorous stirring. The gel possessed the following molar composition: NaAlO₂: TEOS: TPAOH: NaCl: spermine: H₂O = 0.3: 8.1: 2.4: 3.9:

0.6: 1000. The ageing step took place during 1 h. Afterwards, the mixture was transferred in a stainless steel autoclave (75 mL) and heated at 443 K under autogenous pressure for 161 h. The solid was filtered and washed with distilled water over a nylon membrane and dried in an oven at 383 K for 4 h. The zeolite was then ion exchanged with NH_4NO_3 (3 times) at 353 K during 3 h and calcined at 823 K overnight in static air. Hence, the zeolite synthesized by double templating (DT-ZSM-5) was obtained in its H-form.

3.1.1.2. Characterizations

Different characterizations have been performed in order to observe the effect of the second template spermine on the DT-ZSM-5 zeolite crystallization and its intrinsic properties.

XRD analysis

Figure 3.12 shows the XRD pattern of well-crystalline ZSM-5 catalyst synthesized *via* the double templating approach. The DT-ZSM-5 zeolite exhibits the sole characteristic diffraction reflections of MFI type material. The addition of the second template did not affect the crystallization toward the MFI structure.

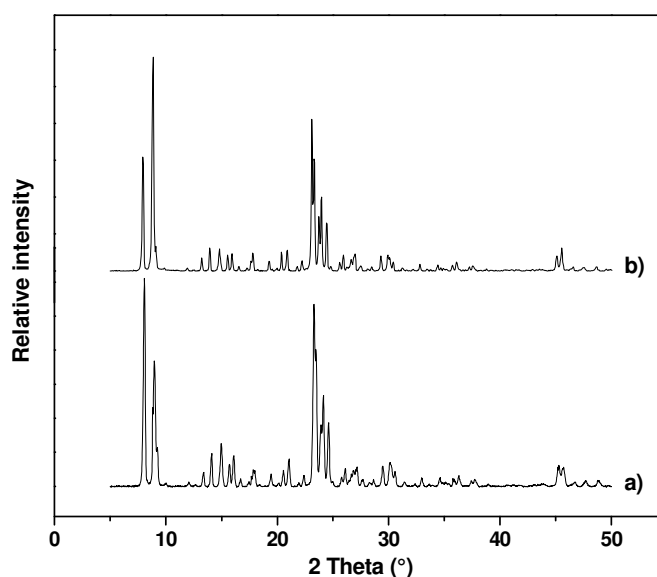


Figure 3.12 XRD patterns of the a) pristine and b) DT-ZSM-5 zeolites

SEM analyses

The DT-ZSM-5 zeolite crystals exhibit a conventional coffin-shape for MFI zeolite (Figure 3.13). In addition, their outer surfaces present a high roughness, as shown in the higher magnified image. This roughness may suggest the formation of inter-crystalline mesoporosity during the crystallization.

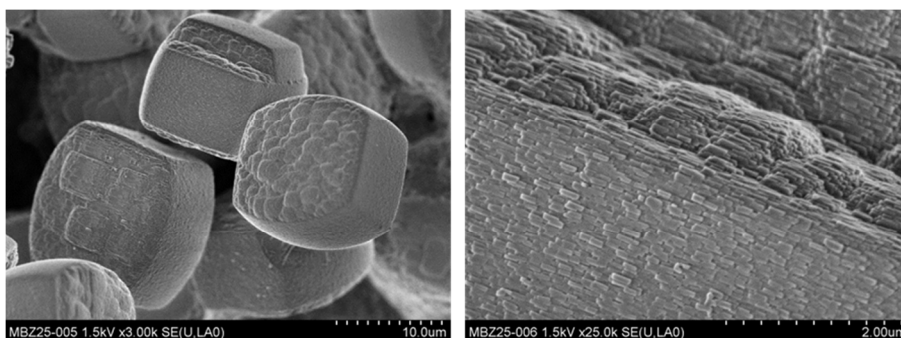


Figure 3.13 SEM images of DT-ZSM-5 zeolite at different magnifications

N₂ adsorption-desorption measurements

Figure 3.14 presents N₂ adsorption-desorption isotherm and BJH adsorption pore size distribution obtained for the zeolite synthesized *via* the double templating method.

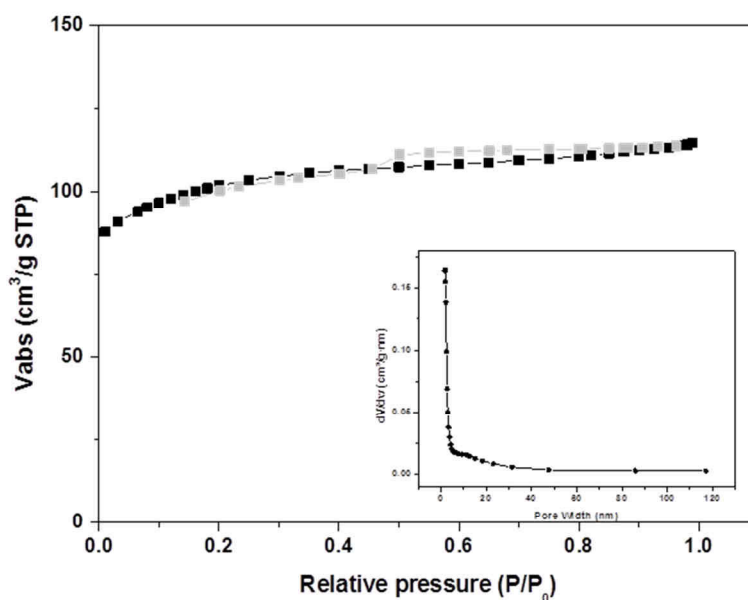


Figure 3.14 N₂ adsorption and desorption isotherm at 77 K and BJH adsorption pore size distribution (inset) of DT-ZSM-5

One can observe that the isotherm is of type I with a plateau at higher relative pressures, confirming the microporous nature. Moreover, the BJH pore size distribution derived from the adsorption branch of the isotherm does not show any mesoporosity in ZSM-5 DT. In conclusion, the addition of spermine as second template in the synthesis gel does not lead to the creation of an additional mesoporosity.

The textural properties of ZSM-5 DT zeolite are shown in Table 3.7. The zeolite exhibits classical BET surface area and total pore volume expected for microporous zeolite, being 333 m²/g and 0.24 m³/g, respectively. Moreover, no significant mesoporous volume has been created during the synthesis.

Table 3.7 Textural properties of ZSM-5 DT zeolite

Zeolite	S _{BET} ^a [m ² /g]	V _{tot} ^a [m ³ /g]
ZSM-5 DT	333	0.24

^a BET method applied to the N₂ isotherm

3.2 Destructive synthesis strategy

3.2.1. Dealumination

3.2.1.1. Procedures

Steaming treatments

Home-made Y zeolite and powdered ZSM-5 zeolite (Zeolyst International, CBV 5020, Si/Al=25, NH₄⁺-form) were calcined in static air at 823 K overnight using a heating rate of 10 K/min. The resulting samples, denoted as parent (P), were subjected to different dealumination treatments.

Pristine ZSM-5P sample suffered mild and severe steamings under different water vapor pressures. The first step was the activation of the catalyst (700 mg) under N₂ flow at the steaming temperature, followed by the steaming treatment at given flow rates and

temperatures for a defined time (see Table 3.8). The ZSM-5 ST2 sample was prepared by repeating the ZSM-5 ST1 procedure twice.

Table 3.8 Steaming conditions of dealuminated zeolites

Sample	Flow rate [mL.min ⁻¹]	Partial water vapor [mmol.h ⁻¹]	Temperature [°K]	Treatment duration [h]
ZSM-5 or Y ST1	40	2.3	723	15
ZSM-5 or Y STS	40	11.6	823	24

Chemical treatment

Steamed ZSM-5 ST1 and STS and the commercial USY samples were further modified with an ethylenediamine-tetraacetic acid disodium salt dihydrate solution (Na₂.H₂-EDTA) to remove the excess of extra-framework aluminum species present in zeolite micropores. The samples (300 mg) were dispersed in a Na₂.H₂-EDTA solution (0.1 M aq., 30 mL, ≥ 99%, Aldrich), stirred at 650 rpm and heated at 335 K for one day. The zeolite was then filtered and washed with distilled water over a nylon membrane and finally dried in an oven at 383 K overnight. The zeolites obtained in their Na-forms were ion exchanged three times with a NH₄NO₃ solution (0.1 M, 20 mL) at 353 K. The zeolites in their H-form (ZSM-5 ST1-EDTA, ZSM-5 STS-EDTA and USY-EDTA, respectively) were obtained after a calcination step at 823 K overnight in air.

Acid treatment

The pristine zeolite (1 g) was dispersed in 20 mL of oxalic acid solution (1 M aq., Aldrich), stirred and heated under reflux for 1 h. After cooling to room temperature, the solid was filtered, washed with distilled water over a nylon membrane and dried at 383 K in an oven for 10 minutes. The ZSM-5 OA was finally calcined in static air at 823 K overnight.

3.2.1.2. Characterizations

Chemical composition

The elementary analysis of alkaline catalysts was performed by X-Ray Fluorescence (XRF, XEPOS, AMETEK). H/D exchange isotope technique was used to determine the total

number of Brønsted acid sites. The silicon to aluminum ratio (Si/Al) and the Brønsted acidity are given in Table 3.9.

All dealuminated zeolites present higher Si/Al ratios with respect to pristine ZSM-5P zeolite, which could be attributed to the extraction of aluminum atoms from the microporous framework. Indeed, it is well-known that steaming treatment induces the extraction of Al atoms from the zeolite framework to create EFAl species [15]. ZSM-5 ST and STS samples exhibit rather similar and constant Si/Al ratio compared with pristine zeolite (*i.e.*, 34 and 34 vs. 31) since EFAl species formed during the hydrothermal treatment are not leached out of the solid.

Table 3.9 Chemical composition of dealuminated zeolites

Entry	Si/Al ratio	Brønsted acidity [mmol H ⁺ .g ⁻¹]
ZSM-5 P	25	0.86
ZSM-5 ST1	34	0.83
ZSM-5 ST1-EDTA	41	-
ZSM-5 ST2	-	1.01
ZSM-5 STS	35	0.51
ZSM-5 STS-EDTA	40	-
ZSM-5 OA	-	1.00

However, the leaching of EFAl species with EDTA leads to further increase in the Si/Al ratio, *i.e.*, 41 and 40 for ZSM-5 ST1-EDTA and STS-EDTA, respectively, vs. 25 for pristine zeolite.

Finally, the Brønsted acidity was slightly affected by the steaming treatment severity. Indeed, ZSM-5 ST1 and STS samples see their acidities vanished, *i.e.*, 0.83 and 0.51, respectively vs. 0.86 mmol_{H⁺}.g⁻¹ for pristine ZSM-5). In contrast, ZSM-5 ST2 and OA zeolites exhibit higher Brønsted acidities, which might be attributed to the re-insertion of EFAl species in the zeolite framework, as reported by Almutairi *et al.* [16].

[15] a) C. S. Trianta, A. G. Vlessidis, L. Nalbandian, N. P. Evmiridis, *Microporous Mesoporous Mater.* **2001**, *47*, 369–388.

[16] S. M. T. Almutairi, B. Mezari, E. A. Pidko, P. C. M. M. Magusin, E. J. M. Hensen, *J. Catal.* **2013**, *307*, 194–203.

XRD analyses

Figure 3.15 shows the XRD patterns of several dealuminated ZSM-5 zeolites. All dealuminated samples exhibit the sole characteristic diffraction reflections of MFI type material. One could also notice that no significant amorphous phase is formed during dealumination treatments. Thus, all zeolites present high crystallinities.

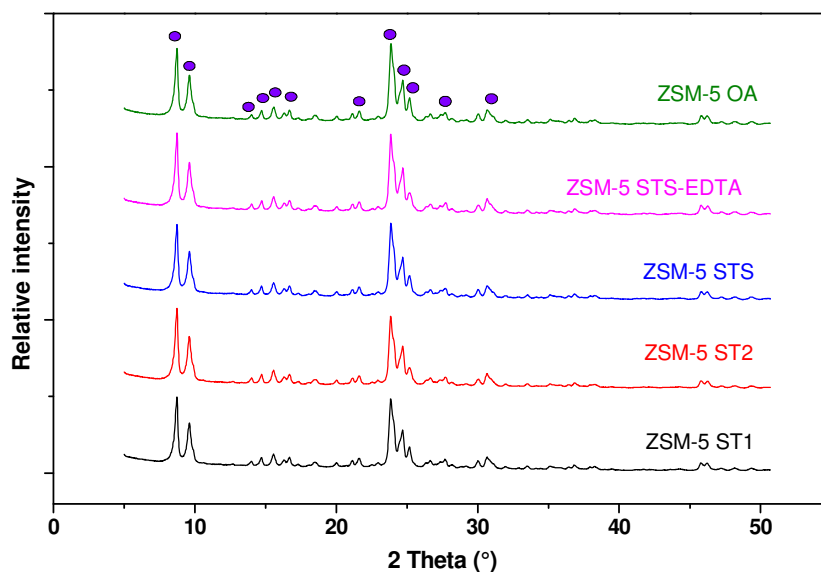


Figure 3.15 XRD patterns of the dealuminated ZSM-5 zeolites

N₂ adsorption-desorption measurements

The specific surface areas (S_{BET}) of the samples varied between 356 and 406 $\text{m}^2\cdot\text{g}^{-1}$ (Table 3.10). For steam-treated catalysts, BET surfaces were observed to decrease, especially the strong steamed ZSM-5 STS suffered a BET surface decrease compared with pristine zeolite (357 vs. 402 $\text{m}^2\cdot\text{g}^{-1}$, respectively). This behavior could be explained by the fact that during the steaming, extra-framework aluminum species (EFAl) are created and could hinder the pores' accessibility. For ZSM-5 ST1 sample, this effect is less pronounced. The EFAl complexation by EDTA treatment did not allow the ZSM-5 ST1 to recover its initial surface area. Nevertheless, EDTA treatment led to partial EFAl leaching outside the porous system (see also NMR analyses) for ZSM-5 STS sample. Finally, the dealuminated ZSM-5 zeolite with oxalic acid shows similar textural properties with respect to ZSM-5 ST1 sample.

Besides, the total pore volume (V_{tot}) of dealuminated ZSM-5 zeolites varied slightly from 0.24 to 0.27 $\text{cm}^3 \cdot \text{g}^{-1}$. The drastic steaming treatment led to the higher V_{tot} , but there is no clear evidence for the formation of significant mesoporosity in treated zeolites.

The leaching of EFAl species in USY EDTA sample allowed to increase both BET surface area and total pore volume with respect to pristine USY zeolite (*i.e.*, 693 $\text{m}^2 \cdot \text{g}^{-1}$ and 0.44 $\text{cm}^3 \cdot \text{g}^{-1}$ vs. 642 and 0.38).

Table 3.10 Textural properties of dealuminated zeolites

Zeolite	$S_{\text{BET}}^{\text{a}}$ [$\text{m}^2 \cdot \text{g}^{-1}$]	$V_{\text{tot}}^{\text{a}}$ [$\text{cm}^3 \cdot \text{g}^{-1}$]
ZSM-5 P	402	0.25
ZSM-5 ST1	386	0.25
ZSM-5 ST1-EDTA	383	0.25
ZSM-5 STS	357	0.24
ZSM-5 STS-EDTA	406	0.27
ZSM-5 OA	377	0.24
USY P	642	0.38
USY EDTA	693	0.44

^a BET method applied to the N_2 isotherm

Figure 3.16 presents the N_2 adsorption-desorption isotherms of dealuminated ZSM-5 catalysts. Typical type I isotherms with no distinct hysteresis loop were found for the most part of samples, being characteristic for conventional microporous zeolites. One can note the apparition of a weak hysteresis in strong steamed ZSM-5 STS. The intensity of this hysteresis slightly increased with the extraction of EFAl species (ZSM-5 STS-EDTA) from the porous architecture and in oxalic acid treated sample (ZSM-5 OA).

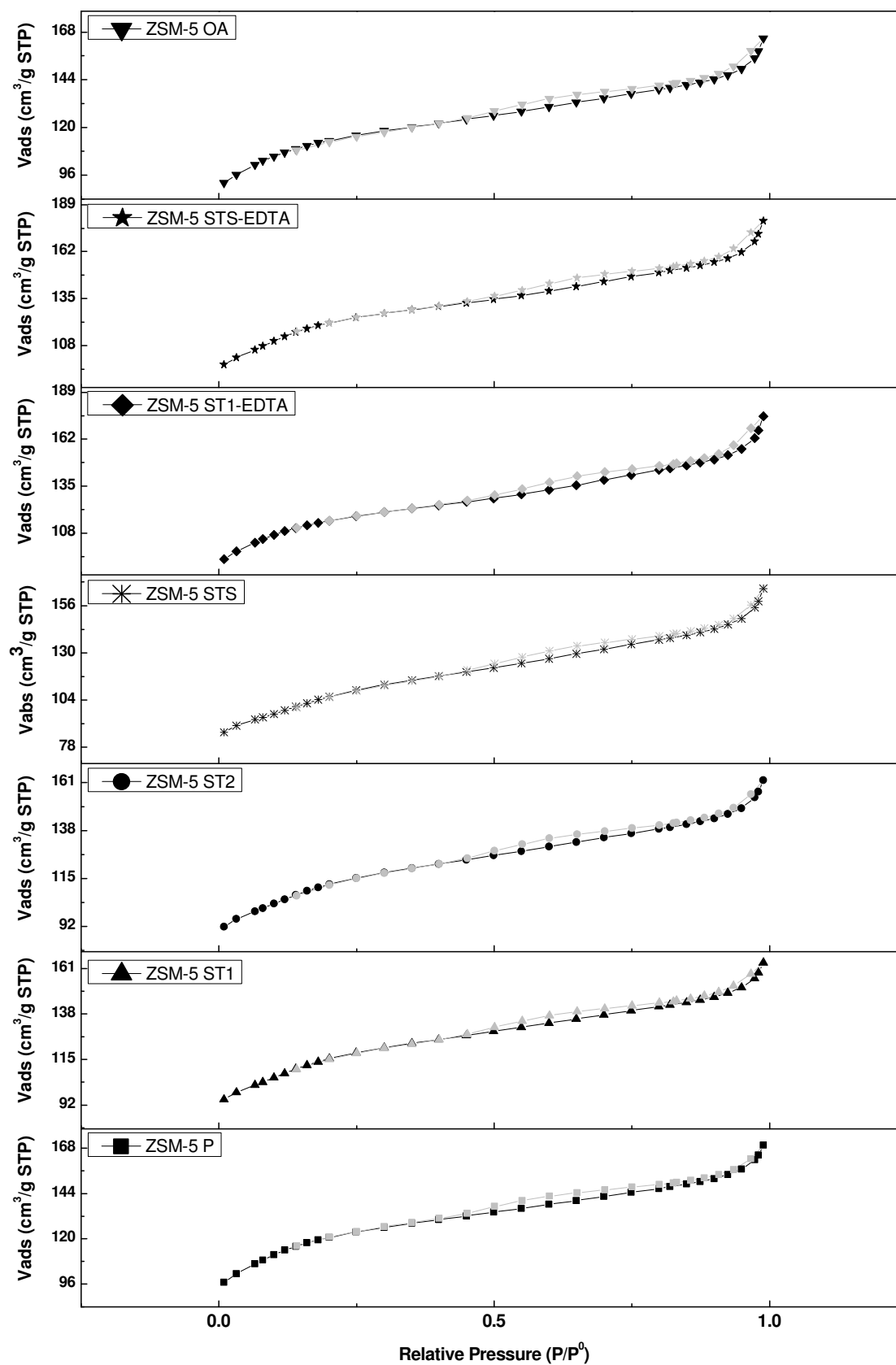


Figure 3.16 N_2 adsorption and desorption isotherms at 77 K of dealuminated ZSM-5 zeolites

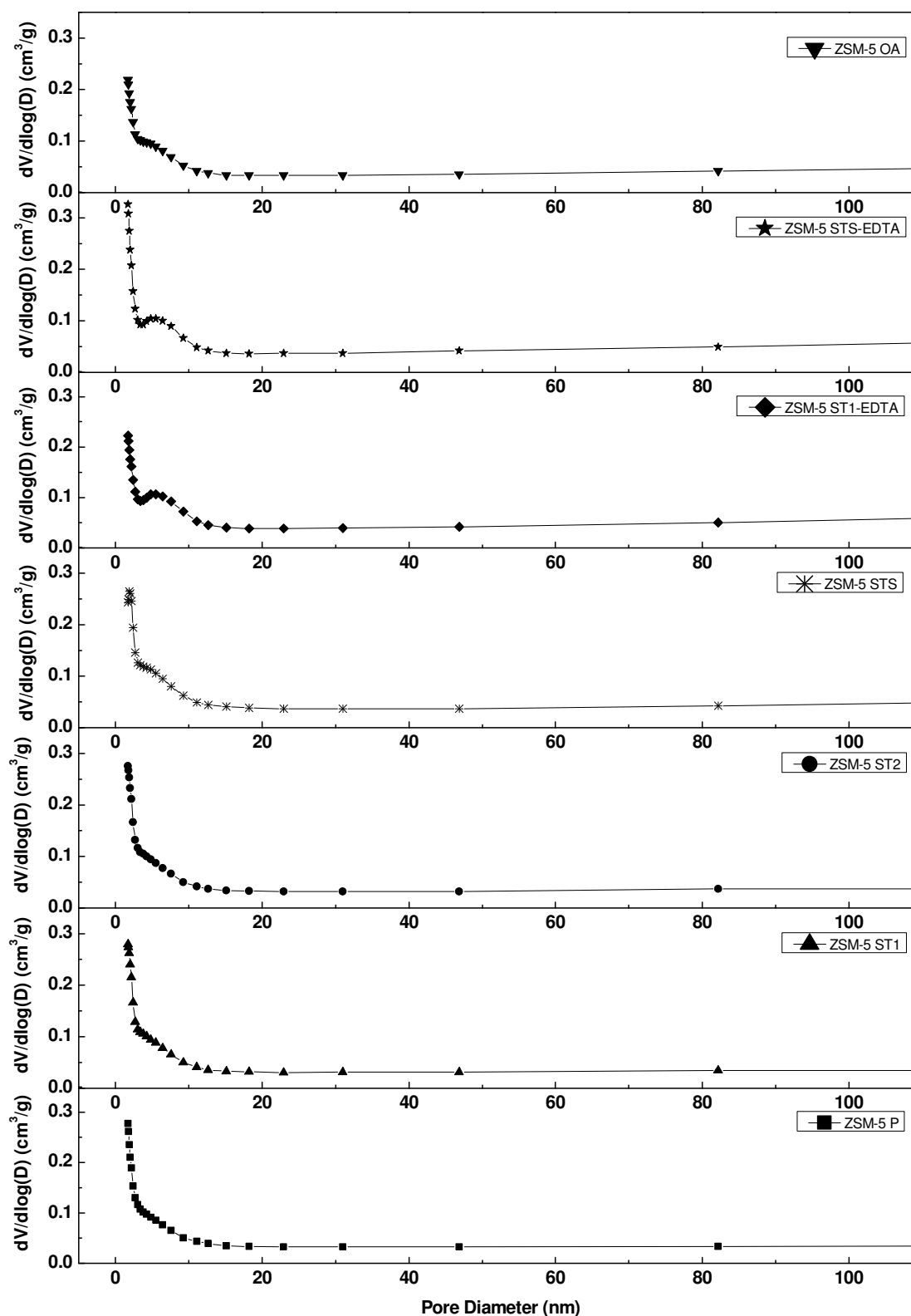


Figure 3.17 Pore size distribution of the dealuminated ZSM-5 zeolites

Pore size distributions were obtained by applying the BJH model derived from the adsorption branch, as shown in Figure 3.17. The BJH mesopore distribution did not show intracrystalline mesopores for the most dealuminated zeolites. Only the samples treated with EDTA present a development of a broad pore-size distribution centered at 7 nm.

The N_2 isotherms of FAU zeolites, *i.e.*, USY and USY EDTA in Figure 3.18 left, display enhanced uptake at intermediate pressures being a typical finger-print of hierarchical porous zeolites. The higher hysteresis loop of USY EDTA sample compared with pristine USY evidences an increased mesoporosity associated with the leaching of EFAl species out of the porous channels. The BJH pore size distribution of USY EDTA sample (Figure 3.18 right solid line) shows an increase of mesopores centered at 4 nm and the creation of greater mesoporous channel of approximately 20 nm.

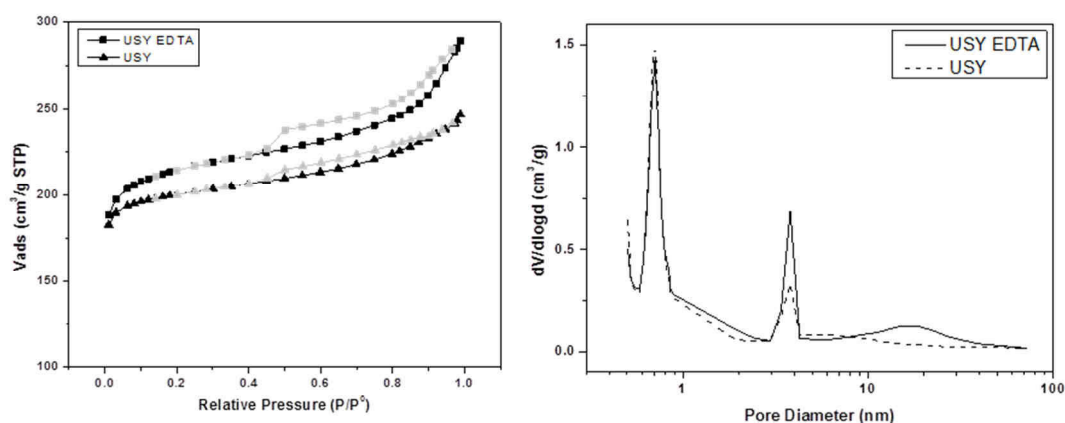


Figure 3.18 N_2 isotherms at 77 K of the pristine and dealuminated USY zeolites (left) and the corresponding adsorption BJH pore size distributions (right)

^{27}Al MAS NMR

Solid-state ^{27}Al MAS NMR spectra were collected for selected samples (MFI and FAU types) in order to determine the effect of dealumination treatment on the distribution of aluminum atoms in the zeolite framework and particularly the disappearance of the characteristic signal attributed to octahedral species (EFAl) at nearly 0 ppm (Figure 3.19 and Figure 3.20).

Firstly, in the case of FAU type zeolites, two distinct signals were detected over pristine H-USY zeolite (before EDTA treatment): one located at 50 ppm and one broad near 0 ppm (Figure 3.19b).

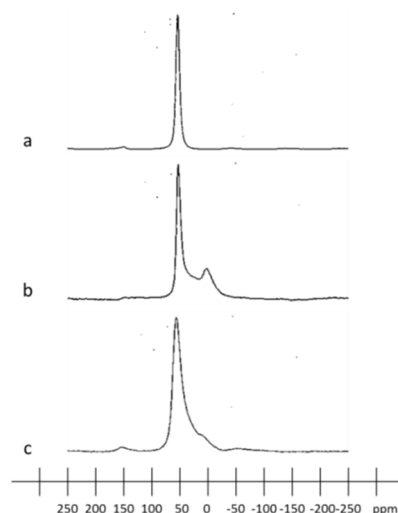


Figure 3.19 ^{27}Al MAS NMR spectra of a) H-Y, b) H-USY-P and c) H-USY EDTA zeolites

These signals correspond to tetrahedral framework aluminum species and to octahedral extra-framework aluminum (EFAl) species, respectively. The later species represent nearly 29% of the total aluminum present within the zeolite. Figure 3.19c, corresponding to H-USY after one EDTA treatment, shows the quasi-disappearance of the EFAl signal with 12% of the remaining aluminum present as EFAl species within the zeolite channels. It appears therefore that one EDTA treatment alone did not remove all the EFAl species in the H-USY. However, it has been previously shown in the laboratory that two EDTA treatments removed all EFAl species. As a control experiment, no EFAl could be detected in the H-Y spectrum (Figure 3.19a), all aluminum cations being present as framework T-atoms.

Moreover, similar studies have been performed for MFI zeolites (Figure 3.20). The spectra clearly show the creation of EFAl species after steaming treatments. The spectrum of parent zeolite (Figure 3.20a) contains a strong signal around 50 ppm and a weak signal at 0 ppm. A ratio of octahedral/tetrahedral species of 0.55 could be estimated qualitatively.

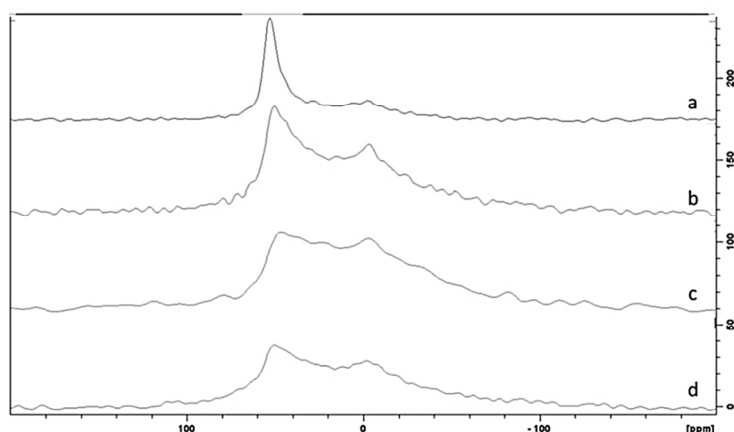


Figure 3.20 ^{27}Al MAS NMR spectra of dealuminated ZSM-5 zeolites, a) ZSM-5 P, b) ZSM-5 ST1, c) ZSM-5 STS and d) ZSM-5 STS-EDTA

After one steaming treatment, one can see the partial extraction of framework Al atoms to extra-framework positions and a ratio Octa/Td = 2.56 was reached (Figure 3.20b). This effect is even more visible in the strong steaming case (Figure 3.20c). The intensity of tetrahedral aluminum peak drastically diminished with respect to mild steamed ZSM-5 zeolite. Likewise to FAU zeolite, the leaching of EFAl species by one EDTA treatment did not lead to the complete removal of EFAl fragments (Figure 3.20d).

FTIR analyses

The FTIR spectra in the $\nu(\text{OH})$ regions of dealuminated ZSM-5 samples and parent ZSM-5 zeolite are shown in Figure 3.21.

The spectrum of pristine ZSM-5 P zeolite exhibits three well-separated bands at 3620 cm^{-1} , 3670 cm^{-1} and 3749 cm^{-1} corresponding to the O-H stretching of acidic bridging hydroxyl Si-OH-Al groups, hydroxyls linked to extra-framework aluminum (EFAl) species partially extracted from the zeolite framework (strong acidic Al-OH groups) [17,18] and isolated silanols Si-OH located at the outer surface, respectively. The strong and sharp band

[17] a) A. Zecchina, S. Bordiga, G. Spoto, D. Scarano, G. Petrini, G. Leofanti, M. Padovan, C. O. Areàn, *J. Chem. Soc. Faraday Trans.* **1992**, *88*, 2959-2969. b) K. Chakarova, K. Hadjiivanov, *J. Phys. Chem. C* **2011**, *115*, 4806–4817. c) M. Trombetta, T. Armaroli, A. Gutiérrez Alejandro, J. Ramirez Solis, G. Busca, *Appl. Catal. A* **2000**, *192*, 125–136.

[18] a) M. B. Sayed, R. A. Kydd, R. P. Cooney, *J. Catal.* **1984**, *88*, 137–149. b) L. M. Kustov, V. B. Kazansky, S. Beran, L. Kubelkova, P. Jiru, *J. Phys. Chem.* **1987**, *91*, 5247–5251.

at 3749 cm^{-1} , due to isolated external silanols, contains a low-frequency tail at 3737 cm^{-1} associated with internal terminal silanols (Scheme 3.1).

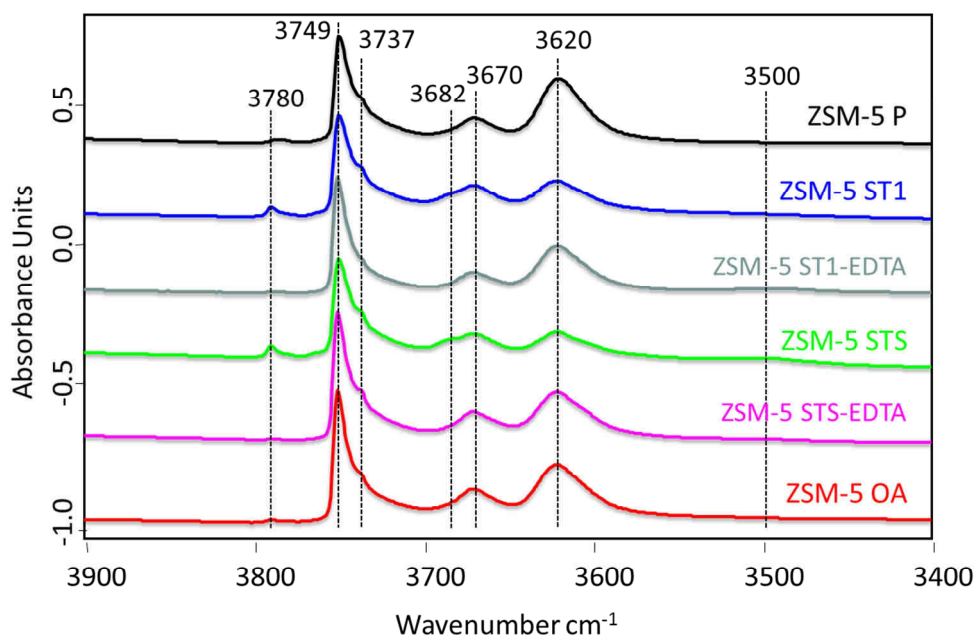
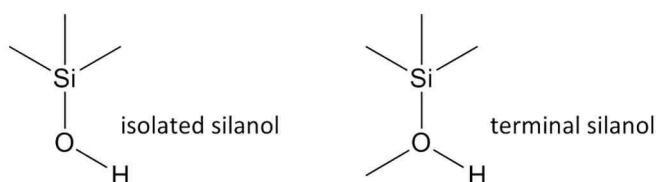


Figure 3.21 FTIR spectra in the $\nu(\text{OH})$ region ($3900 - 3400\text{ cm}^{-1}$) at low temperature of parent ZSM-5 and dealuminated ZSM-5 zeolites. Spectra normalized to $10\text{ mg}\cdot\text{cm}^{-2}$



Scheme 3.1 Isolated and terminal silanols [17a]

A weaker band at 3780 cm^{-1} could be assigned to Al-OH groups, which is due to EFAl species in the form of Al_2O_3 nano-particles type [15a]. In contrast, the 3780 cm^{-1} band was also attributed to tri-coordinated Al connected to the framework in beta zeolite [19]. These data and the relative intensity of $\nu(\text{OH})$ bands characterize our parent sample as a typical H-ZSM-5 zeolite with high Al content and significant amounts of extra-framework alumina.

[19] I. Kiricsi, C. Flego, G. Pazzuconi, W. O. J. Parker, R. Millini, C. Perego, G. Bellussi, *J. Phys. Chem.* **1994**, *98*, 4627–4634.

In addition, the steamed samples spectra present two additional bands at 3500 cm^{-1} corresponding to silanols nests (ZSM-5 STS; Figure 3.22) [20] and at 3682 cm^{-1} due to hydroxyls linked to EFAl species.

The large band at 3620 cm^{-1} (including probably a band at 3605 cm^{-1}) suffered a strong decrease after the different steaming treatments; the stronger the steaming was, the more this band vanished (Figure 3.21 ZSM-5 STS). However, the intensity remains stronger after washing with EDTA but without restoring its initial intensity. Hence, the EDTA treatment allows to regenerate certain Brønsted acid sites. Moreover, the steaming leads to the appearance of a new band located at 3682 cm^{-1} whose intensity increases with the severity of the steaming treatment. This new band could be attributed to new EFAl species created by extraction of aluminum from the framework. The spectrum of the ZSM-5 STS-EDTA sample shows the disappearance of these EFAl species. The EDTA treatment favored the leaching of EFAl species, giving birth to a band at 3682 cm^{-1} , but did not allow the leaching of all EFAl fragments present in the parent zeolite (3670 cm^{-1}). Likewise, bands at 3749 cm^{-1} and 3737 cm^{-1} , associated with silanols, are not affected by the EDTA treatment. Finally, the steaming treatments result in the increase of the vibration at 3780 cm^{-1} due to the creation of new EFAl debris within the zeolite pores. The complete vanishing of this band after EDTA treatment proves the leaching of these EFAl species. These data are in agreement with observations gained by NMR spectroscopy. Hence, one sole EDTA treatment is not sufficient to warrant the removal of all EFAl fragments present in the zeolite framework.

Finally, the sample prepared by dealumination with oxalic acid exhibits an IR spectrum similar to that of ZSM-5 STS-EDTA catalyst. The sole difference relies in the most intense band at 3620 cm^{-1} , being however smaller than pristine zeolite.

In Figure 3.22, one can observe more significantly the presence of the vibration related to silanols nests at 3500 cm^{-1} for ZSM-5 STS sample.

[20] a) B. Gil, Ł. Mokrzycki, B. Sulikowski, Z. Olejniczak, S. Walas, *Catal. Today* **2010**, 152, 24–32. b) M. S. Holm, S. Svelle, F. Joensen, P. Beato, C. H. Christensen, S. Bordiga, M. Bjørgen, *Appl. Catal. A* **2009**, 356, 23–30.

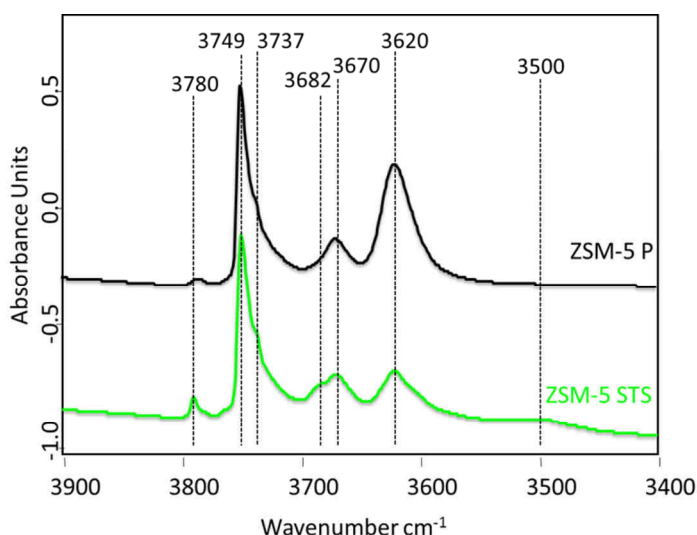


Figure 3.22 FTIR spectra in the $\nu(\text{OH})$ region ($3900 - 3400 \text{ cm}^{-1}$) at low temperature for ZSM-5 P and ZSM-5 STS zeolites. Spectra normalized to $10 \text{ mg}\cdot\text{cm}^{-2}$

The presence and the relative interaction strengths between CO and the Brønsted acid site (BAS) and Lewis acid site (LAS) in zeolite were also determined by FTIR spectroscopy of adsorbed CO at 77 K (Figures 3.22-3.26). CO is a probe molecule having a weak acidity which could be adsorbed end-on through the carbon on polarizing sites, being represented by protons in zeolites. The acid/base link between the $\text{CO}\cdots\text{OH}$ adducts formed during the adsorption perturbs the vibration modes of the $\nu(\text{OH})$ and the $\nu(\text{CO})$ regions. Thus, the O-H bond will be weakened and its vibrational frequency will shift towards lower frequencies (red-shift). On the contrary, the $\text{C}\equiv\text{O}$ bond will be strengthened by electron donation and its vibrational frequency will therefore be blue-shifted. The OH-CO interaction strength is proportional to the magnitude of these frequency shifts, and thus the Brønsted and Lewis acid strength could be determined for each zeolite. CO molecule possesses the ability to discriminate the acid type and strength of a catalyst with respect to other probe molecules such as pyridine or NH_3 .

Figure 3.23 shows the IR spectra of all four representative ZSM-5 zeolites (ZSM-5 P, ZSM-5 ST1, ZSM-5 STS and ZSM-5 STS-EDTA) in both $\nu(\text{OH})$ and $\nu(\text{CO})$ regions at 77 K with respect to CO coverage (between 0.1 and $10.7 \mu\text{mol}$ of CO). The consumption of free OH groups (negative bands) by CO adsorption, providing $\text{OH}\cdots\text{CO}$ adducts, leads to a red-shift in

the $\nu(\text{OH})$ modes (positive bands). Whatever the sample, the strongly acidic $\text{OH}_{\text{Brønsted}}$ sites (BAS) are firstly consumed (at low CO coverage).

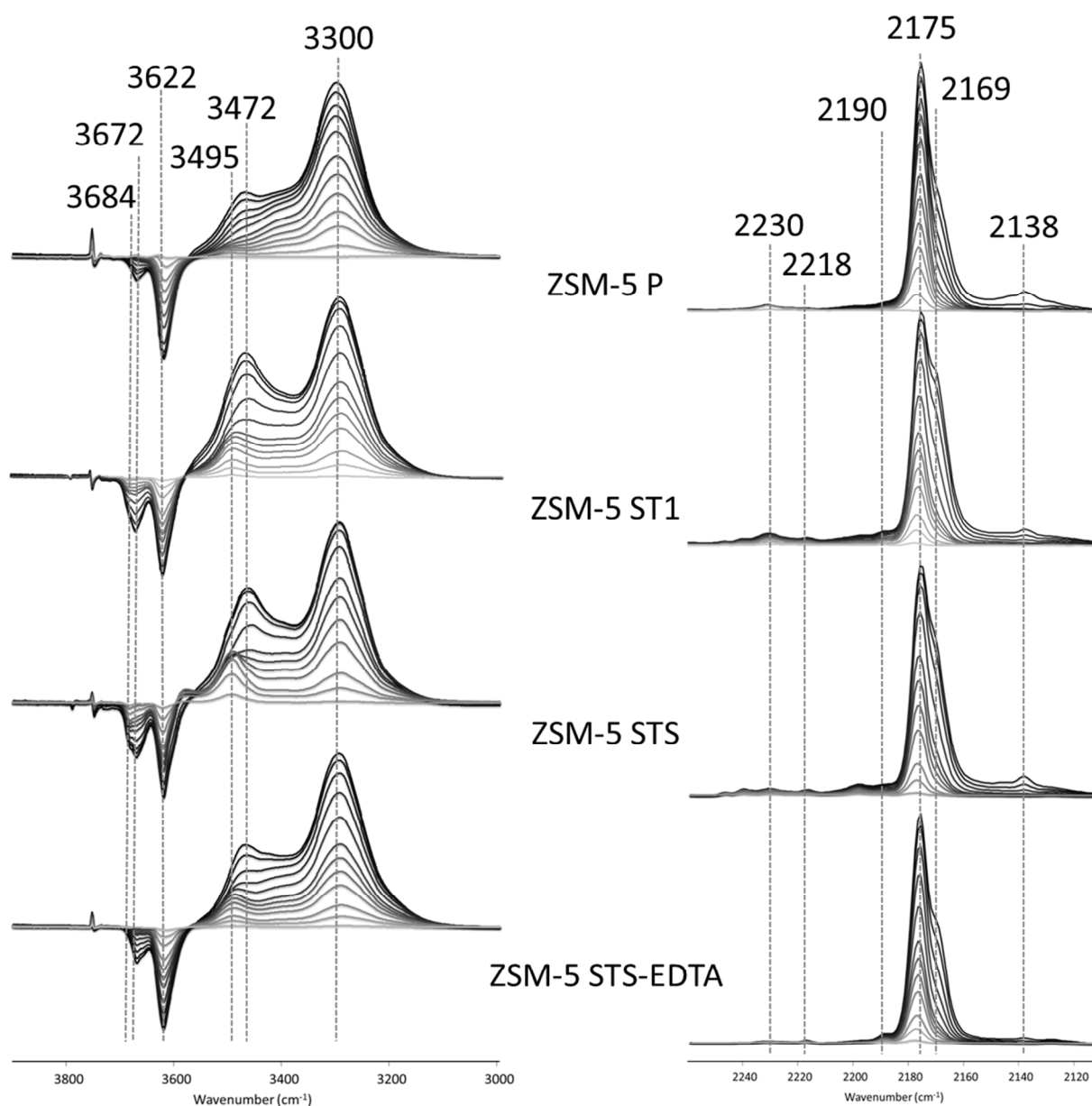


Figure 3.23 FTIR difference spectra of dealuminated ZSM-5-P, ZSM-5 STS and ZSM-5 STS-EDTA following CO adsorption at 77K. Left panel: the $\nu(\text{OH})$ region; right panel: the $\nu(\text{CO})$ region. The CO coverage increases successively from spectra light grey line to dark line in each series.

It is worthy to mention that the figures' annotations correspond to average wavenumbers. In the case of pristine zeolite, a negative band at 3621 cm^{-1} is observed which could be associated to a positive band at 3302 cm^{-1} . These two bands are associated with the strongest BAS (Si-OH-Al) and a $\Delta\nu(\text{OH})$ of 319 cm^{-1} could be calculated. For the ZSM-5 STS

and its EDTA washed counterpart, the maxima of previous positive bands are at 3295 cm^{-1} , providing $\Delta\nu(\text{OH})$ of 326 cm^{-1} . These higher red-shifts indicate stronger acid strengths for dealuminated samples. Whatever the sample, the negative band at 3672 cm^{-1} is associated to the positive band at 3472 cm^{-1} . The $\Delta\nu(\text{OH})$ of 200 cm^{-1} indicates an identical strength of the BAS, associated with Al-OH bonds linked with EFAl species) with an intermediate acidity [21]. One can note that steamed samples (ZSM-5 ST1 and STS) present an additional negative shoulder at 3684 cm^{-1} which could probably be associated to a positive band at 3495 cm^{-1} , thus to a $\Delta\nu(\text{OH})$ of 189 cm^{-1} (Figure 3.23 and Figure 3.24). These bands are also attributed to weakly acidic Al-OH groups (likely related to EFAl species). It is worthy to mention that pristine zeolite also presents this band in the form of a weak shoulder. Except acid treated ZSM-5 zeolite, all dealuminated samples show higher red-shifts for the strong BAS compared with ZSM-5 P, thus signifying slightly higher acid strength properties.

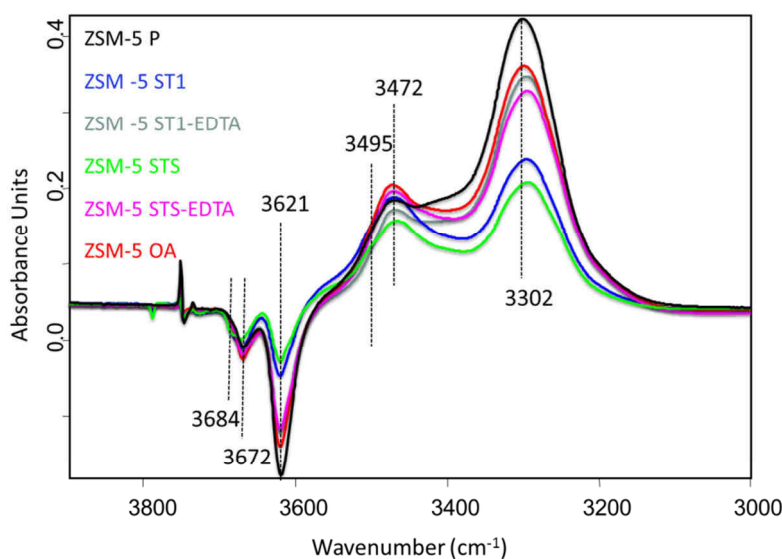


Figure 3.24 FTIR spectra in the $\nu(\text{OH})$ region ($3900 - 3000\text{ cm}^{-1}$) of H-ZSM-5 zeolites after CO adsorption ($110\text{ }\mu\text{mol}$) at 77 K . Spectra normalized to $10\text{ mg}\cdot\text{cm}^{-2}$

The spectra representing the $\nu(\text{CO})$ mode are displayed in the right part of Figure 3.23 with respect to CO coverage. The main bands could be attributed as following (Figure 3.23): (i) $2230 - 2210\text{ cm}^{-1}$: CO adsorbed on strong LAS (Al-CO), (ii) $2210 - 2190\text{ cm}^{-1}$: CO adsorbed on trigonal Al^{3+} (iii) 2175 cm^{-1} : CO adsorbed on strong BAS (Si-OH-Al), (iv) 2169 cm^{-1}

[21] S. M. T. Almutairi, B. Mezari, E. A. Pidko, P. C. M. M. Magusin, E. J. M. Hensen, *J. Catal.* **2013**, *307*, 194–203.

(shoulder): CO adsorbed on hydroxyls linked to EFAl species (AlOH-CO), (ν) 2138 cm^{-1} : CO condensed in the micropores = liquid like CO [17a-b,22].

For all samples, a band at 2175 cm^{-1} appeared first at low CO coverage, which was assigned to Brønsted OH groups. Another band at 2230 cm^{-1} attributed to LAS also grow at low CO coverage for pristine and steamed ZSM-5 zeolites (ST1 and STS). Higher CO pressures led to a raise of a shoulder at 2169 cm^{-1} related to interaction of hydroxyls on EFAl species with CO (AlOH-CO). This shoulder is highly pronounced for ZSM-5 ST1 and ZSM-5 STS samples, indicating a larger amount of weaker BAS in these steamed zeolites.

Figure 3.25 and Figure 3.26 show the spectra after CO adsorption (110 μmol) at 77 K on parent H-ZSM-5 and dealuminated H-ZSM-5 zeolites. The respective assignments of each band was described previously. The steaming treatments strongly affect the band associated to strong BAS. Indeed, the more the steaming is severe, the more the intensity of this band vanished. However, after complexation with EDTA, the magnitude of this band is again more intense. This treatment seems to partially restore the Brønsted acidity of the catalyst (Figure 3.26). In contrast, the treatment with oxalic acid seems to have only a limited impact.

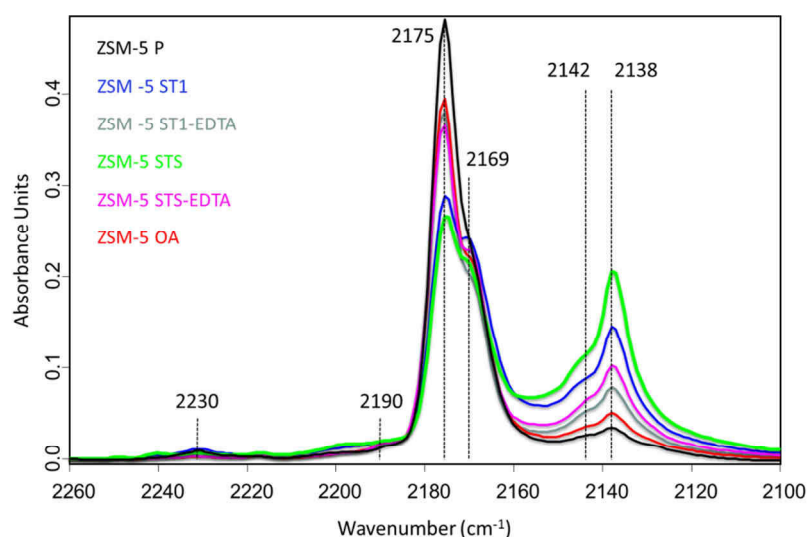


Figure 3.25 FTIR spectra after CO adsorption (110 μmol) at 77 K in the $\nu(\text{CO})$ region (2260 - 2100 cm^{-1}) of dealuminated ZSM-5 zeolites. Spectra normalized to 10 $\text{mg}\cdot\text{cm}^{-2}$

[22] O. Cairon, T. Chevreau, J.-C. Lavalley, *J. Chem. Soc. Faraday Trans.* **1998**, *94*, 3039–3047.

The shoulder attributed to the interaction with EFAl fragments is weak, even almost non-existent, in the spectrum of pristine zeolite compared with steamed samples. Such stronger shoulder confirms the extraction of aluminum from the zeolite framework. The leaching of these fragments by EDTA (ZSM-5 STS-EDTA) is not complete since the band at 2169 cm^{-1} did not disappear after the washing (Figure 3.26 right). Likewise, the ZSM-5 OA sample still exhibits few EFAl species in its micropores.

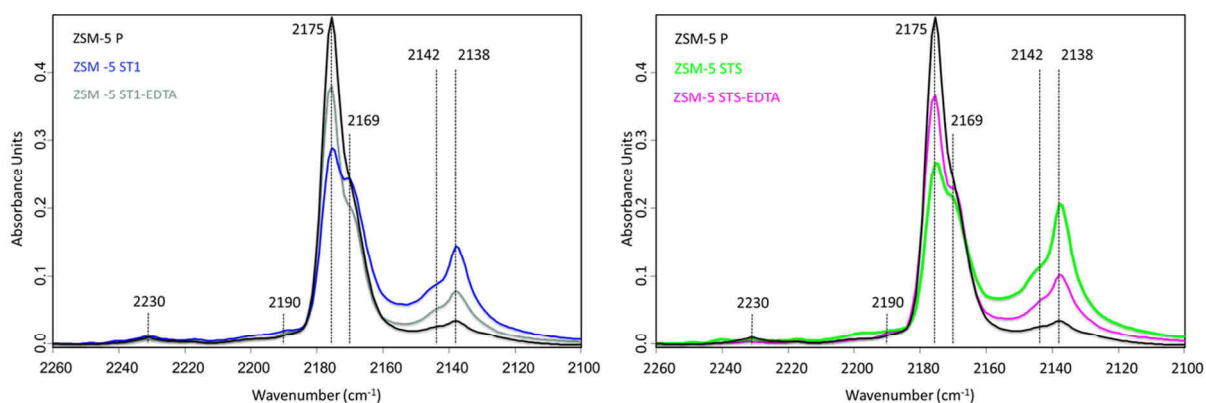


Figure 3.26 FTIR spectra after CO adsorption ($110\ \mu\text{mol}$) at $77\ \text{K}$ in the $\nu(\text{CO})$ region ($2260 - 2100\ \text{cm}^{-1}$) of dealuminated ZSM-5 zeolites. Spectra normalized to $10\ \text{mg}\cdot\text{cm}^{-2}$

In the spectra given in Figure 3.27, one can observe the bands representative of LAS. These sites are characterized by two complex massifs; the first is located between 2250 and $2210\ \text{cm}^{-1}$ and the second between 2210 and $2185\ \text{cm}^{-1}$. These above-mentioned bands were preferentially formed after an adsorption of a small amount of CO and their detailed assignments are rather difficult. However, these massifs were assigned to CO adducts with extra-framework Al^{3+} or $(\text{Al}\equiv\text{O})^+$ [23]. Thanks to these FTIR data, one can ascertain the existence of several LAS with significant abilities to polarize CO as aforementioned (Section 3.2.2.2). Furthermore, the nature of the dealumination procedure significantly affects the nature and distribution of these LAS.

[23] L. M. Kustov, V. B. Kazansky, S. Beran, L. Kubelkova, P. Jiru, *J. Phys. Chem.* **1987**, *91*, 5247–5251.

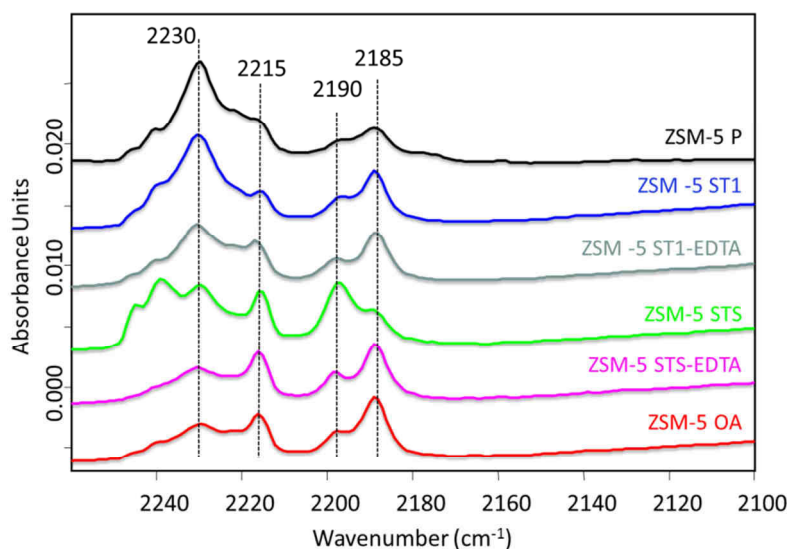


Figure 3.27 FTIR spectra after CO adsorption (110 μmol) at 77 K in the $\nu(\text{CO})$ region (zoom between 2260 - 2100 cm^{-1}) on H-ZSM-5 zeolites. Spectra normalized to $10 \text{ mg}\cdot\text{cm}^{-2}$

3.2.2. Desilication

3.2.2.1. Procedures

Powdered ZSM-5 zeolites from Zeolyst International (CBV 5020 and 8020, Si/Al=25 and 42 respectively, NH_4 -form) were calcined in static air at 823 K overnight using a heating rate of $10^\circ\cdot\text{min}^{-1}$. The resulting samples, denoted as parents (P), were subjected to two different alkaline treatments. NaOH (alkaline treatment) and TPAOH (organic treatment) aqueous solutions were used to perform desilication. In the case of NaOH treatment, the pristine zeolite was dispersed in a solution of sodium hydroxide (0.2 M, Aldrich) and the mixture was stirred and heated at 338 K for 30 min. After cooling down in an ice-water bath, the zeolite was filtered, washed with distilled water over a nylon membrane until neutral pH and dried in an oven at 373 K. The Na^+ -form was ion exchanged three times with a NH_4NO_3 solution (0.1 M) at 353 K. The H^+ -form (ZSM-5 IDS) was obtained after a calcination step at 823 K overnight in air. The same procedure was followed for TPAOH treatment with a 1 M aqueous solution and without the ion exchange step. ZSM-5 ODS zeolite was obtained.

3.2.2.2. Characterizations

Chemical composition

Table 3.11 presents the Si/Al ratios of parent ZSM-5 zeolite (Zeolyst, CBV5020) and as-desilicated ZSM-5 zeolites (determined by EDX). The desilicated sample in the presence of NaOH presents a higher Si/Al ratio with respect to pristine ZSM-5, 35 vs. 25 respectively. Surprisingly, the zeolite treated with TPAOH exhibits a too low Si/Al ratio of 3. A too drastic treatment could explain this result and a large part of the silicon has been extracted during the treatment.

Table 3.11 Si/Al ratios of parent and desilicated ZSM-5 zeolites

Entry	Si/Al ratio
ZSM-5 P	25
ZSM-5 IDS1	35
ZSM-5 ODS	3

TEM analyses

TEM micrograph (Figure 3.28) reveals the generation of mesopores in ZSM-5 IDS1 zeolite. As expected for such destructive method, the mesoporous holes are randomly distributed throughout the crystal.

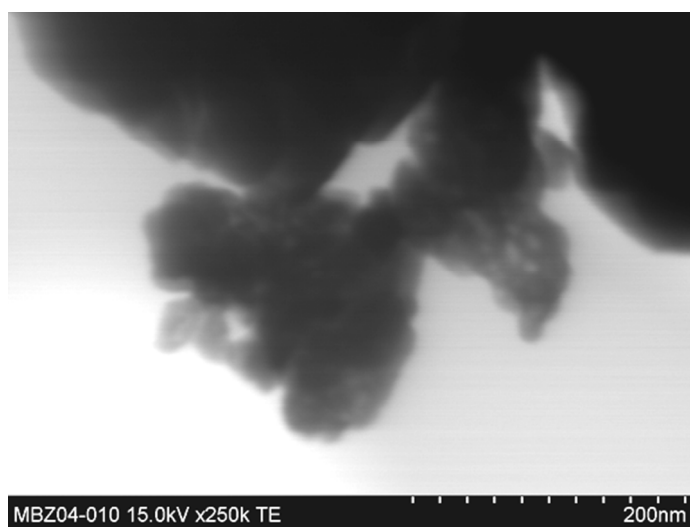


Figure 3.28 TEM image of ZSM-5 IDS1

FTIR analyses

IR spectra of surface hydroxyl groups of different ZSM-5 samples pre-treated by outgassing at 773 K are given in Figure 3.29. The interpretation of the pristine zeolite spectrum has been done in Section 3.2.1.2.

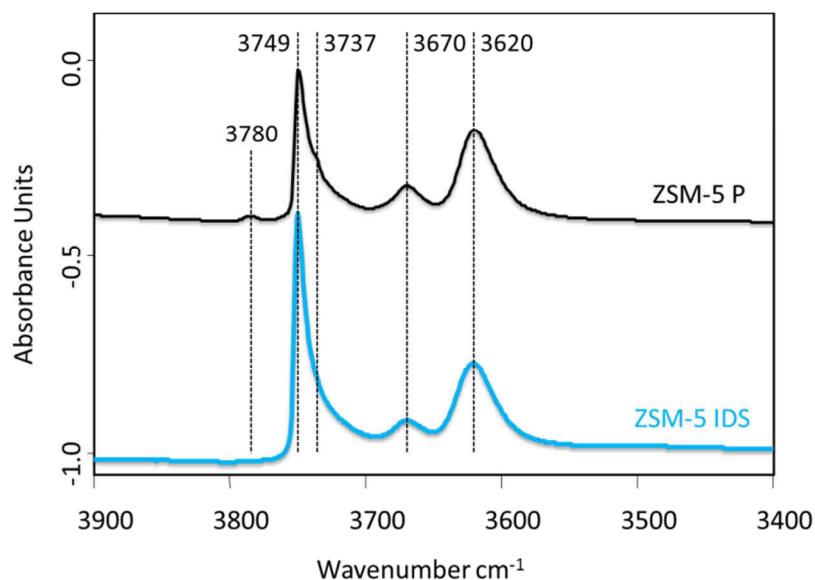


Figure 3.29 FTIR spectra in the $\nu(\text{OH})$ region at low temperature of parent ZSM-5 and NaOH desilicated ZSM-5 zeolites

The desilicated sample spectrum (ZSM-5 IDS) exhibits rather clear differences with respect to the parent spectrum. First of all, the intensity of the 3749 cm^{-1} band compared to the vibration related to Brønsted acid site (3620 cm^{-1}) was enhanced after desilication. This band has been previously attributed to isolated external silanols. Based on this statement, one may claim that NaOH treatment leads to a substantial raise in the number of isolated silanols, which could be assigned to silanols present in mesopore walls. This phenomenon may be related to an enhanced external surface area associated to the creation of an intracrystalline mesoporosity [24]. One can also mention the disappearance of the shoulder at 3737 cm^{-1} attributed to internal terminal silanols (defects). It can therefore be stated that Si atoms bonded to one hydroxyl and to other three silicon (defects) are less stable (thus less strong) than the other Si atoms bonded to four Si atoms and are readily removed by NaOH treatment. In addition, the band associated to external EFAl species (3670 cm^{-1}) and the

[24] S. Abello, A. Bonilla, J. Pérez-Ramírez, *Appl. Catal. A* **2009**, 364, 191–198.

other band associated with EFAl species (3780 cm^{-1}) suffered a slight diminution and a complete disappearance respectively, compared with parent zeolite. The alkaline treatment led to a slight dealumination of the zeolite, generally observed after such treatment. This phenomenon had a higher impact on the weakest Al-OH groups (band at 3780 cm^{-1}) which are removed first [16]. Finally, one may conclude that a partial destruction of the zeolite framework occurred based on the slight decrease of the 3620 cm^{-1} band related to bridging hydroxyl groups.

Figure 3.30 and Figure 3.31 show the FTIR spectra after adsorption of $110\text{ }\mu\text{mol}$ of CO at 77 K in $\nu(\text{CO})$ and $\nu(\text{OH})$ regions for the two zeolites, respectively. The desilication treatment with NaOH led to a raise in the band related to LAS (2230 cm^{-1}). Two maxima around 2230 and 2220 cm^{-1} have been reported previously, but their exact assignment remain unclear [25]. However, these LAS in zeolites are generally associated to EFAl species [26]. The exact nature of these EFAl species is not known yet, but different neutral species and oxoaluminum cations have been suggested [26].

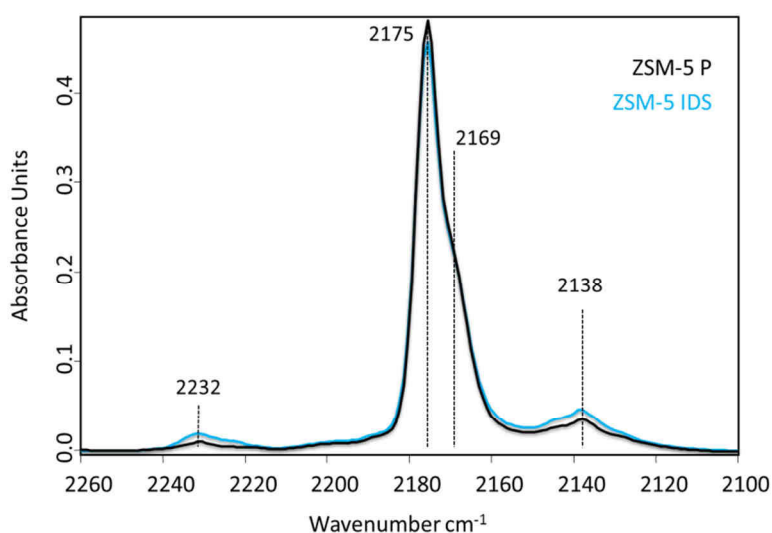


Figure 3.30 FTIR spectra after insertion of CO ($110\text{ }\mu\text{mol}$) in the $\nu(\text{CO})$ region at 77 K of parent ZSM-5 and of NaOH desilicated ZSM-5 zeolites. Spectra normalized to $10\text{ mg}\cdot\text{cm}^{-2}$

[25] H. V Brand, A. Redondo, P. J. Hay, *J. Mol. Catal. A* **1997**, *121*, 45–62.

[26] C. Pazé, S. Bordiga, C. Lamberti, M. Salvalaggio, A. Zecchina, G. Bellussi, *J. Phys. Chem. B* **1997**, *101*, 4740–4751.

Additionally, the interaction between CO and OH group was also used to determine the acid strength of Brønsted acid site (BAS) [17]. It is worthy to note the presence of two positive bands and two negative bands in both spectra (Figure 3.31).

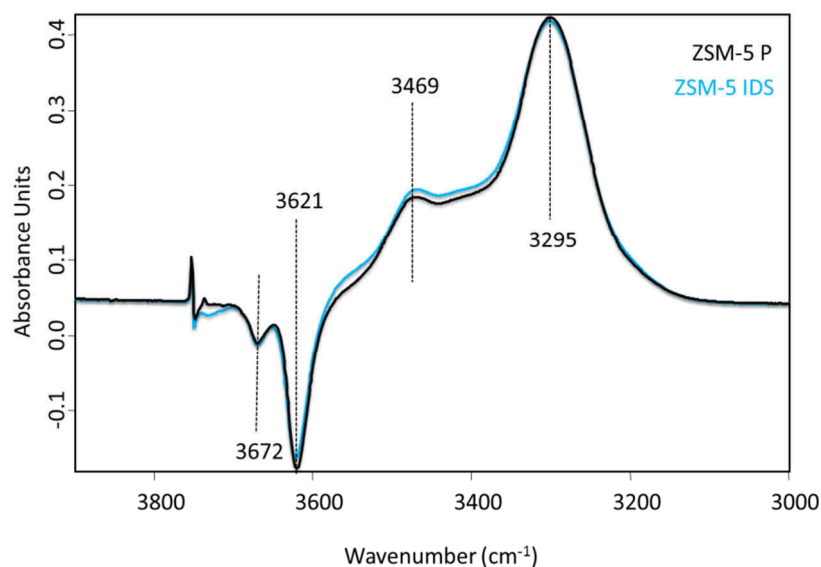


Figure 3.31 FTIR spectra in the $\nu(\text{OH})$ region ($3900 - 3000 \text{ cm}^{-1}$) after CO insertion ($110 \mu\text{mol}$) at 77 K on H-ZSM-5 zeolites. Spectra normalized to $10 \text{ mg}\cdot\text{cm}^{-2}$

The positive band at 3295 cm^{-1} is related to the negative one at 3621 cm^{-1} and are assigned to BAS (Si-OH-Al); these bands exhibit a $\Delta\nu(\text{OH})$ of 321 cm^{-1} in the case of parent ZSM-5 zeolite. The desilicated sample shows the positive band at 3302 cm^{-1} and the negative one at 3672 cm^{-1} with a $\Delta\nu(\text{OH})$ of 319 cm^{-1} . The magnitude of these shifts is representative for ZSM-5 type zeolite [26]. Based on these data, one can conclude that NaOH treatment did not affect the acid strength of the BAS group since the desilicated sample possesses a similar red-shift compared to pristine zeolite [27]. In contrast, the high frequency shoulder at 3469 cm^{-1} is ascribed to perturbed OH groups of EFAl species originally adsorbing at 3672 cm^{-1} . This OH group presents a red-shift of 203 cm^{-1} for both samples. Thus, the acid strength of this group is not perturbed by the desilication treatment.

[27] B. Gil, Ł. Mokrzycki, B. Sulikowski, Z. Olejniczak, S. Walas, *Catal. Today* **2010**, *152*, 24–32.

4. Conclusion

Various zeolites have been successfully prepared *via* different synthesis procedures. All as-prepared catalysts were thoroughly characterized by BET, XRD, SEM, ^{27}Al MAS NMR and FTIR.

Zeolites were synthesized according either to a classical alkaline route or a fluoride-mediated route. Zeolites having different topology and properties have been obtained such as FAU, EMT and MFI types. The ZSM-5 zeolites synthesized *via* the fluoride-mediated route present various crystal size and crystallinity thanks to variations in the synthesis conditions such as silicon source, Si/Al ratio and the acid type (HF or HCl).

Besides, mesoporous zeolites (mainly ZSM-5 type) have been prepared following different methods. Indeed, a constructive route, *via* the double templating method, has been used to synthesize a ZSM-5 zeolite having an apparent inter-crystalline mesoporosity. In order to achieve this goal, spermine molecule was introduced in the zeolite gel as second template. Furthermore, two destructive routes were employed to obtain mesoporous zeolites. Firstly, NaOH and TPAOH aqueous solutions have been used in order to perform desilication. ZSM-5 zeolites with intra-crystalline mesoporosity were obtained. Finally, dealumination *via* a steaming treatment has been studied over ZSM-5 and FAU type zeolites. Depending on the harshness of the steaming treatment, ZSM-5 and FAU samples have been obtained possessing various mesoporous and intrinsic properties. The strong steaming treatment associated with the EDTA treatment seemed to be a good compromise to achieve an optimal candidate in terms of acidity and mesoporosity.

In summary, the rational design of these inorganic solids with highly crystalline structure is warranted thanks to the combination of a proper chemical composition, a hierarchical porosity, an appropriate crystal size and also a proper shape at the reactor level (Chapter 6).

**Chapter 4. CONVERSION OF METHANOL INTO
LIGHT OLEFINS OVER ZSM-5 ZEOLITES**

ABSTRACT

ZSM-5 zeolites having different crystal sizes, acid site densities and morphologies were evaluated as catalysts in the Methanol-to-Olefins (MTO) reaction.

In a first part, the catalytic activities of a micron-sized, a nanoscopic, a mesoporous and a giant-sized (fluoride-mediated route) ZSM-5 zeolites were compared. Propylene to ethylene ratios above 5 were achieved over the zeolite prepared in fluoride medium along with a high methanol conversion (98%). Its surprising superior selectivity was tentatively ascribed to its low density of strong Brønsted acid sites in combination with a long diffusion pathway and few crystal defects. The intrinsic properties of fluoride-mediated ZSM-5 catalyst were deeply investigated in a second part. A weak Brønsted acid site density (Si/Al = 136) and crystal volume of $540 \mu\text{m}^3$ were found to be optimal features needed to design a competitive MTP-catalyst.

Furthermore, aiming in a possible industrial application, the synthesis medium has to be modified, thus avoiding harmful hydrofluoric acid use. Hydrochloric acid was therefore chosen as an alternative and resulted in the same prismatic crystal morphologies and hence to similar catalytic performance.

1. Introduction

The rational design of heterogeneous catalysts to optimize activity and selectivity in a targeted reaction often remains a key challenge in state-of-the-art catalysis research [1]. In this context, zeolites occupy a prominent place since they are used in numerous acid-catalyzed reactions [2]. Discovered in Mobil laboratories, the transformation of methanol-to-hydrocarbons (MTH) to produce high-octane gasoline [3,4], represents a timely and valuable process involving zeolite catalysts. Indeed, the MTH technology has received considerable industrial interest [5]. For instance, the Mobil Oil methanol to gasoline (MTG) process, the Topsøe integrated gasoline synthesis (TIGAS) process, the Lurgi methanol to propene (MTP) process and the Norsk Hydro/UOP's methanol to olefins (MTO) process, have either been commercialized or are ready for commercialization [6].

The MTO reaction is a valuable option for the valorization of stranded gas reserves, and therefore several studies devoted either to the reaction mechanism or to the technology were undertaken [7]. In addition, the worldwide market demand toward ethylene and propylene is gradually raising and projected growth rates in coming decades are expected to remain high [8]. SAPO-34 silico-aluminophosphate, having the CHA structure, is also recognized as a valuable catalyst to generate a high selectivity to light olefins due to its moderate acid strength and small pore opening. However, a high rate of

[1] a) M.-P. Pileni, *Acc. Chem. Res.* **2007**, *40*, 685–93. b) J. M. Thomas, J. C. Hernandez-Garrido, R. Raja, R. G. Bell, *Phys. Chem. Chem. Phys.* **2009**, *11*, 2799–825. c) B. Louis, G. Laugel, P. Pale, M. M. Pereira, *ChemCatChem* **2011**, *3*, 1263–1272. d) J. C. Védrine, *Appl. Catal. A* **2014**, *474*, 40–50.

[2] A. Corma, *Chem. Rev.* **1995**, *95*, 559–614.

[3] C. D. Chang, A. J. Silvestri, *J. Catal.* **1977**, *47*, 249–259.

[4] C. D. Chang, *Catal. Rev. Sci. Eng.* **1983**, *25*, 1–118.

[5] a) S. Kvisle, T. Fuglerud, S. Kolboe, U. Olsbye, K. P. Lillerud, B. V. Vora, in *Handb. Heterog. Catal.* (Eds.: G. Ertl, H. Knözinger, F. Schüth, J. Weitkamp), **2008**, pp. 2950–2965. b) M. Stöcker, *Microporous Mesoporous Mater.* **1999**, *29*, 3–48.

[6] U. Olsbye, S. Svelle, M. Bjørgen, P. Beato, T. V. W. Janssens, F. Joensen, S. Bordiga, K. P. Lillerud, *Angew. Chemie Int. Ed.* **2012**, *51*, 5810–5831.

[7] a) F. C. Patcas, *J. Catal.* **2005**, *231*, 194–200. b) I. Štich, J. D. Gale, K. Terakura, M. C. Payne, *J. Am. Chem. Soc.* **1999**, *121*, 3292–3302. c) M. Bjørgen, U. Olsbye, S. Kolboe, *J. Catal.* **2003**, *215*, 30–44.

[8] G. A. Olah, A. Goepfert, G. K. S. Prakash, *Beyond Oil and Gas: The Methanol Economy*, Wiley-VCH Verlag GmbH & Co. KGaA, **2009**.

deactivation is usually observed over this zeolite due to rapid coke formation [9,10]. ZSM-5 zeolites are therefore often used despite usually yielding lower olefin yield [11,12].

Several strategies targeted to achieve an increasing selectivity toward light olefins over MFI catalysts have been tempted: modification of the reaction conditions, raising the steric constraints to increase shape selectivity, change in the reactor configuration [13], or proper tailoring of Brønsted acidity (density and strength) [11b,14]. Likewise, to limit/inhibit the consecutive formation of higher alkenes, alkanes and aromatics, the development of new catalyst design at the mesoscopic and macro-scale have also been explored [11]. Unfortunately, the preparation of such catalysts remains often complex and quite costly.

During the past decade, the exploration of ethane-rich shale gas in the US rendered ethane crackers economically favorable over naphta crackers, and led to the construction of ethane crackers as well as retrofitting of naphta crackers. Naphta cracker co-products such as propene are therefore in increasingly short supply, and tuning of MTH selectivity toward propene becomes increasingly attractive. Only few studies have been devoted to the optimization of propene yields in the MTH reaction over ZSM-5 catalysts.

Chang *et al.* explored the interplay between Si/Al ratio, temperature and pressure in MTH reaction over ZSM-5 zeolite [15]. Two Si/Al ratios were tested, *i.e.*, 18 and 835, while intermediate Brønsted acid site densities were obtained by partial H⁺-Na⁺ cationic exchange. At 370 °C and full conversion, the C₂-C₄ olefins selectivity increased from 30% to 46% for Si/Al = 18 and 835, respectively. Raising the temperature to 500 °C led to higher olefins selectivities; with a maximum of 38% propene selectivity and a propene to ethene ratio of 4.9 at full methanol conversion for the highly siliceous catalyst. Lower Si/Al ratios led to

[9] G. Qi, Z. Xie, W. Yang, S. Zhong, H. Liu, C. Zhang, Q. Chen, *Fuel Process. Technol.* **2007**, *88*, 437–441.

[10] D. Chen, K. Moljord, T. Fuglerud, A. Holmen, *Microporous Mesoporous Mater.* **1999**, *29*, 191–203.

[11] a) S. Ivanova, E. Vanhaecke, B. Louis, S. Libs, M.-J. Ledoux, S. Rigolet, C. Marichal, C. Pham, F. Luck, C. Pham-Huu, *ChemSusChem* **2008**, *1*, 851–857. b) S. Ivanova, B. Louis, B. Madani, J.-P. Tessonnier, M.-J. Ledoux, C. Pham-Huu, *J. Phys. Chem. C* **2007**, *111*, 4368–4374. c) S. Ivanova, B. Louis, M.-J. Ledoux, C. Pham-Huu, *J. Am. Chem. Soc.* **2007**, *129*, 3383–3391.

[12] S. Svelle, F. Joensen, J. Nerlov, U. Olsbye, K.-P. Lillerud, S. Kolboe, M. Bjørgen, *J. Am. Chem. Soc.* **2006**, *128*, 14770–14771.

[13] K. P. Möller, W. Böhringer, A. E. Schnitzler, E. Van Steen, C. T. O'Connor, *Microporous Mesoporous Mater.* **1999**, *29*, 127–144.

[14] A. G. Gayubo, P. L. Benito, A. T. Aguayo, M. Olazar, J. Bilbao, *J. Chem. Technol. Biotechnol.* **1996**, *65*, 186–192.

[15] C. D. Chang, C. T.-W. Chu, R. F. Socha, *J. Catal.* **1984**, *86*, 289–296.

higher ethene selectivities and lower propene selectivities, e.g. 10.5 and 22.6%, respectively, for Si/Al = 18 [15].

In line with those results, Prinz and Riekert tested ZSM-5 catalysts with different Si/Al ratios (34 – 660) or crystal sizes (0.5 - 8 μm) in the MTO reaction between 280–350 °C in a continuous-stirred-tank reactor [16]. They reported that increasing Si/Al ratios led to higher light olefins selectivities and propene-to-ethene ratios. A similar effect was reported while diminishing crystal sizes (0.5 versus 2x2x6 micron-sized crystals). It is however worth noting that conversions exceeding 80%, differences in selectivity vanished [16]. Recently, Hua *et al.* reported that mesopore formation by desilication of ZSM-5 zeolite with Si/Al ratio 72 led to enhanced propene selectivities; up to 42% with a propene to ethene ratio of 10 at full methanol conversion at 470 °C. The authors ascribed such selectivity increase to shorter diffusion pathways [17].

Zhao *et al.* studied the effect of adding ZrO₂ and H₃PO₄ to H-ZSM-5 zeolite (Si/Al = 84) and reached a propene to ethene ratio of 10 (45% propene selectivity) at 450 °C and full DME conversion. After 30 h on stream, the propene to ethene ratio increased to 16, due to lower ethene selectivity, still at full conversion and 45% propene selectivity [18]. The authors ascribed the propene yield improvements to the modification of acid strength towards lower values while raising the number of acid sites. A slight reduction of pore width was also observed. Later, Hua *et al.* tested ZSM-5 samples with Si/Al ratios ranging from 12 to 360 at 460 °C, and observed a gradual increase in propene selectivity from 16% to 52%, respectively, at full methanol conversion [19]. Concurrently, the propene to ethene ratio increased from 2.0 to 6.5. Screening tests of Si/Al = 220 sample after modification with a large variety of promoting elements showed that phosphorus led to the highest propene selectivity, 56%, at full methanol conversion, with a propene to ethene ratio of 7. Aromatics production was almost fully suppressed (< 1% selectivity) after P modification. The P/ZSM-5 catalyst was thoroughly characterized. It was found that the main change induced by P doping was the reduction of the number and strength of acid sites, while the pore size was maintained or slightly increased [19].

[16] D. Prinz, L. Riekert, *Appl. Catal.* **1988**, *37*, 139–154.

[17] C. Mei, P. Wen, Z. Liu, H. Liu, Y. Wang, W. Yang, Z. Xie, W. Hua, Z. Gao, *J. Catal.* **2008**, *258*, 243–249.

[18] T.-S. Zhao, T. Takemoto, N. Tsubaki, *Catal. Commun.* **2006**, *7*, 647–650.

[19] J. Liu, C. Zhang, Z. Shen, W. Hua, Y. Tang, W. Shen, Y. Yue, H. Xu, *Catal. Commun.* **2009**, *10*, 1506–1509.

In the present work, we investigate the influence of Brønsted acid site density and also crystal size in the MTO reaction. The principle aim was to raise and then maintain a high selectivity toward propene, and therefore develop a simple strategy to design a new generation of MTP (methanol-to-propene) catalyst exhibiting the MFI structure.

2. Preliminary results

Four ZSM-5 zeolite materials with varying crystal size, acid site density and morphology were prepared, characterized by BET, XRD, SEM, FT-IR, H/D exchange and n-hexane cracking experiments and tested as catalysts in the MTO reaction at 623 K, WHSV = 1.8 g_{MeOH}/g_{catalyst}·h⁻¹ under atmospheric pressure.

2.1 Characterization of the zeolites

The XRD patterns of each zeolite confirmed the sole MFI structure [20]. Figure 4.1 shows the SEM images of the four catalysts. ZSM-5R and ZSM-5MS exhibited the classical coffin-shape morphology (Figure 4.1a and d) along with crystal sizes of 5 and 2 μm, respectively. The material prepared *via* the fluoride-mediated route led to the formation of large prismatic crystals having ~15 - 20 μm in size (Figure 4.1b). In contrast, ZSM-5N catalyst consisted of rectangular nanocrystals, 0.05 - 0.10 μm in size, which assembled into a spherical superstructure of approximately 1 - 2 μm (Figure 4.1c).

[20] a) H. Robson, K. P. Lillerud, Eds., *Verified Syntheses of Zeolitic Materials*, Elsevier B.V., Amsterdam, **2001**. b) F. Ocampo, H. Yun, M. M. Pereira, J.-P. Tessonnier, B. Louis, *Cryst. Growth Des.* **2009**, *9*, 3721–3729. c) F. Ocampo, J. A. Cunha, M. R. de Lima Santos, J.-P. Tessonnier, M. M. Pereira, B. Louis, *Appl. Catal. A* **2010**, *390*, 102–109.

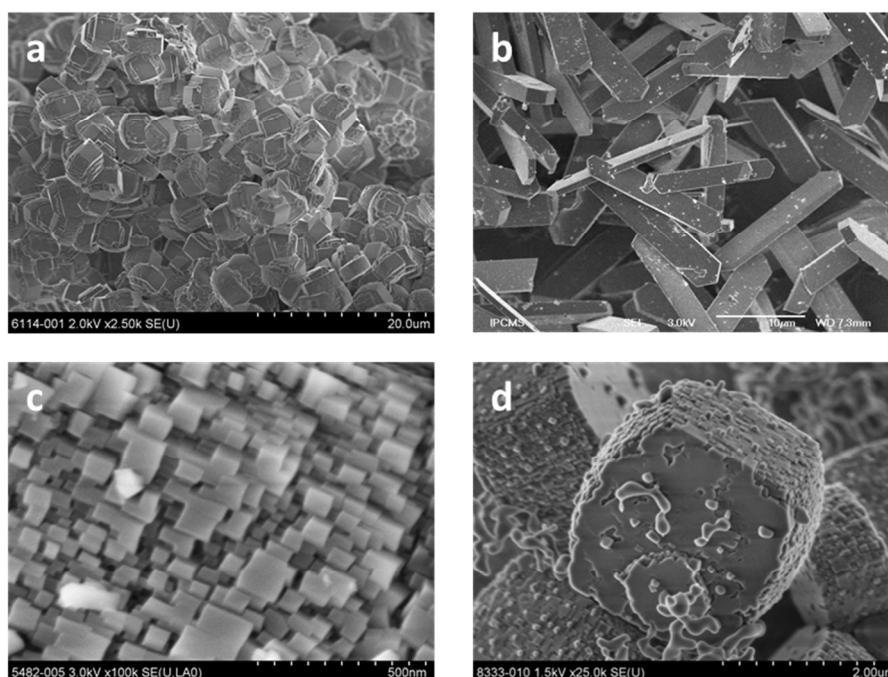


Figure 4.1 SEM micrographs of as-made zeolites: a) ZSM-5R, b) ZSM-5F, c) ZSM-5N and d) ZSM-5MS

Table 4.1 presents the BET surface areas (S_{BET}), the total number of Brønsted acid sites, Si/Al ratios, crystal sizes and the rate of n-hexane cracking for all catalysts. S_{BET} values are in line with those usually found for ZSM-5 zeolites. However, ZSM-5MS exhibited a higher S_{BET} value of 453 m^2/g . This finding is in line with previous HRTEM measurements which showed that it contains 10 - 20 nanometer-sized mesopores [20b]. EDX analysis allowed to estimate the Si/Al ratio of the different zeolites (Table 4.1).

Table 4.1 BET surface areas, Si/Al ratio, crystal sizes, number of Brønsted acid sites and rate of n-hexane cracking

Catalyst	Si/Al	Crystal size [μm]	S_{BET} [m^2/g]	Brønsted acid sites [mmol/g]	Rate of n-hexane cracking [mmol/g.min]
ZSM-5R	25	5	320	1.00	120
ZSM-5F	53	15 - 20	305	0.31	107
ZSM-5N	19	0.05 - 0.10	345	0.78	183
ZSM-5MS	43	2	453	0.26	322

H/D isotope exchange was performed to evaluate the number of Brønsted acid sites present in the different materials. It appears that the Brønsted acid site density diminished

among the zeolites in the order: ZSM-5R > ZSM-5N > ZSM-5F > ZSM-5MS. It is noteworthy that the fluoride-mediated route allowed a decrease in the total number of Brønsted acid sites when compared with MFI catalyst prepared under alkaline conditions. Such influence of the preparation method on the density of Brønsted acid sites for ZSM-5 and [F]ZSM-5 zeolites has already been reported in an earlier study [21]. In parallel to this acidity loss, the Si/Al ratio was enhanced as expected. The ZSM-5MS sample exhibited a low number of acid sites, 0.26 mmol/g; however it is important to remember that this structured composite contained only 34 wt.% of zeolite crystals coated on a glass monolith. The catalytic activity of these zeolites was evaluated in n-hexane cracking reaction and nearly the same rate was achieved over ZSM-5R and ZSM-5F zeolites, 120 and 107 mmol_{n-hexane} converted/g.min, respectively, despite higher Al content in ZSM-5R. This result is further discussed below. Zeolite nanocrystals (ZSM-5N) led to an improved reactivity for n-hexane cracking, thus confirming the higher effectiveness of nanocrystals (183 mmol_{n-C6} converted/g.min) compared to their micrometer counterparts [22-23]. Interestingly, ZSM-5MS zeolite led to a higher rate of n-hexane cracking, *i.e.*, 322 mmol_{n-hexane} converted/g min, thus suggesting a facilitated diffusion of the alkane through the mesoporous zeolite.

Figure 4.2 shows the IR spectra of ZSM-5N, ZSM-5F, ZSM-5R, and ZSM-5MS zeolites in the range 3800 - 3000 cm⁻¹ (ν(OH) region).

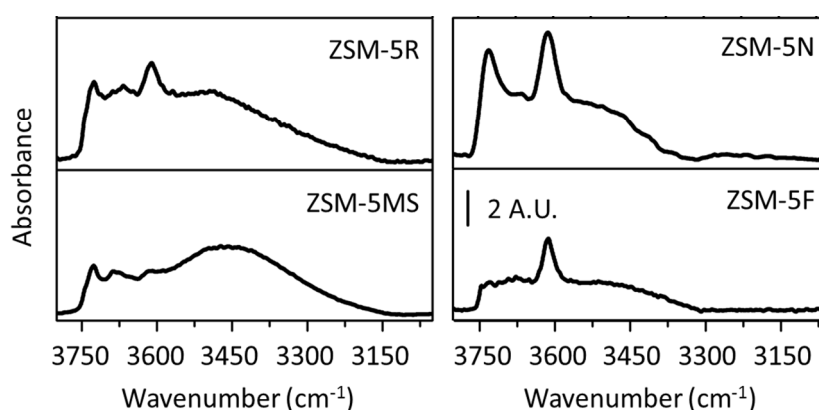


Figure 4.2 FTIR spectra (ν(OH) region) of ZSM-5X samples collected at room temperature after vacuum outgassing at 773 K for 1 h. These spectra are normalized to the overtone modes in the 1944–2092 cm⁻¹ region

[21] J. Arichi, B. Louis, *Cryst. Growth Des.* **2008**, *8*, 3999–4005.

[22] P. B. Venuto, *Microporous Mater.* **1994**, *2*, 297–411.

[23] B. Louis, A. Vicente, C. Fernandez, V. Valtchev, *J. Phys. Chem. C* **2011**, *115*, 18603–18610.

The wavenumbers and assignment of IR bands are given in Table 4.2. These IR spectra support the observations taken from other methods: isolated silanol peak at 3750 cm^{-1} increased in abundance with a decrease in zeolite crystal size, in line with the SEM images in Figure 4.1 (ZSM-5F > ZSM-5R > ZSM-5MS > ZSM-5 N). All samples contain Si-OH-Al bridging sites, as well as extra-framework aluminum (EFAL) species. The mesoporous sample, ZSM-5MS, still exhibits a significant amount of silanol nests.

Table 4.2 Assignments of IR bands

Wavenumber (cm^{-1})	Assignments
3745 (intense)	Isolated external silanol (Si-OH)
3663 (small band)	Extra-framework aluminum species (Al-OH)
3612 (intense)	Bridging hydroxyls (Si-OH-Al)
3510 (broad)	Silanol nests
2174	CO interacting with bridging OH
2169	CO interacting with EFAL
2157	CO interaction with silanol
2138	Liquid like CO

Spectra acquired during interaction with CO at 77 K are presented in Figure 4.3. The peak of the Brønsted acid sites (3610 cm^{-1}) was red shifted to 3305 cm^{-1} for all samples upon interaction with CO, indicating similar acid strength in all samples. When considering the $\nu(\text{CO})$ region ($2050 - 2250\text{ cm}^{-1}$) the main peak was observed at 2174 cm^{-1} for all samples, corresponding to an interaction with Si-OH-Al bridging sites. Furthermore, a significant component centered at 2169 cm^{-1} , associated to CO interaction with EFAL sites, was observed, in particular for ZSM-5R sample, followed by ZSM-5F sample.

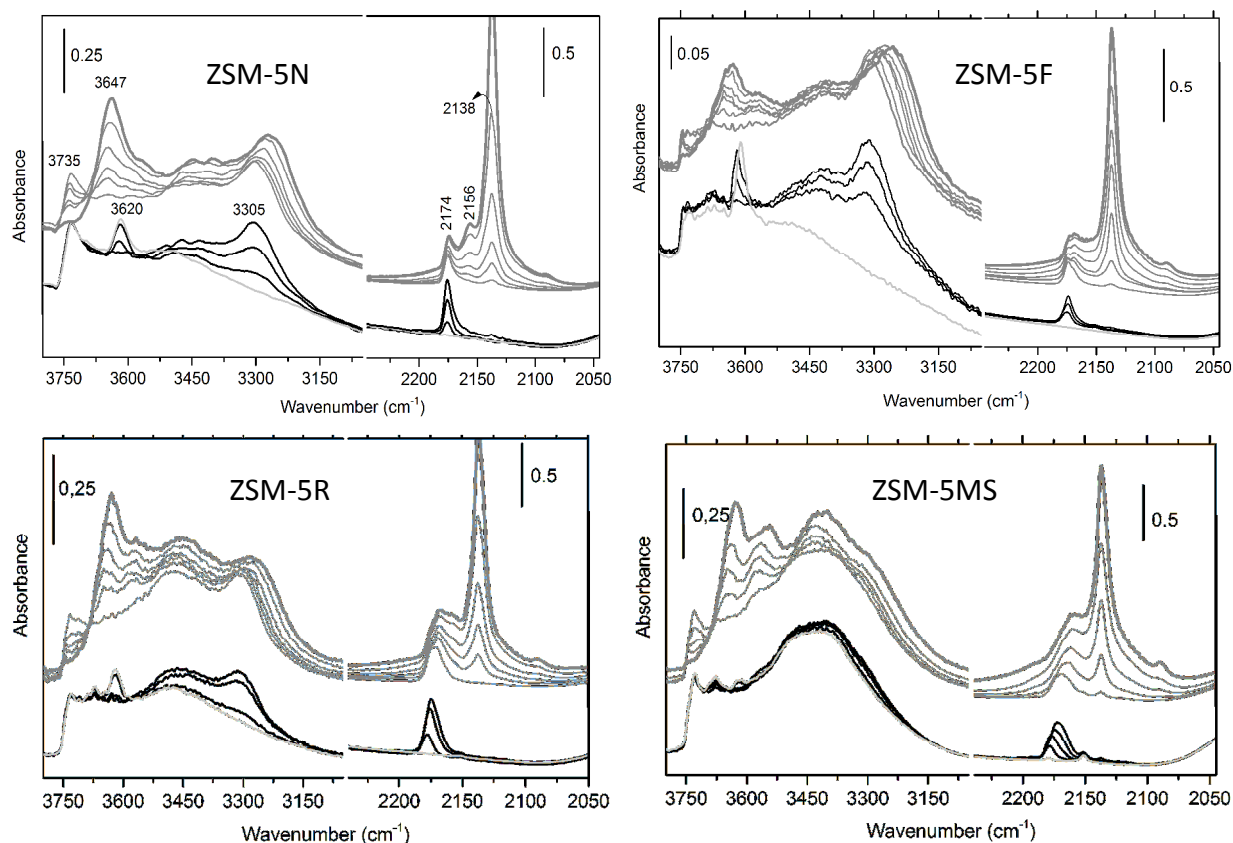


Figure 4.3 FTIR spectra of different ZSM-5-X pretreated at 773 K for 1 h, following CO adsorption at 77 K. Left panel: the $\nu(\text{OH})$ region; right panel: the $\nu(\text{CO})$ region. The CO coverage decreases successively from bold gray curve to light gray curve in each series.

The significantly lower n-hexane cracking rate observed for sample ZSM-5R compared with ZSM-5N in Table 4.1 and aforementioned, in spite of similar Si/Al ratios, may be explained by the higher fraction of EFAL sites present in ZSM-5R zeolite, when assuming that a high acid strength is required for alkane activation.

2.2 Evaluation of catalytic properties in the methanol to hydrocarbons (MTH) reaction

The catalytic data for the four aforementioned samples are shown in Table 4.3. All catalysts gave an initial conversion close to 100%. This total initial conversion is necessary to

obtain comparable deactivation behaviors for all catalysts [24]. Indeed, one can assume that only reaction between methanol and aromatic species leads to coke formation. The initial C_3/C_2 ratio in the product stream increased from 1.6 over ZSM-5N, *via* 1.8 over ZSM-5R, to 2.5 over ZSM-5MS and finally to 5.5 over ZSM-5F, thus following the order:

$$\text{ZSM-5F} > \text{ZSM-5MS} > \text{ZSM-5R} > \text{ZSM-5N}$$

An inverse correlation was found between the C_3/C_2 ratio and the hydrogen transfer index (HTI), which was calculated for the C_4 fraction [*i.e.* $\sum C_{4-} / (\sum C_{4-} + \sum C_{4=})$]. As one would expect, a positive correlation was found between the HTI and the selectivity toward aromatics (Table 4.3).

Table 4.3 Catalytic data for the MTO reaction over ZSM-5 zeolites at 623 K

Catalyst	Conv. [%]	TOS [min]	Selectivities [%]							$C_3/C_2=$	$C_4/C_{4=}$	HTI (C_4)
			C_2	C_3	$C_{4=}$	C_{4-}	C_5	$C_{6+ ar}$	$C_{6+ al}$			
ZSM-5R	99	5	15	27	14	13	11	9	10	1.8	0.9	0.5
ZSM-5N	100	5	14	23	11	17	10	17	7	1.6	1.5	0.6
ZSM-5MS	99	5	12	30	18	9	11	9	11	2.5	0.5	0.3
ZSM-5F	98	5	7	36	23	4	13	5	12	5.5	0.2	0.2

From the catalytic profiles as a function of time on stream (Figure 4.4), no direct correlation was found between product selectivity and deactivation rate. The deactivation rate decreased in the order:

$$\text{ZSM-5R} > \text{ZSM-5MS} > \text{ZSM-5N} \sim \text{ZSM-5F}$$

At higher times on stream, a raise in the C_3/C_2 ratio and a decrease in HTI were observed for all catalysts. The reference catalyst, ZSM-5R, was the sole which deactivated below 50% conversion. At those low conversions, C_2 selectivity increased faster than C_3 selectivity, leading to a gradual decrease in the propene-to-ethene ratio while diminishing

[24] T. V. W. Janssens, S. Svelle, U. Olsbye, *J. Catal.* **2013**, *308*, 122–130.

conversion. Since the aim of this study was to design a MTP-catalyst, more tests were carried out with the most promising ZSM-5F material, at different contact times. Product yield versus methanol conversion data are plotted in Figure 4.5. The yield versus conversion curves were linear for all products in the 2 to 98% methanol conversion range, and the C_3/C_2 ratio was in the range 5 - 7 at all contact times. The yield toward aromatics never exceeded 5%.

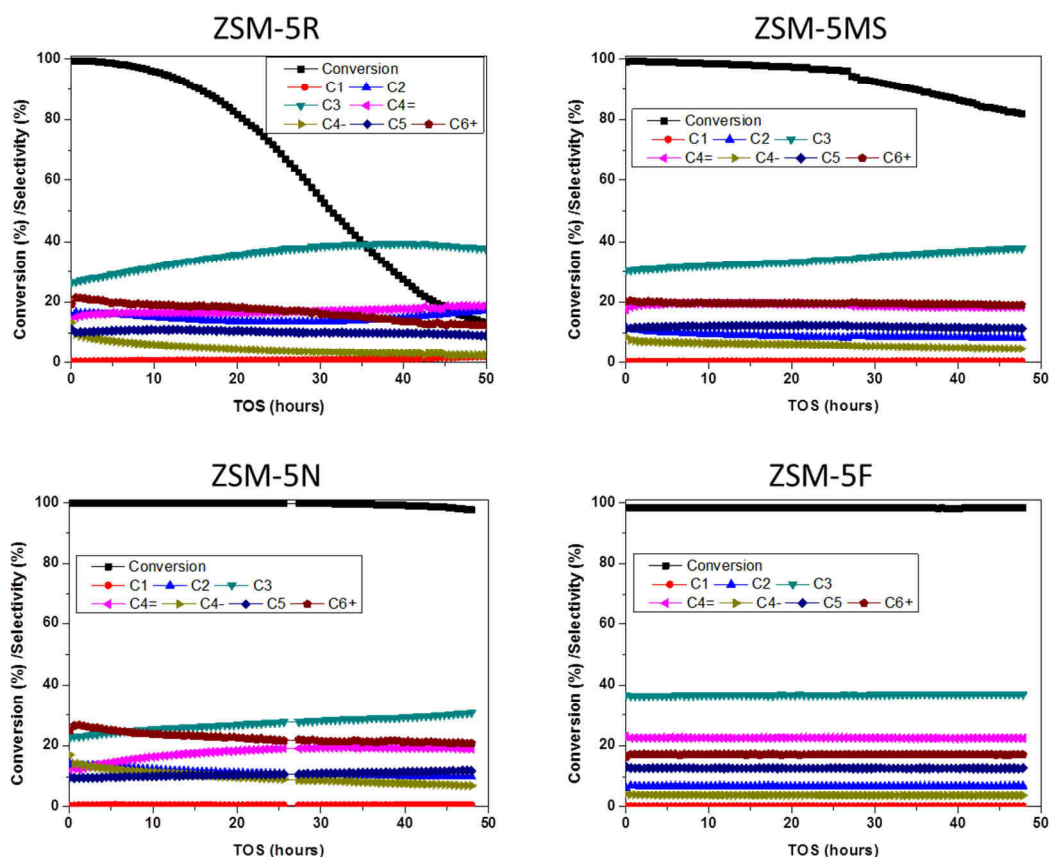


Figure 4.4 MTH test data for the four ZSM-5 samples
Conditions: T=623 K, 60 mg H-ZSM-5F activated 1h at 823 K, WHSV = $1.8 \text{ g}_{\text{MeOH}}/\text{g}_{\text{cat}}\cdot\text{h}^{-1}$, TOS = 48 h

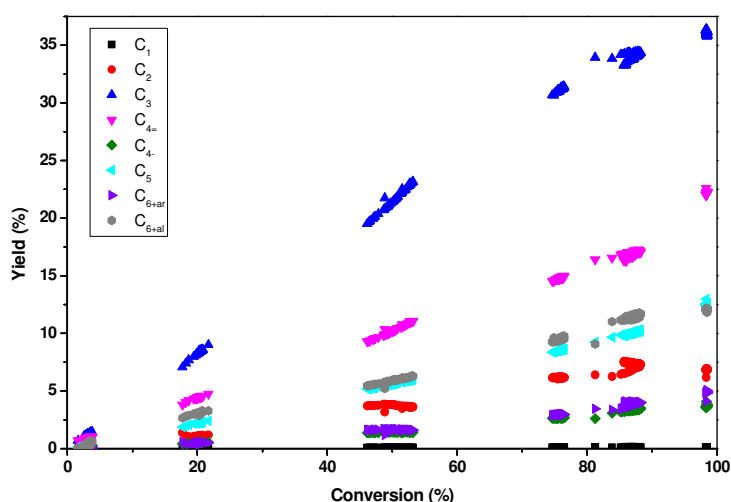


Figure 4.5 Methanol conversion – yield in different product plot for ZSM-5F at 623 K

2.3 Discussion

In order to rationalize these data, a brief recapitulation of the mechanistic aspects of the Methanol to Hydrocarbons (MTH) reaction is required: Chang and Silvestri published the first study using a ZSM-5 catalyst in 1977 [3]. They showed how product selectivity was shifted from light olefins to a mixture of aromatics and alkanes with increasing contact times. Two years later, Chen and Reagan replotted the rate versus contact time data and suggested that the reaction was autocatalytic, olefins acting as autocatalytic species [25]. During the past three decades, huge efforts have been made to reveal further mechanistic details of the MTH reaction. Today, the general view is that both C_{3+} alkenes and various arenes, polymethylated benzenes in particular, may act as autocatalytic species in ZSM-5 (see ref. [6] and references therein). Methylation of C_{3+} alkenes have been found to produce mainly propylene by cracking reactions, while methylation of polymethylated benzenes have been shown to produce mainly ethylene and propene, in ZSM-5 zeolite [12,26].

Taking the mechanistic aspects into account, a high C_3/C_2 ratio, and a low selectivity to aromatics, may be ascribed either to low acid site density and/or low diffusion hindrance,

[25] N. Y. Chen, W. J. Reagan, *J. Catal.* **1979**, *59*, 123–129.

[26] M. Bjørgen, S. Svelle, F. Joensen, J. Nerlov, S. Kolboe, F. Bonino, L. Palumbo, S. Bordiga, U. Olsbye, *J. Catal.* **2007**, *249*, 195–207.

thus facilitating transport of alkene products out of the catalyst before being eventually converted to aromatics. Such a hypothesis has already been validated by previous studies referred in the Introduction, which indicated that high Si/Al ratios, as well as small crystal sizes, favor light olefins selectivity and elevated propene-to-ethene ratios [15–17]. An alternative hypothesis could be an enhanced selectivity for one or the other catalytic cycle, *i.e.*, alkene-mediated versus arene-mediated, beyond the two parameters already mentioned. Such an explanation would be in line with the studies showing that addition of phosphorous to the ZSM-5 zeolite led to lower acid strengths and concurrently to higher propene-to-ethene ratios and high light olefins selectivities [18,19]. A key challenge when comparing several catalysts for a targeted reaction is that the materials normally differ by more than one parameter, and that several parameters may influence product selectivity. This is the case for the four samples under investigation. Let us therefore compare product selectivities versus each of the parameters suggested above: Overall, the selectivity to C₂–C₄ olefins diminishes in the order:

ZSM-5F (66%) > ZSM-5MS (60%) > ZSM-5R (56%) > ZSM-5N (48%)

Furthermore, the propene-to-ethene ratio decreases in the order:

ZSM-5F (5.1) > ZSM-5MS (2.5) > ZSM-5R (1.8) > ZSM-5N (1.6)

2.3.1. Product selectivity versus crystal size

The crystal size of the materials decreases in the order:

ZSM-5F (15 – 20 μm) > ZSM-5R (5 μm) > ZSM-5MS (2 μm) > ZSM-5N (0.05 – 0.10 μm)

A larger crystal size represents longer characteristic diffusion lengths, but also a lower fraction of external sites. A positive correlation between crystal size and light olefins selectivity was indicated when considering the two ends of the row. However, an inversion

was observed for the two materials in the middle, thus suggesting that there is no direct correlation between crystal size and selectivities for the samples studied here.

2.3.2. Product selectivity versus Brønsted acid sites

The number of Brønsted acid sites in the materials decreases in the order:

ZSM-5R (1.00) > ZSM-5N (0.78) > ZSM-5F (0.31) > ZSM-5MS (0.26) (H/D titration)
ZSM-5MS (322) > ZSM-5N (183) > ZSM-5R (120) > ZSM-5F (107) (n-hexane cracking)

The two methods gave quite different results, possibly because H/D exchange may take place at Si-OH-Al bridging sites as well as hydroxyls linked to EFAL species, while n-hexane cracking may only proceed at Si-OH-Al bridging sites with higher acid strength. The FTIR spectra indicated that the acid strength of the Si-OH-Al bridging sites is similar for all materials. However, they further suggested that the fraction of hydroxyls associated with EFAL species is highest for ZSM-5R, followed by ZSM-5F, while ZSM-5MS and ZSM-5N contain a small fraction of those hydroxyls. In either case, it is not obvious that there is a direct correlation between the number of Si-OH-Al bridging sites and selectivity in the materials tested.

2.3.3. Tentative reaction path occurring for raising propylene formation

The aforementioned results remain quite difficult to explain in terms of reaction pathway occurring especially in the ZSM-5F giant crystals. Indeed, the nearly five-times higher propylene formation versus ethylene may involve a rather complex mechanism. It is important to remind that Froment and Park have already presented a detailed MTO mechanism involving 726 elementary steps including protonation, deprotonation, hydride transfer, methyl-shift, methylation, oligomerization, cracking [27]. Nevertheless, one may expect that under specific reaction conditions or catalyst formulation, it can be conceived

[27] T.-Y. Park, G. F. Froment, *Ind. Eng. Chem. Res.* **2001**, *40*, 4172–4186.

that one path becomes dominant with respect to the others. Wu *et al.* [28] have demonstrated, while co-feeding methanol and C₂–C₆ alkenes in a multi-stage adiabatic fixed-bed reactor, that methylation and cracking of C₄–C₇ olefins became predominant. The question arises what would induce this impressive propylene selectivity at complete methanol conversion over ZSM-5F synthesized *via* the fluoride-mediated route?

Following the Mulhouse's group key researches [29,30], it is now well admitted that larger zeolite crystals with fewer defects are produced *via* the non-alkaline procedure. In addition, the F⁻ anion has been reported to be occluded in [4¹5²6²] cage, pentacoordinated and interacting with a silicon framework atom, thus forming [SiO_{4/2}F]⁻ entities [31]. Guth and Kessler have reported a possible modification of the catalytic properties in calcined materials even after complete fluorine removal. Indeed, the co-templating role of fluoride anion contributes to the stabilization of small 4MR cavities [30,31] and may also induce distortion in the geometry of tetrapropylammonium (TPA) cations located at the channel intersections. Besides those materials exhibit very few connectivity defects and thus allow the synthesis of rather hydrophobic zeolites.

The main difference between ZSM-5R and ZSM-5F zeolites relies in different BA sites densities. Whereas the later catalyst exhibits a three- to four-times larger crystal size, it possesses at the same time nearly one third of BA sites. One can therefore roughly estimate a ten-times higher density of BA sites per crystal of ZSM-5R zeolite. The higher deactivation rate observed is directly connected to this high acidity. A higher density of BA sites should also induce more proximity among these sites, thus to ease consecutive reactions up to extensive coke formation. If we consider a high dispersion of BA sites in the ZSM-5F regular prismatic crystals, whilst ZSM-5R presents a high degree of twinning, one can understand the higher selectivity toward light olefins over the former catalysts. In spite of their huge diffusion length, giant ZSM-5F crystals which contain few defects, being rather hydrophobic, exhibit few BA sites and warrant therefore reduced aromatization reactions (and thus lower extend of aromatics hydrocarbon pool), allowing the catalyst to maintain its steady-state

[28] W. Wu, W. Guo, W. Xiao, M. Luo, *Chem. Eng. Sci.* **2011**, *66*, 4722–4732.

[29] M. Estermann, L. B. Mc Cusker, C. Baerlocher, A. Merrouche, H. Kessler, *Nature* **1991**, *352*, 320–323.

[30] A. Jakob, V. Valtchev, M. Soulard, J. Patarin, D. Faye, *Stud. Surf. Sci. Catal.* **2008**, *174A*, 677–680.

[31] E. Aubert, F. Porcher, M. Souhassou, V. Petricek, C. Lecomte, *J. Phys. Chem. B* **2002**, *106*, 1110–1117.

behavior during the whole course of the reaction (Figure 4.4). Figure 4.6 tends to rationalize the main reaction path occurring over this highly MTP-selective zeolite. The reduced acidity of ZSM-5F catalyst with respect to ZSM-5R plays in favor of higher propylene selectivity as already observed by Liu *et al.* [19] while reducing the acidity of ZSM-5 zeolites by doping with phosphorous.

In line with these tentative explanations, a TPO experiment was performed to quantify the coke amount after long-term experiments by flowing methanol at 400 °C over the two zeolites prepared either in alkaline or fluoride-media. It appeared that the amount of carbon present on the former ZSM-5R zeolite was about nine times higher than for ZSM-5F zeolite [32]. One can therefore conclude that the zeolite prepared *via* the fluoride route is much more resistant to coke formation when compared with other zeolites. Thanks to its reduced number of Brønsted acid sites and an important diffusion length, thus to a drastically reduced density of acid sites, ZSM-5F appears to be at the same time an active and stable MTP-catalyst. Whereas the peculiar behavior of this catalyst remains partly unrevealed, the high selectivity to propene may be related to (some extend at least) aforementioned peculiarities: lower BA sites density, huge diffusion length, absence of crystal twinning, presence of EFAL. Figure 4.6 tempts to summarize an eventually favored alkene methylation-cracking cycle over large ZSM-5F crystals. Further studies are under progress to evaluate the exact nature of coke formed over these zeolites.

[32] G. Laugel, X. Nitsch, F. Ocampo, B. Louis, *Appl. Catal. A* **2011**, 402, 139–145.

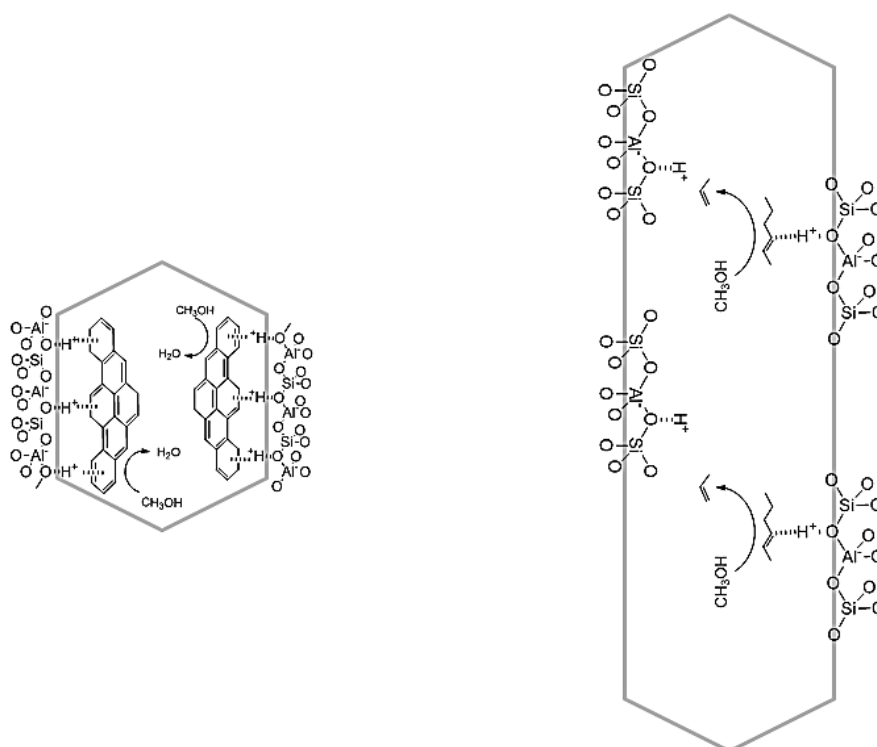


Figure 4.6 Schematic representation of methanol reaction over Brønsted acid sites in ZSM-5R and ZSM-5F crystals

2.4 Summary

Different ZSM-5 zeolites possessing various crystal sizes and acid site densities were synthesized and thoroughly characterized by BET, XRD, SEM, FT-IR and H/D exchange techniques.

Their catalytic activities were evaluated in the Methanol to Olefins (MTO) reaction with the objective to maximize the propylene selectivity.

A high propylene to ethylene ratios (~ 5) was achieved over ZSM-5F catalyst prepared *via* the fluoride route. The superior selectivity of this promising MTP-catalyst was tentatively ascribed to the lower density of strong Brønsted acid sites in combination with a long diffusion pathway and few crystal defects.

3. Toward the design of a second generation of MTP-catalysts

The crystalline ZSM-5 prepared in fluoride medium offers the possibility of selectively converting methanol to propene at high degrees of conversion. The aim of this section was therefore to design a MTP-catalyst *via* the development of a fluoride-mediated ZSM-5 zeolite having the appropriate chemical composition and crystal size.

The synthesis procedures and characterizations of all ZSM-5F zeolites were described in Section 0. The catalytic tests for MTO reaction were performed according to the procedure described in Section Chapter 2.1.2.

3.1 Influence of the Si/Al ratio

Several H-ZSM-5F catalysts having different Si/Al ratio (SAR) were tested to see whether the density of acid site has an influence on fluoride-mediated catalyst performance. Figure 4.7 shows the degrees of conversion and the related C_3/C_2 ratio as functions of SAR.

It can be clearly seen that the conversion degrees increase with increasing Si/Al ratio. As the amount of Brønsted acid sites is directly proportional to the Al content of the zeolite, an increase in the SAR leads to a decrease of bridging OH groups. Surprisingly low acid site densities in fluoride-mediated zeolite crystals allowed to obtain high catalytic activities in the conversion of methanol to light olefins. Hence, catalysts, having a SAR of approximately 20, presented less than 1% methanol conversion. In contrast, a $SAR \geq 130$ led to convert between 75 and 95% of methanol.

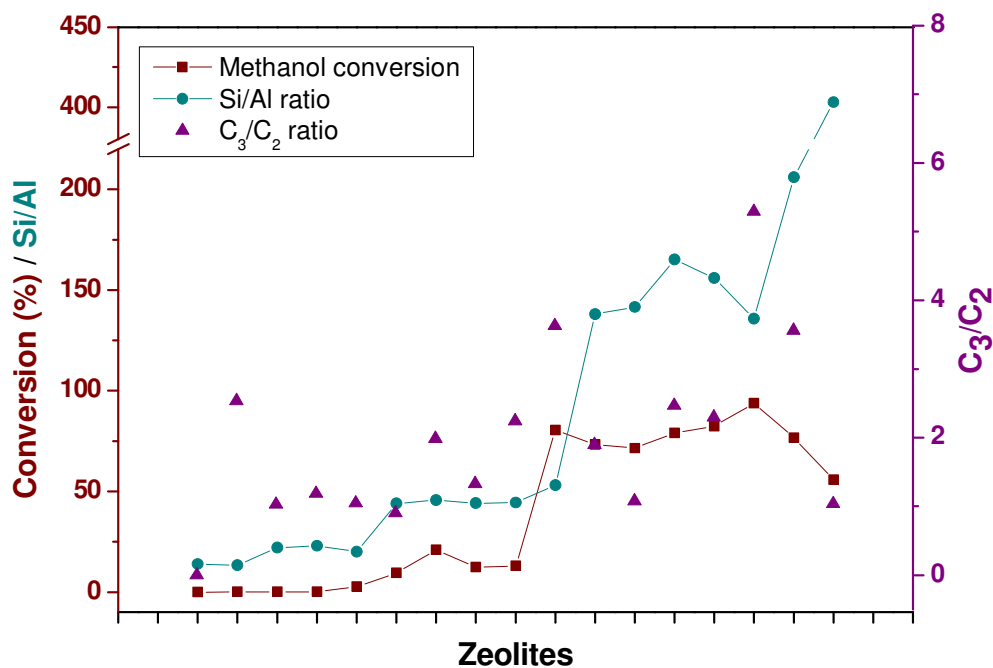


Figure 4.7 Conversion and C_3/C_2 ratio for different ZSM-5F zeolites having various Si/Al ratio
 Conditions: $T=698$ K, 60 mg H-ZSM-5F activated 1 h at 823 K, $WHSV = 1.12 \text{ g}_{\text{MeOH}}/\text{g}_{\text{cat}} \cdot \text{h}^{-1}$, TOS = 2 h

These results seem contradictory, but it is also known that the acid strength of a given site could increase when there is a decrease in the number of Al atoms in next nearest neighbor positions (NNN) of the Al atom which supports the acid site [33]. Moreover, it is well known in the literature that the MTO process requires a catalyst with moderate acidity to hinder aromatization reactions, and thus deactivation by coking [34].

Furthermore, the C_3/C_2 ratio seems to follow the same tendency as the methanol conversion. Although its distribution is not very clear, one can see that zeolites with a high acid site density exhibit rather low C_3/C_2 ratio ≤ 1 . Whereas zeolites with high SAR allow to reach $2 < C_3/C_2 < 6$, expected for zeolite with the highest SAR.

These data and considerations allow us to conclude that the acid site density plays an important role in both methanol conversion and selectivities towards ethylene and propylene. Moreover, the most effective catalyst tested during this work is the F2 sample

[33] A. Corma, *Chem. Rev.* **1995**, 95, 559–614.

[34] a) S. Wilson, P. Barger, *Microporous Mesoporous Mater.* **1999**, 29, 117–126. b) D. Mores, J. Kornatowski, U. Olsbye, B. M. Weckhuysen, *Chem. Eur. J.* **2011**, 17, 2874–2884. c) H. Schulz, *Catal. Today* **2010**, 154, 183–194. d) S. M. T. Almutairi, B. Mezari, E. A. Pidko, P. C. M. Magusin, E. J. M. Hensen, *J. Catal.* **2013**, 307, 194–203.

presenting a high crystallinity with crystals having 30 μm in length. This catalyst prepared in fluoride medium allowed, to reach a 94% conversion along with a selectivity towards light olefins $\text{C}_2\text{-C}_4$ of 85%. Hence, the C_3/C_2 ratio was 5.3. Long time on stream experiments are presented in Figure 4.8. Likewise the preliminary tests, this new ZSM-5F catalyst presents a very stable behavior versus time on stream.

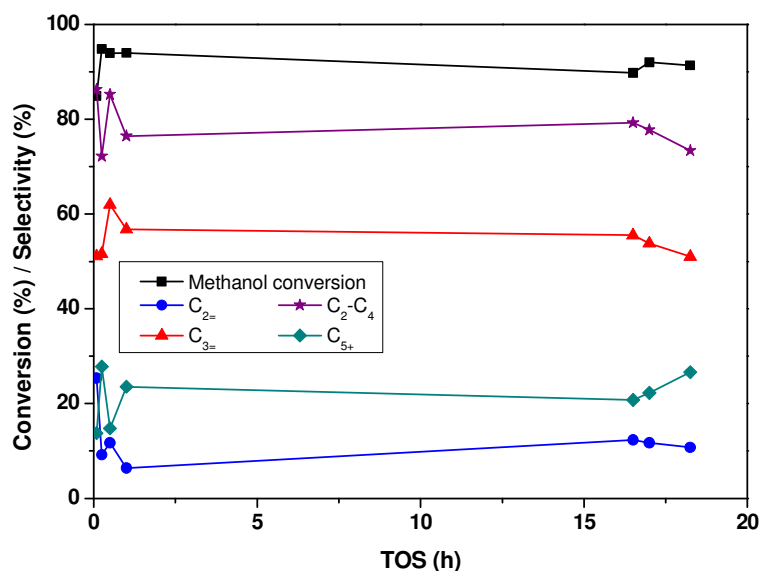


Figure 4.8 Catalytic profile of most efficient catalyst (F2) versus time on stream
Conditions: $T=698\text{ K}$, 60 mg H-ZSM-5F activated 1 h at 823 K, $\text{WHSV} = 1.12\text{ g}_{\text{MeOH}}/\text{g}_{\text{cat}} \cdot \text{h}^{-1}$, TOS = 19 h

3.2 Influence of the crystal size

Among all fluoride-mediated ZSM-5 zeolites, various crystal sizes have been obtained (see Table 3.5 in Section Chapter 3.2.2.2). Figure 4.9 presents the catalytic performances of four representative ZSM-5F catalysts, having the same SAR (100), as functions of their crystal size. One can firstly see that the increase in crystal size has a negative impact on both methanol conversion and C_3/C_2 ratio. Indeed, the higher the crystal size was, the lower the catalytic performances were recorded; *i.e.* a methanol conversion of 98% could be achieved for the catalyst having crystal size of 540 μm^3 vs. 56% over crystals with volume of 6250 μm^3 . In the preliminary experiments, we observed that fluoride-mediated ZSM-5 with the larger crystal size, were the optimal catalyst. However, among the fluoride-mediated zeolite family,

the “smallest” crystals gave the higher catalytic activity. This behavior could be explained by diffusion limitations observed for crystals size superior to $1500 \mu\text{m}^3$, which thus hindered the reaction.

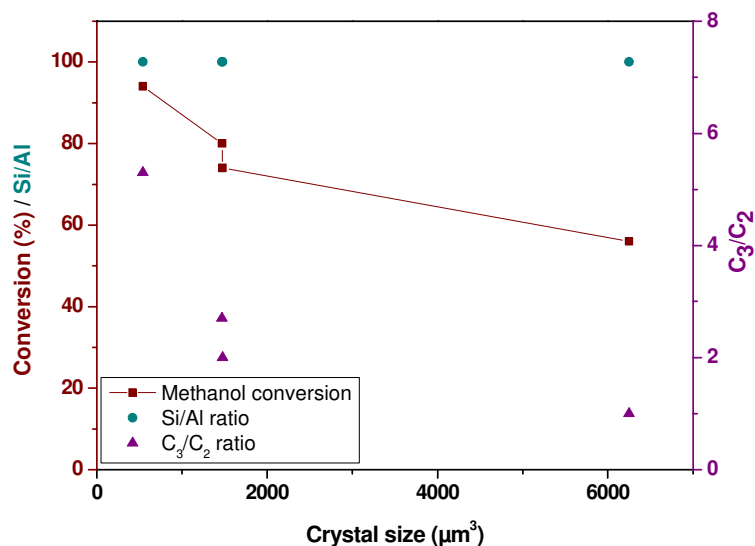


Figure 4.9 Influence of crystal size on the catalytic performance in MTO reaction
Conditions: $T=698 \text{ K}$, 60 mg H-ZSM-5F activated 1 h at 823 K , $\text{WHSV} = 1.12 \text{ g}_{\text{MeOH}}/\text{g}_{\text{cat}} \cdot \text{h}^{-1}$, $\text{TOS} = 2 \text{ h}$

3.3 Replacement of HF by HCl

The influence of both Brønsted acid sites density and crystal size on activity / selectivity has been previously investigated in the MTO reaction. The main goal was to raise and then maintain a high selectivity toward propylene, hence to develop a simple strategy for designing a MTP catalyst with the MFI structure. With these promising results in hand, it was decided to further optimize ZSM-5 zeolites synthesized under fluoride conditions. Indeed, hydrofluoric acid has to be replaced to warrant industrial catalyst implementation. This study will therefore focus on the design of a novel MTP-catalyst generation, synthesized in the absence of HF. Thus, hydrochloric acid was chosen to replace HF.

The pH, the Si/Al and the Si/ NH_4F of the syntheses as well as reactivity data are summarized in Table 4.4. It is worthy to mention that whatever the H-ZSM-5FCl zeolites were, the same amount of HCl was introduced in the synthesis gel (1 mL) and a neutral pH was obtained. The absence of alkalinity is important in fluoride-mediated synthesis, to avoid

any competition between hydroxide and fluoride mineralizer anions. Besides, all zeolites are giant-sized (superior to 20 μm) with comparable crystal volumes (see Table 3.5 in Section Chapter 3.2.2.2).

Parent ZSM-5F (entry F2 in Table 4.4) appears to be more active MTP-catalyst when compared with its HCl-modified homologue (entry F11). Indeed, ZSM-5FCl catalyst showed lower degree of conversion and selectivity toward propylene. However, this more environmental-friendly catalyst exhibited non-negligible catalytic activity. Other ZSM-5FCl samples have therefore been prepared to tempt raising either activity or selectivity. The longer synthesis duration led to a slight increase in methanol conversion (entry F12; *i.e.* 67% vs. 64%) with no change in the products distribution. As seen in SEM images (Figure 3.10), samples prepared in the presence of HCl exhibited lower crystallinities compared to their HF homologues. Hence, the addition of NH_4F in the synthesis gel (entries F13 and F14) led to higher apparent crystallinities with an optimum for F13 sample. It is worthy to mention that the F13 catalyst achieved the higher catalytic performance recorded for HCl-mediated family. More detailed characterizations on their intrinsic acidity, such as ^1H MAS NMR and/or infrared spectroscopies, seem to be necessary to explain more precisely their catalytic activities. Nevertheless, their intrinsic acidity appears to be different with respect to their HF counterparts. Probably, the content in silanol defects might be associated with the selectivities' inversion between ethene and propene. Bearing this in mind, one can ascertain that the apparent crystallinity is an important parameter to design an efficient catalyst.

Table 4.4 Textural properties and catalytic performances of as-prepared catalysts

Entry	Catalyst	Synthesis duration	Si/Al ratio ^a	NH_4F gel ^b	MeOH conv. ^c [%]	S_{C_2} ^c [%]	S_{C_3} ^c [%]	$S_{\text{C}_2-\text{C}_4}$ ^c [%]	C_3/C_2 ratio ^a
F2	H-ZSM-5F	48	136	112	94	12	62	85	5.3
F11	H-ZSM-5FCl	48	-	112	64	27	33	69	1.2
F12	H-ZSM-5FCl	166	196	112	67	29	32	69	1.1
F13	H-ZSM-5FCl	161	230	168	73	21	37	68	1.7
F14	H-ZSM-5FCl	161	237	224	69	25	35	76	1.4

^a determined by X-Ray Fluorescence

^b molar ratio

^c after 2 h on stream

Additionally, Figure 4.10 shows the catalytic profiles of F14 ZSM-5FCl zeolite during two days on stream. It is noteworthy that the replacement of HF by HCl in the gel led to stable catalysts which kept the methanol conversion constant at 70% during 48h on stream.

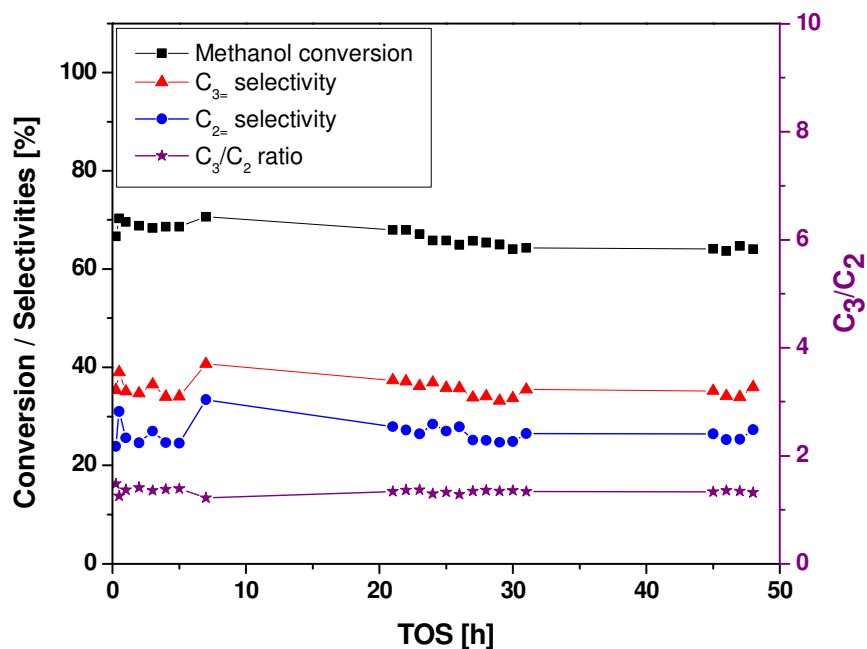


Figure 4.10 Conversion/Selectivities toward ethylene and propylene and C_3/C_2 ratio for ZSM-5FCl catalyst (entry F14).

Conditions: $T=698$ K, 60 mg H-ZSM-5F activated 1 h at 823 K, $WHSV = 1.12 \text{ g}_{\text{MeOH}}/\text{g}_{\text{cat}} \cdot \text{h}^{-1}$, TOS = 48 h

As a conclusion, this study shows that hydrofluoric acid can be efficiently replaced by another acid. Although their lower conversion and selectivity toward propylene (which might be even improved in future work), HCl ZSM-5 zeolite homologues preserved the high stability of fluoride-mediated ZSM-5 catalysts.

3.4 Total conversion capacity

In order to get a more precise and quantitative measure of the improvement of the catalytic performances of our most effective catalysts, we have decided to use a method

developed by Bjørngen *et al.* in 2008, named the total conversion capacity [35]. This data is obtained by plotting the methanol conversion with respect to the cumulative methanol converted per gram of catalyst and extrapolating to zero conversion. This method allows calculating an estimated catalytic capacity of MTO catalysts until their complete loss of activity. The total conversion capacity of two different ZSM-5F (F2 and F5) is plotted in Figure 4.11.

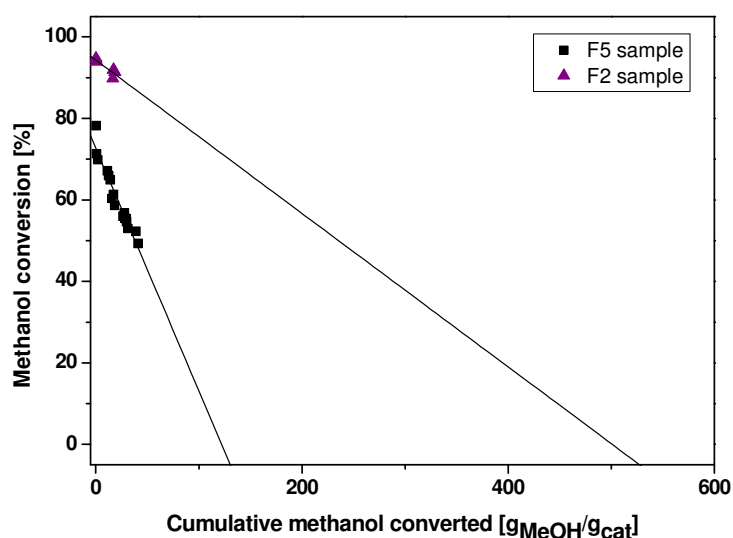


Figure 4.11 Methanol conversion as functions of cumulative methanol converted for two different ZSM-5F

A conversion capacity of $122 \text{ g}_{\text{MeOH}}/\text{g}_{\text{catalyst}}$ is achieved over F5 zeolite, whereas for our most effective ZSM-5F catalyst (F2) a conversion capacity of $502 \text{ g}_{\text{MeOH}}/\text{g}_{\text{catalyst}}$ was obtained. By taking into account the respective selectivity towards light olefins of each catalyst, one can estimate the total mass of light olefins produced per gram of catalyst (Table 4.5). ZSM-5 F2 zeolite allowed to obtain high conversion, selectivity toward light olefins and even stability.

[35] M. Bjørngen, F. Joensen, M. Spangsborg Holm, U. Olsbye, K.-P. Lillerud, S. Svelle, *Appl. Catal. A* **2008**, 345, 43–50.

Table 4.5 Light olefins production of ZSM-5F zeolites

Catalyst	Light olefins production [g(C ₂ =C ₄ =)/g _{catalyst}]
ZSM-5 F2	167
ZSM-5 F5	35

One can cite a recent study from Valtchev *et al.* who used this total conversion capacity data to compare their fluoride-mediated ZSM-5 zeolite against classical ZSM-5 synthesized in alkaline medium [36]. Indeed, they have found a cumulative conversion of $1000 \text{ g}_{\text{MeOH}}/\text{g}_{\text{catalyst}}$ for their fluoride-mediated catalyst, being 1.6 times higher than the alkaline-synthesized ZSM-5. Compared to our results, their ZSM-5F zeolite seems to be more competitive and efficient. However, if we take into account the fact that their catalyst owns a greater Brønsted acidity, we can try to reformulate the total conversion capacity in terms of the acidity of the material (Si/Al ratio). Thus, the new values, taking into account the acidity of each catalyst, are $47,710$ and $131,489 \text{ mol}_{\text{MeOH converted}}/\text{mol}_{\text{Al}}$ for the ZSM-5 synthesized by the team of Valtchev and our ZSM-5F zeolite, respectively. As a conclusion, the reformulated conversion capacity was enhanced by a 2.8 factor for our most effective catalyst. One could explain this result by comparing the intrinsic properties of both F-catalysts. Although the fluoride-mediated catalyst from Valtchev *et al.* possesses low amount of external and internal silanols with respect to their alkaline-mediated catalyst, it presents a significant quantity of silanol defects. Thus, the higher performance of our F2 zeolite can be attributed to the absence of silanol defects. Furthermore, as previously exposed, our “giant” crystals with low acid site density allow to hinder consecutive reactions and thus deactivation due to the formation of coke species, being not the case for nanocrystals with high acid site density.

[36] Z. Qin, L. Lakiss, L. Tosheva, J.-P. Gilson, A. Vicente, C. Fernandez, V. Valtchev, *Adv. Funct. Mater.* **2014**, *24*, 257–264.

4. Conclusion

The work described in this Chapter has demonstrated the primary role or importance of F⁻ anions in the design of an efficient and competitive MTO/MTP-catalyst.

A first generation of promising MTP-catalyst was successfully developed by adapting the ZSM-5 zeolite preparation procedure, along with a tailored Brønsted acidity and crystal size. High propylene to ethylene ratios (> 5) were achieved over a ZSM-5 zeolite prepared *via* fluoride route. The superior selectivity of this MTP-catalyst was tentatively ascribed to the low density of strong Brønsted acid sites in combination with a long diffusion path throughout the crystal.

A novel generation of MTO-catalyst was successfully developed by adapting the fluoride ZSM-5 zeolite preparation procedure. The influences of both SAR and crystal volume were analyzed. A Si/Al ratio of 100 and a low acid site density along with crystal volume around 540 μm³ seemed to be required properties to design a competitive and efficient MTP-candidate. Moreover, the crystallinity of giant crystals synthesized in fluoride medium have to be the highest possible.

On the other hand, high propylene to ethylene ratios (> 5) were achieved over a ZSM-5 zeolite prepared *via* the fluoride route. Consequently it was tried to render the synthesis in fluoride medium more environmental friendly. The different zeolites obtained in the presence of hydrochloric acid exhibited interesting MTO-features, such as high stability and light olefins selectivity.

Finally, the total conversion capacity of our most effective catalyst was able to be determined and compared with a fluoride-mediated catalyst developed by the team of Valtchev. A 2.8 times higher cumulative conversion, taking into account the respective Brønsted acid site densities, was achieved over our home-made ZSM-5F candidate.

**Chapter 5. AROMATIC CHLORINATION WITH
TRICHLOROISOCYANURIC ACID OVER ZEOLITES**

ABSTRACT

This chapter focuses on the evaluation of zeolite catalysts in chlorination reactions of several aromatics in the presence of trichloroisocyanuric acid (TCCA).

The first part deals with preliminary results obtained over solid acids under liquid phase conditions. TCCA reactivity is highly affected by the acid strength of the reaction medium. Our experimental results, along with DFT calculations highlight that the chlorination over solid acid is feasible, thus leading to a possible replacement of nasty liquid acids to promote this superelectrophilic reaction. We have tested several solid acids, showing the synergic need between acid strength and adapted pore size for performing the reaction.

The second section is dedicated to the catalytic evaluation of zeolites in chlorination reactions (nitrobenzene and chlorobenzene) under semi-continuous gas-solid conditions. A large screening of solids was made to design an optimal catalyst for each aromatic substrate. Reaction condition optimizations along with kinetic studies were investigated.

In an environmental-friendly way of thinking, catalyst recyclability was verified. Finally, several hierarchical zeolites (FAU and MFI-types), developed by different methods, were tested in both aromatics' chlorination. Nanosized and dealuminated zeolites were found to be promising catalysts for chlorobenzene chlorination ($X_{\text{PhCl}} = 44\text{-}89\%$, $S_{\text{monochlorination}} = 96\text{-}56\%$).

1. Introduction

Electrophilic reagents that exhibit greatly enhanced reactivities in the presence of superacids are said to form protonated or protosolvated species, named as superelectrophiles [1]. The concept of using charge-charge repulsion in the reagents to decrease the activation barrier was explored for a series of reactions, especially by Klumpp and co-workers [2]. We have been using this concept for halogenating organic substrates using trihaloisocyanuric acids (TXCA, Figure 5.1) [3].

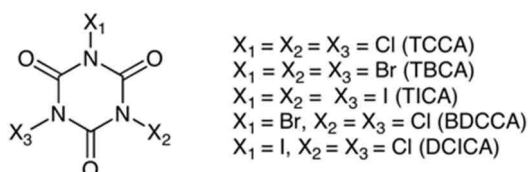


Figure 5.1 Some trihaloisocyanuric acids

Trichloroisocyanuric acid (TCCA) is a safe commercially available reagent [4], whilst tribromo- and triiodoisocyanuric acids (TBCA and TICA, respectively) can be prepared from readily available commercial sources [5]. These reagents can perform the electrophilic halogenation of diverse substrates, such as alkenes [6] and carbonyl compounds [7]. The different trihaloisocyanuric acids are also powerful regioselective halogenating agents [8].

[1] G. A. Olah, *Angew. Chem. Int. Ed.* **1993**, *32*, 767–788.

[2] a) D. a Klumpp, Y. Zhang, M. J. O'Connor, P. M. Esteves, L. S. de Almeida, *Org. Lett.* **2007**, *9*, 3085–3088. b) G. A. Olah, D. A. Klumpp, *Superelectrophiles and Their Chemistry*, Wiley, New York, **2008**.

[3] a) G. F. Mendonça, M. R. Senra, P. M. Esteves, M. C. S. de Mattos, *Appl. Catal. A* **2011**, *401*, 176–181. b) L. S. de Almeida, P. M. Esteves, M. C. S. de Mattos, *Tetrahedron Lett.* **2009**, *50*, 3001–3004. c) R. S. da Ribeiro, P. M. Esteves, M. C. S. de Mattos, *Synthesis* **2011**, 739–744.

[4] U. Tilstam, H. Weinmann, *Org. Process Res. Dev.* **2002**, *6*, 384–393.

[5] a) R. D. S. Ribeiro, P. M. Esteves, M. C. S. de Mattos, *Tetrahedron Lett.* **2007**, *48*, 8747–8751. b) L. de Almeida, P. M. Esteves, M. C. S. De Mattos, *Synlett* **2006**, *2006*, 1515–1518.

[6] a) G. F. Mendonça, A. M. Sanseverino, M. C. S. De Mattos, *Synthesis* **2003**, 45–48. b) L. T. C. Crespo, R. da S. Ribeiro, M. C. S. de Mattos, P. M. Esteves, *Synthesis* **2010**, 2379–2382.

[7] G. F. Mendonça, H. C. Sindra, L. S. de Almeida, P. M. Esteves, M. C. S. de Mattos, *Tetrahedron Lett.* **2009**, *50*, 473–475.

[8] a) L. S. de Almeida, P. M. Esteves, M. C. S. de Mattos, *Synlett* **2007**, 1687–1690. b) R. da S. Ribeiro, P. M. Esteves, M. C. S. de Mattos, *J. Braz. Chem. Soc.* **2012**, *23*, 228–235.

Trihaloisocyanuric acids can also be efficiently selected to introduce halogen atoms in electron rich arenes [9]. Besides, the reaction with deactivated arenes is only possible under strong acidic conditions [10], the reactivity being highly influenced by the acidity of the reaction medium [3a]. As an example, nitrobenzene has been fully brominated to pentabromonitrobenzene by TBCA in 2 minutes at room temperature, using 65% oleum as solvent [3b]. Other impressive results are the electrophilic chlorination [3a], bromination [3c], and iodination [3c] of *m*-dinitrobenzene respectively by TCCA, TBCA and TICA in 98% H₂SO₄, which afforded the corresponding halogenated products in good yields.

The use of strong acids is however a drawback due to their high corrosive nature and environmental problems. In order to solve this problem and render the halogenating process safer, we have considered the use of solid acids as an alternative. Indeed, recently zeolites and other solid acids have been shown to be attractive catalysts because in addition to maintain the electrophilic character of the medium sharp. In addition, they did not generate waste and were easily removed at the end of the reaction by simple filtration [11]. Despite being less acidic than 98% H₂SO₄, they possess numerous properties based on their structure that can influence the progress of reactions [12]. One typical feature relies on the presence of Brønsted and Lewis acid sites [13].

Zeolites have been used in electrophilic aromatic substitution reactions [14]. Various reagents have been used in zeolite-catalyzed chlorination of arenes [14b]. However, they are not safe (Cl₂, *t*-butyl hypochlorite, sulfonyl chloride, to name a few) or the reactions suffer from a lack of chemoselectivity. On the other hand, limited studies have been reported involving the use of *N*-halo compounds in halogenations catalyzed by solid acids [15].

[9] a) R. da S. Ribeiro, P. M. Esteves, M. C. S. de Mattos, *J. Braz. Chem. Soc.* **2008**, *19*, 1239–1243. b) G. F. Mendonça, M. C. S. de Mattos, *Quim. Nova* **2008**, *31*, 798–801. c) L. S. de Almeida, P. M. Esteves, M. C. S. de Mattos, *Synthesis* **2006**, 221–223.

[10] G. F. Mendonça, R. R. Magalhães, M. C. S. de Mattos, P. M. Esteves, *J. Braz. Chem. Soc.* **2005**, *16*, 695–698.

[11] a) A. S. S. Sido, S. Chassaing, M. Kumarraja, P. Pale, J. Sommer, *Tetrahedron Lett.* **2007**, *48*, 5911–5914. b) A. Corma, *Chem. Rev.* **1995**, *95*, 559–614.

[12] K. Smith, G. A. El-Hiti, *Curr. Org. Chem.* **2006**, *10*, 1603–1625. b) I. Fechete, Y. Wang, J. C. Védrine, *Catal. Today* **2012**, *189*, 2–27.

[13] R. A. Van Santen, G. J. Kramer, *Chem. Rev.* **1995**, *95*, 637–660.

[14] a) P. Ratnasamy, A. P. Singh, S. Sharma, *Appl. Catal. A* **1996**, *135*, 25–55. b) K. Smith, G. A. El-Hiti, *Green Chem.* **2011**, *13*, 1579–1608. c) K. Y. Koltunov, S. Walspurger, J. Sommer, *Chem. Comm.* **2004**, 1754–1755.

[15] B. Karimi, D. Zareyee, *Tetrahedron Lett.* **2005**, *46*, 4661–4665.

2. Preliminary results

2.1 Liquid-phase chlorination

Thanks to a collaboration with the team of M. C. S. de Mattos (UFRJ, Rio de Janeiro), preliminary results have been obtained for the chlorination of different aromatics over solid acids. In previous studies, they have demonstrated the chlorination capacity of various substrates with the use of trichloroisocyanuric acid (TCCA) in sulfuric acid medium [3a].

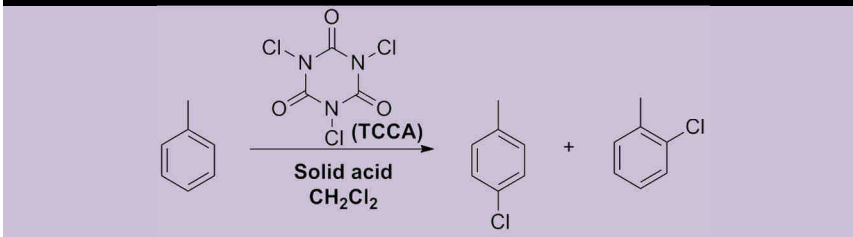
We have first tested the reaction between TCCA and model arenes possessing different nucleophilic degrees (with decreasing order of reactivity toward an electrophile): toluene, chlorobenzene, and nitrobenzene. Table 5.1 presents the different solid acids tested as catalysts for these reactions. Chlorination reactions were typically performed in a round bottom flask under magnetic stirring, using 1 mmol of aromatic substrate, TCCA (0.34 mol equiv.), a given amount (corresponding to 0.3 mol equiv. of H⁺) of solid acid and CH₂Cl₂ or 1,2-dichloroethane as solvents. All chlorination tests were performed following the procedure described in Section Chapter 2.1.1.2.

Table 5.1 Solid acids used in the reaction of arenes with TCCA

Solid acid	Characteristic	Pore size [Å]	Brønsted acidity [mmol H ⁺ /g]	Si/Al
H-USY	microporous zeolite	7.4	3.9	2.9
H-BEA	microporous zeolite	5.6 x 5.6 6.7 x 6.6	1.1	13.6
H-EMT	microporous zeolite	7.4	2.4	6.5
H-MOR	microporous zeolite	7.0 x 6.5 5.7 x 2.6	1.9	5
H-ZSM-5	microporous zeolite	5.5	1.0	15
NAFION/MCM-41	polymer on MCM-41	20	1.0	-
H-SAPO-5	microporous zeolite	7.3	0.8	0.3
SO ₄ ⁻² /ZrO ₂	supported acid	-	0.3	-
H ₃ PW ₁₂ O ₄₀	heteropolyacid	-	0.9	-

The results of the reaction of toluene with TCCA using these acids are presented in Table 5.2.

Table 5.2 Reaction between toluene and TCCA over solid acids



Solid acid	Time [h]	Conversion [%] ^a	<i>o/p</i> ratio ^a
-	24	3	0.6
H-USY	6	100	1.0
H-BEA	24	98	1.6
H-EMT	24	98	1.2
H-MOR	48	87	1.5
H-ZSM-5	48	82	1.2
H-SAPO-5	48	40	3.1
SO ₄ ⁻² /ZrO ₂	48	48	1.3
NAFION/MCM-41	24	98	1.4
H ₃ PW ₁₂ O ₄	48	48	1.3

Conditions: PhCH₃: TCCA: H⁺ (on catalyst) = 1: 0.34: 0.3.

^a Determined by GC.

It is worthy to mention that the methyl substituent of toluene is an activating and *ortho-para* directing group, due to its electron-donor ability. The previous study of de Mattos *et al.* have shown that in liquid acid medium the selectivity followed the statistical formation of two *ortho* positions for only one *para* position [3a]. Indeed, they observed higher *ortho* selectivities (*i.e.*, *o/p* ratio of 2:1) whatever the composition of the medium.

In this preliminary study, we observed that the presence of solid acids improves significantly the conversion and changes the *o/p* ratio with respect to the blank test and sulfuric acid medium. Thus, the presence of organized porous structures and particularly zeolite framework allowed to obtain almost the same amount of *ortho*- and *para*-

chlorination products. In contrast, non-porous acid solids, *i.e.*, sulfated zirconia and heteropolyacid, did not exhibit a high degree of toluene conversion.

Figure 5.2 summarizes the conversion profile versus time over various solids. One can see that the best results were achieved with H-USY and H-EMT zeolites, yielding to a highest conversion in shorter times.

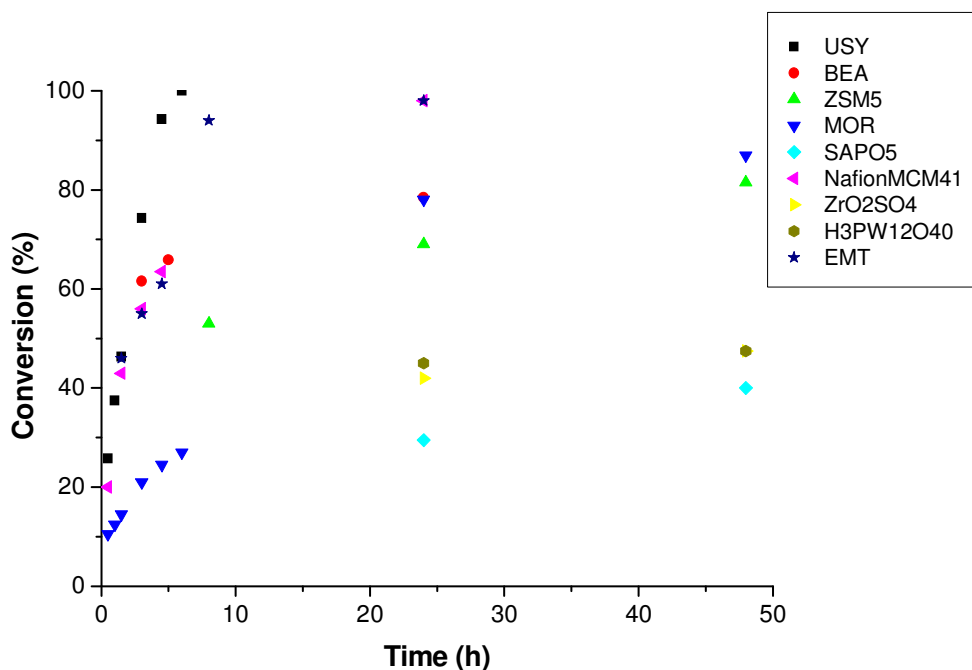


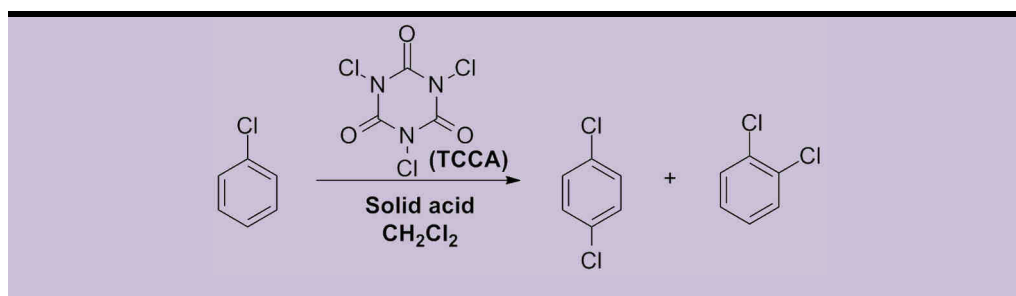
Figure 5.2 Conversion of toluene as a function of time and nature of the catalyst. Conditions: T = r.t., PhCl: TCCA: H⁺ (on catalyst) = 1: 0.34: 0.3

Catalysts with high surface acidity but barely porous (*i.e.*, ZrO₂/SO₄⁻² or H₃PW₁₂O₄), or containing small pores (*i.e.*, H-ZSM-5) did not exhibit good performance. In contrast, solids with combined acidity with micro- and/or mesoporosity, exhibit much higher catalytic activity. For instance, Nafion perfluorinated catalyst grafted in a MCM-41 mesoporous matrix led to high conversions (98% after 24 h). It appears therefore as a valuable chlorination catalyst for activated aromatics.

This indicates that the reaction is favored by both an appropriate pore structure and acidity. This can be due to entropic factors driving the reaction as well as the need for appropriate (strong) acidity of the solid. Weak acidity of the catalyst, as in H-SAPO-5, also negatively influences the conversion.

In order to better understand the role of the catalyst acidity, the chlorination reaction of a slightly deactivated arene, chlorobenzene, with TCCA was attempted and the results are shown in Table 5.3. Halogenated substituents are known to be deactivating, due to their unshared pair of electrons which destabilizes the aromatic ring by its electron-withdrawing effect. In addition, halogens are *ortho/para*-directors.

Table 5.3 Reaction between chlorobenzene and TCCA over solid acids



Solid acid	Solvent	Temp. [°C]	Time [h]	Conv. [%] ^a	<i>o/p</i> ratio ^a
-	CH ₂ Cl ₂	r.t.	96	0	-
-	Cl(CH ₂) ₂ Cl	80	24	0	-
H-ZSM5	CH ₂ Cl ₂	r.t.	96	15	2.9
H-MOR	CH ₂ Cl ₂	r.t.	96	27	<i>n.d.</i>
H-EMT	CH ₂ Cl ₂	r.t.	96	47	4.4
	Cl(CH ₂) ₂ Cl	80	24	73	<i>n.d.</i>
H-USY	CH ₂ Cl ₂	r.t.	96	30	1.8
	Cl(CH ₂) ₂ Cl	80	24	72	1.7
H-BEA	Cl(CH ₂) ₂ Cl	80	24	50	2.6

Conditions: PhCl: TCCA: H⁺ (on catalyst) = 1: 0.34: 0.3.

^a Determined by GC.

Blank tests involving only chlorobenzene and TCCA in CH₂Cl₂ or 1,2-dichloroethane (DCE) did not lead to any conversion after several hours at different temperatures. However, the use of acidic zeolites catalyzes the reaction and the conversion once more depends on the zeolite pore structure. Zeolites with small pores exhibit lower degree of conversion compared with those with larger pores. For instance, H-EMT and H-USY yielded the highest conversions. To improve the conversion, reactions using H-USY and H-EMT catalysts were carried out in 1,2-DCE, a solvent with higher boiling point. The increase in the temperature from room temperature to 80 °C led to an increase in chlorobenzene conversion (*i.e.*, from

30% to 72%) and to reduced reaction times (from 96 h to 24 h). The *ortho-para* ratio was found to be 1.6 for the reaction of chlorobenzene with TCCA catalyzed by H-USY, contrasting with the 0.6 (*o/p*) value obtained in HOAc/H₂SO₄ (1:1) medium [3]. Hence, it seems that porous acid zeolites favor the *ortho*-position in relation to the *para*-position. One might assign these higher *ortho*-selectivities to an isomerization step which occurs after the chlorination reaction outside the zeolite channels and favor the statistical position.

Finally, we tempted to chlorinate nitrobenzene. The nitro-substituent present on the aromatic ring possesses inductive and resonance electron-withdrawing effects, which destabilize the aromatic ring. Thus, nitrobenzene is considered as a deactivated aromatic. Moreover, the nitro-group is a *meta*-directing substituent since its resonance forms present positive charge at *ortho*- and *para*-positions hindering the SEAr reaction at these positions (Figure 5.3).

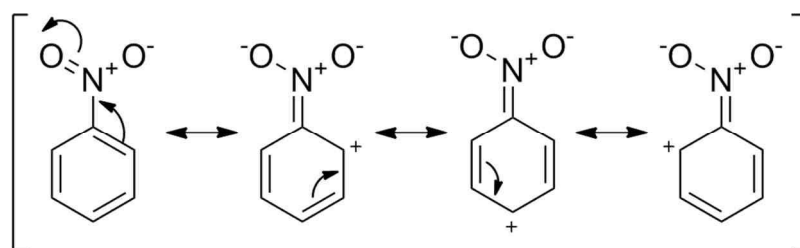
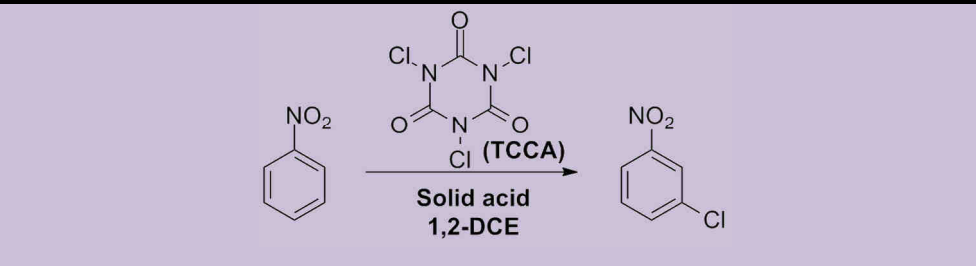


Figure 5.3 Resonance forms of nitrobenzene

Nevertheless, nitrobenzene is not reactive with TCCA in ordinary conditions, but gave 30% conversion and 100% *meta*-selectivity in the presence of H-USY zeolite (Table 5.4).

Table 5.4 Reaction between nitrobenzene and TCCA over H-USY zeolite


The reaction scheme shows nitrobenzene (a benzene ring with an NO₂ group) reacting with trichloroisocyanuric acid (TCCA), which is a six-membered ring with three carbonyl groups and three chlorine atoms on the nitrogen atoms. The reaction is catalyzed by a solid acid in 1,2-dichloroethane (DCE). The product is 3-chloronitrobenzene (a benzene ring with an NO₂ group and a chlorine atom at the meta position).

Solid acid	Solvent	Temp. [°C]	Time [h]	Conv. [%] ^a
-	Cl(CH ₂) ₂ Cl	80	120	0
H-USY	Cl(CH ₂) ₂ Cl	80	24	30

Conditions: PhNO₂: TCCA: H⁺ (on catalyst) = 1: 0.34: 0.3.

^a Determined by GC.

2.2 DFT calculations

In order to get insights on the reaction mechanism, DFT calculations were performed at IEFPCM(H₂O)/M06-2X/6-31++G**+ECP(Si,Al,Cl) level for the reaction of TCCA with benzene catalyzed by an acid zeolite. We have considered the cluster T5, containing four silicon atoms and an aluminum atom, as a model for the zeolite active site. The acid form of the zeolite site is denominated HT5. This cluster has been shown to be large enough to mimic the local acid site properties of zeolites.

The whole process and results of the calculations are presented in Figure 5.4 and Figure 5.5. Firstly, optimized reactants (benzene, abbreviated as PhH, and TCCA) geometries were optimized together in the present model of the zeolite acid site (HT5), in order to form the complex PhH.TCCA.HT5 (Figure 5.4). This complex basically consists of the TCCA molecule hydrogen-bonded through the carbonyl group to the acid site (O⁻H distance of 1.749 Å), while benzene stays around this complex being 3.304 Å away from the nearest chlorine atom from TCCA. This adsorption step is exothermic by 15.8 kcal/mol (Figure 5.5). From this structure, a transition state leading to benzene ring chlorination was found (TS), with an activation enthalpy of 21.8 kcal/mol, leading to a σ -complex (σ -complex 1).

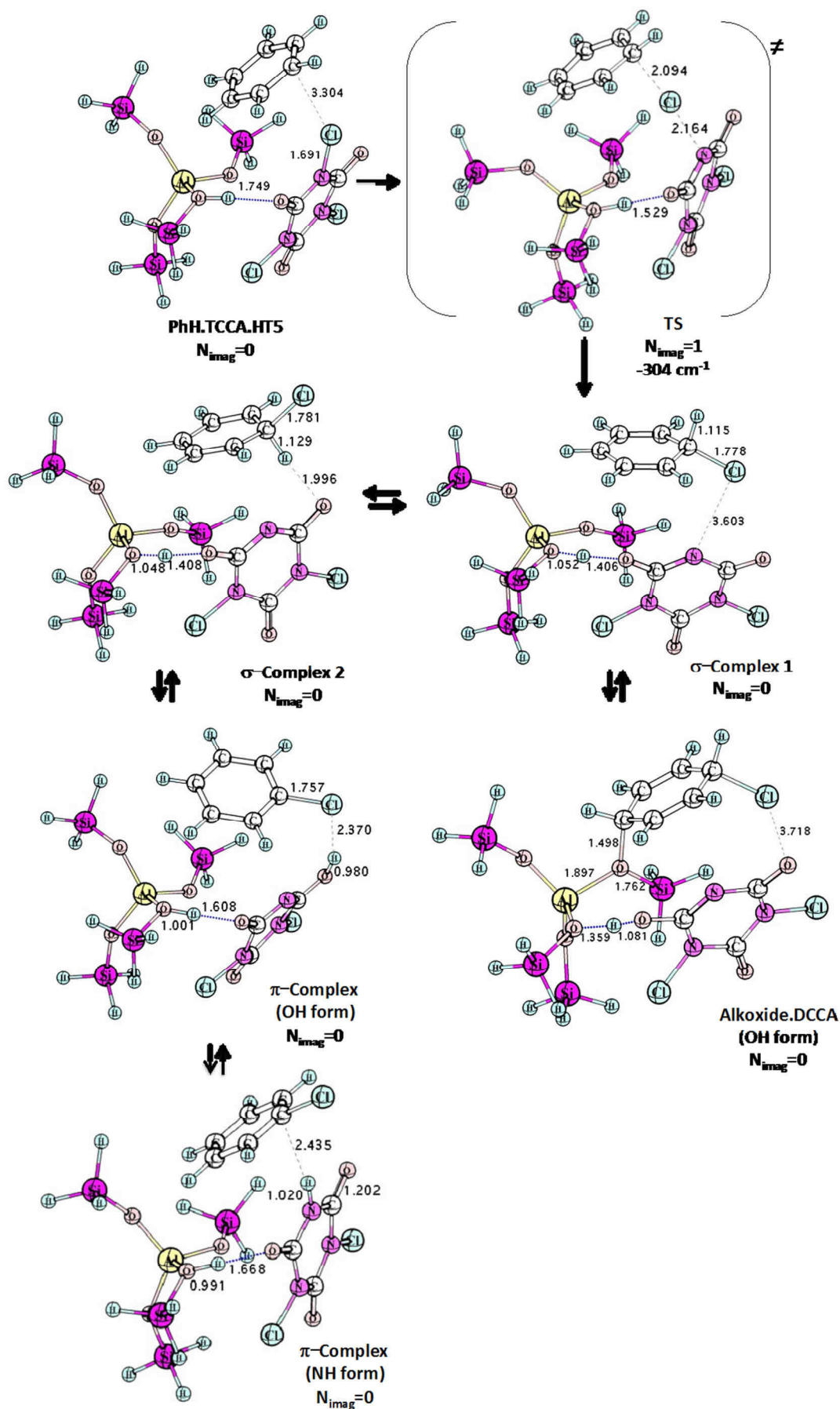


Figure 5.4 Optimized geometries at IEFPCM(H₂O)/M06-2X/6-31++G**+ECP(Si,Al,Cl)

This transition state has an imaginary frequency of 304 cm^{-1} and bond lengths $N_{\text{TCCA}}\cdots\text{Cl}$ of 2.164 \AA , contrasting with the 1.691 \AA found in the complex PhH.TCCA.HT5 , and $\text{Cl}\cdots\text{C}_{\text{PhH}}$ of 2.094 \AA , being much smaller than the 3.304 \AA calculated for PhH.TCCA.HT5 complex. IRC calculations from the transition state TS confirmed that it connects the initial adsorption complex, PhH.TCCA.HT5 , to a σ -complex. This complex (σ -complex 1), for its turn, was characterized as true minimum on the potential energy surface, since it shows no imaginary frequency after vibrational analysis, and lies 7.0 kcal/mol above PhH.TCCA.HT5 adsorption complex. This complex stays 3.603 \AA from the other reactants, typical distance found for π -complexes. It has two reaction outcomes: (a) adsorption on the zeolite surface, leading to an alkoxide complex (indicated as $\text{alkoxide.DCCA (OH form)}$ in Figure 5.4 and Figure 5.5), 10.5 kcal/mol ($= 3.5 + 7.0\text{ kcal/mol}$) lower in energy in relation to σ -complex 1, but which does not lead to any product; and (b) undergo rotation to afford σ -complex 2, in which the proton of the arenium ion is pointing towards the zeolite surface. This complex is 2.0 kcal/mol more stable than σ -complex 1, probably due to the higher proximity and better hydrogen interaction between the arenium ion and the DCCA species. This complex can undergo deprotonation affording the π -complex (indicated in Figures 5.4 and 5.5 as π -complex (OH form)) leading to the product, chlorobenzene (PhCl), dichloroisocyanuric acid (DCCA) in its phenolic (OH) form and regenerated acid site, HT5. This deprotonation is exothermic by 39.9 kcal/mol ($5.0 + 34.5\text{ kcal/mol}$). Further isomerization of this complex leads to the complex involving the imide form of DCCA (NH form), lying 9.8 kcal/mol below the energy from OH isomer. Full dissociation of this complex in DCCA (NH isomer), PhCl and HT5 is endothermic by 19.1 kcal/mol .

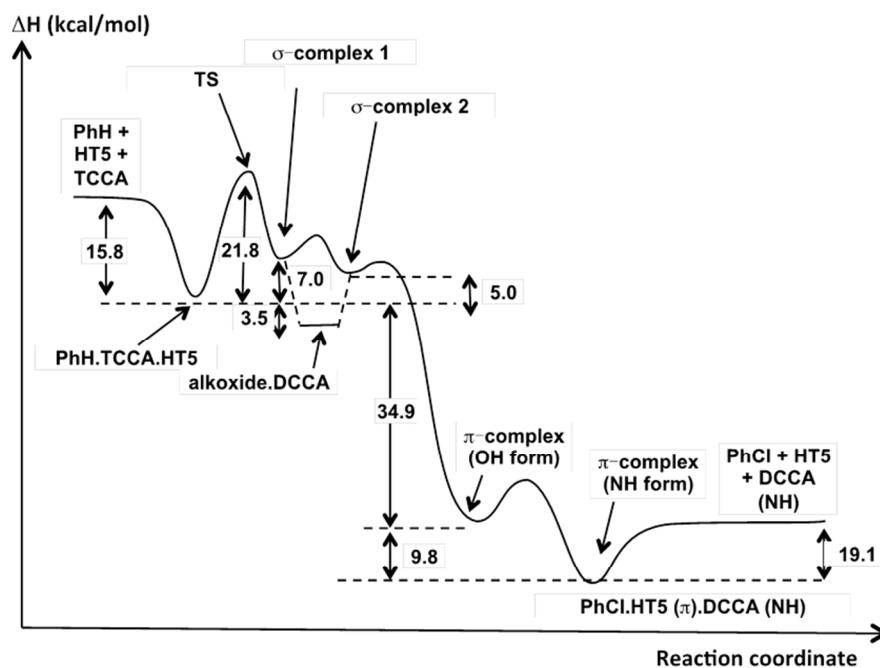


Figure 5.5 Pictorial representation of the reaction coordinate for the reaction between HT5, TCCA and benzene, at IEFPCM(H₂O)/M06-2X/6-31++G**+ECP(Si,Al,Cl)

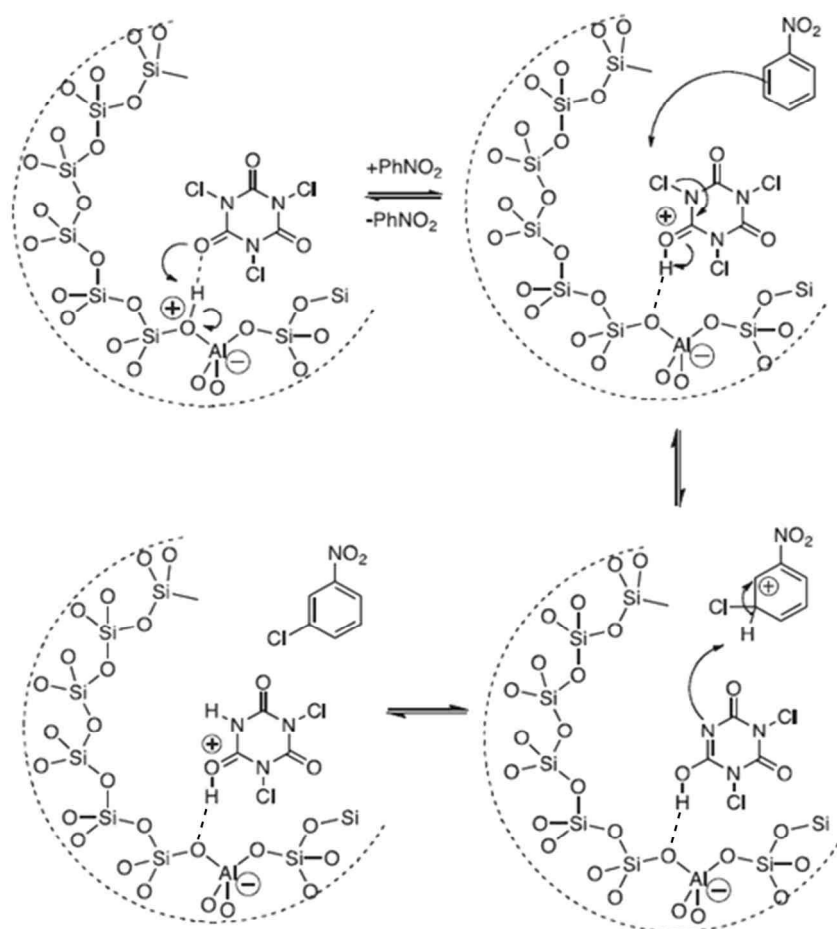
Thermodynamically, the overall process is exothermic (41.4 kcal/mol) and should exhibit an apparent enthalpy of activation of 25.1 kJ/mol (6 kcal/mol), thus able to occur even at room temperature.

These computational results support the model of acid catalysis of TCCA towards electrophilic attack on simple aromatic rings, leading to relatively low apparent activation energies.

2.3 Chlorination reaction mechanism

Scheme 5.1 tempts to rationalize the Brønsted acid-catalyzed activation of one TCCA molecule within the zeolite pores and cavities, thus raising the electrophilicity of Cl-atom. The first step is the adsorption and activation of one TCCA molecule by the acid site of the zeolite. The electrophilicity of Cl-atom is thus increased and the aromatic ring can attack this chlorine in a second step. Finally, to restore the aromaticity of nitrobenzene ring, dichloroisocyanuric acid (DCCA), through its nitrogen electron pair, attacks the hydrogen

atom. Hence, the electrophilic aromatic substitution remains therefore favored on the aromatic ring of nitrobenzene.



Scheme 5.1 Brønsted acid-catalyzed activation of TCCA within the zeolite framework

2.4 Summary

The aforementioned results support our claim that zeolites can successfully substitute liquid acids in superelectrophilic chlorination of aromatic compounds. From these preliminary results, one can conclude that electrophilic chlorination of aromatic rings can be achieved using cheap TCCA as chlorine source over acidic zeolites. Indeed, the successful chlorination of various activated and deactivated aromatics in the presence of zeolites shows that the acid strength of this medium is strong enough to form protosolvated (superelectrophilic) species which can transfer Cl⁺ to arenes. This opens up the possibilities

to use this safe and easily handling reactant for superelectrophilic aromatic substitution *via* an heterogeneous process. This is an interesting alternative to strong liquid acids which have been employed in the development of superelectrophilic chemistry of TXCA by the team of de Mattos [3a].

DFT calculations suggest that a mechanism involving protosolvated TCCA simultaneously transferring Cl^+ to the aromatic ring to afford σ -complexes, which eventually form the chlorinated products, is a viable process and should present low apparent activation energies, in the order of 6 kcal/mol. This is in agreement with the findings that the reaction is taking place at relatively low temperatures with substrates such as toluene.

3. Semi-continuous chlorination

With these results in hand, we have decided to develop an original process for aromatics' chlorination in gaseous phase. The main objective was to conceive a semi-continuous flow reactor system to obtain an environmental-friendly process. The experimental setup is detailed in Section Chapter 2.1.1.3.

3.1 Screening of solid acid catalysts

3.1.1. Nitrobenzene chlorination

It is important to remind that all reactions have been performed at iso-Brønsted acid site conditions.

Figure 5.6 shows the degree of nitrobenzene conversion and the selectivity to mono-chloronitrobenzenes and *meta*-chloronitrobenzene among the different zeolite catalysts. It is noteworthy that *m*-chloronitrobenzene was always found as prominent isomer, *i.e.*, > 90% with respect to the *ortho*- and *para*-chloronitrobenzene, as *a priori* expected from its nitro electron-withdrawing group. However, one can observe that ZSM-5 zeolite presents a slightly lower *m*-chloronitrobenzene selectivity, *i.e.*, 74%, compared with other zeolites. This

behavior could be explained by the narrower pore openings in MFI topology. Thus, the *m*-isomer formation could be hindered by steric constraints.

As previously exposed (in liquid phase reaction), the zeolite pore size acts as a limiting factor for this reaction. Whilst no reaction occurred over H-FER zeolite (~ 0.4 nm pore aperture), nitrobenzene reacted with TCCA over medium pore H-ZSM-5 zeolite, which possesses a rather narrow pore size of 0.55 nm, affording 21% conversion. In contrast, 39% of nitrobenzene was converted over H-USY (~ 0.74 nm). This tends to support an effect of higher accessibility of those large organic molecules to the catalytic sites within H-USY zeolite [16].

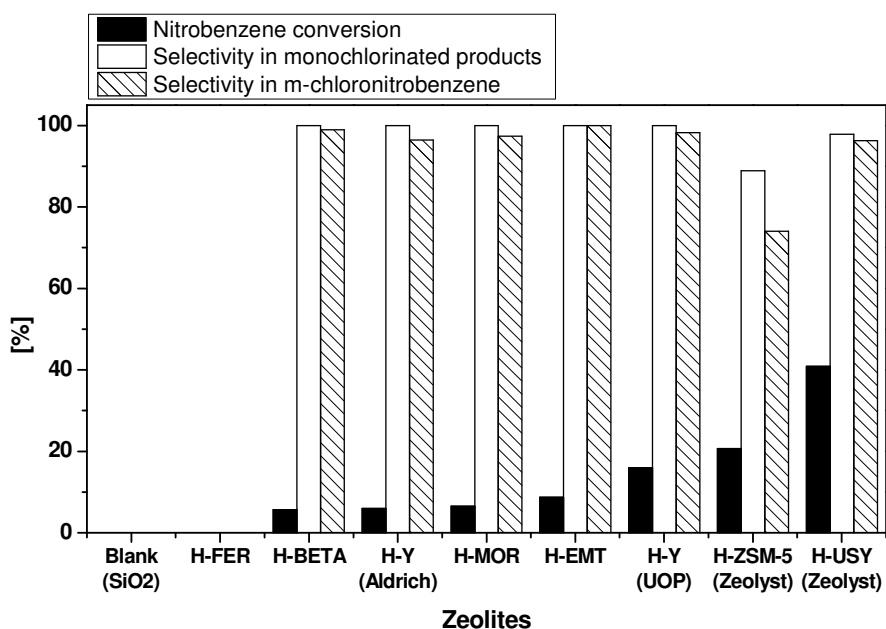


Figure 5.6 Nitrobenzene chlorination and selectivity toward mono- and *m*-chlorinated products. Conditions: T = 150 °C, TCCA: H⁺: PhNO₂ = 1: 3: 3, Flow = 100 mL/min, TOS = 5 h

On the other hand, the chlorination reaction appears to be positively influenced by the channel architecture of zeolite frameworks. Indeed, the SAC-13 catalyst (Nafion-H supported over MCM-41), being a polymer-grafted on mesoporous silica, only led to a 5% nitrobenzene

[16] P. Kuhn, P. Pale, J. Sommer, B. Louis, *J. Phys. Chem. C* **2009**, *113*, 2903–2910.

conversion (Figure 5.7). Likewise, gallium-doped mesoporous silica (Ga-SBA-15) [17] also led to poor catalytic performance (conversion of 7%) with respect to zeolites.

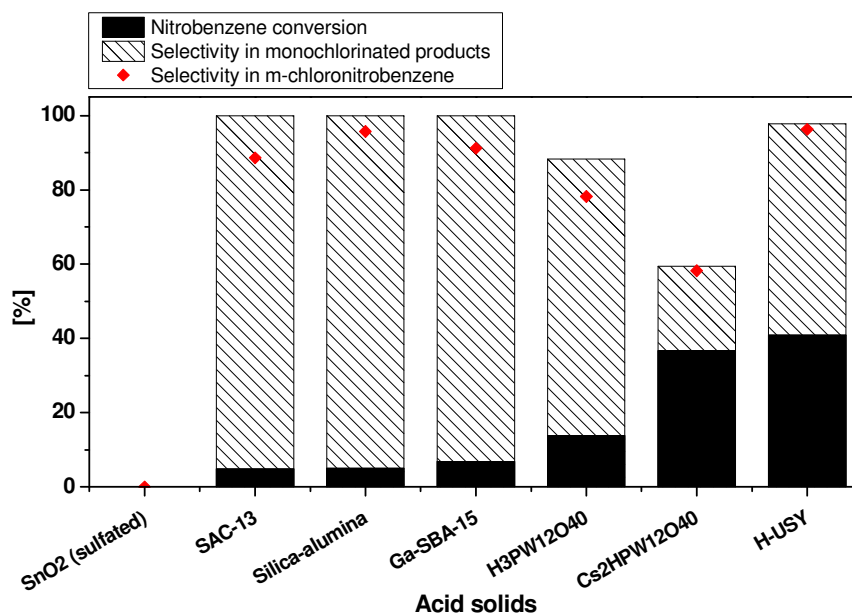


Figure 5.7 Nitrobenzene chlorination and selectivity toward mono- and *m*-chlorinated products. Conditions: T = 150 °C; TCCA: H⁺: PhNO₂ = 1: 3: 3; Flow = 100 mL/min; TOS = 5 h

Following the same trend, the selectivity toward monochlorination is also governed by the zeolite porosity. In parallel, the beneficial effect of microporosity has been further evidenced by the use of strongly acidic polyoxometalate H₃PW₁₂O₄₀. Whereas, this non porous solid acid led to an appreciable degree of nitrobenzene conversion (14%), in contrast the selectivity drastically diminished with respect to zeolites in favor of dichlorination products. However, Cs₂HPW₁₂O₄₀ that exhibits a higher SSA value (123 m²/g) and porosity with respect to pristine protonic counterpart (5 m²/g) led to 2.6 fold increase in activity. The same behavior was observed over amorphous silica-alumina, which converted only 5% of nitrobenzene probably due to the absence of an organized pore architecture.

In addition, a non-conventional acid catalyst, sulfated tin dioxide, was also tested. This SnO₂/SO₄²⁻ catalyst, which possesses mainly Lewis acid sites and almost no porosity, did not exhibit any activity at all.

[17] Z. El Berrichi, B. Louis, J.-P. Tessonnier, O. Ersen, L. Cherif, M. J. Ledoux, C. Pham-Huu, *Appl. Catal. A* **2007**, 316, 219–225.

Besides, a rather surprising difference in reactivity between H-Y and H-USY zeolites was observed (Figure 5.6). H-USY zeolite is usually obtained by dealumination *via* a high temperature steaming of pristine H-Y zeolite [18]. The dealumination process consists of removing framework aluminum atoms and thus to create new extra-framework aluminum species (EFAl) present either as amorphous species (pseudo Al₂O₃) [19] or aluminum species exhibiting exalted Lewis acidity (AlOOH, AlO⁺ species *etc.*) [20]. This phenomenon is beneficial for the chlorination process since the conversion of nitrobenzene was drastically improved to 39% with H-USY compared with HY zeolite (16%).

To summarize these preliminary tests, one can observe that an optimal catalyst for performing the chlorination of nitrobenzene remains the H-USY zeolite. Indeed, the faujasite structure allows catalyzing the chlorination of nitrobenzene by combining a high selectivity in monochlorinated compounds (99%) at an acceptable degree of nitrobenzene conversion.

To complete these results, we have tested and compared with the classical USY zeolite another FAU-type zeolite (*i.e.*, EMC-1) and a pure hexagonal analogue of faujasite (*i.e.*, EMC-2) possessing EMT topology. The synthesis procedures and the intrinsic features of these zeolites are detailed in Section Chapter 3.2.1.1.4. Though these zeolites presented different Si/Al ratio, thus variations in their acid site densities (Table 3.1), the catalyst mass has been adjusted to keep iso-site conditions.

Figure 5.8 presents the nitrobenzene conversion and the selectivity in monochlorinated products for the three catalysts (H-EMC-1, H-EMC-2 and H-USY). It is noteworthy that the H-EMC-2 zeolite exhibits a nearly 30% higher performance with respect to pristine H-USY zeolite, *i.e.*, 51% versus 39%. Likewise, the selectivity toward monochlorination was 100% for the former H-EMC-2 zeolite, being higher than those obtained with the H-EMC-1 (95%) catalyst. Among the products formed, *meta*-chloronitrobenzene was always found as major isomer, *i.e.*, > 90% with respect to *ortho*- and *para*-chloronitrobenzene.

[18] S. Altwasser, J. Jiao, S. Steuernagel, J. Weitkamp, M. Hunger, *Stud. Surf. Sci. Catal.* **2004**, 154B, 1212–1213.

[19] C. R. Moreira, M. H. Herbst, P. R. de la Piscina, J.-L. G. Fierro, N. Homs, M. M. Pereira, *Microporous Mesoporous Mater.* **2008**, 115, 253–260.

[20] C. Mirodatos, D. Barthomeuf, *J. Chem. Soc., Chem. Commun.* **1981**, 39–40.

These results led us conclude that the acid site density appears to be an important factor for nitrobenzene chlorination. Although the catalytic tests were performed at iso-site conditions, the nitrobenzene chlorination is favored over the higher acidic concentrated catalysts (*i.e.*, 4,6 mmol H⁺/g for H-EMC-1 and 4.4 mmol H⁺/g for H-EMC-2 vs. 3.9 mmol H⁺/g for H-USY). Thus, nitrobenzene chlorination reaction could allow to “quantify” the relative acid strength present in a same zeolite topology family.

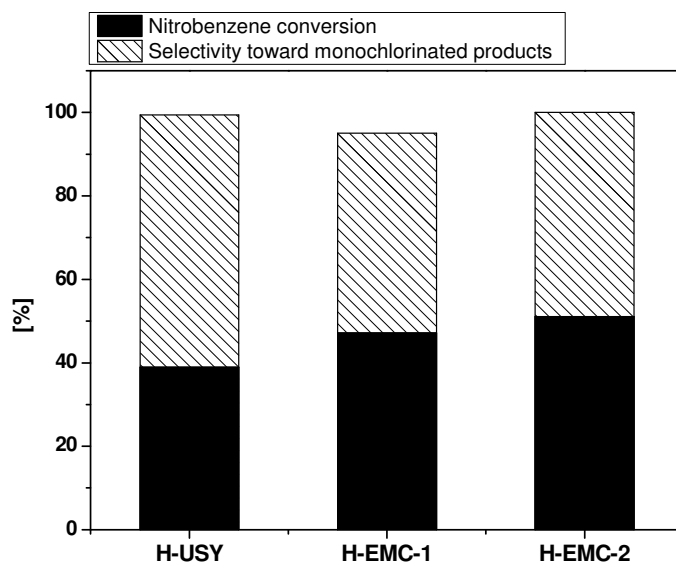


Figure 5.8 Nitrobenzene conversion and selectivity toward chlorination products. Conditions: T = 150 °C; TCCA: H⁺: PhNO₂ = 1: 3: 3; Flow = 100 mL/min; TOS = 5 h

3.1.2. Chlorobenzene chlorination

The chlorination of chlorobenzene was also evaluated under semi-continuous flow conditions over several zeolite types, as shown in Figure 5.9.

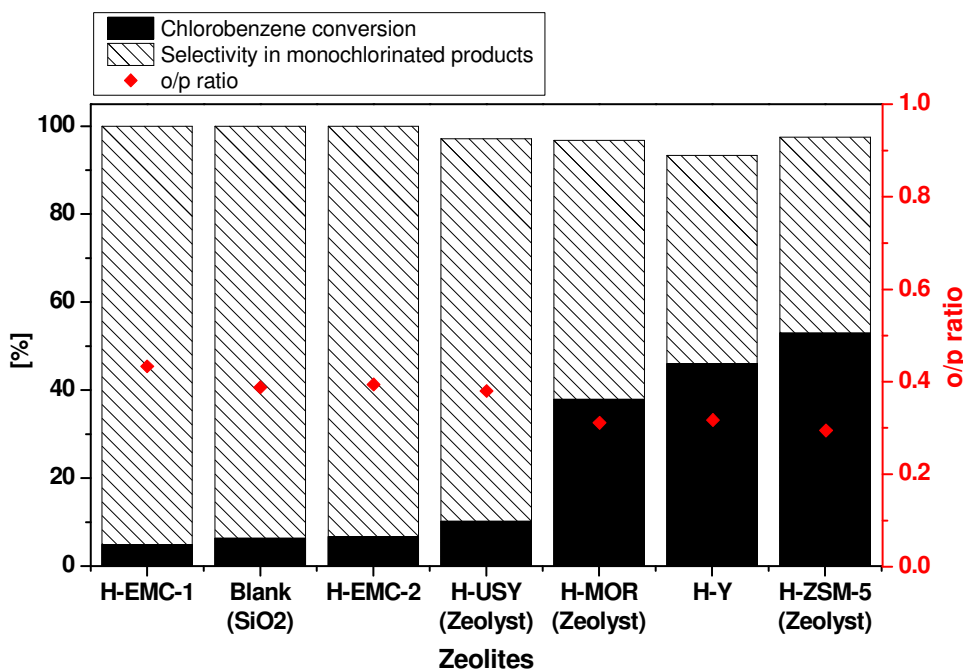


Figure 5.9 Chlorobenzene chlorination, selectivity toward monochlorinated products and *o/p* ratio. Conditions: T = 150 °C, TCCA: H⁺: PhCl = 1: 0.8: 1, Flow = 25 mL/min, TOS = 3 h

Likewise nitrobenzene chlorination, all experiments were undertaken by keeping the number of acid sites constant. It is noteworthy that less acid sites are needed to convert chlorobenzene with respect to nitrobenzene. Although chlorobenzene is less deactivated than nitrobenzene, the selectivity toward monochlorinated products for all zeolites remains higher than 90%.

Firstly, we observed that part of chlorobenzene can be chlorinated over silica contrary to nitrobenzene which is too deactivated for such weak acid. Hence, the catalytic bed for the chlorination of chlorobenzene was diluted in inactive glass rings.

Contrarily to nitrobenzene chlorination, zeolite pore size did not act as a limiting factor. Indeed, the higher catalytic performance is achieved over the zeolite with the smallest pore size: ZSM-5 zeolite. ZSM-5 catalysts allowed to convert 53% of chlorobenzene in 3 h along with a selectivity to monochlorinated products of 98% and *o/p* ratio of 0.3. Whilst H-USY zeolite (*i.e.*, the optimal catalyst for nitrobenzene chlorination) converted only 10% of chlorobenzene. In general, FAU-type zeolites (EMC-1, EMC-2 and USY) did not seem to be adequate candidates for chlorobenzene chlorination. Furthermore, H-MOR and H-Y zeolite

presented good catalytic activities (*i.e.*, > 35% of chlorobenzene conversion) along with high selectivities in monochlorinated products.

The influence of acid site density in MFI zeolites has also been investigated. Three commercial ZSM-5 having different Si/Al ratios (*i.e.*, Zeolyst CBV 8020, 5020 and 2314), were tested and the results are given in Table 5.5.

Table 5.5 Catalytic results of three H-ZSM-5 zeolites in chlorobenzene chlorination

Zeolite	Si/Al ratio	Conversion [%]	Selectivity in mono-chlorination products [%]	TOF [$\text{mol}_{\text{PhCl conv.}} \cdot \text{mol}_{\text{Al}}^{-1} \cdot \text{s}^{-1}$]
H-ZSM-5 (8020)	40	26	99	2.2×10^{-4}
H-ZSM-5 (5020)	25	53	98	2.9×10^{-4}
H-ZSM-5 (2314)	12	58	64	1.5×10^{-4}

Conditions: TCCA: PhCl = 1: 1, 248 mg of catalyst

These catalytic tests were performed under iso-mass conditions. One can observe that the H-ZSM-5 with the lower Si/Al ratio exhibited the higher catalytic activity in terms of chlorobenzene conversion (*i.e.*, 58%). This phenomenon can be related to the amount of acid sites present in this sample which favors its reactivity. Moreover, the lower selectivity toward monochlorination product over this ZSM-5 (*i.e.*, 64%) can also be attributed to its higher acidic properties. Nevertheless, TOF values have been calculated taking into account the relative Al atoms content in each ZSM-5 in order to analyze the acid site density effect. Surprisingly, TOF values in the same order of magnitude were obtained whatever the Si/Al ratio in the ZSM-5 zeolite. Contrarily to nitrobenzene chlorination, the acid site density did not drastically influence the catalytic activities of ZSM-5 zeolites in chlorobenzene halogenation.

3.1.3. Differences between ZSM-5 and USY zeolites in chlorination reactions

According to Spartan calculations, the diameter of chlorobenzene molecule measures approximately 0.56 nm whereas nitrobenzene molecule has a diameter of about 0.6 nm. Hence, nitrobenzene can rather enter through the H-USY pores than in ZSM-5 pores. Moreover, the nitro-group has the ability to make hydrogen bonds which can stabilize the aromatic. The acid site density in H-USY zeolite is higher than in ZSM-5 zeolite. Thus, the probability of stabilization of nitrobenzene molecules by H-bonds nearby TCCA adsorption site in FAU catalyst is higher than in MFI and could explain the higher catalytic activity of the former in nitrobenzene chlorination.

In contrast, the relative size of chlorobenzene molecules is close to ZSM-5 pore apertures; *i.e.*, 0.56 and 0.55 nm, respectively. According to Derouane confinement effect and particularly its “floating molecule” concept (see Section Chapter 1.1.2.3.3 [21]), one may assume that the diffusion of chlorobenzene molecules is improved and thus the chlorination reaction is favored in ZSM-5 zeolite. Furthermore, this confinement effect could explain the higher selectivity toward *para*-isomers.

3.2 Optimization of the reaction conditions

3.2.1. Nitrobenzene chlorination

We have further optimized the reaction conditions by changing the quantities of TCCA and H-USY zeolite (WHSV alteration).

Figure 5.10 shows the results obtained for different quantities of H-USY catalyst. We realized these experiments in comparison to the reference, where the ratio between TCCA and H-USY was 1/3 (based on the number of Brønsted acid sites). It is important to note that the value 0.15 mmol corresponds to $n_{\text{TCCA}}/n_{\text{Brønsted acid sites}} = 1$. Hence, this implies that 3 chlorine atoms could be potentially involved in the reaction ($n_{\text{Cl}}/n_{\text{H}^+} = 3$). Based on the results depicted in Figure 5.10, it can be concluded that the optimal amount of catalyst for

[21] a) E. G. Derouane, *Chem. Phys. Lett.* **1987**, *142*, 200–204. b) E. G. Derouane, J.-M. Andre, A. A. Lucas, *J. Catal.* **1988**, *110*, 58–73.

reaching maximal conversion corresponds to a $n_{\text{TCCA}}/n_{\text{Brønsted acid sites}} = 1$ ratio (0.15 mmol H^+). This ratio allowed the conversion of 24% of nitrobenzene with an excellent selectivity toward monochlorinated products of 95%.

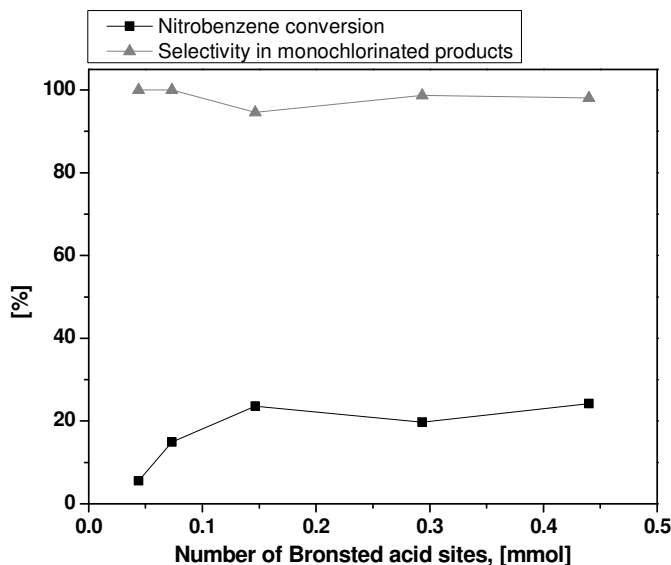


Figure 5.10 Influence of the HUSY catalyst loading on the nitrobenzene conversion. It is worthy to mention that 0.15 mmol H^+ corresponds to $n_{\text{TCCA}}/n_{\text{Brønsted acid sites}} = 1$ (or $n_{\text{Cl}}/n_{\text{H}^+} = 3$). Conditions: $T = 150\text{ }^\circ\text{C}$; $n_{\text{TCCA}} = 0.15\text{ mmol}$; TOS = 5 h

In parallel, the quantity of TCCA was also varied (Figure 5.11). It is noteworthy that a raise in the TCCA amount led to an increase in the conversion of nitrobenzene while keeping a high selectivity toward monochlorinated products. These experiments confirmed that the optimal ratio between TCCA and the number of Brønsted acid sites was 1 (0.45 mmol TCCA, referring to $n_{\text{Cl}}/n_{\text{H}^+} = 3$). These new conditions allowed converting 53% of nitrobenzene with a high selectivity of 94% toward monochlorination products.

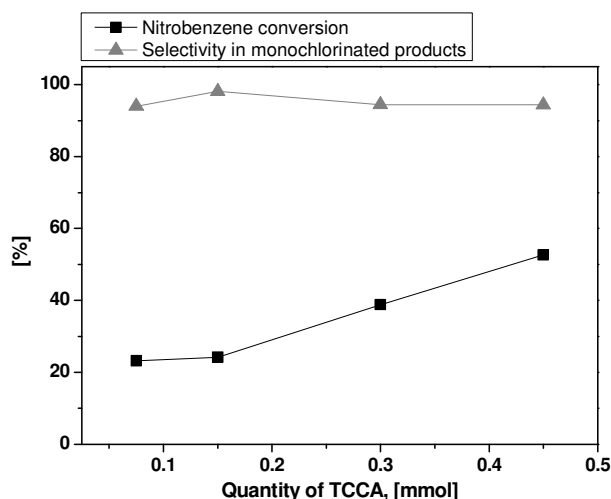


Figure 5.11 Effect of TCCA quantity on the chlorination of nitrobenzene over HUSY zeolite. The equimolar ratio between the number of Brønsted acid sites and TCCA ($n_{\text{Cl}}/n_{\text{H}^+} = 3$) corresponds to 0.45 mmol. Conditions: $T = 150\text{ }^{\circ}\text{C}$; $n_{\text{H}^+} = 0.44\text{ mmol}$; TOS = 5 h

In other words, these optimal conditions (TCCA: H^+ : $\text{PhNO}_2 = 1: 1: 1$) led to the production of 1.0 kg of chlorination products per $\text{kg}_{\text{catalyst}}$ per day, along with a high selectivity toward monochlorinated compounds (*i.e.*, 94%).

3.2.2. Chlorobenzene chlorination

Figure 5.12 presents the chlorobenzene chlorination as a function of Brønsted acid sites. The chlorobenzene conversion is linearly proportional to the quantity of ZSM-5 catalyst. The optimal conditions for the chlorobenzene chlorination were set as follows: TCCA: H^+ : $\text{PhCl} = 1: 0.8: 1$ and allowed to convert 53% of chlorobenzene along with a 98% selectivity in monochlorinated compounds. Hence, 1.4 kg of chlorination products can be produced per $\text{kg}_{\text{catalyst}}$ per day.

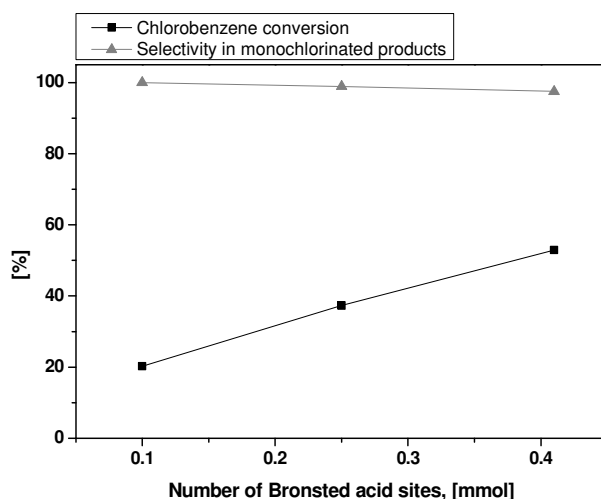


Figure 5.12 Influence of H-ZSM-5 catalyst loading on the chlorobenzene conversion. It is worthy to mention that 0.22 mmol H^+ corresponds to $n_{TCCA}/n_{Bronsted\ acid\ sites} = 0.8$. Conditions: $T = 150\ ^\circ C$; $n_{TCCA} = 0.51\ mmol$; TOS = 3 h

3.2.1. Effect of the space-time

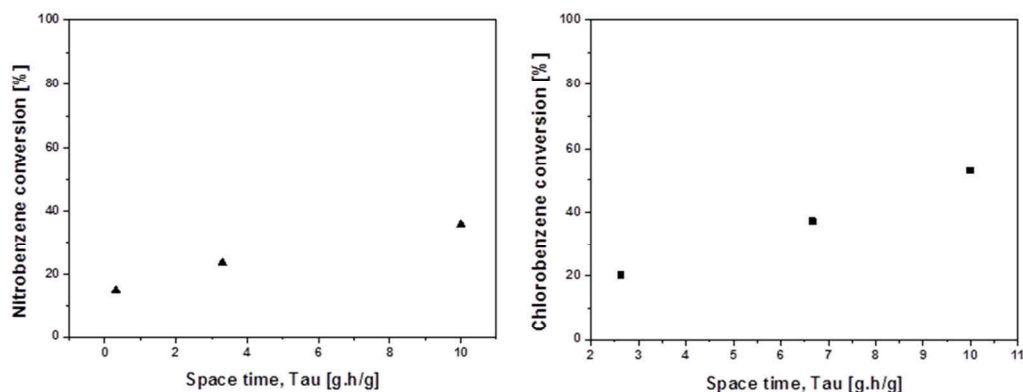
The space-time was varied in order to see whether the catalytic data should be examined by the differential or integral method of kinetics analysis [22]. These values were calculated using Equation 5.1.

Equation 5.1

$$\tau = \frac{1}{WHSV}$$

Figure 5.13 shows the respective aromatics' conversion as function of space-time τ . In both cases, it can be observed that aromatics' conversion increase linearly with τ . This indicates that the reactor can be operated in a differential manner. Thus, aromatics' concentration can be regarded as nearly constant along the reactor, *i.e.*, the rate of aromatic can be assume constant over the entire catalytic bed.

[22] G. F. Froment, K. B. Bischoff, *Chemical Reactor Analysis and Design*, John Wiley & Sons, New York, 1990, pp. 219-255.

Figure 5.13 Aromatic conversions versus space-time τ

3.3 Kinetics study

3.3.1. Mass transfer limitations

Internal mass transfer is known to limit many reactions catalyzed by zeolites [23]. The estimation of Thiele-Weisz modulus could provide informations on these diffusional limitations according to Equation 5.2.

Equation 5.2

$$\phi = \frac{R \times d_p^2}{D_{eff} \times C_{gas}}$$

where

- R = reaction rate
- d_p = particle size
- D_{eff} = diffusion coefficient
- C_{gas} = surface concentration

The diffusion coefficient of benzene in ZSM-5 zeolite has been estimated by Kärger and Ruthven to be in the order of $D_{eff} = 10^{-14} \text{ m}^2/\text{s}$ [24]. With a crystal size of approximately 300 nm for both USY and ZSM-5 zeolite, a Thiele-Weisz modulus of the order of 10^{-2} can be calculated in both cases. In conclusion, the influence of internal mass transfer on the observed reaction rate can be neglected.

[23] a) B. Louis, F. Ocampo, H. Yun, J.-P. Tessonnier, M. M. Pereira, *Chem. Eng. J.* **2010**, *161*, 397–402. b) J. Pérez-Ramírez, C. H. Christensen, K. Egeblad, J. C. Groen, *Chem. Soc. Rev.* **2008**, *37*, 2530–2542.

[24] J. Kärger, D. M. Ruthven, Eds., *Diffusion in Zeolites and Other Microporous Solids*, John Wiley & Sons, New York, **1992**.

3.3.2. Nitrobenzene chlorination

Figure 5.14 shows the results of nitrobenzene chlorination reaction at different reaction temperatures. As *a priori* expected, a raise in the temperature led to higher nitrobenzene conversion, but at the expense of the selectivity in monochlorination products. The decrease in selectivity is due to the formation of di- and trichlorination products. For instance, the selectivity toward monochlorination was diminished to 63% at 200 °C. Selectivities in di- and trichlorinated products were 32% and 5%, respectively. Among the products of dichlorination, 1,4-dichloro-2-nitrobenzene was formed as a major isomer (71%), whilst 1,2-dichloro-4-nitrobenzene represented nearly 28% selectivity among the products. It is therefore worthy to mention that the second chlorination (involving deactivated *meta*-chloronitrobenzene) is favored in ortho and para positions of chlorine atom. The higher selectivity in 1,4-dichloro-2-nitrobenzene major isomer might be explain by lower steric hindrance than 1,2-dichloro-4-nitrobenzene isomer. Based on these results, we have arbitrary chosen the temperature of 150 °C as an optimal temperature, since a good compromise between a high selectivity and a reasonable nitrobenzene conversion was achieved.

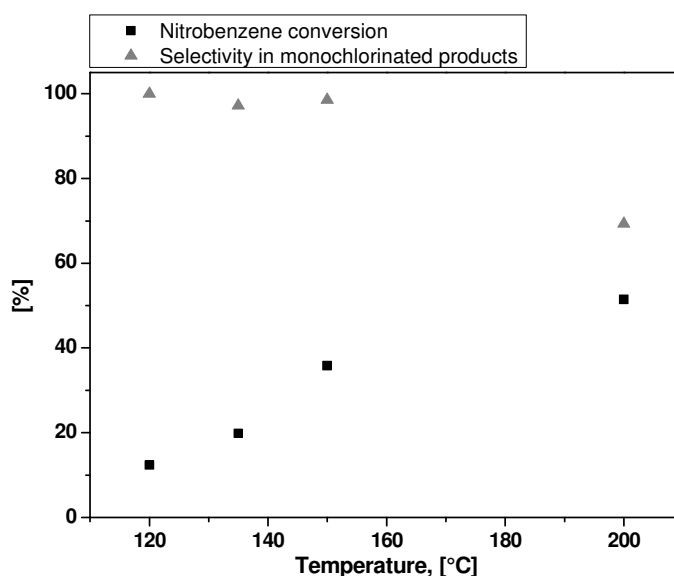


Figure 5.14 Influence of temperature on nitrobenzene conversion and selectivity in monochlorinated products over H-USY catalyst.

Conditions: TCCA: H⁺: PhNO₂ = 1: 3: 3; Flow = 100 mL/min; TOS = 5 h

Arrhenius equation, given in Equation 5.3, is a very useful tool in kinetics to estimate the activation energy of any reaction. Indeed, the fit of the plot of $\ln(k)$ versus $1/T$, called Arrhenius plot, can be used to determine the apparent activation energy (E_a) and the constant A values (in the case of straight line).

Equation 5.3
$$k = Ae^{-E_a/(RT)}$$

From aforementioned data, reaction rates were calculated at different temperatures to provide the constant rate (k) at each temperature. This value has been calculated using the rate law, given in Equation 5.4 for a generic reaction such as $x A + y B \rightarrow z C$ without intermediate steps (A=aromatic and B= TCCA).

Equation 5.4
$$r = k [A]^x \cdot [B]^y$$

Where: r : reaction rate
 k : rate constant or coefficient of the reaction
 A and B express the concentration of the species A and B
 x and y are partial order of reaction determined experimentally

Thanks to the results obtained by DFT calculations (Figure 5.5), one could assume that the major rate-limiting step is the formation of transition state of aromatic ring and not the DCCA desorption step (21.8 kcal/mol vs. 19.1 kcal/mol, respectively). Besides, the rate law could be simplified by removing the reactant B (Equation 5.5), since TCCA molecule is not directly implied in this step. Finally, one could assume a partial order of 1 since only one aromatic molecule is involved in the transition state.

Equation 5.5
$$r = k [A]^1$$

Figure 5.15 presents the Arrhenius plot of nitrobenzene chlorination over H-USY catalyst.

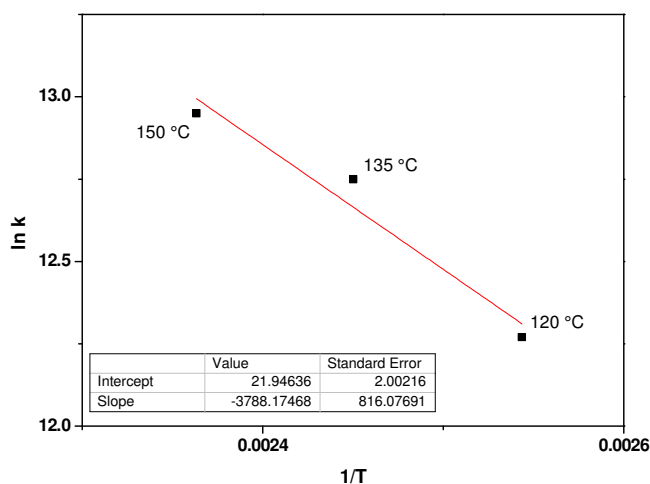


Figure 5.15 Arrhenius plot for nitrobenzene chlorination over H-USY catalyst

From the slope of the curve, one can obtain E_a . Thus, an apparent activation energy of approximately 31.5 kJ/mol was found. This value is in agreement with the activation energy obtained by the DFT calculations for benzene chlorination in Section 2.2 (*i.e.*, 25.1 kJ/mol).

3.3.3. Chlorobenzene chlorination

Figure 5.16 shows the influence of temperature on chlorobenzene conversion and selectivity toward monochlorinated products over H-ZSM-5 (Zeolyst CBV 50/20) catalyst.

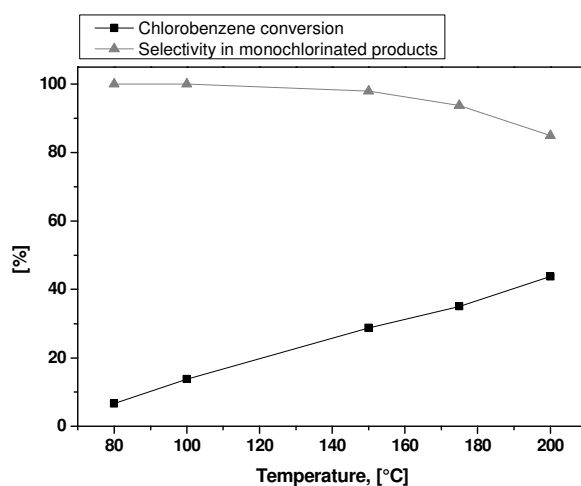


Figure 5.16 Influence of temperature on chlorobenzene conversion and selectivity in monochlorinated products over H-ZSM-5 catalyst.

Conditions: TCCA: H^+ : PhCl = 1: 0.8: 3; Flow = 25 mL/min; TOS = 3 h

Again, an increase in temperature led to a raise in chlorobenzene conversion. From 180 °C, the selectivity toward monochlorinated products vanishes in favor of polychlorinated compounds (di- and trichlorinated products). Thus, at 200 °C the selectivity in di- and trichlorination reached 13% and 2%, respectively. The optimal temperature of 150 °C was chosen for the conversion of chlorobenzene along with high selectivity in monochlorination.

Figure 5.17 presents the Arrhenius plot obtained for chlorobenzene conversion over H-ZSM-5 zeolite at the lowest temperature. The calculated apparent activation energy was 17.6 kJ/mol. This lower value obtained for chlorobenzene is probably due to its lower deactivation effect compared to nitrobenzene, thus being more difficult to halogenate.

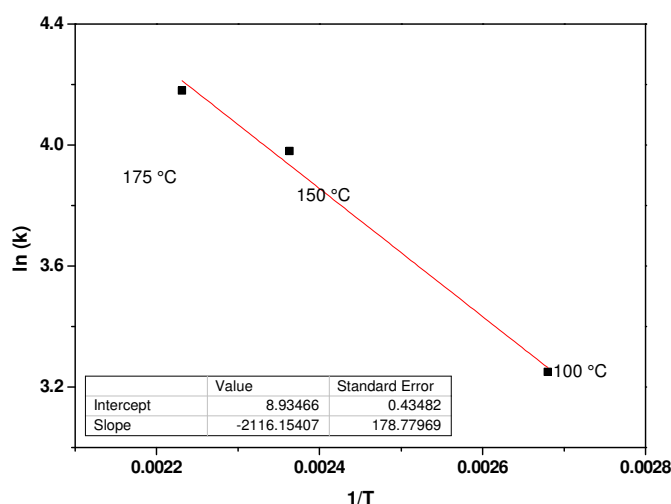


Figure 5.17 Arrhenius plot of chlorobenzene chlorination over H-ZSM-5 catalyst

In addition, Figure 5.18 gives the Arrhenius plot of chlorobenzene chlorination over H-USY catalyst. It is worthy to mention that the molar ratios between reactants of these experiments were not similar to those used over H-ZSM-5 zeolite (*i.e.*, TCCA: H⁺: PhCl = 1: 0.8: 1 vs. TCCA: H⁺: PhCl = 1: 0.8: 3 for H-USY and H-ZSM-5, respectively).

The apparent activation energy found in this case was lower than the one obtained over H-ZSM-5 zeolite (*i.e.*, 14.6 kJ/mol). Such variation in the apparent activation energy regarding the zeolite used could be directly related to the entropy. Indeed, zeolites have different entropy values what could have an impact on the adsorption step ΔH value and thus change the apparent activation energy.

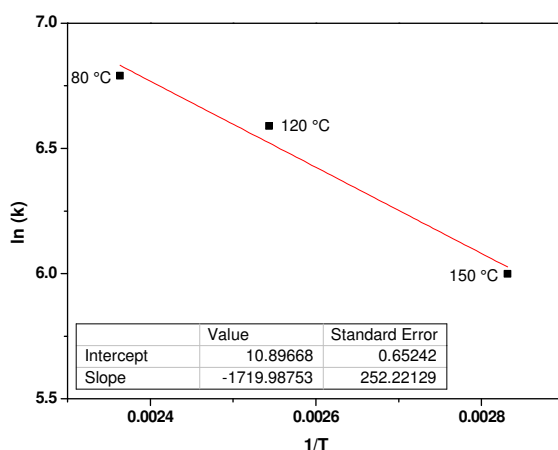


Figure 5.18 Arrhenius plot of chlorobenzene chlorination over H-USY catalyst

3.4 Catalyst recycling

3.4.1. Nitrobenzene chlorination

To fulfill our study in a green chemistry context, the recyclability of our “optimal” H-USY catalyst was tested during five successive runs without changing the catalyst bed. To be able to regenerate the zeolite after each run, the catalytic reaction was performed without the use of silica. The absence of inert material led to a decrease in the aromatic conversion (*i.e.*, ~ 37% in relative). After each run, the catalyst was treated at 550 °C under air during one night after reaction to remove all organics from its surface. After calcination, new TCCA (*i.e.*, the same amount as the first run) was added and mixed with the catalyst. Figure 5.19 shows that after the first run the catalyst lost nearly 25% of relative activity but without further loss during the four consecutive runs. This loss in activity could be explained by an irreversible damage during chlorination process in the zeolite. The zeolite structure and probably some Brønsted acid sites might be altered and the calcination step did not restore their full activity [25]. Furthermore, it is worthy to mention that the catalyst held a constant and high selectivity toward monochlorinated compounds.

[25] T. M. Wortel, D. Oudijn, C. J. Vleugel, D. P. Roelofsen, H. van Bekkum, *J. Catal.* **1979**, *60*, 110–120.

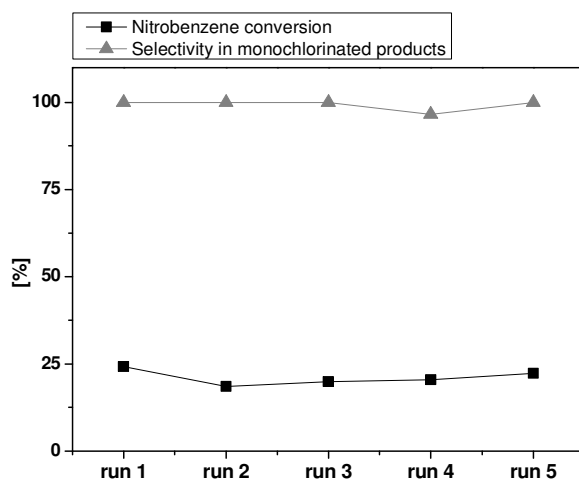


Figure 5.19 Recyclability of H-USY catalyst during five consecutive runs. Conditions: T = 150 °C; TCCA: H⁺: PhNO₂ = 1: 1: 1; Flow = 100 mL/min; TOS = 5 h

3.4.2. Chlorobenzene chlorination

Likewise, the recycling of the catalyst was done according to the same procedure. The recyclability of the most effective catalyst for chlorobenzene chlorination (*i.e.*, ZSM-5 zeolite) follows the same trend than H-USY in nitrobenzene chlorination (Figure 5.20). The ZSM-5 catalyst showed after the first run an irreversible loss in activity of about 25%. However, the selectivity toward monochlorinated compounds remains nearly stable throughout the runs.

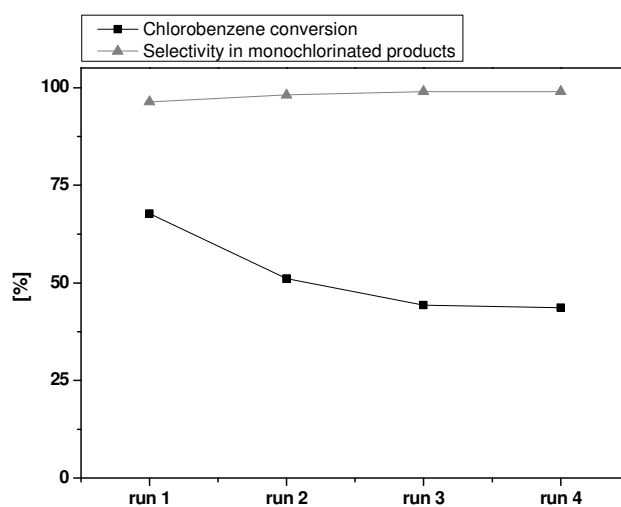


Figure 5.20 Recyclability of H-ZSM-5 catalyst during four consecutive runs. Conditions: T = 150 °C; TCCA: H⁺: PhCl = 1: 0.8: 1; Flow = 25 mL/min; TOS = 3 h

3.5 Chlorine consumption and catalyst stability versus time

To evaluate a possible viable application, a long-term experiment was conducted during 15 h on stream without any extra-TCCA addition over H-USY catalyst (Figure 5.21). Unfortunately, the nitrobenzene conversion dropped from nearly 50% (relative value) after 10 h on stream, due to less chlorine available in the reactor. However, the global chlorine consumption into final products (mono- and dichlorination) was further enhanced and reached 55% after 15 h on stream. Nevertheless, the selectivity toward monochlorinated compounds remains almost unchanged and higher than 90%.

Figure 5.21 confirms that chlorine consumption increases linearly throughout time on stream. Nearly 60% of total available chlorine is consumed after 15 h on stream. In other words, almost 2/3 of chlorine atoms available in one TCCA molecule were transferred to the products, with regard to chlorination with Cl_2 which only allow to achieve 50% atom efficiency at maximum.

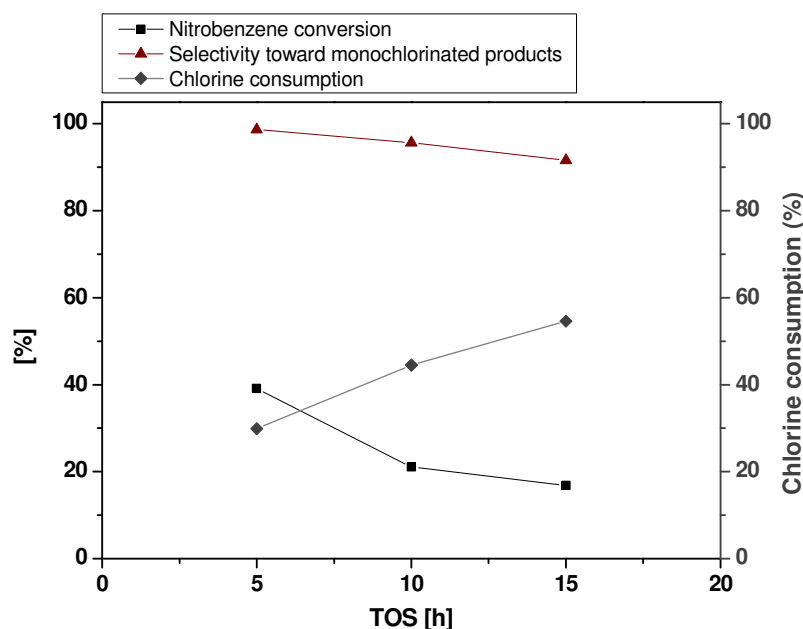


Figure 5.21 Nitrobenzene conversion, selectivity in chlorination products and chlorine consumption versus time on stream.

Conditions: T = 150 °C; TCCA: H⁺: PhNO₂ = 1: 1: 1; Flow = 100 mL/min

3.6 Silylation of zeolite surface

Post-synthesis modification by chemical liquid deposition (CLD) consists of the coverage of the external surface of zeolites by using silicon alkoxides like tetraethylorthosilicate (TEOS). The diameter of one TEOS molecule being higher than the apertures of the pores, a layer of silica is formed at the outer surface close to the pores' opening. Selective coverage of the external surface has been intensively studied during past decades [26]. It is well-known that this surface modification enhances the shape selectivity and sorption processes in ZSM-5 zeolites [27].

In this work, the surface of commercial ZSM-5 zeolite (Zeolyst CBV5020, named ZSM-5NC) was silylated by a chemical liquid deposition technique using TEOS (Section Chapter 3.2.1.1.3). The impact of these post-synthesis treatments was evaluated in nitro- and chlorobenzene chlorinations.

3.6.1. Nitrobenzene chlorination

Figure 5.22 gives the influence of silylation on the catalytic performance of H-ZSM-5 zeolite in nitrobenzene chlorination. One can observe that after the first passivation procedure the ZSM-5 zeolite presented a drastic decrease in nitrobenzene conversion degree compared to pristine catalyst, *i.e.*, 6% vs. 20%, respectively.

Nitrobenzene conversion are extremely affected by the surface modification since the catalysts silylated ZSM-5NCP2 and ZSM-5NCP3 exhibited almost no activities. These results can be explained by the lower access of reactants inside zeolite micropores. Indeed, the SiO₂ layer formed during the silylation procedure covers the external surface and the perimeter of the pore openings and thus reduces the pore diameter. Consequently, nitrobenzene and TCCA molecules can not enter through the pores and react on Brønsted acid sites.

[26] a) R. W. Weber, K. P. Möller, C. T. O'Connor, *Microporous Mesoporous Mater.* **2000**, 35-36, 533–543. b) S. Zheng, H. R. Heydenrych, A. Jentys, J. A. Lercher, *J. Phys. Chem. B* **2002**, 106, 9552–9558. c) F. Bauer, W. Chen, E. Bilz, A. Freyer, V. Sauerland, S. Liu, *J. Catal.* **2007**, 251, 258–270. d) J. H. Ahn, R. Kolvenbach, S. S. Al-Khattaf, A. Jentys, J. A. Lercher, *Chem. Comm.* **2013**, 49, 10584–6.

[27] S. J. Reitmeier, O. C. Gobin, A. Jentys, J. A. Lercher, *Angew. Chem. Int. Ed.* **2009**, 48, 533–538.

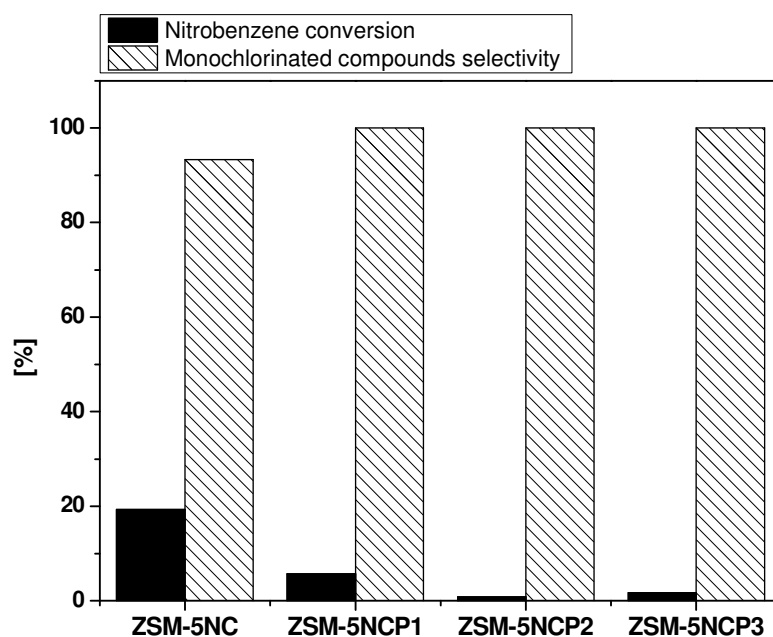


Figure 5.22 Nitrobenzene conversion and selectivity toward monochlorinated products over silylated H-ZSM-5 catalysts.

Conditions: T = 150 °C; TCCA: H⁺: PhNO₂ = 1: 1: 1; Flow = 100 mL/min; TOS = 5 h

In addition, Figure 5.22 shows that the selectivity in monochlorinated products of all passivated catalyst is higher than pristine zeolite (*i.e.*, 100% vs. 93%). Hence, one can conclude that according to the narrower pore openings after surface modification, the steric hindrance led to the (exclusive) formation of monochlorinated products.

3.6.2. Chlorobenzene chlorination

All silylated ZSM-5 catalysts were also tested in chlorobenzene chlorination and the catalytic results are summarized in Figure 5.23. Likewise, a similar behavior was observed: the catalyst passivated once led to a three-times lower conversion than pristine zeolite. ZSM-5NCP2 and ZSM-5NCP3 zeolites presented chlorobenzene conversion degrees < 10%.

The silylation of the external surface led also to the inertization of the external surface acid sites [28]. These external acid sites, which could be assimilated to silica acid sites, could also be active to perform the chlorination. Indeed, chlorobenzene chlorination can be

[28] C. T. O'Connor, K. P. Möller, H. Manstein, *J. Mol. Catal. A* **2002**, 181, 15–24.

catalyzed by silica (see Section 3.1.2). The drastic loss in chlorobenzene conversion after one silylation procedure could be attributed to a decrease in internal acid site accessibility combined with the inertization of external surface acid sites. In addition, the selectivity in monochlorinated products and *o/p* ratios were not affected by surface modifications.

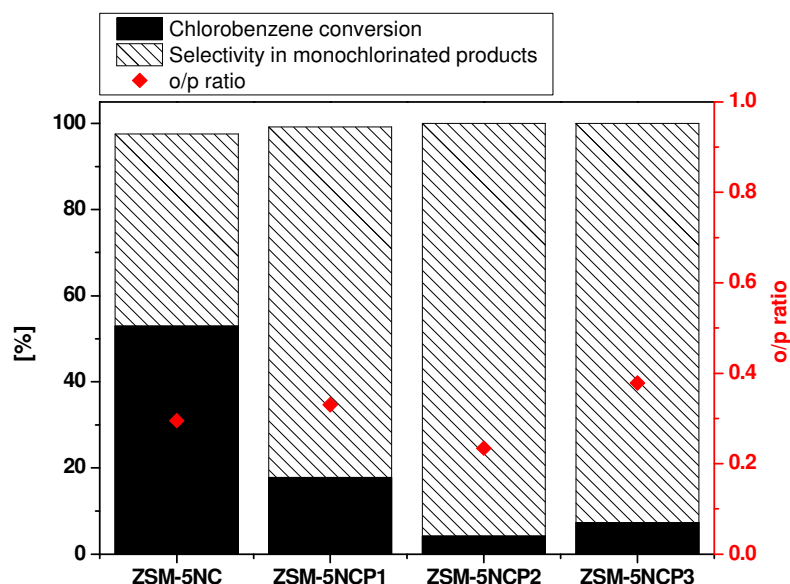


Figure 5.23 Chlorobenzene conversion and selectivity toward monochlorination products over passivated H-ZSM-5.

Conditions: T = 150 °C; TCCA: H⁺: PhCl = 1: 0.8: 1; Flow = 25 mL/min; TOS = 3 h

As a conclusion, one can assume that chloro- and particularly nitrobenzene chlorination reactions require the zeolite internal Brønsted acidity and thus take place inside the zeolite pores.

3.7 Hierarchical zeolites in chlorination reactions

The semi-continuous gas–solid chlorination of deactivated arenes using TCCA as a chlorination agent was chosen to compare the catalytic performances of various hierarchical catalysts. Indeed, one could expect a difference in the catalytic behavior with respect to the presence of mesoporosity. Various methods of inter- and/or intracrystalline mesoporosity generation, *i.e.*, nanosized zeolites, dealumination and desilication, were investigated and their catalytic performance analyzed in the reaction.

3.7.1. Nanosized zeolites

Thanks to a collaboration with Jean Daou (IS2M, UHA, Mulhouse), we compared the catalytic activities of four MFI zeolites exhibiting distinct crystal morphologies (nanocrystals, nanosheets and conventional coffin-shape micro-crystals) or distinct surfaces (by external surface passivation). The different procedures are summarized in Section Chapter 3.2.1.1.

The influence of crystal morphology on nitro- and chlorobenzene chlorinations was depicted in Figure 5.24 and Figure 5.25, respectively. It is worthy to mention that all catalytic tests were performed under iso-mass conditions.

The selectivity toward monochlorination products are nearly the same for both nanoscopic zeolites, being 60% *meta*-chloronitrobenzene produced as shown in Figure 5.24. Likewise, the selectivities toward *o,p*-dichlorobenzenes remained nearly the same over the latter two zeolites (Figure 5.25).

Besides, one can observe that micron-sized ZSM-5R exhibits almost no activity (< 1%). These results can be explained by a hindered diffusion in those large crystals with respect to nano-sized ZSM-5 zeolites.

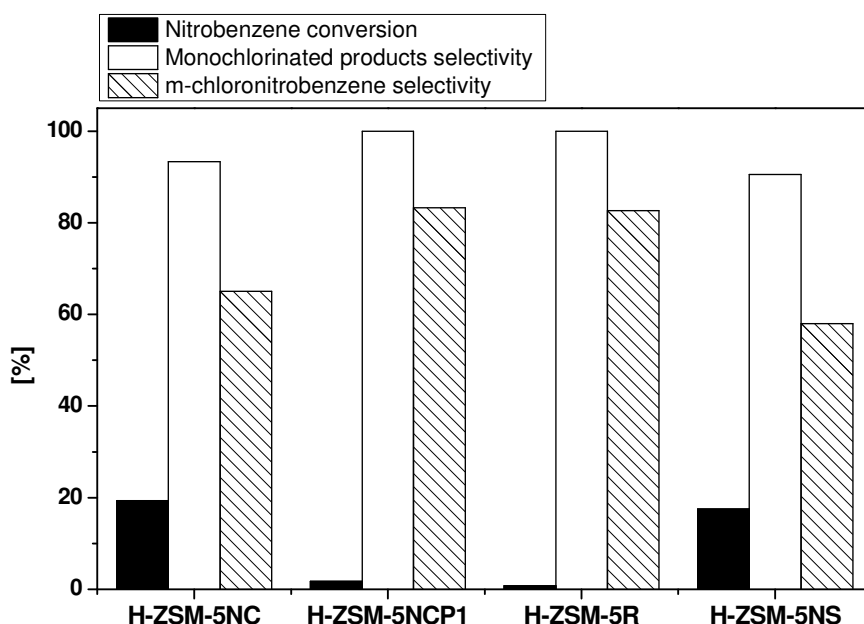


Figure 5.24 Nitrobenzene chlorination reaction over the four MFI-type zeolite samples. Conditions: T = 150 °C; TCCA: PhNO₂ = 1: 1; 214 mg of catalyst; Flow = 100 mL/min; TOS = 5 h

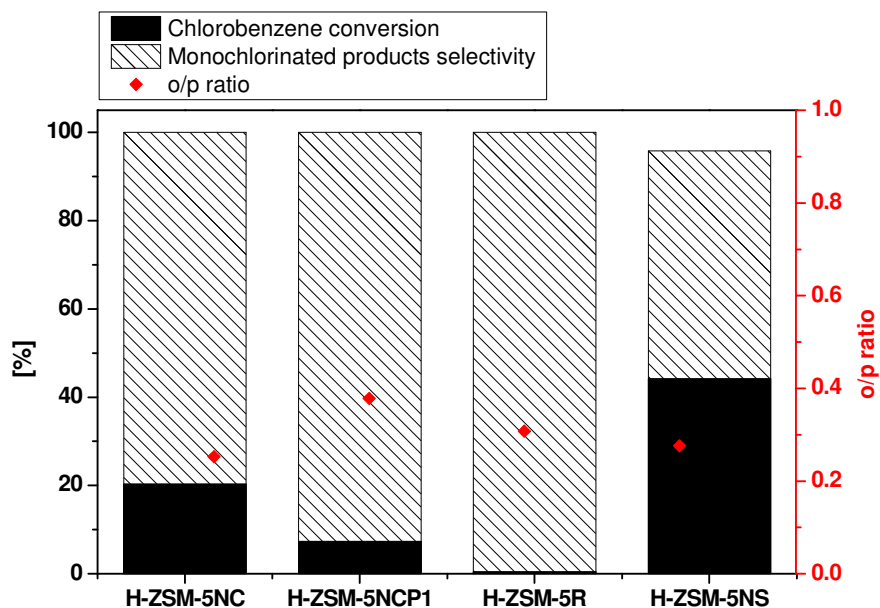


Figure 5.25 Chlorobenzene chlorination reaction over the four MFI-type zeolite samples. Conditions: T = 150 °C; TCCA: PhCl = 1: 1; 62 mg of catalyst; Flow = 25 mL/min; TOS = 3 h

In heterogeneous-catalyzed reactions by zeolites, especially involving bulky molecules, internal mass transfer limitations have to be taken into account [23]. The estimation of Thiele-Weisz modulus has therefore been undertaken according to the following formula: $\phi = L(k/D_{\text{eff}})^{(1/2)}$, in which L represents the diffusion length, k the rate coefficient, and D_{eff} the effective diffusivity of a monosubstituted aromatic in zeolite pores. A Thiele-Weisz modulus for micron-sized ZSM-5R $\phi_{\text{big crystals}} \sim 18$ was estimated, whereas $\phi_{\text{nanocrystals}} \sim 0.01$ and $\phi_{\text{nanosheets}} \sim 10^{-5}$ were obtained for ZSM-5NC and ZSM-5NS zeolites, respectively. In terms of intra-particle transport, the latter two (low) values for Weisz modulus (admitted when $\phi < 0.1$) confirm a full utilization of zeolite catalyst particle, thus the reaction rate equals the intrinsic reaction rate [29,30]. In contrast, mass transfer issues completely hinder the reaction in micron-sized ZSM-5R ($\phi_{\text{big crystals}} \sim 18$). The superior catalytic performance of zeolite nanocrystals and nanosheets can therefore be rationalized by enhanced diffusion properties.

To further highlight the importance of diffusion phenomena, a comparison was drawn before and after external surface passivation of ZSM-5NC zeolite. It appeared that silylated

[29] a) M. Baerns, H. Hofmann, A. Renken, *Chemische Reaktionstechnik*, Georg Thieme Verlag, Stuttgart, Germany, 3rd ed., 1999. b) B. Louis, P. Reuse, L. Kiwi-Minsker, A. Renken, *Ind. Eng. Chem. Res.* **2001**, *40*, 1454–1459.

[30] O. Levenspiel, *Chemical Reaction Engineering*, John Wiley & Sons, New York, United States, 3rd ed., 1999.

catalyst exhibited a lower activity for both aromatics, *i.e.*, 2% versus 19% for nitrobenzene (Figure 5.24), 7% versus 20% for chlorobenzene (Figure 5.25), respectively. The drastic loss in activity observed in aromatics chlorination can be explained by both phenomena: reduced microporous volume accessibility and decrease in BET surface area (*i.e.*, 321 m²/g versus 402 m²/g), which may impact nitrobenzene/chlorobenzene adsorption on the acid sites within ZSM-5 channels. Based on Weisz modulus estimations, internal mass transfer limitations could be excluded for these two nano-sized MFI zeolites.

In spite of such extremely low values for Weisz modulus, one cannot neglect surface permeability barriers which are readily to occur in nanocrystals [31]. Krishna highlighted discrepancies in the modelling of diffusion kinetics at high surface coverage by reactants/products along with strong confinement effects [31a]. Likewise, Karger *et al.* confirmed that these surface barriers may differ up to a factor 2, thus indicating a higher resistance for bulky molecules to enter inside the pores of smaller nanocrystals [31b].

The difference between those two zeolites relied on their three-dimensional arrangement and on their textural properties. ZSM-5NC zeolite exhibits a specific surface area of 402 m²/g and a mesoporous volume of 0.08 cm³/g, whereas ZSM-5NS zeolite possesses a specific surface area above 500 m²/g and a mesoporous volume of 0.48 cm³/g. In addition, ZSM-5NS sample exhibits a 30% higher number of Brønsted acid sites (1.17 versus 0.90 mmol H⁺/g for ZSM-5NC).

In the case of nitrobenzene chlorination (Figure 5.24), the two ZSM-5 catalysts led to nearly the same nitrobenzene conversion, *i.e.*, 19% for ZSM-5NC zeolite and 18% for ZSM-5NS zeolite. It is noteworthy that ZSM-5 nano-sized crystals/nanosheets improved significantly the catalytic performance of MFI-type catalysts compared with conventional coffin-shaped big crystals. Unfortunately, the three-dimensional architecture of ZSM-5 nanosheets did not further raise the nitrobenzene reactivity with respect to nano-sized ZSM-5 zeolites. In contrast, a 36% higher TOF was achieved over ZSM-5NC catalyst, *i.e.*, 1.8.10⁻⁴ mol_{nitrobenzene} converted per acid site per m².g⁻¹ in one hour. The TOF values were corrected by the specific surface area values to avoid its influence.

[31] a) R. Baur, R. Krishna, *Catal. Today* **2005**, *105*, 173–179. b) D. Tzoulaki, L. Heinke, H. Lim, J. Li, D. Olson, J. Caro, R. Krishna, C. Chmelik, J. Kärger, *Angew. Chem. Int. Ed.* **2009**, *48*, 3525–3528. c) L. Karwacki, M. H. F. Kox, D. A. Matthijs de Winter, M. R. Drury, J. D. Meeldijk, E. Stavitski, W. Schmidt, M. Mertens, P. Cubillas, N. John, *et al.*, *Nature Mater.* **2009**, *8*, 959–965.

The two nano-sized MFI zeolites exhibited different activities in chlorobenzene chlorination (Figure 5.25). Indeed, ZSM-5NS zeolite led to a twice higher conversion, with respect to ZSM-5NC zeolite, *i.e.*, 44% versus 20%. By taking into account TOF values, $1,9 \cdot 10^{-3}$ and $2,8 \cdot 10^{-3} \text{ mol}_{\text{conv. PhCl}} \cdot \text{mol}_{\text{H}^+}^{-1} \cdot \text{m}^{-2} \cdot \text{g}^{-1} \cdot \text{h}^{-1}$ over ZSM-5NC and ZSM-5NS zeolites (respectively), a nearly 33% higher productivity was achieved over ZSM-5 nanosheets. Hence, this suggests that the layered nanosheets morphology plays an important role in the chlorination performance. Ryoo and co-workers outlined the point that MFI nanosheets, thanks to their larger number of external acid sites, exhibited a higher catalytic activity for large organic molecules [32].

Nevertheless, the reverse tendency was observed for nitrobenzene chlorination which requires a stronger acidity due to the presence of deactivating nitro- group (TOF diminished by approx. 35%). Since the TOF values for the two nano-sized zeolites deviate from approx. $\pm 33\text{-}36\%$ ranging from chlorobenzene to nitrobenzene, one can roughly estimate the density of external silanol groups present at the nanosheets' outer surface, representing thus nearly one third of the total amount of their Brønsted acid sites.

To summarize, the ZSM-5 zeolite organization into nanosheet layers led to a 33% raise in the TOF for chlorobenzene halogenation, suggesting that all O-H groups from the catalyst are accessible and probably involved in the catalytic reaction whatever their localization and strength. In contrast, the chlorination of nitrobenzene requires stronger Brønsted acid sites to protonate TCCA molecule, as previously exposed in Section 3.1.1. A rough estimation of mildly acidic external silanol groups fraction in ZSM-5NS zeolite to 1/3 of the total amount of Brønsted acid sites can therefore be made.

Mota *et al.* have developed a method to assess the acid strength of different solid acid catalysts with the use of linear free energy relationship for the H/D exchange with mono-substituted aromatics [33]. A combination of H/D exchange technique (to determine the whole number of O-H groups present in the zeolite) [34] with the present strategy to perform the halogenation reaction of various deactivated aromatics can therefore be used as a tool to estimate the fraction of acid sites involved in those electrophilic aromatic

[32] a) M. Choi, K. Na, J. Kim, Y. Sakamoto, O. Terasaki, R. Ryoo, *Nature* **2009**, *461*, 246–249. b) K. Na, M. Choi, W. Park, Y. Sakamoto, O. Terasaki, R. Ryoo, *J. Am. Chem. Soc.* **2010**, *132*, 4169–4177.

[33] V. L. C. Gonçalves, R. C. Rodrigues, R. Lorençato, C. J. A. Mota, *J. Catal.* **2007**, *248*, 158–164.

[34] B. Louis, A. Vicente, C. Fernandez, V. Valtchev, *J. Phys. Chem. C* **2011**, *115*, 18603–18610.

substitution reactions. Hence, one may distinguish the quantity of sites possessing milder acidity by tailoring the basicity of the probe molecule used for the reaction.

To summarize, the gas-solid phase chlorination of deactivated arenes (chlorobenzene and nitrobenzene) using TCCA, was successfully performed over two nano-sized ZSM-5 zeolites. Whilst no change in the selectivity toward the reaction products could be evidenced, significant variations in TOF values were observed, *i.e.*, $1.9 \cdot 10^{-3}$ and $2.8 \cdot 10^{-3}$ $\text{mol}_{\text{conv. PhCl}} \cdot \text{mol}_{\text{H}^+}^{-1} \cdot \text{m}^{-2} \cdot \text{g}^{-1} \cdot \text{h}^{-1}$ for ZSM-5 nanocrystals and nanosheets, respectively. In contrast, the reverse performance was observed for nitrobenzene where a 35% higher TOF was achieved over ZSM-5NC zeolite with respect to ZSM-5NS zeolite.

3.7.2. Dealuminated zeolites

In this study, FAU and MFI-type zeolites were dealuminated through several methods. Different steaming treatments were conducted over home-made Y and commercial ZSM-5 (Zeolyst CBV5020) zeolites to provide zeolites with various dealumination degrees. Thus, three degrees of steaming have been conducted: mild, intermediate and severe, named ST1, ST2 and ST3 respectively for each zeolite type. Furthermore, commercial H-USY (Zeolyst CBV500) and the mild and severe steamed ZSM-5 zeolites were further treated with EDTA to leach EFAl species out of the micropores. Finally, pristine ZSM-5 zeolite was acid treated with oxalic acid (ZSM-5 OA). The detailed procedures and characterizations are described in Section Chapter 3.3.2.1. Hierarchical zeolites were tested in both nitro- and chlorobenzene chlorinations.

3.7.2.1. Nitrobenzene chlorination

Figure 5.26 shows the catalytic data obtained with commercial H-USY zeolite treated and non-treated with EDTA. The characterization by ^{27}Al MAS NMR of EDTA treated H-USY zeolite has shown the almost disappearance of the signal at 0 ppm, thus indicating the leaching of almost all EFAl debris from the micropores.

It is noteworthy that the presence or not of EFAl species strongly influences the catalytic performance of FAU zeolite. Indeed, the EDTA treatment led to a significant raise in nitrobenzene conversion, up to 82% while the selectivity in monochlorinated products remained unchanged. This phenomenon could be due to the higher accessibility of the reactants to the active sites within the pores, emptied from their alumina aggregates [35]. Hence, the molecules easily access to the active sites, thus raising the conversion of nitrobenzene to mono- and dichlorinated products. To summarize, Lewis acidity provided by EFAl species did not play a direct role in the reaction but the creation of mesoporosity in the H-USY (by the removal of EFAl fragments) enhanced the catalyst performance.

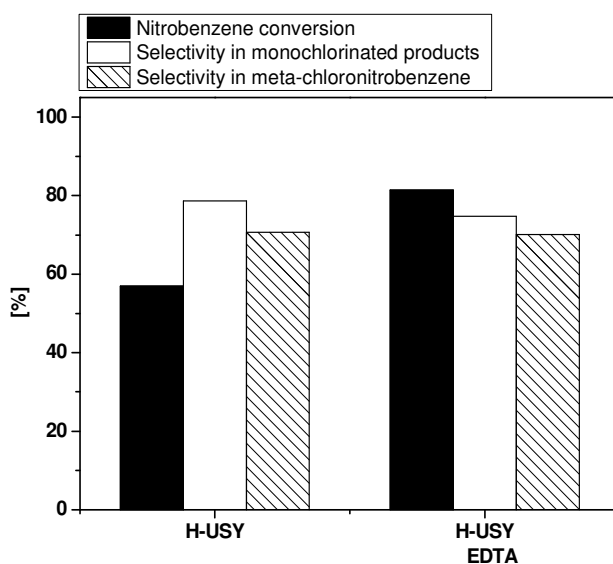


Figure 5.26 Comparison in terms of nitrobenzene conversion and selectivity toward mono- and m-chlorinated products between H-USY zeolite and H-USY treated by EDTA.

Conditions: T = 150 °C; TCCA: PhNO₂ = 1: 1; 66 mg of catalyst ; Flow = 100 mL/min; TOS = 5 h

Besides, the family of dealuminated ZSM-5 zeolites was tested in nitrobenzene chlorination (Figure 5.27). All catalytic tests were performed at iso-mass conditions. One can observe that excepted ZSM-5 ST2 catalyst, all steamed catalysts exhibit lower conversions compared with pristine ZSM-5. Indeed, the more severe the steaming treatment was, the lower the catalytic activity was. It is noteworthy that steamed ZSM-5 zeolites possess EFAl species in their microporous channel, as characterized by ²⁷Al MAS NMR.

[35] C. R. Moreira, M. H. Herbst, P. R. de la Piscina, J.-L. G. Fierro, N. Homs, M. M. Pereira, *Microporous Mesoporous Mater.* **2008**, *115*, 253–260.

Moreover, the characterization of these samples by FTIR analyses has evidenced the Lewis acid sites presence due to EFAl species in steamed zeolites, as well as silanols nests and lower Brønsted acidity. From our characterization data which are in line with literature [36], one can conclude that severe steaming results in a strong decrease in the framework Al content, agglomeration of EFAl species and decrease in Brønsted acidity. In addition, BET measurements have shown that steamed zeolites did not exhibit noticeable mesoporosity, except ZSM-5 STS which presented a small hysteresis in N₂ adsorption-desorption isotherm. This phenomenon could be attributed to the presence of EFAl debris hindering the accessibility to freshly formed mesopores. The combination of these properties had an negative impact on nitrobenzene conversion.

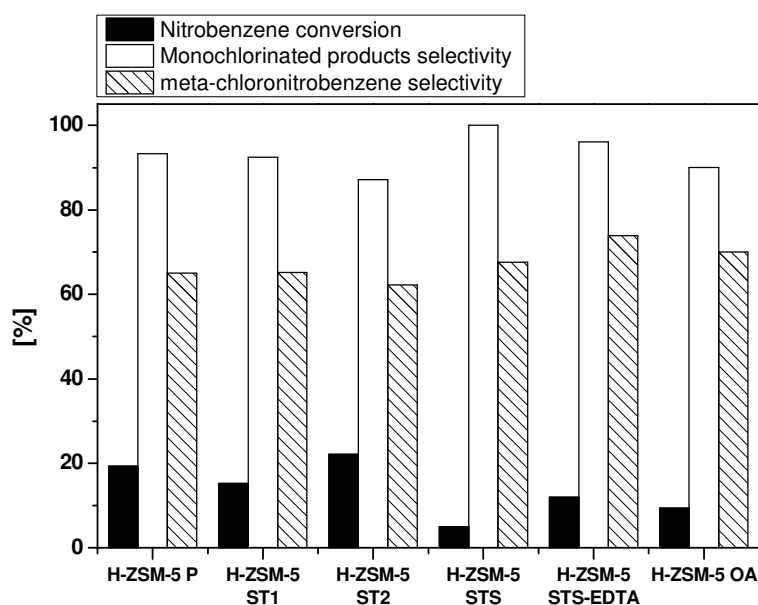


Figure 5.27 Nitrobenzene conversion and selectivities in mono- and m-chlorinated products over dealuminated MFI-type zeolites.

Conditions: T = 150 °C; TCCA: PhNO₂ = 1: 1; 250 mg of catalyst; Flow = 100 mL/min; TOS = 3 h

Surprisingly, ZSM-5 ST2 sample exhibits the highest catalytic activity (*i.e.*, 22% conversion). Unfortunately, this catalyst was not well characterized like other steamed zeolites. The only data collected for this sample is its BAS concentration which is the highest among all steamed zeolites (*i.e.*, 1.0 vs. 0.86 mmol H⁺/g for parent ZSM-5). Almutairi *et al.* performed a complete study on intrinsic properties and catalytic activities in MTO for various

[36] S. M. T. Almutairi, B. Mezari, E. A. Pidko, P. C. M. M. Magusin, E. J. M. Hensen, *J. Catal.* **2013**, *307*, 194–203.

steamed ZSM-5 zeolites [36]. They observed the highest propane conversion for a mildly steamed sample. They correlated this higher catalytic activity to the higher concentration of BAS determined by IR spectroscopy of adsorbed pyridine. They attributed this phenomenon to the partial reinsertion of EFAl species into the zeolite framework. Based on H/D exchange characterization of ZSM-5 ST2 sample showing a higher amount of BAS and catalytic results, one may assume that our intermediate steamed ZSM-5 possesses similar properties as their mildly steamed zeolite. The higher BAS concentration allowed to improve the catalytic performance of pristine zeolite. Indeed, as exposed previously in this Section, the nitrobenzene chlorination is a reaction which requires high acid site density.

The leaching of EFAl moieties in severe steamed ZSM-5 zeolite allows to partially restore the catalytic performance but still inferior than parent ZSM-5. This phenomenon could be ascribed to a higher accessibility to the acid sites and higher diffusion abilities compared with steamed zeolites. Thanks to BET measurements, we observed that EDTA washed catalysts exhibited significant mesoporosity (with diameter around 7 nm). Nevertheless, ZSM-5 STS-EDTA catalyst possesses lower intrinsic acidity since its Si/Al ratio is higher than pristine ZSM-5 zeolite (*i.e.*, 40 vs. 25, respectively) that can explain its lower nitrobenzene conversion.

The dealumination by oxalic acid had a negative impact on the catalyst performance, *i.e.*, 9% conversion.

Finally, selectivities toward monochlorination and *m*-chloronitrobenzene did not seem to be affected by dealumination treatments. Dealuminated catalyst kept high selectivity toward monochlorinated products > 85%. One can note that ZSM-5 STS-EDTA sample allowed to increase the selectivity in *m*-chloronitrobenzene compared to pristine zeolite, 74% and 65% respectively. This can be attributed to the lower steric hindrance due to mesopores presence in ZSM-5 STS-EDTA catalyst.

3.7.2.2. Chlorobenzene chlorination

The catalytic performances of dealuminated faujasite and ZSM-5 zeolites in chlorobenzene chlorination reaction are depicted in Figure 5.28 and Figure 5.29.

All catalytic tests over FAU-type zeolites were conducted at iso-mass conditions. First of all, one can observe that steaming treatments of H-Y catalyst led to vanished catalytic activities (Figure 5.28). Indeed, the more the steaming treatment was severe, the more the conversion degree was decreased. H-Y STS catalyst exhibited 2% of chlorobenzene conversion versus 46% for pristine H-Y zeolite. The selectivity toward monochlorinated products remained unchanged whatever the severity of the steaming process (*i.e.*, > 90%). Concerning the *o/p* ratios, the mild and intermediate steaming treatments did not affect this parameter, whilst the severe treatment led to an increase in *o/p* ratio value, thus to higher formation of *ortho*-isomer. This behavior could be ascribed to weaker steric hindrance after severe steaming modification. In fact, a weak hysteresis was observed in ZSM-5 STS zeolite by N₂ adsorption-desorption isotherm. One could expect the same effect for severe steamed Y zeolite. Nevertheless, the presence of EFAl species in steamed Y zeolites seems to inhibit the reaction by vanishing the acid site accessibility within the zeolite pores.

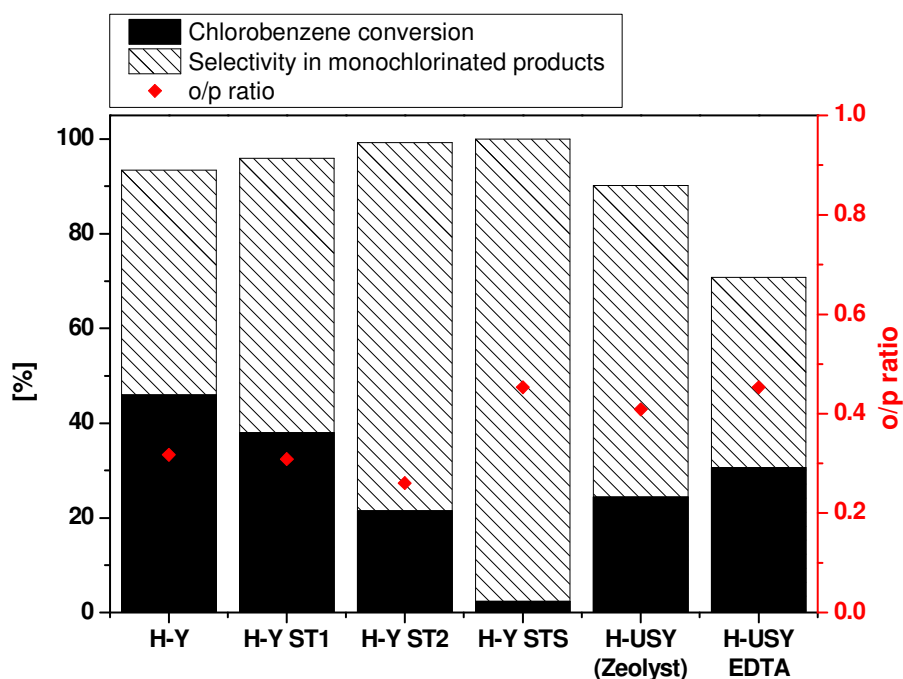


Figure 5.28 Chlorobenzene conversion and selectivity in monochlorinated compounds over dealuminated FAU-type zeolites.

Conditions: T = 150 °C; TCCA: PhCl = 1: 1; 76 mg of catalyst; Flow = 25 mL/min; TOS = 3 h

The catalytic test of commercial H-USY zeolite presented similar results as our intermediate steamed H-Y zeolite (H-Y ST2). Likewise to nitrobenzene chlorination over ZSM-

5 STS-EDTA catalyst, the partial leaching of EFAl species probed by ^{27}Al MAS NMR allowed to improve the catalytic performance of H-USY zeolite. Moreover, the selectivity in monochlorinated products is strongly decreased with respect to H-Y catalyst (*i.e.*, 71%). In conclusion, the presence of both mesoporosity and LAS through EFAl aggregates in FAU zeolite did not allow to improve the catalytic performance in chlorobenzene chlorination.

The catalytic activities of dealuminated ZSM-5 zeolites in chlorobenzene chlorination are completely different compared with dealuminated FAU-type zeolites (Figure 5.29). Except the intermediate steamed ZSM-5 (H-ZSM-5 ST2), all dealuminated catalysts led to improved catalytic activities with respect to parent ZSM-5 zeolite. The mildly and severe steamed ZSM-5 zeolites allowed to convert 67% and 58% of chlorobenzene respectively, along with slightly lower selectivities in monochlorinated products (*i.e.*, 91% and 97% vs. 98% for ZSM-5 P).

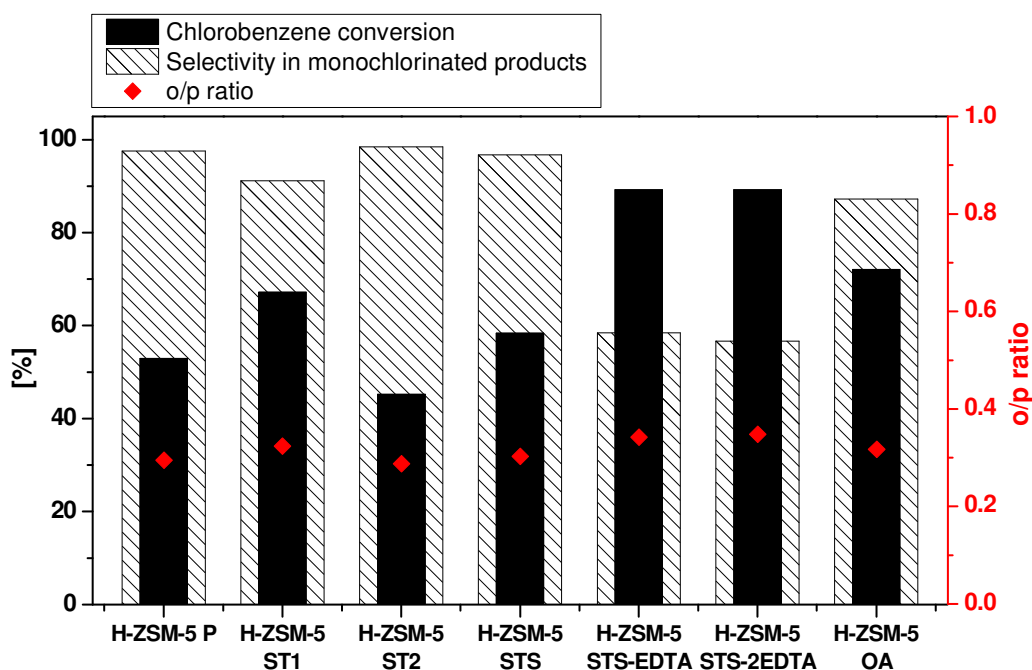


Figure 5.29 Chlorobenzene conversion and selectivity in monochlorinated products over dealuminated MFI-type zeolites.
Conditions: T = 150 °C; TCCA: PhCl = 1: 1; 248 mg of catalyst; Flow = 25 mL/min; TOS = 3 h

Earlier studies attributed the higher efficiency of steamed zeolites in various reactions to a synergy between EFAl moieties and BAS which improves the Brønsted acid strength [37]. Although the BAS concentration is decreased by steaming treatments (probed by titration and FTIR analyses), the higher conversion achieved over steamed ZSM-5 zeolites could be attributed to the synergy between LAS and BAS which improve the acid strength of the zeolite. In the case of severe steamed ZSM-5 zeolite, one might ascribed its lower activity compared to the mild steamed one, to a lower accessibility to the acid sites because of EFAl aggregates.

The EFAl removal in ZSM-5 STS sample by EDTA treatment allowed to significantly enhance the chlorobenzene conversion (*i.e.*, 89%) but at the expense of selectivity in monochlorinated products which strongly vanished (*i.e.*, 58%). One can assign this result to both higher accessibility inside microporous channels and mesoporosity formation. Hence, this hierarchical ZSM-5 zeolite presented lower diffusion limitations which positively influences the chlorination rate. In contrast to nitrobenzene chlorination, the milder acidity in H-ZSM-5 STS-EDTA sample did not hinder the reaction. The second EDTA treatment did not lead to further improvement.

Finally, the dealumination of ZSM-5 zeolite with oxalic acid permitted to reach the same catalytic activity as ZSM-5 ST1 sample. Although this catalyst exhibited similar acid properties as ZSM-5 STS-EDTA, the lower mesoporosity created in ZSM-5 OA sample diminished its reactivity.

Thanks to this study, it seems that the chlorination of nitro- and chlorobenzene are not influenced by the same factors. Whilst nitrobenzene chlorination is strongly depending on acid site density and slightly influenced by the presence of mesoporosity, chlorobenzene chlorination is extremely favored over mesoporous zeolites.

[37] a) C. Mirodatos, D. Barthomeuf, *J. Chem. Soc., Chem. Commun.* **1981**, 39–40. b) A. Corma, V. Fornes, F. Rey, *Appl. Catal.* **1990**, *59*, 267–274. c) S. Li, A. Zheng, Y. Su, H. Zhang, L. Chen, J. Yang, C. Ye, F. Deng, *J. Am. Chem. Soc.* **2007**, *129*, 11161–71.

3.7.3. Desilicated zeolites

Several desilicated ZSM-5 zeolites were tested in chlorobenzene chlorination. Commercial ZSM-5 zeolite (Zeolyst CBV2314) has been alkaline-treated under various conditions, as summarized in Table 5.6. More characterization data of ZSM-5 IDS1 sample are provided in Section Chapter 3.3.2.2.2.

Table 5.6 Alkaline treatment conditions

Entry	NaOH concentration [mol.L ⁻¹]	Duration [min]	Temperature [°C]
ZSM-5 IDS1	0.2	45	65
ZSM-5 IDS2	0.2	75	65
ZSM-5 IDS3	0.2	105	65
ZSM-5 IDS4	0.5	75	65
ZSM-5 IDS5	1.0	75	65

The specific surface area (S_{BET}) of the samples varied between 287 and 427 m²/g (see Table 5.7). For mild alkaline treated catalysts, BET areas and mesopore volumes were increased (*i.e.*, 427 and 0.13 and 409 m²/g and 0.13 cm³/g for ZSM-5 IDS1 and IDS2 samples, respectively). These samples are characterized by similar mesoporosity creation after alkaline treatment whatever its duration.

Table 5.7 Textural properties of dealuminated ZSM-5 zeolites

Entry	$S_{\text{BET}}^{\text{a}}$ [m ² /g]	$V_{\text{micro}}^{\text{b}}$ [cm ³ /g]	$V_{\text{meso}}^{\text{c}}$ [cm ³ /g]	$V_{\text{tot}}^{\text{a}}$ [cm ³ /g]
ZSM-5 P	376	0.13	0.07	0.20
ZSM-5 IDS1	427	0.13	0.13	0.26
ZSM-5 IDS2	409	0.12	0.13	0.25
ZSM-5 IDS4	287	0.08	0.15	0.23

^a BET method applied to the N₂ isotherm

^b t-plot method

^c $V_{\text{meso}} = V_{\text{tot}} - V_{\text{micro}}$. V_{tot} was determined from the amount of N₂ adsorbed at $P/P_0 = 0.97$

Although the more severe alkaline treated sample (ZSM-5 IDS4) presents a higher mesoporous volume (*i.e.*, 0.17 cm³/g), its BET surface area and microporous volume vanished (*i.e.*, 287 m²/g and 0.08 cm³/g, respectively). These results indicate that more severe alkaline treatment led to a partial destruction of the microporous channels.

Figure 5.30 gives the N₂ adsorption-desorption isotherms of desilicated ZSM-5 catalysts. Typical type I isotherm with a weak hysteresis loop was found for pristine zeolite, being characteristic for conventional microporous zeolites with mesoporosity due to inter-crystalline diffusion.

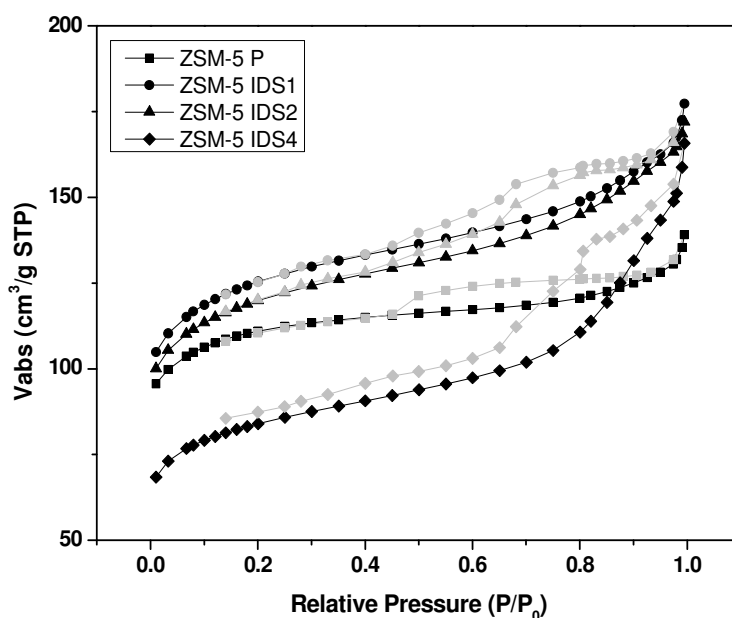


Figure 5.30 N₂ adsorption and desorption isotherms at 77 K of desilicated ZSM-5 zeolites

Upon alkaline treatment all zeolites show an enhanced N₂ uptake at higher relative pressures accompanied by a hysteresis loop, being indicative of extra mesoporosity. The more mesoporous catalyst is ZSM-5 IDS4 sample since it exhibits a higher hysteresis loop compared with other samples. The more severe the alkaline treatment is, the more the zeolite presents mesoporosity but sometimes at the expense of the microporous network crystallinity.

The catalytic tests were conducted under iso-mass conditions and the results are presented in Figure 5.31. Except H-ZSM-5 IDS3 sample, all alkaline-treated materials exhibited higher catalytic performances compared to pristine ZSM-5 zeolite. Three samples presented significant improvement in chlorobenzene conversion up to 48%, *i.e.*, HZSM-5 IDS2, IDS4 and IDS5 zeolites.

Mesoporosity properties present in these materials could decrease diffusion limitations in zeolite channels and thus facilitate the reactivity. Although the severity of the treatment performed on the H-ZSM-5 IDS5 was high, this material exhibited the higher conversion but at the expense of the selectivity toward monochlorination. This lower selectivity can be due to a high mesoporosity providing enough space for further chlorination of monohalogenated products.

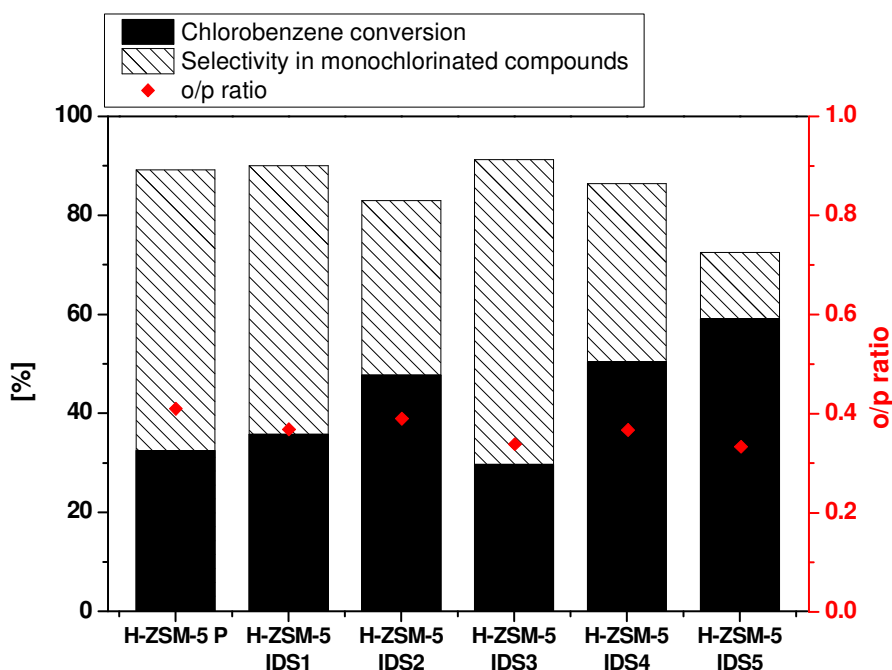


Figure 5.31 Chlorobenzene conversion and selectivity in monochlorinated products. Conditions: T = 150 °C; TCCA: PhCl = 1: 1; 62 mg of catalyst; Flow = 25 mL/min; TOS = 3 h

Finally, the zeolite treated by TPAOH was tested in nitro- and chlorobenzene chlorination reactions. Unfortunately, no conversions could be observed. One can assume thanks to the characterization data that this catalyst suffered from partial destruction of the microporous framework.

Likewise dealuminated ZSM-5 zeolites, the chlorobenzene chlorination is favored over desilicated zeolites. The insertion of mesoporosity inside ZSM-5 crystals allows to significantly improve the activity by facilitating reactants and products diffusion.

4. Conclusions

The present chapter describes the development of a green route to perform the chlorination of deactivated aromatics in the presence of zeolites and TCCA.

Preliminary results have shown that TCCA reacts with arenes in liquid-phase and its reactivity is highly affected by the acid strength of the reaction medium. Several arenes are efficiently chlorinated by TCCA over solid acids. Unfortunately, according to temperature limitation in liquid phase conditions, the chlorination of nitrobenzene was not feasible.

According to DFT calculations, we have demonstrated that TCCA can easily be activated by solid acid catalyst, thus leading to possible replacement of strong liquid acids to promote this superelectrophilic reaction. We have tested several solid acids, showing the synergy between acid strength and pore size for promoting the reaction.

Afterwards, further developments of the chlorination process have been made to render the chlorination process more environmental-friendly. A semi-continuous flow system has been designed to perform nitrobenzene and chlorobenzene halogenation under gas-solid conditions. H-USY zeolite was found the more promising catalyst for the chlorination of nitrobenzene, with good conversions (39–64%) at excellent selectivities toward monochlorinated products (90–99%). In contrast, an optimal catalytic activity in terms of chlorobenzene conversion and selectivity in monochlorination was achieved over H-ZSM-5 zeolite, which allowed to convert 53% of aromatic substrate into 98% of monochlorination products. According to the narrower ZSM-5 pore openings and smaller chlorobenzene average size with respect to nitrobenzene, confinement effects like “floating molecules” concept could explain this activity.

The potential reuse of these optimal catalysts has been demonstrated but with an irreversible loss in activity after the first run (only), which remained stable after the successive runs.

Optimization of experimental conditions in both chlorobenzene and nitrobenzene halogenations led to define an appropriate molar ratio between the reactants and synthesis temperature, being TCCA: H⁺: PhNO₂ = 1: 1: 1 at 150 °C and TCCA: H⁺: PhCl = 1: 0.8: 1 at 150 °C.

Kinetic studies have been performed for both aromatics and apparent activation energies calculated were in agreement with the value found by DFT calculations for benzene chlorination (*i.e.*, 16.7 and 26.8 kJ/mol for chlorobenzene and nitrobenzene chlorination, respectively).

A deeper focus on TCCA activation over H-USY zeolite in nitrobenzene chlorination was given. Thus, 2/3 of chlorine atoms in TCCA molecule can be integrated in final products.

Additionally, surface modification of ZSM-5 zeolite through silylation procedure allowed us to assume that chlorination reactions take place inside the porous network of zeolites.

The influence of (intra- or inter-crystalline) mesoporosity on chlorination reactions has been investigated thanks to the design of various hierarchical FAU and MFI-type zeolites. Mass transfer limitations were evaluated by reacting either chloro- or nitrobenzene through a ZSM-5 zeolite porous network with different crystal sizes and morphologies. Whereas, the reaction rate was completely controlled by internal diffusion in 10–15 μm-sized big ZSM-5 zeolite crystals (Weisz modulus, Φ big crystals = 18), the impact of mass transfer limitations could be ruled out for ZSM-5 nanocrystals (200–400 nm) and in stacked ZSM-5 nanosheets (thickness 2 nm). Based on reactivity differences in arene chlorination between the two nano-sized ZSM-5 zeolites, we were able to estimate the quantity of mild acidic silanol groups in ZSM-5 nanosheets to roughly 1/3 of the total amount of Brønsted acid sites.

Finally, the reactivity of nitrobenzene was strongly influenced by the acid site density in zeolite crystals. Despite a raise in mesoporosity, rendering easier the diffusion of reactants and products inside the microporous channels, the loss of active sites seems to govern the conversion in both FAU and MFI-type zeolites. In contrast, the reaction with chlorobenzene appeared to be positively influenced by mesoporosity regardless the method used to produce the hierarchical zeolite.

In conclusion, depending on the aromatic used, the chlorination reaction can be used as a powerful tool to quantify the intrinsic acidity of zeolites, in terms of acid site density and strength.

**Chapter 6. SYNTHESIS AND APPLICABILITY OF
ZEOLITE COATINGS ON SILICON-CONTAINING
SUPPORT**

ABSTRACT

Several syntheses have been performed to allow the growth of zeolite crystals on silicon-containing supports.

The first section describes the preparation and characterization of zeolite coatings on glass monoliths. ZSM-5 crystals have been grown on the glass surface at the expense of the monolithic structure.

Afterwards, numerous zeolite coatings on silicon carbide (SiC) supports were achieved. α -SiC foams, exhibiting a duplex macroporous structure, were successfully coated with different zeolite types. Indeed, this relatively inert material was partly recrystallized into ANA, LTA and MFI zeolites. Different gel compositions have been investigated to analyze their effect on zeolite coatings, including syntheses without additional Si-source. ANA/ α -SiC composites were unexpectedly obtained through the self-recrystallization of silicon contained in α -SiC substrate. In addition, the size of icositetrahedral ANA crystals was controlled to nearly 35 μm , thanks to α -SiC open cells templating effect. The quantity of zeolite coating as well as the coverage by ANA zeolite crystals on α -SiC surface were determined by both SEM observations and adsorption measurements.

Finally, catalytic activities of ANA/ α -SiC and ZSM-5/ β -SiC composites were evaluated in the methanol to hydrocarbons reaction. While ANA/ α -SiC composite allowed to convert methanol into dimethylether, high selectivities toward light olefins were achieved over ZSM-5/ β -SiC composite.

1. Introduction

The microporous structure as well as the defined pore architecture and size of zeolites are well established. In addition, these crystalline aluminosilicates have found widespread applications as ionic exchangers [1], molecular sieves [2], cracking catalysts [3] and more recently as confinement media [4]. Zeolites are considered as *green* catalysts. A proper control of their chemical composition and microstructure is ensured during the synthesis. In contrast, zeolites are mainly used in fixed beds in the form of randomly packed microgranules or extrudated pellets having few millimeters in size. Their macrostructure remains therefore fairly undefined.

Although zeolites exhibit many advantages, their industrial implementation can be hindered by the following drawbacks in a fixed bed-use; (i) high-pressure drop, (ii) limited heat and mass transports, (iii) axial dispersion leading to loss of selectivity, and (iv) susceptibility to fouling by dust [5].

During past decades, a deeper attention has been paid to the development of zeolite coatings on various macro-shaped supports [6]. Studying new active phase formulations, numerous researches have also been devoted to the development of structured composites (catalyst + support), which could provide an easier access of the reactants to the active sites

[1] S. Kulprathipanja, *Zeolites in Industrial Separation and Catalysis*, Wiley-VCH Verlag GmbH & Co. KGaA, Weinheim, Germany, **2010**.

[2] A. Corma, *Chem. Rev.* **1997**, *97*, 2373–2420.

[3] a) T. F. Degan, *Top. Catal.* **2000**, *13*, 349–356. b) F. V. Pinto, A. S. Escobar, B. G. de Oliveira, Y. L. Lam, H. S. Cerqueira, B. Louis, J.-P. Tessonnier, D. S. Su, M. M. Pereira, *Appl. Catal. A* **2010**, *388*, 15–21. c) B. Louis, M. M. Pereira, F. M. Santos, P. M. Esteves, J. Sommer, *Chem. Eur. J.* **2010**, *16*, 573–576.

[4] a) A. Corma, S. Zones, *Zeolites and Catalysis Synthesis, Reactions and Applications*, Wiley-VCH Verlag GmbH & Co. KGaA, Weinheim, Germany, **2010**. b) A. Olmos, S. Rigolet, B. Louis, P. Pale, *J. Phys. Chem. C* **2012**, *116*, 13661–13670. c) P. M. Esteves, B. Louis, *J. Phys. Chem. B* **2006**, *110*, 16793–16800.

[5] a) S. Ivanova, B. Louis, M.-J. Ledoux, C. Pham-Huu, *J. Am. Chem. Soc.* **2007**, *129*, 3383–3391. b) D. Edouard, M. Lacroix, C. Pham, M. Mbodji, C. Pham-Huu, *AIChE J.* **2008**, *54*, 2823–2832. c) M. N. Kashid, A. Renken, L. Kiwi-Minsker, *Chem. Eng. Sci.* **2011**, *66*, 1480–1489. d) A. Renken, L. Kiwi-Minsker, *Adv. Catal.* **2010**, *53*, 47–122.

[6] a) A. Cybulski, J. A. Moulijn, Eds., *Structured Catalysts and Reactors*, CRC, Taylor & Francis Group, United States, **2005**. b) S. Lopez-Orozco, A. Inayat, A. Schwab, T. Selvam, W. Schwieger, *Adv. Mater.* **2011**, *23*, 2602–2615. c) V. Valtchev, M. Smihi, A.-C. Faust, L. Vidal, *Angew. Chem. Int. Ed.* **2003**, *42*, 2782–2785.

and also avoid mass transport limitations [7]. There have been various attempts to grow of zeolite crystals on macroscopic inert materials. One can cite for instance, both meso- and macroporous glass monoliths [8], alumina [9], metals [10], ceramics [5,11], sacrificial biological supports [6c,12], which have been used as supports for the development of structured catalytic beds.

Among aforementioned materials, zeolite synthesis on siliceous materials represents a great advantage for the coating of zeolites. Indeed, according to the silicon present, a deeper affinity between crystalline Si zeolite and amorphous Si support could be expected. Louis et al. made an attempt to allow the crystallization of zeolites on porous glass supports under strong alkaline conditions [8d]. The glass monolith was partially transformed into zeolite crystals giving birth to a composite material with a bimodal pore system.

Following this strategy, the aim of the present work was to prepare new binderless and structured ZSM-5 coatings *via* an *in-situ* hydrothermal synthesis on perfectly defined glass and silicon carbide monoliths. Furthermore, silicon carbide (SiC) appears as a promising support due to its robustness. Indeed, these porous ceramics exhibit the necessary intrinsic properties required to become valuable candidates as zeolite support. In general, silicon

-
- [7] a) M. T. Kreuzer, F. Kapteijn, J. A. Moulijn, *Catal. Today* **2006**, *111*, 111–118. b) R. J. Berger, E. H. Stitt, G. B. Marin, F. Kapteijn, J. A. Moulijn, *CATTECH* **2001**, *5*, 30–60. c) N. Navascues, M. Escuin, Y. Rodas, S. Irusta, R. Mallada, J. Santamaria, *Ind. Eng. Chem. Res.* **2010**, *49*, 6941–6947. d) M. P. Pina, R. Mallada, M. Arruebo, M. Urbiztondo, N. Navascués, O. de la Iglesia, J. Santamaria, *Microporous Mesoporous Mater.* **2011**, *144*, 19–27.
- [8] a) M. Rauscher, T. Selvam, W. Schwieger, D. Freude, *Microporous Mesoporous Mater.* **2004**, *75*, 195–202. b) F. Ocampo, H. Yun, M. M. Pereira, J.-P. Tessonnier, B. Louis, *Cryst. Growth Des.* **2009**, *9*, 3721–3729. c) B. Louis, F. Ocampo, H. Yun, J.-P. Tessonnier, M. M. Pereira, *Chem. Eng. J.* **2010**, *161*, 397–402. d) B. Louis, C. Tezel, L. Kiwi-Minsker, A. Renken, *Catal. Today* **2001**, *69*, 365–370.
- [9] N. van der Puil, F. M. Dautzenberg, H. van Bekkum, J. C. Jansen, *Microporous Mesoporous Mater.* **1999**, *27*, 95–106.
- [10] a) B. Louis, P. Reuse, L. Kiwi-Minsker, A. Renken, *Appl. Catal. A* **2001**, *210*, 103–109. b) S. Mintova, J. Hedlund, B. Schoeman, V. Valtchev, J. Sterte, *Chem. Comm.* **1997**, 15–16. c) V. Valtchev, S. Mintova, *Zeolites* **1995**, *15*, 171–175.
- [11] a) A. Zampieri, P. Colombo, G. T. P. Mabande, T. Selvam, W. Schwieger, F. Scheffler, *Adv. Mater.* **2004**, *16*, 819–823. b) A. Zampieri, H. Sieber, T. Selvam, G. T. P. Mabande, W. Schwieger, F. Scheffler, M. Scheffler, P. Greil, *Adv. Mater.* **2005**, *17*, 344–349. c) F.-C. Buciuman, B. Kraushaar-Czarnetzki, *Catal. Today* **2001**, *69*, 337–342. d) G. B. F. Seijger, O. L. Oudshoorn, W. E. J. van Kooten, J. C. Jansen, H. van Bekkum, C. M. van den Bleek, H. P. A. Calis, *Microporous Mesoporous Mater.* **2000**, *39*, 195–204. e) S. Ivanova, B. Louis, B. Madani, J.-P. Tessonnier, M.-J. Ledoux, C. Pham-Huu, *J. Phys. Chem. C* **2007**, *111*, 4368–4374. f) S. Ivanova, E. Vanhaecke, B. Louis, S. Libs, M.-J. Ledoux, S. Rigolet, C. Marichal, C. Pham, F. Luck, C. Pham-Huu, *ChemSusChem* **2008**, *1*, 851–857.
- [12] a) A. Zampieri, G. T. P. Mabande, T. Selvam, W. Schwieger, A. Rudolph, R. Hermann, H. Sieber, P. Greil, *Mater. Sci. Eng. C* **2006**, *26*, 130–135. b) M. W. Anderson, S. M. Holmes, N. Hanif, C. S. Cundy, *Angew. Chem. Int. Ed.* **2000**, *39*, 2707–2710.

carbide polymorphs possess high thermal conductivity, high mechanical strength, excellent resistance to oxidation, chemical inertness and ease of shaping [13]. In contrast to β -polymorph, α -SiC demonstrates a higher thermal conductivity and better resistance to attrition [14]. SiC porous substrates have been widely used as filters, membranes, catalyst supports, thermal insulation, gas-burner media, and refractory materials owing to their superior properties, such as: low bulk density, high permeability, high temperature stability, and erosion resistance [15]. Silicon carbide possesses a low density which significantly reduces the fraction of useless weight within the overall weight of the composite. Finally, β -SiC synthesized according to the shape-memory-synthesis [13] exhibits a medium surface area, rendering it suitable for the dispersion of zeolite crystals on its surface [5,11e].

2. Structured catalyst synthesis

2.1 Zeolite coated on glass monolith

2.1.1. Glass support

The glass matrix used for the preparation of structured zeolitic materials was provided by the center for future technology from Korea (Dr. H. S. Yun, KIMS).

Gel pastes for robotic deposition were prepared using tetraethyl orthosilicate (TEOS) as inorganic precursor, a triblock copolymer, poly(ethylene oxide)-poly(propylene oxide)-poly(ethylene oxide) (Pluronic P123, $\text{EO}_{20}\text{PO}_{70}\text{EO}_{20}$, $M_{\text{av}} = 5750$), as meso-structure-directing agent through an evaporation-induced self-assembly process, and methyl cellulose (MC,

[13] a) M. J. Ledoux, C. Pham-Huu, *Cattech* **2001**, *5*, 226–246. b) W. J. Lackey, D. P. Stinton, G. A. Cerny, A. C. Schaffhauser, L. L. Fehrenbacher, *Adv. Ceram. Mater.* **1987**, *2*, 24–30.

[14] a) I.-H. Song, I.-M. Kwon, H.-D. Kim, Y.-W. Kim, *J. Eur. Ceram. Soc.* **2010**, *30*, 2671–2676. b) M. Lacroix, P. Nguyen, D. Schweich, C. Pham Huu, S. Savin-Poncet, D. Edouard, *Chem. Eng. Sci.* **2007**, *62*, 3259–3267.

[15] a) P. Sepulveda, *Am. Ceram. Soc. Bull.* **1997**, *76*, 61–65. b) F. F. Lange, K. T. Miller, *Adv. Ceram. Mater.* **1987**, *2*, 827–831. c) J. Saggio-Woyansky, C. E. Scott, W. P. Minnear, *Am. Ceram. Soc. Bull.* **1992**, *71*, 1674–1682.

$M_{av} = 86000$), acting both as semi-macro-structure-directing agent and binder [16]. In a typical synthesis, 2.28 g of P123 was dissolved in 18.67 mL of ethanol (EtOH). Stock solutions, which were prepared by mixing 6 mL of TEOS, 0.95 mL of HCl (1M), 7.62 mL of EtOH and 2.86 mL of H₂O, were added to this solution after stirring for 1 h separately and were vigorously stirred together for another 4 h at 40 °C. The reactant solution, sealed and aged at 40 °C for 24 h without stirring, was then evaporated at 40 °C for 10-24 h without the seal until the volume of solution reduces to one-fifth. Later, 1.4 g of MC was then mixed with this solution to render homogeneous the gel paste. 3D scaffolds were fabricated by directly extruding the paste gel onto a heated substrate using a robotic deposition device. A commercially available gantry robotic deposition apparatus was used with specially altered systems such as an actuator and heat-control to verify the right position of deposition nozzle for scaffold fabrication. The gel paste housed in the syringe was deposited through a cylindrical nozzle (17-26 gauge (G), 24 G ($\approx 500 \mu\text{m}$) generally used). A linear actuator served to depress the plunger of the syringe at a fixed speed such that the volumetric flow rate could be precisely controlled. The extrusion strength and speed were set to 200-250 $\mu\text{L}/\text{min}$ and 5-10 mm/s, respectively, depending on the viscosity of the gel paste. Shapes and sizes of scaffold can be designed at discretion and were automated by computer system. The fabricated organic-inorganic hybrid scaffolds were aged at 40 °C for 24 h and treated at 500-700 °C to remove the organic polymer template for obtaining the final calcined porous scaffolds.

The glass monolith exhibits three types of porosities (Figure 6.1): giant sized pores (300-500 μm) produced by the rapid prototyping technique (Figure 6.1a), macro-sized pores (10-100 μm) formed by of methyl cellulose template (Figure 6.1b) and meso-sized pores (4-5 nm) having 2D hexagonal pore structure produced by P123 triblock copolymer self-assembly (Figure 6.1c).

[16] a) H. Yun, S. Kim, Y. Hyun, S. Heo, J. Shin, *Chem. Mater.* **2007**, *19*, 6363–6366. b) H. Yun, S. Kim, Y. Hyeon, *Chem. Comm.* **2007**, 2139–2141.

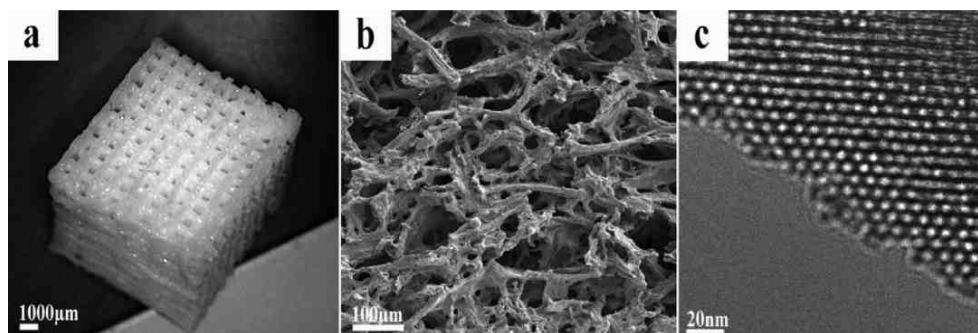


Figure 6.1 Optical (a), FE-SEM (b), and TEM (c) images of hierarchically giantporous (a), macroporous (b), and mesoporous (c) glass monolith

2.1.2. Preparation of the zeolite coating on glass monolith

The zeolite coating was performed according to an earlier procedure developed in the laboratory [8b]. The gel was prepared at room temperature by adding sodium aluminate, sodium chloride, tetrapropylammonium hydroxide and tetraethyl orthosilicate in distilled water. The molar ratio was as follows: NaAlO_2 : NaCl : TPAOH: TEOS: H_2O = 0.15: 1.93: 1.20: 4.02: 1000. The gel was stirred and aged for 150 min. Afterwards, a piece of mesoporous glass monolith (439 mg) was added to the mixture. The gel was then poured into a 75 mL Teflon-lined autoclave containing the support. The gel was heated within 1 h up to 170 °C and pursued for 14 h. The glass monolith was recovered by filtration over Nylon membrane and washed with water. Finally, the composite was calcined at 550 °C in air overnight to remove the template.

2.1.3. Glass composite characterization

After filtration, we obtained both the piece of mesoporous glass and unsupported zeolite powder. However, ZSM-5/glass monolith composite was partially dissolved during the synthesis. This phenomenon is attributed to the strong alkalinity of the medium required for zeolite formation ($\text{pH} = 13$). Hence, several pieces of starting monolith could be recovered and analyzed.

SEM analyses

Figure 6.2 shows SEM micrographs of ZSM-5/glass monolith composite at different magnifications. According to alkaline medium, the glass grid was partially dissolved during the reaction. Nevertheless, one can assess the characteristic prismatic crystals of MFI structure, which homogeneously cover the surface of the glass substrate. At higher magnification (Figure 6.2 right) it appears that ZSM-5 crystals reached 8 μm whereas 3 μm in length was achieved for the crystals present in unsupported powder.

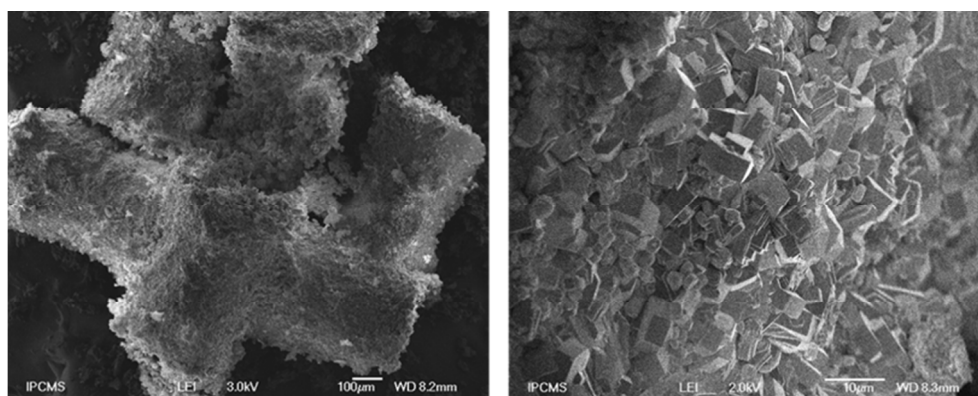


Figure 6.2 SEM images of ZSM-5/glass monolith at different magnifications

TEM analyses

The microstructure of alkaline-prepared composite was investigated by transmission electron microscopy. TEM images of ZSM-5/glass monolith are presented in Figure 6.3 and shows the core of ZSM-5 crystals.

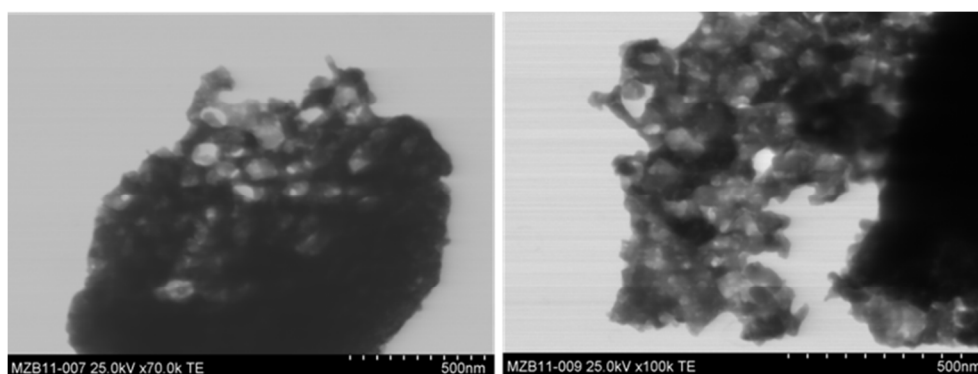


Figure 6.3 TEM images of ZSM-5/glass monolith

The partial dissolution of the glass monolith allows to form mesoporous ZSM-5 crystals. Indeed, the initial meso-structured glass monolith recrystallized immediately into ZSM-5 crystals while maintaining mesoporosity properties, thus leading to the formation of meso-/microporous zeolite.

2.2 Zeolite coatings on silicon carbide

2.2.1. Silicon carbide supports

β -SiC beads supports were obtained from SICAT company. Furthermore, α -SiC foams were prepared at the Engineering Ceramics Group (KIMS) [17]. α -SiC was added as inert filler while Al_2O_3 and Y_2O_3 were used as sintering additives. Two kinds of pore formers: expandable microspheres of approximately 38 μm (461DU40, Expancel, Sundsvall, Sweden) and poly(methyl methacrylate) (PMMA) spheres (particle size 8 μm , Sunjin, Korea), were used to generate duplex pore structure, (Figure 6.4). SEM micrographs clearly show the sponge structure of α -SiC foam provided by macropores of approximately 7 μm .

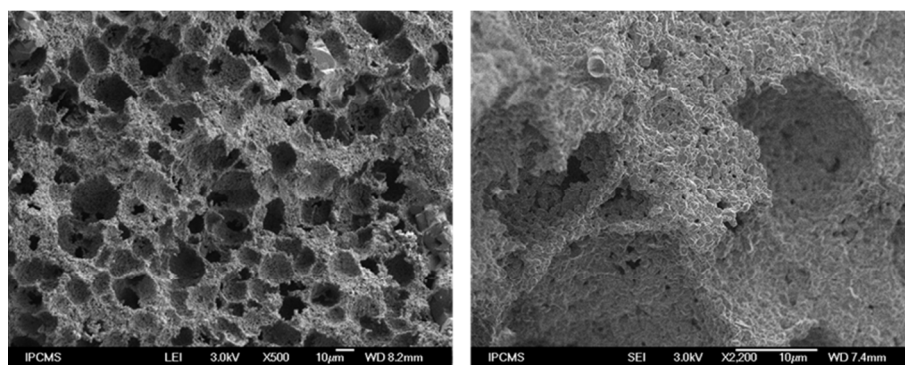


Figure 6.4 SEM images of α -SiC foam

2.2.2. Procedure for zeolite coatings on SiC

Prior to zeolite syntheses, α - and β -silicon carbide monolith pieces (0.2 g – 0.5 g) have been calcined in static air at 550 °C during 18 h to obtain a SiO_2 layer at the topmost surface.

[17] I.-H. Song, I.-M. Kwon, H.-D. Kim, Y.-W. Kim, *J. Eur. Ceram. Soc.* **2010**, *30*, 2671–2676.

Several gel compositions were used to prepare zeolite/SiC composites and the molar ratios between reactants are summarized in Table 6.1. Entries 1 to 13 and 16 to 18 concern the preparation in alkaline medium on α -SiC and β -SiC supports, respectively. Whereas, entries F14 and F15 report the zeolite coatings conditions on α -SiC in fluoride medium. The gel was vigorously stirred and aged for several hours at room temperature. The mixture was then transferred to an autoclave (75 mL) and heated at 170 °C under autogenous pressure for several days (Table 6.1). Again, the solid formed was filtered over a nylon membrane and dried in an oven at 115 °C overnight. Finally, sonication tests (VWR ultrasonic cleaner, 45 kHz, 80 W) were performed during 5 min on several zeolite/ α -SiC composites to verify the coating strength. A maximum 2% mass loss for all composites was obtained after sonication.

Table 6.1 Summary of synthesis conditions of zeolites coatings on SiC supports

Composite	NaAlO ₂	TEOS	TPAOH/ TPABr	NaCl/ NH ₄ F	NaOH	H ₂ O	Ageing [h]	SiC [g]	Duration [h]
1	1	27	8	13	-	5555	2	2.62	66
2	1	-	8	13	-	5555	2	0.77	48
3	1	-	8	13	-	5555	2	0.29	60
4	1	-	8	13	-	5555	2	0.31	333
5	1	-	8	13	-	5555	2	0.11	768
6	1	-	8	13	-	5555	2	0.33	2300
7	1	-	14	-	13	5555	2	0.23	192
8	1	-	14	-	13	5555	2	0.07	333
9	1	-	22	-	13	5555	2	0.15	192
10	1	-	14	-	8	5555	2	0.13	97
11	1	-	14	-	8	5555	2	0.15	192
12	1	-	14	-	8	5555	2	0.10	504
13	1	-	22	-	8	5555	2	0.11	258
F14	1	-	6	184	-	7831	3	0.68	138
F15	1	164	6	184	-	6505	3	0.29	138
16	1	-	14	-	8	5555	2	0.16	185
17	1	-	14	-	8	5555	2	0.10	504
18	1	-	8	13	-	5555	2	0.29	64

Furthermore, zeolite coatings on β -SiC beads were prepared in a larger scale with the use of TEOS to enhance the zeolite layer thickness. Thus, the procedure was adapted from Ivanova *et al.* [11e]. The gel was as follows: NaAlO₂: TPAOH: NaCl: TEOS: H₂O = 1: 17: 26: 43: 7690. After 4 h of ageing, β -SiC beads (2.55 g, ~ 30 beads) were added to the mixture and transferred to a Teflon-lined autoclave and heated at 170 °C for 66 h. Afterwards, β -SiC beads were filtrated over a nylon membrane and washed with distilled water. β -SiC composites were divided in two parts, one being re-engaged in a second coating procedure. These beads were placed in a fresh solution having the same composition as the previous step. Both series of β -SiC beads were sonicated during 5 min to remove loosely attached crystals. The organic template was removed by calcination in air at 550 °C overnight. The materials, named ZSM-5/ β -SiC single layer and ZSM-5/ β -SiC double layer, were then three times ion-exchanged with an aqueous 1M NH₄NO₃ solution for 3 h at 65 °C, and subsequently calcined at 550 °C overnight to leave the zeolite H-form.

2.2.3. Zeolite/SiC composites characterization

SEM analyses

All as-synthesized structured materials were analyzed by SEM. It is noteworthy that the addition of TEOS as an external silica-source led to the sole formation of MFI-zeolite crystals onto macroporous SiC foam (Figure 6.5-1 and Figure 6.8-F15).

In contrast, analcime (ANA) crystals were observed to grow *via* the self-recrystallization procedure of the SiC substrate (entries 2-5). Likewise, Ivanova *et al.* reported that sodium cation often plays the role of the template during ANA crystallization [18]. It is therefore shown that the absence of any TEOS extra-addition led to the crystallization of high Al-containing ANA framework. By following this non-conventional strategy for the coating, a high Al-content zeolite material was produced with respect to the *a priori* expected growth (due to TPA⁺ template presence) of low Al content MFI zeolite. This result will be discussed below. Moreover, the use of sodium aluminate in the gel instead of

[18] J. M. Martínez Blanes, B. M. Szyja, F. Romero-Sarria, M. Á. Centeno, E. J. M. Hensen, J. A. Odriozola, S. Ivanova, *Chem. Eur. J.* **2013**, *19*, 2122–2130.

aluminum sulfate, should allow the growth of analcime's porous form [19]. The Al content of α -SiC foam (due to Al_2O_3 presence) could further favor the formation of high Al-containing ANA structure. SEM observations have shown that crystals having diameters up to $60\ \mu\text{m}$ were produced in the solution (Figure not presented), with respect to the narrow crystal size distribution of their coated counterparts. This phenomenon is probably due to a slow raise of silicate-species concentration in the medium *via* dissolution/recrystallization processes.

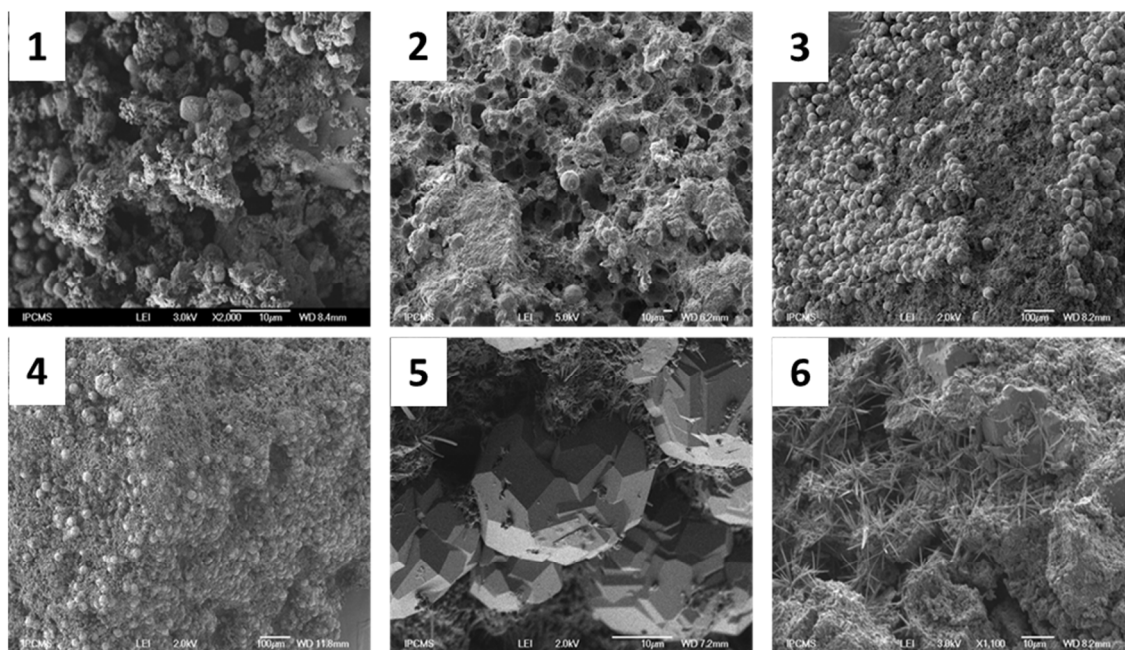


Figure 6.5 SEM images of as-synthesized structured materials on α -SiC support *via* alkaline route (entries 1 to 6 in Table 6.1)

It is noteworthy that a relationship between synthesis duration and α -SiC surface coverage by crystals (at least qualitatively) can be built. A low coverage was achieved on α -SiC surface after 48 h synthesis duration (Figure 6.5-2) by few icositetrahedral crystals. By prolonging the coating procedure up to 768 h, the presence of more crystals could be evidenced by SEM (Figure 6.5-5). Nevertheless, a higher increase in synthesis duration led to the formation of threads and any ANA crystals were observed. According to the metastable property of zeolites, one could assume that a longer synthesis duration induces a shift in gel composition and thus to a new zeolite phase formation (Figure 6.5-6).

[19] H. Robson, K. P. Lillerud, Eds., *Verified Syntheses of Zeolitic Materials*, Elsevier B.V., Amsterdam, **2001** pp. 107-109.

The morphology of the crystal and the nature of the coating usually involve an aggregation process following either a layer-by-layer or an island growth-mode [20]. A growth unit is therefore adsorbed on the growing face and migrates to find its optimum location. Hence, the aggregate may behave as a nutrient-recipient pair in consistency with Thompson's "tugging-chain" mechanism [21]. Besides, the dissolution of these nuclei can lead to the further growth of zeolite crystals within the gel.

Figure 6.6 and Figure 6.7 show SEM micrographs of zeolite coatings on α -SiC synthesized with different gel compositions. A rise in alkalinity through the replacement of NaCl by NaOH and increase in TPAOH concentration seems to inhibit the formation of ANA phase. Indeed, the gel composition of entry 7 induced the growth of threads on the α -SiC outer surface. Unfortunately, XRD analyses did not permit to determine the zeolite topology since no additional diffraction lines except those of α -SiC were observed. An increase in synthesis duration or in TPAOH amount, led to any crystal coating (entries 8 and 9 in Table 6.1).

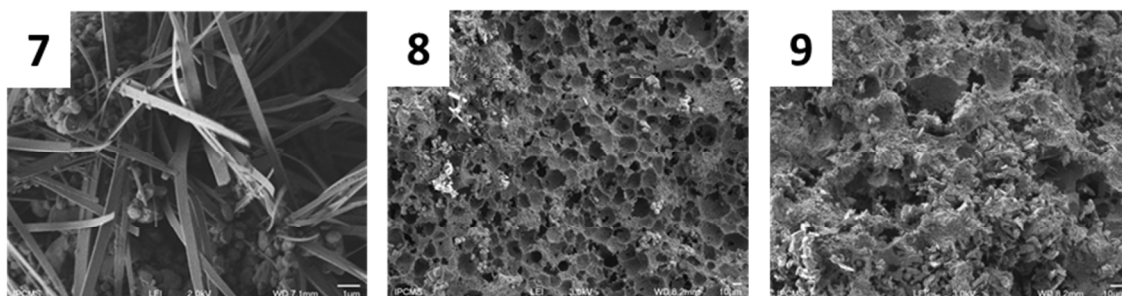


Figure 6.6 SEM micrographs of as-synthesized structured materials on α -SiC support *via* alkaline route [entries 7 to 9 in Table 6.1]

In addition, a lower amount of NaOH with respect to entry 7, resulted in the development of cubic crystals of approximately 20 μm (Figure 6.7-10). This crystal morphology let us speculate the formation of low Si/Al containing LTA zeolite [22]. Although

[20] M. Volmer, *Kinetik der Phasenbildung*, Steinkopff, Dresden, **1939**.

[21] a) R. W. Thompson, in *Molecular Sieves* (Eds.: H.G. Karge, J. Weitkamp), Springer-Verlag, Berlin, Germany, **1998**. b) S. Wong, V. Kitaev, G. A. Ozin, *J. Am. Chem. Soc.* **2003**, *125*, 15589–15598.

[22] H. Robson, K. P. Lillerud, Eds., *Verified Syntheses of Zeolitic Materials*, Elsevier B.V., Amsterdam, **2001** pp. 182-183.

LTA synthesis requires tetramethylammonium hydroxide (TMAOH) as a template [23], it has been shown that A zeolite can be obtained without the use of organic template [24]. Likewise, similarly to the formation of ANA zeolite, the gel and α -SiC foam compositions could enhance the support recrystallization into LTA topology.

Formation of threads was obtained *via* longer synthesis duration for entry 11 (Figure 6.7-11) compared with entry 10 (*i.e.*, 192 and 97 h, respectively).

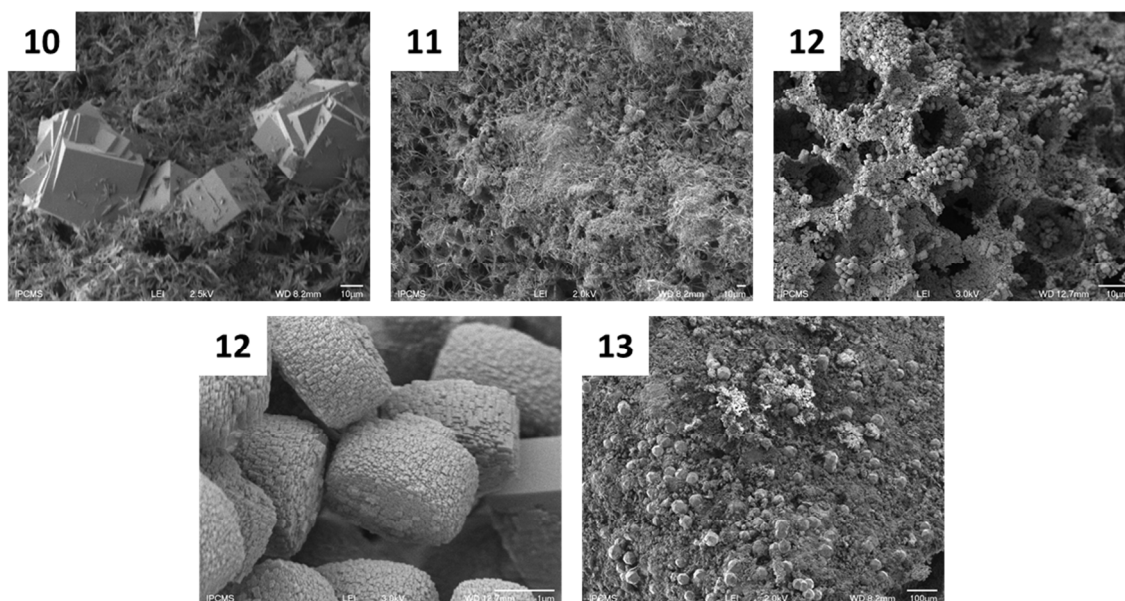


Figure 6.7 SEM images of as-synthesized structured materials on α -SiC support *via* alkaline route [entries 10 to 13 in Table 6.1]

In contrast, a synthesis duration of 504 h (entry 12 and Figure 6.7-12) allowed the recrystallization of surface into MFI type crystals. Indeed, typical coffin-shape ZSM-5 crystals with highly rough surfaces were coated on α -SiC foam. Surprisingly, ANA crystals (entry 13) have been obtained while increasing the TPAOH concentration with respect to entry 12.

The procedure without any additional Si-source addition (entry F14) in fluoride medium resulted in ZSM-5 zeolite formation, but at the expense of the SiC foam morphology, as shown in Figure 6.8-F14.

[23] L. Tosheva, V. Valtchev, *Chem. Mater.* **2005**, *17*, 2494–2513.

[24] S. Alfaro, C. Rodríguez, M. A. Valenzuela, P. Bosch, *Mater. Lett.* **2007**, *61*, 4655–4658.

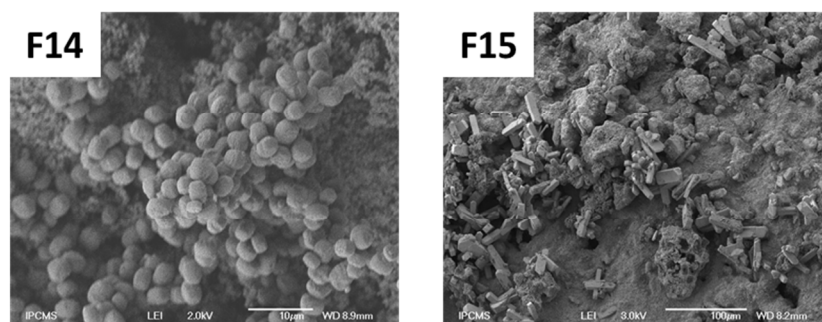


Figure 6.8 SEM images of as-synthesized zeolites on α -SiC support *via* fluoride route [entries F14 and F15 in Table 6.1]

To complete these results and understand the influence of α -SiC support, we have performed similar syntheses on β -SiC beads. The formation of threads for entries 16 and 17 was achieved over β -SiC beads (Figure 6.9-16 and 17) while using similar gel compositions as entries 11 and 12, respectively. In contrast, the use of the same gel composition as entry 3, leading to ANA/ α -SiC composite, resulted in LTA cubic crystals formation (Figure 6.9-18). The shift from α - to β -polymorph seriously influences the nature of the zeolite. In spite of using an additional Si source in the gel, the support composition and structure play an important role in the recrystallization of the SiC supports to produce zeolite crystals. Although a high Al-containing zeolite (*i.e.*, LTA) has been coated on β -SiC beads, ANA crystals were not able to form using the same gel composition.

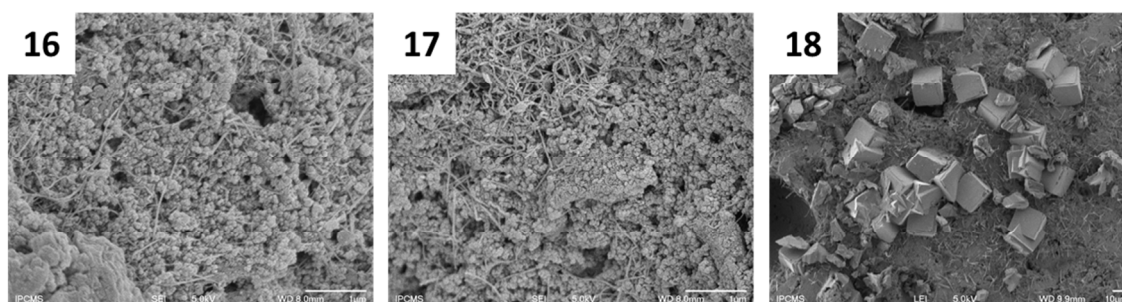


Figure 6.9 SEM images of as-synthesized zeolites on β -SiC beads *via* alkaline route [entries 16 to 18 in Table 6.1]

Finally, Figure 6.10 presents SEM micrographs of single and double layered ZSM-5/ β -SiC composites prepared in the presence of Si source. Although, the coverage of starting carrier is nearly homogeneous, and the shape of the support was not altered during the synthesis, SEM micrograph of single layered ZSM-5/ β -SiC composite reveals the formation of

two kinds of ZSM-5 crystals (Figure 6.10a-c). Indeed, typical coffin-shape and highly rough crystals were coated on β -SiC surface and exhibited heterogeneous sizes (2 and 9 μm in length).

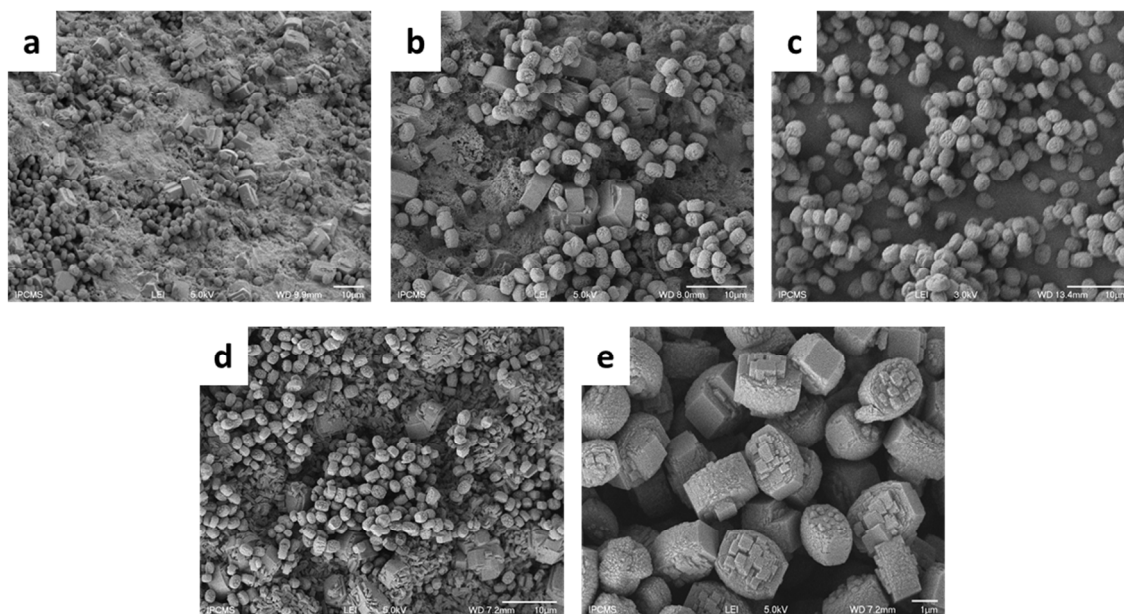


Figure 6.10 SEM micrographs of (a-c) single and (d,e) double-layered ZSM-5/ β -SiC composites

Moreover, after repeated coating procedures unsupported powder was formed (Figure 6.10c and e). Crystals exhibit similar size and morphology as the smaller crystals coated on the support raising approximately 2-3 μm in length. The second coating procedure allowed to increase the zeolite layer thickness since no more β -SiC surface is visible on SEM images. Likewise the single-layered composite, ZSM-5 crystals also exhibit two distinct morphologies with highly heterogeneous sizes (*i.e.*, 2 and 9 μm in length).

XRD analyses

Figure 6.11 presents XRD patterns of bare α -SiC, ANA/ α -SiC composite and detached powdered material.

Figure 6.11a presents the XRD patterns of the support prior to the synthesis. The pattern of pristine support confirms the sole presence of α -type polymorph for the silicon carbide substrate. Figure 6.11b confirms the presence, after the coating procedure, of two main characteristic diffraction lines of ANA structure at $2\theta = 15.88^\circ$ and $2\theta = 26.08^\circ$, corresponding to (211) and (400) planes, respectively [19].

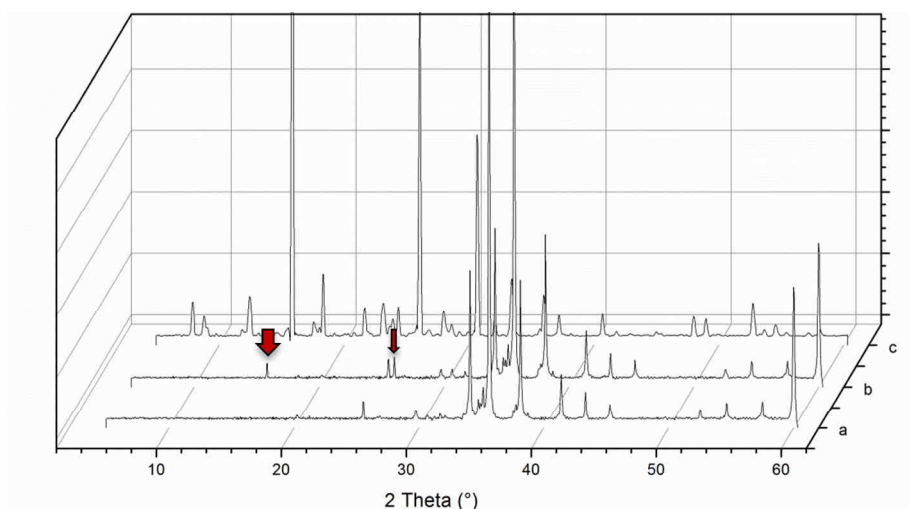


Figure 6.11 XRD patterns of a) α -SiC, b) ANA/ α -SiC composite and c) recovered powder

Likewise to ANA/ α -SiC, unsupported powder also exhibits pure ANA zeolite structure (Figure 6.11c). These XRD data thus support the successful growth of ANA crystals on α -SiC surface. Besides, pure ANA phase has been detected for powdered material recovered at the bottom of the reactor vessel.

Tentative mechanism of ANA crystals growth on α -SiC surface

The experimental factors which govern the self-assembly of zeolite crystals onto support surfaces in thin films or other coating morphologies are not well understood yet. Nevertheless, the T-O-T bond making and bond breaking (where T = Si or Al), based upon nucleophilic reactions, facilitate structural modifications catalyzed by hydroxyl ions. Furthermore, it appears that this strategy of self-transformation of α -SiC support, allows the formation of ANA zeolite crystals, which can grow with defined size but also *via* a tailored surface coverage depending on operating conditions (pH, mineralizer nature, time).

Figure 6.12 tentatively aims to summarize how the zeolite precursors organize at the vicinity of the SiC surface and allow a preferential growth of one zeolite type or another. After calcination at high temperature, barely reactive SiC support is partially oxidized at the topmost surface into a thin and homogeneous layer of an amorphous mixed phase of silica and silicon oxycarbide (SiO_xC_y) having few nanometers in size [11f].

After, the surface is placed in contact with the reagents present in the gel: aluminum source, template cation, sodium cation and eventually as shown in case B (Figure 6.12)

external silicon source (TEOS for MFI synthesis). The synthesis of MFI prismatic crystals can therefore be performed in open cells within the α -SiC foam but also outside and at the expense of the ceramic support (Figure 6.5-1) after a fluoride-mediated procedure. In contrast, ANA crystals grew mainly within the 38 μm cell aperture of α -SiC (case A, Figure 6.12). A shape-memory synthesis is therefore occurring restricting the size of final ANA crystals. At the present stage, it is rather easy to understand that a high Al-containing zeolite is produced since AlO_4^- species are present at the vicinity of support silanol groups and Na^+ cations. The hydroxyl anion mineralizer favors the condensation of aluminate and silicate species and hence zeolite nucleation.

A conventional synthesis of ANA zeolite requires only 24 h to produce giant 180 μm -sized crystals [19]. However, since no other source of silicon as SiC external surface is present in the gel, less Si-containing species are accessible and more time is required to partially dissolve it from the support. α -SiC is thus acting as a Si-nutrient reservoir. A slower crystal growth process is therefore taking place, being also confined within the foam cell (Figure 6.12-A). Na^+ cations, aluminates and hydroxyl anions can self-organize around this reservoir *via* van der Waals attractive forces. A prolongation of the synthesis duration is necessary for these ion pairs to assemble around the reservoir of nutrients surface, acting as a nodal point, and hence raise the number of centers allowing crystal growth. The self-assembly of these nutrient species can therefore be influenced by a higher rate of solvent evaporation with respect to the rate of crystal growth. Hence, the local conditions (water pressure, temperature, nutrient concentrations) probably induced an isothermal heating-evaporation-induced self-assembly effect (IHEISA) [25]. Moreover, by changing the nutrients concentrations, one may expect the formation of other high Al-containing zeolites as reported for coatings over glass monoliths [8b,c].

[25] S. Wong, V. Kitaev, G. A. Ozin, *J. Am. Chem. Soc.* **2003**, *125*, 15589–15598.

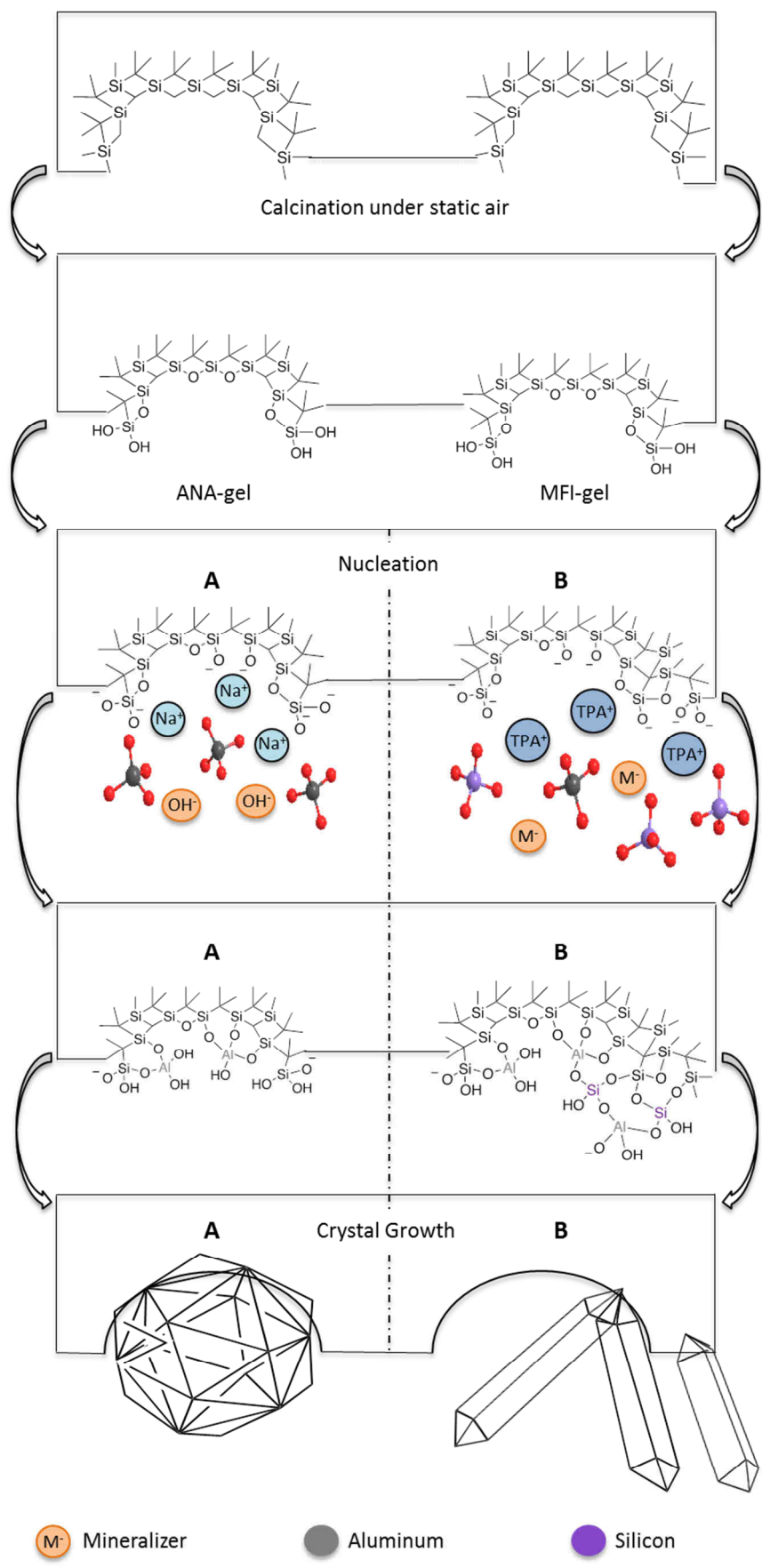


Figure 6.12 Schematic representation of zeolites crystal growth on α -SiC; **A** Alkaline route for ANA-growth, **B** Alkaline or fluorine route for MFI-growth

Whereas previous studies reported the use of covalent linkers [26], or proteins [27], to guide the assembly of zeolite crystals, we have successfully demonstrated that a controlled surface coverage by tailored-size ANA zeolite crystals can be achieved over α -SiC support and additionally without any chemical binder use.

Nevertheless, the question arises why ANA structure has been produced in our study? Zeolites are known to be metastable phases, from which it is possible to shift from one structure to another by modifying synthesis parameters (duration, alkalinity, concentration) [28,29]. At the present stage, it can be barely understood why only ANA crystals were grown on SiC surface. The recent outstanding contribution from Rimer *et al.* addressed the complexity to understand the zeolite phase(s) formation given the numerous parameters and even parameter combinations involved in zeolite synthesis [30].

In addition, it is worthy to mention that this approach can warrant further catalytic application, as already shown for MFI crystals coated on β -SiC polymorph [5a,b,11e] but also for membrane applications [31]. ANA zeolite was already used in membrane technology namely for the adsorption of surfactants [31c].

Textural properties analyses

In view of aforementioned results, we have focused our study to detailed textural properties analysis of ANA/ α -SiC composites. The evaluation of nitrogen adsorption isotherms and high-pressure mercury porosimetry techniques have been performed for as-synthesized catalysts. These results are summarized in Table 6.2. In parallel, pore-size distribution (PSD) curves are depicted in Figure 6.13. It can be clearly seen that all samples possess rather low inner surface area as well as an intrusion volume in line with meso- and/or macroporous structures of tested samples (Table 6.2 and Figure 6.13).

[26] a) K. Ha, Y. J. Lee, H. J. Lee, K. B. Yoon, *Adv. Mater.* **2000**, *12*, 1114–1117. b) Y. Yan, T. Bein, *J. Phys. Chem.* **1992**, *96*, 9387–9393.

[27] a) S. H. Um, G. S. Lee, Y. Lee, K. Koo, C. Lee, K. B. Yoon, *Langmuir* **2002**, *18*, 4455–4459. b) J. H. Jung, Y. Ono, K. Hanabusa, S. Shinkai, *J. Am. Chem. Soc.* **2000**, *122*, 5008–5009.

[28] C. S. Cundy, P. A. Cox, *Microporous Mesoporous Mater.* **2005**, *82*, 1–78.

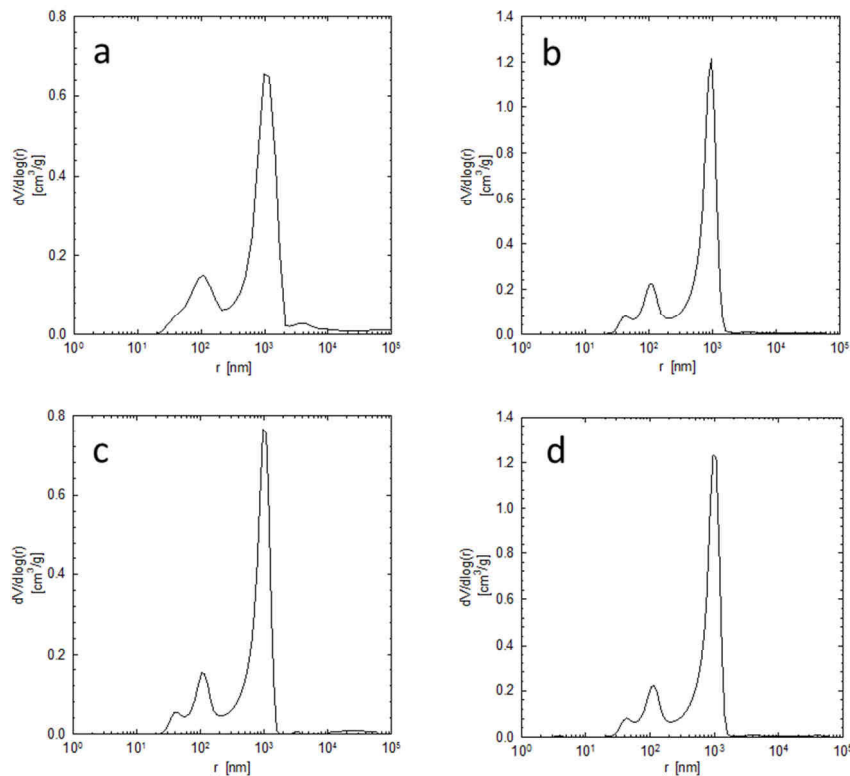
[29] R. W. Thompson, in R. C. A. Catlow, (Ed.), *Modelling of structure and reactivity in zeolites*, Academic Press, London, **1992**; pp. 231.

[30] M. Maldonado, M. D. Oleksiak, S. Chinta, J. D. Rimer, *J. Am. Chem. Soc.* **2013**, *135*, 2641–2652.

[31] a) J. Caro, M. Noack, *Microporous Mesoporous Mater.* **2008**, *115*, 215–233. b) B. S. Liu, D. C. Tang, C. T. Au, *Microporous Mesoporous Mater.* **2005**, *86*, 106–111. c) A. Potdar, A. Shukla, A. Kumar, *J. Memb. Sci.* **2002**, *210*, 209–225.

Table 6.2 Basic textural properties of ANA zeolites supported on α -SiC foams determined by nitrogen physisorption at 77 K and high-pressure mercury porosimetry methods

ANA/ α -SiC composite	S_{BET} [m ² /g]	S_{meso} [m ² /g]	V_{micro} [mm ³ _{liq} /g]	V_{intr} [cm ³ /g]	ρ_{He} [g/cm ³]	ρ_{Hg} [g/cm ³]	ϵ [-]
α -SiC	1.7	1.6	0.22	0.38	3.44	1.25	0.64
3 ^a (60 h)	3.0	3.0	0.33	0.43	3.40	1.22	0.64
4 ^a (333 h)	2.4	1.9	0.36	0.28	3.44	1.13	0.67
5 ^a (78 h)	2.5	2.3	0.32	0.44	3.40	1.21	0.64

 S_{BET} : BET surface area V_{intr} : total intrusion volume from high-pressure mercury porosimetry S_{meso} : mesopore surface area ρ_{He} : true (skeletal) density V_{micro} : micropore volume ρ_{Hg} : apparent (bulk) density^a correspond to composites presented in Table 6.1**Figure 6.13** Pore-size distribution curve for: (a) α -SiC support, (b) [entry 3 in Table 6.1] 60 h, (c) [entry 5] 728 h and (d) [entry 4] 333 h

PSD functions were evaluated from mercury porosimetry data. However, it must be stated that this technique provides reliable information about microstructure properties of SiC supports rather than zeolites. The results clearly indicate a bi-dispersed pore structure including macropores of SiC material (Figure 6.13). On the other hand, after the zeolite

coating process (Figure 6.13b–d), a new kind of pores appears with a mean pore radius of approximately 45 nm, which resulted in an increase of the inner surface area of supported zeolites. This type of porosity may be due to the cavities of the zeolite coating on α -SiC foam jagged surface. Nevertheless, the values of true densities as well as porosities are nearly identical for both SiC support and ANA/ α -SiC composites (Table 6.2).

These porosimetry values were used to estimate the surface coverage by zeolite crystals. This coverage can firstly be calculated in a mass/mass ratio, using the literature values of S_{BET} and V_{micro} for ANA zeolite [32] ($S_{\text{BET}} = 34.3 \text{ m}^2/\text{g}$, Total pore volume = $0.032 \text{ cm}^3/\text{g}$). The mass of used α -SiC piece with its density ($\rho = 1.01 \text{ g/cm}^3$) is converted to its volume and lastly, by a cubic approximation, to its surface according to Equation 6.1:

Equation 6.1
$$S = 6 \times \left(\frac{m}{\rho}\right)^{\frac{2}{3}} [\text{m}^2]$$

Finally, we can get a mass/surface ratio for the coating of ANA/ α -SiC composite, as listed in Table 6.3. The relatively high differences in the specific surface areas (ΔS_{BET}) between the α -SiC support and the composites prove that we are in the presence of porous ANA zeolite form. This difference reflects the rate of crystal growth on the surface of the entire material and is used for the calculation of surface coverage. These values indicate that an optimal surface coverage was achieved after 60 h where a maximum of ANA crystals were coated on the support.

Table 6.3 Estimation of the surface coating of different ANA/ α -SiC materials as a function of the synthesis duration

ANA/ α -SiC composite	S_{BET} [m^2/g]	ΔS_{BET} [m^2/g]	Coating rate [wt.%]	Surface coating ^b [g/m^2]	V_p [$\text{mm}^3_{\text{liq}}/\text{g}$]	ΔV_p [$\text{mm}^3_{\text{liq}}/\text{g}$]	Coating rate [wt.%]	Surface coating ^b [g/m^2]
α -SiC	1.7	0	0	0	2.44	0	0	0
3 ^a (60 h)	3.0	1.3	4.3	55.1	4.01	1.57	4.9	55.1
4 ^a (333 h)	2.4	0.7	2.3	29.2	3.15	0.71	2.2	27.5
5 ^a (728 h)	2.5	0.8	2.7	20.8	3.44	1	3.1	24.1

^a correspond to composites presented in Table 6.1

^b surface coatings correspond to coated zeolite mass related to geometric surface of the support

[32] S. N. Azizi, M. Yousefpour, *Z. Anorg. Allg. Chem.* **2011**, 637, 759–765.

Surprisingly, a further prolongation of the duration led to diminish the extend coating. This can be explained by the raise of silicates concentration at the support surface formed *via* the crystallization–dissolution of already produced zeolite nuclei [5a,8b].

3. Catalytic activity of zeolite coatings on SiC supports in MTH reaction

Methanol-to-Hydrocarbons reactions have been carried out according to the same experimental set-up as fluoride zeolites (Section Chapter 2.1.2.2) to evaluate the catalytic activities of zeolite coatings on SiC supports.

3.1 Catalytic activity of ANA/ α -SiC composite

The catalytic evaluation of ANA/ α -SiC composite (entry 5 in Table 6.1) was performed in methanol dehydration reaction. Table 6.4 presents the relative methanol conversion (where the powdered form was set to 100) and the selectivities toward dimethylether (DME) and C₂–C₄ olefins.

Table 6.4 Catalytic activity in the methanol dehydration of ANA/ α -SiC composite

Material	Mass [mg]	Relative conv. ^a [%]	S(DME) [%]	S(C ₂ -C ₄) [%]
α -SiC (calcined)	104	5	98.8	1.2
ANA/ α -SiC ^b	98	5	97.9	2.1
SiO ₂ /Al ₂ O ₃	60	100	99.9	0.1

^a Relative conversion was calculated by referring the conversion achieved by the composite to the one of powdered catalyst

^b ANA/ α -SiC composite corresponds to composite 5 in Table 6.1

It is noteworthy that the composite was slightly active in the reaction and led to produce DME at selectivities above 95%. The activity of calcined and therefore partially oxidized SiC support is nearly the same as ANA/ α -SiC composite. The only effect of ANA zeolite structure results in a slightly higher selectivity in ethylene, propylene and butylenes (2.1% versus 1.2%).

The catalytic test was also performed to estimate the surface coverage of the SiC support by the different zeolite phases (while assuming nearly the same catalytic behavior for non-supported and as-grown crystals onto the support). Hence, a coverage of 23.7 g/m² could be estimated for ANA/ α -SiC foam which is in line with the 24.1 g/m² calculated from textural properties measurements (Table 6.3).

3.2 Catalytic activity of ZSM-5/ β -SiC beads

Table 6.5 presents the catalytic activities of single and double-layered H-ZSM-5/ β -SiC composites in the MTO reaction. The corresponding unsupported powder produced during the coating procedure was also tested.

Table 6.5 Catalytic activity in the MTO reaction of ZSM-5/ β -SiC composites

Catalyst	Mass [g]	Conv. [%]	TOS [h]	Selectivities [%]				C ₃ /C ₂
				C ₂₌	C ₃₌	C _{2-C4}	C ₅₊	
ZSM-5 P1	0.060	66	2	19	43	83	17	2.3
ZSM-5/ β -SiC single layer	1.284	30	2	24	41	81	20	1.7
ZSM-5 P2	0.060	72	2	18	44	83	17	2.4
ZSM-5/ β -SiC Double layer	1.198	74	2	15	41	73	27	2.8

The methanol conversion of the double-coated ZSM-5/ β -SiC composite reached 74% and is higher when compared to the single-coated (*i.e.*, 30%) or both powdered zeolite catalysts, *i.e.*, 66% and 72% for unsupported ZSM-5 obtained after the first and second coating, respectively. These results are in line with previous studies from Ivanova *et al.* who

achieved nearly 80% methanol conversion over ZSM-5/ β -SiC foams [33]. The single layered ZSM-5/ β -SiC composite exhibits a slightly lower C_3/C_2 ratio with respect to its relative unsupported powder (*i.e.*, 1.7 vs. 2.3 for ZSM-5 P1), whereas a higher C_3/C_2 ratio (*i.e.*, 2.8) was achieved with the double-layered ZSM-5 composite. Besides, the double-layered ZSM-5/ β -SiC slightly favored the MTH process since it allowed to produce 27% of C_{5+} hydrocarbons (gasoline fraction).

Likewise ANA/ α -SiC composites, these catalytic results can be used to evaluate the surface coverage of β -SiC support after each coating procedure. The zeolite phase coated on β -SiC supports represented 2 and 5 wt.% after the first and second coatings, respectively. The second coating procedure allows to increase the zeolite layer by a factor of 2.5, representing approximately 62 mg of ZSM-5.

Finally, the stability of double-coated ZSM-5/ β -SiC composite over 71 h time on stream was investigated (Figure 6.14). Unfortunately, it appears that ZSM-5 crystals coated on β -SiC beads deactivated linearly after approximately 20 h on stream.

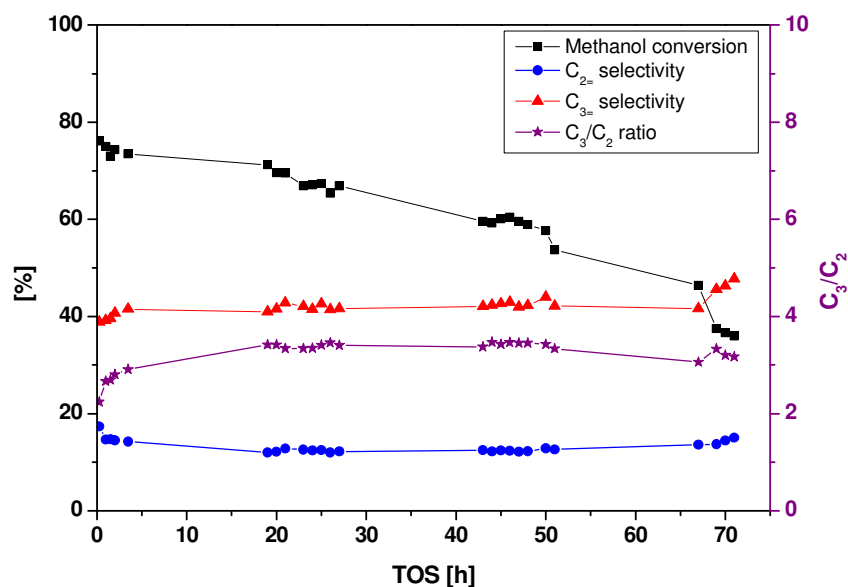


Figure 6.14 Methanol conversion as a function of time on stream for double-layered ZSM-5/ β -SiC composite

The rate of activity loss was linear versus time and achieved 36% in methanol conversion after 71 h on stream. The composite loss approximately 10% (absolute) of activity per 10 h. This loss in activity could be attributed to the macroscopic morphology of β -SiC beads which do not favor the zeolite dispersion compared with β -SiC foams [33]. However, in terms of selectivities toward ethene and propene, the double layer composite exhibited a stable behavior versus time: the C_3/C_2 ratio was kept higher than 3.

4. Conclusions

This chapter was focused on the design of structured catalytic beds using silicon-containing supports.

Firstly, the development of ZSM-5 coatings on glass monoliths was envisaged through the addition of external silicon source. SEM characterizations have shown the formation of zeolite crystals on the support surface but at the expense of the monolith structure. A partial dissolution of the glass support occurred due to the high alkalinity of the synthesis gel.

On the other hand, numerous zeolite coatings have been successfully achieved over two kinds of SiC support, *i.e.*, α -SiC foam and β -SiC beads. This study demonstrates that depending on the presence (or not) of an external Si-source and gel composition, different zeolites can be synthesized on α -SiC foam surface. MFI crystals could be grown following a conventional procedure (with the addition of Si nutrients). In contrast, ANA zeolite structure was formed without any additional Si-source. The surface coverage and the size of ANA crystals have been tailored in view of future application of these composites. Adapting the gel composition allowed to recrystallize the α -SiC foam surface into ZSM-5 and LTA crystals. Merging the huge number of zeolite structures, the possibilities to influence the synthesis conditions and the quantity of available silicon species in the ceramic, offer a high degree of freedom for engineering new zeolite/SiC composites with controlled size and shape, and thus suitable properties for targeted applications.

It is therefore recommended to use a self-recrystallization approach to guarantee high loadings of zeolite, along with a strong chemical bond with the substrate surface. In order to

overcome the difficult coating of active phases on α -SiC polymorph [13a], the control of self-assembly processes of non-siliceous zeolite precursors at the topmost SiC oxidized surface appears to be a suitable strategy. Indeed, the silica source is solely provided by the support surface containing oxygen-silicon species, thus one can expect a reorganization of the gel *via* solid–solid transformations of precursors having few nanometers in size.

Single and double-coated ZSM-5 on β -SiC beads, prepared with the use of an additional Si source, were tested in the MTH reaction. The zeolite crystals were well-anchored on the foam surface, resulting in a full-covered surface by crystals ranging from 2 to 9 μm in length. Under these reaction conditions, the composites exhibit interesting results in terms of conversion of methanol to propene as principal product as well as a high selectivity toward C_2 - C_4 fraction. Unfortunately, the composite stability versus time on stream was limited with a deactivation rate of nearly 1% per hour. However, its C_3/C_2 ratio remains stable during the reaction.

GENERAL CONCLUSIONS AND FUTURE PROSPECTS

This Thesis includes several studies involving the design of zeolites at different scales, *i.e.*, active site level, microstructure and reactor scale, and their applications in acid-catalyzed reactions.

Several approaches have been tempted to design zeolite catalysts depending on their future application. Throughout these studies, the link between the activities/selectivities of each catalyst and their intrinsic properties is highlighted.

The influence of both crystal size and acid site density of ZSM-5 zeolites was analyzed in the MTO reaction (Chapter 4). “Giant” ZSM-5 crystals with low acid site density have been prepared according to the fluoride route. Higher catalytic performances in MTO reaction, selectivity in propene and stability, were achieved over those catalysts. A compromise between crystal size, acid site density and crystallinity has to be settled to design a competitive MTP-catalyst. Moreover, our studies have demonstrated the possibility of replacing hydrofluoric acid, unappropriated for an industrial application, by hydrochloric acid. Further investigations such as mesoporosity introduction in such “giant” crystals could lead to enhanced catalytic performances.

The development of an environmental-friendly semi-continuous chlorination process allowed us to investigate the intrinsic properties required for either nitro- and chlorobenzene chlorination over zeolite catalysts (Chapter 5).

First, the acid site density appears to be an important parameter for nitrobenzene chlorination. Although the catalytic tests were performed at iso-site conditions over FAU-type zeolites, the nitrobenzene chlorination was favored over the zeolite having the highest acid site density. In addition, the higher performance of hierarchical zeolites, in particular ZSM-5 type, prepared through various methods, *i.e.*, nanosized, desilication and dealumination, has been demonstrated for either nitro- and chlorobenzene chlorination reactions. Indeed, higher catalytic activities of nanosized ZSM-5 zeolites were shown in both aromatics’ chlorination. The inter-crystalline mesoporosity induced in nanosized catalysts allowed to seriously reduce diffusion limitations encountered in micron-sized zeolites. Moreover, the enhanced catalytic activity of hierarchical ZSM-5 zeolites, prepared *via* post-modifications, was highlighted in chlorobenzene chlorination. The lower acid site densities in

hierarchical zeolites with respect to conventional catalyst particularly highlights their remarkable capacities. In these cases, the apparent enhanced acid site contribution was attributed to an improved accessibility to the acid sites implied by the secondary porosity.

Depending on the aromatic used, chlorination reactions have showed to be an interesting tool for the quantification of intrinsic acidity of zeolites, in terms of acid site density and strength. Thus, by changing the nature or size of the molecule to be halogenated, one could expect to obtain numerous informations on zeolite properties.

Finally, studies on binderless coatings of zeolites on silicon-containing supports have shown a strong link between the support and zeolite crystals (Chapter 6). The strength of this chemical bond was enhanced when the support itself was used as a Si-source. The self-recrystallization approach guarantee high loadings of zeolite, along with a strong chemical bond with the substrate surface. Nevertheless, due to the metastable properties of zeolites, the gel composition has to be appropriate to get the desired zeolite topology. The investigation of catalytic activity of such structured beds in MTH reactions has demonstrated a high potentiality compared with unsupported powders.

In summary, this Thesis provided insights in the triple-scale design of a catalyst module ranging from its chemical composition, an appropriate crystal size, up to a suitable reactor geometry at the macroscopic level (Figure). One should therefore continue the zeolite development in this direction.

From my point of view, the rational design of a quasi-ideal catalyst should combine several aspects in order to exhibit a proper chemical composition (acid site strength and density), a hierarchical porosity, an appropriate crystal size and also a proper shape at the reactor level. Indeed, these properties seem to be necessary to extend the applicability of zeolites in petrochemistry but also in fine chemistry. Each level plays a proper role: nature and density of the acid sites into microporous channels provide activity; the mesopores facilitate intra-crystalline transport; and the macroshape enables practical implementation taking into account engineering considerations. By combining these parameters, one should be able to warrant the introduction of hierarchical zeolites into industrial reactor.

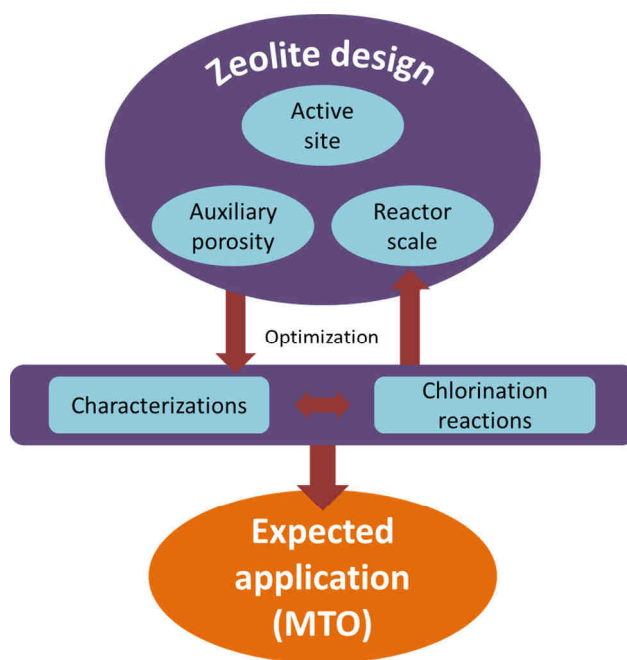


Figure Our application-driven design of zeolite catalysts

PUBLICATIONS

- * M. Boltz, A. Blanc, G. Laugel, P. Pale, B. Louis
Heterogenization of [Cu(2,2'-bpy)Cl₂] and [Cu(1,10-phen)Cl₂] on Polyoxometalates: New Catalysts for the Selective Oxidation of Tetralin, Chinese J. Catal. 32 (2011) 807.
- * F.L. Bleken, S. Chavan, U. Olsbye, M. Boltz, F. Ocampo, B. Louis
Conversion of methanol into light olefins over ZSM-5 zeolite: Strategy to enhance propene selectivity, Appl. Catal. A 447–448 (2012) 178.
- * M. Boltz, M.C.S. de Mattos, P.M. Esteves, P. Pale, B. Louis
Green route for the chlorination of nitrobenzene, Appl. Catal. A 449 (2012) 1.
- * G.F. Mendonça, A.R. Bastos, M. Boltz, B. Louis, P. Pale, P.M. Esteves, M.C.S. de Mattos
Electrophilic Chlorination of Arenes with trichloroisocyanuric acid over Acid Zeolites, Appl. Catal. A 460-461 (2013) 46.
- * T.J. Daou, M. Boltz, L. Tzanis, L. Michelin, B. Louis
Gas-phase chlorination of aromatics over FAU- and EMT-type zeolites, Catal. Commun. 39 (2013) 10.
- * M. Boltz, P. Losch, B. Louis
A general overview on the methanol to olefins reaction: Recent catalyst developments, Adv. Chem. Lett. 1 (2013) 247.
- * P. Losch, M. Boltz, K. Soukup, I.-H. Song, H.S. Yun, B. Louis
Binderless Zeolite Coatings on Macroporous α -SiC Foams, Microporous Mesoporous Mater. 188 (2014) 99.
- * M. Boltz, P. Losch, B. Louis, G. Rioland, L. Tzanis, T.J. Daou, MFI-type Zeolite
Nanosheets for Gas-Phase Aromatics Chlorination: A Strategy to Overcome Mass Transfer Limitations, RSC Advances, 4 (2014) 27242.
- * P. Losch, A. Martinez-Pascual, M. Boltz, S. Ivanova, B. Louis, F. Montilla-Ramos, J.A. Odriozola
Ionic liquid immobilization on carbon nanofibers and zeolites: catalyst design for the liquid-phase toluene chlorination, Comptes Rendus Chimie, submitted.
- * P. Losch, M. Boltz, B. Louis, S. Chavan, U. Olsbye

Catalyst optimization for enhanced propylene formation in the Methanol-To-Olefins reaction, Comptes Rendus Chimie, submitted.

- * C. Carvalho-Rocha, A. Balanqueux, M. Boltz, P. Losch, C. Bernadon, V. Beneteau, P. Pale, M.M. Pereira, B. Louis

Unraveling the importance of zeolite crystal morphology, Actualité Chimique, submitted.

COMMUNICATIONS

Posters

M. Boltz, B. Louis

Procédé de chloration du nitrobenzène en continu catalysé par des acides solides.

Congrès GECat 2012 Kerjouanno, France

M. Boltz, P. Losch et B. Louis

Mise en forme de catalyseurs de type zéolithique sur des supports structurés.

Congrès GECat 2013, Cap d'Agde, France

M. Boltz, M.C.S. de Mattos, P. M. Esteves, P. Pale, B. Louis

Green route for the chlorination of deactivated aromatics.

Congrès ABC-7 2013, Japan

M. Boltz, M.C.S. de Mattos, P. M. Esteves et B. Louis

Etude de la chloration d'aromatiques désactivés en milieu zéolithique : apport de calculs DFT.

Congrès GECat 2014, Cluny, France

Oral presentation

M. Boltz and B. Louis

Design microscopique de zéolithes ZSM-5 pour la conversion du méthanol en oléfines légères.

Congrès GECat (mai 2013) Cap d'Agde, France

Tailor-made conception of zeolites for catalysis: From the active site to the reactor

Résumé

Les zéolithes représentent une importante classe de catalyseurs hétérogènes largement utilisée dans l'industrie. En effet, ce sont des catalyseurs de choix pour de multiples réactions grâce à leurs propriétés uniques largement modulables, à savoir leur forte acidité de Brønsted, leur grande surface spécifique, leur stabilité hydrothermique et leur sélectivité de forme. Cependant, la taille de leurs micropores engendre des difficultés en terme de diffusion, réduisant ainsi leur potentiel catalytique. Une la conception sur mesure, pour satisfaire une application finale, s'avère être une méthode très intéressante pour le développement de nouveaux catalyseurs zéolithiques.

Des zéolithes hiérarchisées ont été synthétisées selon diverses méthodes pré- ou post-synthétiques et testées dans la chloration du nitrobenzène et du chlorobenzène. Par ailleurs, l'activité de ces zéolithes ainsi que des cristaux « géants » de ZSM-5, préparés par voie fluorure, a été évaluée dans le MTO.

La corrélation directe entre l'activité catalytique et les propriétés intrinsèques des zéolithes a permis de souligner les propriétés indispensables à chaque réaction.

Les travaux réalisés au cours de cette Thèse ont pour objectif la conception de zéolithes à trois niveaux : (i) au niveau du site actif en jouant sur la force acide et sur leur accessibilité, (ii) au niveau microscopique par la taille des cristaux et (iii) au niveau du réacteur en les déposant sur divers supports. Ces différentes zéolithes ont été évaluées dans deux réactions de la catalyse acide : la chloration d'aromatiques et la conversion du méthanol en oléfines légères (MTO).

Mots clés: zéolithe, mésoporosité, coating, MTO, chloration, conception sur mesure, FAU, MFI

Abstract

Zeolites are aluminosilicate catalysts of great importance for chemical industries. Their unique properties, *i.e.*, strong Brønsted acidity, high surface area, high hydrothermal stability, and shape selectivity, combined with an extensive tunability, render them the candidate of choice in various reactions. Nevertheless, often only a fraction of their potential is exploited, due to hindered access and diffusion limitations in their micropores. The rational design appears as a valuable method to design new zeolite catalysts, according to their targeted application.

The work described in this Thesis aims in the design of zeolites at three levels: (i) acid site by playing on acid strength and accessibility, (ii) microscopic scale by adapting the crystal size and (iii) reactor level by coating zeolite crystals on different supports. These as-prepared zeolites were evaluated in two acid-catalyzed reactions: the aromatics chlorination and the conversion of methanol in light olefins (MTO).

Hierarchical zeolites were synthesized according to several pre- or post-synthetic modifications and evaluated in nitro- and chlorobenzene chlorinations. Besides, "giant" ZSM-5 zeolites, prepared according to a fluoride-mediated route, as well as zeolite coatings on β -SiC, were tested in the MTO reaction.

Thanks to a direct correlation between catalytic activities and intrinsic properties, optimal catalyst properties were highlighted for both reactions.

Keywords: zeolite, mesoporosity, coating, MTO, chlorination, rational design, FAU, MFI